

Pharmacological and *in silico* investigation of anti-inflammatory diterpenoid compounds isolated from *Dodonaea polyandra*

PhD Thesis

By Matthew Bendikov

Bachelor of Medical and Pharmaceutical Sciences (Honours)

Principal Supervisor: Dr Matt Sykes

Co-Supervisor: Dr Susan Semple

Submitted in fulfilment of the requirements for the degree of

Doctor of Philosophy (Pharmacology)

Sansom Institute for Health Research

School of Pharmacy and Medical Sciences

Division of Health Sciences

University of South Australia

November 2017

Table of Contents

List of Figures VI

List of Tables X

Table of Abbreviations XII

Summary XV

Declaration XVII

Statement of Authorship XVIII

Acknowledgements XXI

Chapter One: Introduction 1

1.1. Project background 1

1.2. Pathways of inflammation 5

1.2.1. Background of PAA and inflammation 5

1.2.2. Characterisation of inflammation 5

1.2.3. Eicosanoids 7

1.2.4. Interleukin-1β (IL-1β) 11

1.2.5. Tumor necrosis factor alpha (TNFα) 13

1.2.6. Interleukin-6 (IL-6) 14

1.2.7. Nitric oxide (NO) 15

1.2.8. Glucocorticoid receptor 16

1.2.9. Summary of PAA and inflammation 18

1.3. Pain, analgesia and opioid receptors 19

1.3.1. Background of PAB and pain 19

1.3.2. Characterisation of pain 19

1.3.3. Action potentials and transmission of pain 20

1.3.4. Treatment of pain or analgesia 21
1.3.5. Opioid receptors 22
1.3.6. Opioid agonists 24
1.3.7. Summary of PAB and pain 26
1.4. Metabolism of drugs 27
1.4.1. Function and biology of metabolism 27
1.4.2. Cytochrome p450 (CYP) enzymes 28
1.4.3. UDP-glucuronosyltransferase (UGT) enzymes 29
1.4.4. Carboxylesterase (hCES) enzymes 30
1.4.5. Other metabolising enzymes and their relative importance 31
1.5. *In vitro* and *in silico* approaches to studying molecules 34
1.5.1. *In vitro* techniques in the pharmaceutical industry 34
1.5.2. *In silico* tools in the pharmaceutical industry 35
1.5.3. Structure-based methods 36
1.5.4. Ligand-based methods 39
1.5.5. Knowledge-based methods 45
1.6. Project aims 48

Chapter Two: The enzymology of human PAA and PAAH metabolism 50

2.1. Introduction 50
2.2. Results and Discussion 52
2.2.1. Incubation of PAA with standard media 52
2.2.2. Incubation of PAA with HLM 53
2.2.3. PAAH to substitute for PAA in further experiments 55
2.2.4. Cytochrome P450 mediated metabolism of PAAH 56
2.2.5. UGT-mediated metabolism of PAAH 59

2.2.6. Sulfotransferase (SULT) mediated metabolism of PAAH 60
2.2.7. Combined CYP and UGT mediated metabolism of PAAH 61
2.2.8. Summary of human hepatic enzyme depletion studies 63
2.2.9. Derived kinetic parameters and *in vitro* / *in vivo* extrapolation 64
2.2.10. Carboxylesterases involved in PAA hydrolysis 66
2.2.11. CYP enzymes involved in PAAH metabolism 69
2.2.12. UGT enzymes involved in PAAH metabolism 73
2.2.13. Summary of specific enzyme contributions 77
2.2.14. Identity of UGT metabolites 78
2.2.15. Identity of CYP metabolites 96
2.3. Conclusions and future directions 105

Chapter Three: Anti-inflammatory investigation of PAA 108

3.1. Introduction 108
3.2. Results and discussion 110
3.2.1. Caspase-1 110
3.2.2. Protein kinase C (PKC) 120
3.2.3. Nuclear factor-κB (NF-κB) 126
3.2.4. Glucocorticoid receptor 133
3.2.5. Additional pathways investigated using an *in silico* approach 148
3.2.6. Discussion of *in silico* implementation 151
3.3. Conclusions and future directions 156

Chapter Four: Opioid investigation of PAB 158

4.1. Introduction 158

4.2. Results and discussion 160

4.2.1. *In silico* investigations and structure-activity relationships 160

4.2.2. Chemical synthesis of methyl polyandrate B 167

4.2.3. *In vitro* opioid screening 172

4.2.4. Post screening *in silico* analysis 173

4.2.5. Discussion of findings 177

4.3. Conclusions and future directions 184

Chapter Five: Thesis overview 185

5.1. Project description 185

5.2. Findings of the metabolism study of PAA and PAAH 186

5.3. Findings of the study of inflammatory pathways of PAA action 190

5.4. Findings of the study of MPB and the μ-opioid receptor 193

5.5. Observations on *in silico* methods 196

5.6. Final thoughts 199

Chapter Six: Methods and materials 200

6.1. Experimental materials, assays and software 200

6.1.1. Chemicals and suppliers 200

6.1.2. Outsourced assays 202

6.1.3. Software 203

6.2. Human enzyme metabolism of PAA and PAAH 204

6.2.1. Collection of human liver microsomes 204
6.2.2. *E. coli* P450 expression 206
6.2.3. Protein content quantification 207
6.2.4. Sample analysis by HPLC 208
6.2.5. Methodology for experimental incubation 209
6.2.6. Specific enzyme studies 213
6.2.7. Recombinant enzyme studies 214
6.2.8. Statistical analysis/data management 214
6.2.9. Metabolite characterisation by hydrolysis 215
6.2.10. Sample analysis by UPLC/MS 215
6.3. Anti-inflammatory investigation of PAA and PAAH 217
6.3.1. Caspase-1 and NF-κB assays 217
6.3.2. Protein kinase testing 218
6.3.3. Glucocorticoid receptor testing 218
6.4. Opioid investigation of PAB and its methyl ester derivative MPB 220
6.4.1. Synthesis of MPB by thionyl chloride reflux 220
6.4.2. Synthesis of MPB by methyl iodide reflux 220
6.4.3. MPB screening against μ-opioid receptor 221
6.5. *In silico* methods 222
6.5.1. 3D-structure generation 222
6.5.2. Webserver screening 222
6.5.3. FILTER screening 223
6.5.4. Docking methods 225
6.5.5. Overlay analysis 226

References 228

List of Figures

Figure 1.1: Photographs of *Dodonaea polyandra*. 2
Figure 1.2: Structures of anti-inflammatory diterpenoids from *D. polyandra.* 3
Figure 1.3: Structures of arachidonic acid, prostaglandin E_2 and leukotriene D_4. 8
Figure 1.4: Production pathway of inflammatory prostaglandin PGE_2. 10
Figure 1.5: Condensed transduction cascade of IL-1β. 12
Figure 1.6: Condensed transduction cascade of TNFα. 14
Figure 1.7: Signal transduction pathway of IL-6. 15
Figure 1.8: Production pathway of RNOS from L-arginine. 16
Figure 1.9: Signal transduction pathway of the glucocorticoid receptor. 17
Figure 1.10: Structure of a nerve cell. 20
Figure 1.11: Structures of opioid agonists. 25
Figure 1.12: Examples of drug metabolites produced by CYP enzymes. 28
Figure 1.13: Examples of drug metabolites produced by UGT enzymes. 30
Figure 1.14: Examples of drug metabolites produced by hCES enzymes. 31
Figure 1.15: Contributions of enzyme families to the metabolism of marketed drugs. 32
Figure 1.16: Crystal structure of the CYP2C9 enzyme. 37
Figure 1.17: Pharmacophore mapping of compound ID 20 performed by a Catalyst Flexible Best Search. 41
Figure 1.18: ROCS model of PAA displaying defined structural features. 43
Figure 1.19: ROCS overlay of PAAH to flurbiprofen. 44

Figure 2.1: Structures of PAA and PAAH. 51
Figure 2.2: Incubation of PAA with standard media. 52
Figure 2.3: Incubation of PAA with HLM. 53
Figure 2.4: Structures of the diterpenoids PAAH and salvinorin A. 55
Figure 2.5: Molecular structure of eserine. 55
Figure 2.6: Incubation of PAAH with HLM and NADPH generating system. 56
Figure 2.7: Incubation of phenacetin with HLM and NADPH generating system. 57
Figure 2.8: Incubation of PAAH with HLM, NADPH generating system and alamethicin. 58
Figure 2.9: Incubation of PAAH with HLM and UDPGA. 59

Figure 2.10: Incubation of PAAH with HLC and PAPS. 60
Figure 2.11: Depletion of PAAH with HLM, UDPGA and NADPH generating system. 62
Figure 2.12: Summary of PAAH depletion by HLM with enzyme cofactors. 63
Figure 2.13: Scaffold of ester functional group. 66
Figure 2.14: Structure of PAA with ester functionality highlighted. 68
Figure 2.15: Effect of the use of enzyme inhibitors on total CYP depletion of PAAH. 70
Figure 2.16: Structures of the selective CYP inhibitors sulfaphenazole and CYP3cide. 71
Figure 2.17: CYP mediated PAAH depletion attributed to recombinant CYP enzymes. 72
Figure 2.18: Effect of the use of enzyme inhibitors on total UGT depletion of PAAH. 74
Figure 2.19: Structure of niflumic acid and fluconazole. 75
Figure 2.20: UGT mediated PAAH depletion attributed to recombinant UGT enzymes. 76
Figure 2.21: XenoSite predicted site of metabolism of PAAH by UGT enzymes in HLM. 79
Figure 2.22: MetaPred Web Server prediction results of PAAH metabolism by UGT enzymes. 81
Figure 2.23: SomUGT prediction of glucuronidation sites in PAAH. 82
Figure 2.24: Formation of metabolite over time by incubation of PAAH with UDPGA. 83
Figure 2.25: UPLC/MS chromatograms of PAAH and PAAH-glucuronide. 85
Figure 2.26: UPLC/MS chromatogram of PAAH-glucuronide metabolites. 86
Figure 2.27: UPLC/MS chromatogram of PAAH-glucuronide metabolites after incubation with β-glucuronidase. 87
Figure 2.28: UPLC/MS chromatogram of PAAH-glucuronide metabolites after incubation with weak base. 88
Figure 2.29: Structure of proposed glucuronide metabolites and glucuronide moiety. 89
Figure 2.30: UPLC/MS chromatograms of PAAH-glucuronide metabolites produced by different enzyme preparations. 91
Figure 2.31: UPLC chromatogram of HLM/UDPGA incubated PAAH sample. 92
Figure 2.32: XenoSite predicted site of metabolism of PAAH by CYP enzymes in HLM. 96
Figure 2.33: MetaPred Web Server prediction results of PAAH metabolism by CYP2C9. 97
Figure 2.34: MetaPred Web Server prediction results of PAAH metabolism by CYP3A4. 98
Figure 2.35: ROCS overlay of flurbiprofen and PAAH. 100
Figure 2.36: Docked structure of PAAH in the CYP2C9 receptor. 101
Figure 2.37: Structures of a furan ring and potential CYP-metabolites. 103
Figure 2.38: Proposed in vitro metabolic pathway of PAAH. 106

Figure 3.1: Overlay of 10 caspase-1 crystallised ligands. 112
Figure 3.2: ROCS overlays of PAA with the four highest ranked caspase-1 inhibitors.... 114
Figure 3.3: Docking pose of PAA and bound ligand, 13, in caspase-1. 116
Figure 3.4: Effects of PAA on pro-IL-1β and IL-1β production by THP-1 cells. 118
Figure 3.5: ROCS overlays of PAA to the four highest ranked PKC inhibitors. 122
Figure 3.6: Complete pharmacophore map for PKC inhibitors. 123
Figure 3.7: ROCS overlays of PAAH to the four highest ranked NF-κB inhibitors. 129
Figure 3.8: Screening results of PAA effects on nitrite production by RAW 264.7 cells as measured colorimetrically using the Griess assay. 131
Figure 3.9: Structures of glucocorticoid agonists. 134
Figure 3.10: Pharmacophore of glucocorticoid receptor agonists. 134
Figure 3.11: ROCS overlay of PAAH and GR9. 137
Figure 3.12: Pharmacophore of glucocorticoid agonists overlaid to GR2. 138
Figure 3.13: Docked pose of PAAH in the active site of the glucocorticoid receptor. 143
Figure 3.14: Overlay of docked PAAH to co-crystallised mometasone furoate. 144
Figure 3.15: Measurement of PAAH and PAA binding to the glucocorticoid receptor.... 146
Figure 3.16: Structures of cacospongiolide E and PAAH. 149
Figure 3.17: Structures of compound 6 and PAAH. 150
Figure 3.18: Compounds docked by FRED into protein kinases. 153

Figure 4.1: Chemical structures of polyandric acid B and salvinorin A. 158
Figure 4.2: Molecular surface of the active site of the κ-opioid receptor. 161
Figure 4.3: Consensus of three SAR studies into salvinorin A. 163
Figure 4.4: Overlay of the docked poses of MPB and herkinorin in the μ-opioid structure 4DKL. 166
Figure 4.5: Proposed reaction pathway of MPB synthesis by reflux with thionyl chloride. 168
Figure 4.6: Likely reaction pathway that occurred during reflux with thionyl chloride. .. 169
Figure 4.7: Intended reaction pathway of MPB synthesis by reflux with methyl iodide. . 170
Figure 4.8: Key correlations observed in the HMBC spectrum of MPB. 172
Figure 4.9: Overlay of docked structures of MPB and herkinorin in the μ-opioid structure 5C1M. 175
Figure 4.10: Chemical structures of co-crystallised opioid ligands. 176

Figure 4.11: ROCS overlay of herkinorin to MPB. 180
Figure 4.12: Proposed binding mode of herkinorin in the μ-opioid receptor. 182

Figure 5.1: Structures of furan containing compounds..... 189

List of Tables

Table 1.1: Multidimensional representations of PAA. 46

Table 2.1: Derived kinetic parameters for PAAH depletion by HLM and co-factors. 65
Table 2.2: Structures of human carboxylesterase substrates. 67
Table 2.3: Knowledge-based predictions of PAAH metabolism by UGT enzymes. 73
Table 2.4: Comparative quantitative analysis of glucuronide metabolites. 93

Table 3.1: List of PDB crystal structures of caspase-1. 110
Table 3.2: ROCS scores of caspase-1 inhibitors with PAA as the query. 113
Table 3.3: ROCS scores of PAA as a query to PKC inhibitors. 121
Table 3.4: Screening results of PAA against various PKC subtypes. 125
Table 3.5: ROCS scores of PAAH as a query to NF-κB inhibitors. 127
Table 3.6: ROCS scores of PAAH as a query to glucocorticoid modulators. 135
Table 3.7: ROCS scores of GR1 as a query to glucocorticoid modulators and PAAH. 139
Table 3.8: List of PDB crystal structures of glucocorticoid receptors. 141
Table 3.9: Docking table of Chemgauss4 scores. 142

Table 4.1: ^{1}H and ^{13}C NMR spectral data of MPB in MeOD-d_4. 171
Table 4.2: In vitro binding of MPB to the μ-opioid receptor. 173
Table 4.3: Parameters of μ-opioid crystal structures. 174

Table 6.1: List of chemical suppliers, chemicals and chemical grade. 200
Table 6.2: Relevant data of human livers used in experiments 204
Table 6.3: Contents of standard tubes for Lowry protein assay. 207
Table 6.4: Universal HPLC conditions for sample analysis 208
Table 6.5: Specific HPLC conditions for sample analysis 209
Table 6.6: Contents of incubation experiment test tubes 210
Table 6.7: General parameters for experimental incubation of samples 211
Table 6.8: Specific parameters for experimental incubation of samples 212
Table 6.9: Contents of NADPH generating system per experiment 212
Table 6.10: List of enzyme inhibitors used in experiments. 213

Table 6.11: Component list of UPLC/MS system 216
Table 6.12: Settings list for UPLC/MS analysis of samples..... 216
Table 6.13: Stepwise dilution scheme of PAA and PAAH for glucocorticoid testing. 219
Table 6.14: Default variables used in Omega for conformer generation..... 222
Table 6.15: List of webservers used for molecular modelling purposes. 223
Table 6.16: List of generic variables for Make Receptor active site generation 226
Table 6.17: List of generic variables for OEDocking screening 226
Table 6.18: List of generic variables for vROCS analysis. 227

Table of Abbreviations

δ-ALA	5-Aminolevulinic acid
ACN	Acetonitrile
AcOH	Acetic acid
ATP	Adenosine triphosphate
cAMP	Cyclic adenosine monophosphate
CNS	Central nervous system
COX	Cyclooxygenase
CYP	Cytochrome P450
D. polyandra	*Dodonaea polyandra*
E. coli	*Escherichia coli*
FDA	Food and Drug Administration
FRED	Fast Rapid Exhaustive Docking
G-6-P	Glucose-6-phosphate
GPCR	G-protein coupled receptor
GR	Glucocorticoid receptor
GST	Glutathione-S-transferase
hCESx	Human carboxylesterase x i.e. hCES1, hCES2
HLC	Human liver cytosol
HLM	Human liver microsomes
HMBC	Heteronuclear multiple-bond correlation
HPLC	High performance liquid chromatography
IL-x	Interleukin-x i.e. IL-1β, IL-6, IL-18
iNOS	Inducible nitric oxide synthase
IPTG	Isopropyl β-D-1-thiogalactopyranoside
IV-IVE	*In vitro – in vivo* extrapolation
LB	Lysogeny broth
LKx_4	Leukotriene x_4 i.e. LKD_4, LKE_4
MeI	Methyl iodide

MeOD-d_4	Deuterated methanol
MeOH	Methanol
MPB	Methyl polyandrate B
MS	Mass spectrometry
NADPH	Nicotinamide adenine dinucleotide phosphate
NF-κB	Nuclear factor kappa B
NMR	Nuclear Magnetic Resonance
NO	Nitric oxide
NSAID	Non-steroidal anti-inflammatory drug
PAx	Polyandric acid x i.e. PAA, PAB
PAAH	Hydrolysed polyandric acid A
PDB	Protein data bank
PGx_2	Prostaglandin x_2 i.e. PGE_2, PGH_2
PKCx	Protein Kinase Cx i.e. PKCα, PKCβ1
PMSF	Phenylmethanesulfonyl fluoride
PNS	Peripheral nervous system
RCSB	Research Collaboratory for Structural Bioinformatics
RMSD	Root mean square deviation
ROCS	Rapid Overlay of Chemical Structures
ROS	Reactive oxygen species
RT	Retention time
SD	Standard deviation
SEM	Standard error of the mean
SMARTS	SMILES arbitrary target specification
SMILES	Simplified molecular-input line-entry system
SRB	Spheroplast resuspension buffer
SULT	Sulfotransferase
TB	Terrific broth
TGA	Therapeutic Goods Administration
TNFα	Tumor necrosis factor alpha
TOF	Time of Flight

TPA	12-O-tetradecanoylphorbol-13-acetate
TR-FRET	Time resolved – fluorescence energy transfer
UDPGA	Uridine diphosphate glucuronic acid
UGT	UDP-glucuronosyl transferase
UPLC	Ultra-performance liquid chromatography
UV	Ultraviolet

Summary

Over the past 30 years the search for new medicines has increasingly turned towards natural products for chemical leads and therapeutic products. Indigenous knowledge is often sought to guide the scientific discovery of medicines derived from natural products. A collaborative project, previously established by the Chuulangun Aboriginal Corporation and the University of South Australia, has explored the medicinal properties of various traditional Australian medicinal plants, including the species *Dodonaea polyandra*. Active components of this plant species have previously been isolated and found to possess anti-inflammatory activity *in vitro* and *in vivo*. The study described in this thesis sought to further develop academic knowledge about the bioactive constituents of *D. polyandra* and to aid the pre-clinical development of a therapeutic product.

In this pharmacological study, active compounds of *D. polyandra,* polyandric acid A and B (PAA and PAB), were investigated by *in vitro* and *in silico* means in relation to three primary areas: drug metabolism, and anti-inflammatory and analgesic mechanisms. Chapter 1 provides a literature review of these three primary areas to provide a background to the areas explored within this thesis.

Chapter 2 describes *in vitro* investigations of the human enzyme metabolism of the anti-inflammatory compound PAA, and its de-esterified metabolite PAAH, including primary mechanisms of metabolism, determination of kinetic parameters and identification of major metabolites. Additionally, *in silico* techniques were used to complement the *in vitro* work. The key findings were the identification of carboxylesterases and UGT enzymes, specifically UGT 1A1 and 2B7, as major clearance enzymes, and CYP enzymes, specifically CYP 2C9 and 3A4, as minor clearance enzymes. The metabolism of PAAH by CYP2C9 was rationalised using both ligand and structure based *in silico* methods. The half-life of PAA by UGT/CYP enzymes was 107±2.12 minutes, and the total hepatic clearance of PAA was estimated at 1.25 L/hr, suggesting metabolism was likely to occur slowly in humans. Furthermore, the identity of the major glucuronide metabolite was determined using LC-MS/MS as an acyl glucuronide, which was in good agreement with the results obtained using *in silico* methods.

While PAA had previously been shown to have anti-inflammatory activity in mice and to modulate the release of inflammatory cytokines in cells, the mechanism of action had

not been established. The study described in Chapter 3 involved a series of *in silico* and *in vitro* investigations into a variety of receptors associated with the inflammation cascade, to determine a mechanism of action for PAA and its de-esterified metabolite. This process took *in vitro* results from whole cell experiments which identified that key pro-inflammatory cytokines: IL-1β, IL-6 and TNFα were modulated by PAA. Studies were undertaken assessing enzymes and protein complexes associated with these cytokines by ligand- and structure-based *in silico* techniques and testing hypotheses with *in vitro* assays. Several targets were screened including caspase-1, NF-κB, protein kinase C and the glucocorticoid receptor, but no significant activity was found with *in vitro* testing of the chosen targets. *In silico* screening of each target involved a combination of ligand-based structural similarity searching and structure-based docking, and it was determined that the ligand-based approach offered better predictive power due to better discernment of positive and negative results.

A previous honours study established a structural relationship between PAB and the opioid agonist, salvinorin A, which led to formation of a hypothesis that PAB may also modulate opioid receptor activity. In Chapter 4, studies are described that investigated this hypothesis by examining literature regarding salvinorin A analogues, as well as structure-based *in silico* investigation of opioid receptors. It was determined that a methyl ester derivative of PAB (MPB) possessed significant similarity to the salvinorin A analogue and μ-opioid selective agonist, herkinorin, suggesting that MPB may have μ-receptor modulating properties. As a result, *in vitro* synthesis and screening of MPB against the μ-receptor was carried out, but no significant activity was determined. Additional analysis was performed in light of a very recent study into herkinorin binding to review this result and it was suggested that key structural differences between MPB and herkinorin, not fully described by previously available literature, may account for the difference in binding activity.

In summary, this thesis details the first human metabolism study of an Australian medicinal plant compound, insight into the field of anti-inflammatory clerodane diterpenoids, assessment of a novel hypothesis of opioid activity, and commentary on *in silico* applications in drug discovery.

Declaration

The work presented in this thesis is carried out by the author and does not incorporate, without due acknowledgement, any material that has been previously submitted for a degree or diploma in any university. To the best of my knowledge, it does not contain materials previously published or written by another person, except where due reference is made in the text; and all substantiative contributions by others to the work presented, including jointly authored publications, are clearly acknowledged.

Matthew Bendikov

Statement of Authorship

Chapter 2: The enzymology of human PAA and PAAH metabolism: An *in vitro* and *in silico* investigation

Chapter 2 focuses on the study of the human enzyme metabolism of polyandric acid A (PAA) and its de-esterified alcohol form (PAAH). The chapter incorporates *in vitro* methodologies, performed at the Flinders Medical Centre under the supervision of Professor John Miners and *in silico* methodologies, performed at the University of South Australia. A majority of experimental work (>90%) presented in this chapter, both *in vitro* and *in silico*, was performed by Matthew Bendikov. The remainder of experimental work in this chapter, the section in regard to MS detection of metabolites, was performed with the assistance of Mr David Elliot. Beyond experimental work, analysis of results was performed primarily by Matthew Bendikov and John Miners with contributions from Matt Sykes and Susan Semple. The *in vitro* results presented in this chapter have been published in *Xenobiotica* in a paper titled: *"In vitro metabolism of the anti-inflammatory clerodane diterpenoid polyandric acid A and its hydrolysis product by human liver microsomes and recombinant cytochrome P450 and UDP-glucuronosyltransferase enzymes"* [1]. Specific authorship contributions of the co-authors are as follows:

Matthew Y. Bendikov performed a majority of experimental work and authored a majority of the paper.

John O. Miners provided guidance to the studies direction as well as significant oversight in preparation of the manuscript.

Bradley S. Simpson was involved in the foundational research for this paper including the initial isolation of PAA from *Dodonaea polyandra.*

David J. Elliot provided assistance with operation of the mass spectrometer for analysis of metabolites.

Susan J. Semple assisted with editing of the manuscript as well as data analysis and acting as a liaison between the University of South Australia and the Chuulangun Aboriginal Corporation.

David J. Claudie was involved in supplying raw plant materials of *D. polyandra* and acting as a liaison between the Chuulangun Aboriginal Corporation and the University of South Australia.

Ross A. McKinnon assisted with editing of the manuscript.

Elizabeth M.J. Gillam assisted with editing of the manuscript as well as providing several recombinant enzymes used in experiments.

Matthew J. Sykes assisted with data analysis, editing and submission of the manuscript.

Chapter 3: Anti-inflammatory investigation of PAA

Chapter 3 focuses on investigations of target based interactions of PAA and PAAH with various enzymes involved in the inflammatory cascade to attempt to elucidate a mechanism of action for the observed anti-inflammatory properties of PAA. The chapter incorporates *in silico* methodologies, all of which were conducted by Matthew Bendikov at the University of South Australia, and *in vitro* methodologies, which were conducted by various people and external services as outlined in the chapter. A portion of this chapter relating to *in silico* investigations of interactions between PAAH and the glucocorticoid receptor were presented at the Royal Australian Chemical Institute (RACI) National Congress 2014 held in Adelaide, South Australia as a poster titled: *"Proposed anti-inflammatory mechanism of the diterpenoid polyandric acid A".*

Chapter 4: Opioid investigation of PAB

Chapter 4 focuses on investigations of structure activity relationships, particularly in regards to polyandric acid B and a unique opioid agonist scaffold, based on salvinorin A. As a general note, the study in this chapter is an extension of previous work conducted as part of an honours study by the candidate titled: *"In silico directed investigation of novel diterpenoid compounds isolated from Dodonaea polyandra"* [2]. As such, within this chapter a number of references are made to this past work. The chapter incorporates *in silico* and *in vitro* methodologies, all of which were conducted by Matthew Bendikov at the

University of South Australia, except for biological screening which was performed by an external organisation as outlined in the chapter. Aspects of this chapter were presented twice in the form of a poster, firstly in a competition hosted by Bionomics and secondly at the RACI Biomolecular Division Conference in 2013. The title of this poster was: *"An in silico directed investigation of novel diterpenoid compounds as potential substrates of opioid receptors"*.

Acknowledgements

Any person who claims that a PhD project is a simple task is either a genius or a fool. Personally, I would never claim anything so obviously silly. The contents of this thesis represent the culmination of thousands of hours of work. Work that would have been impossible without the support, guidance and contributions of many people.

Firstly, I would acknowledge my supervisors: Dr Matt Sykes and Dr Susan Semple. I was told since before I started my studies that a supervisor can make or break a project. I can't imagine how this project would have turned out without both Matt and Sue. Since my very first undergraduate chemistry lecture, Matt has been one of my foremost academic and professional influences. Sue also has been a key influence on my development by demonstrating ethical responsibility in research and imparting its importance to me. I am ever grateful to Matt and Sue for their consistent support, encouragement and patience (especially patience) throughout my studies, but I am most grateful for allowing me the gift of freedom. Freedom to experiment with strange ideas is something that, as I have learned, is a rarity amongst PhD supervisors. I have no idea where I will be ten or twenty years from now, but I know that whatever I will have achieved will be in part because of your positive influences.

I'd also like to thank Prof John Miners for his guidance while working at the Flinders Medical Centre Department of Clinical Pharmacology. While not officially my supervisor, John provided a huge amount of support while studying drug metabolism. My time at Flinders was extremely valuable and was probably the most significant learning experience I have had since my undergraduate studies. John is only one member of the department however, and so I'd also like to acknowledge Dr Andrew Rowland, Dr Ben Lewis, Dr Pramod Nair, David Elliot, Kushari Burns, Nuy Chau and Attarat Pattanawongsa, for sharing their practical and academic experience with me.

Closer to home, I'd like to acknowledge some of the people from the University of South Australia who have supported me along the way. For their various contributions, encouragements, support and general friendship I'd like to thank Steven Nguyen, Dr Theodosia Teo, Sapphire Le, Todd Gillam, Dr Mingfeng Yu, Dr Aik Wye Goh and Courtney De Vries. Great and small you have all, in some way, contributed to making my studies a more enjoyable experience. Also from UniSA I'd like to thank Dr Maurizio Costabile, for improving my knowledge of inflammatory biology, and Assoc. Prof. Bob Milne who has consistently provided oversight and advice throughout the duration of my project.

I'd like to acknowledge financial support received through an Australian Government Research Training Program Scholarship. Also of assistance was OpenEye Scientific Software who provided a free academic license to a suite of *in silico* tools used throughout this project.

More personally I'd like to acknowledge my family, Andrew and Kim, Laura and Greg, Stacey and Lachlan, Iylah, Samuel and Elise, and especially my parents, George and Edwina. Consistently you have encouraged me to work hard and aim for success. To my friends also, your friendship, and at times distraction, has helped me greatly. Regardless of how much, or little, you have all understood about my work, you have continued to ask questions and shown interest. I owe the best parts of who I am to you all.

Finally, and most importantly, I'd like to give my thanks and love to my wife, Bek. Your love and support throughout my studies have been the biggest driving force for me to continue. When I was at my most difficult moments and feeling my lowest, you were the reason I kept working. You believed in me at times when I didn't and inspired me to work harder, and for that I will always be grateful.

Chapter One: Introduction

1.1. Project background

Since ancient times, natural products have been known to be an important source of medicines. Some of the earliest records of this knowledge include ancient Sumerian tablets dated to the third or fourth millennia B.C. referring to *"hul gil"* or *"joy plant"*, meaning *Papaver somniferum*, the opium poppy [3, 4], and the Edwin Smith Papyrus, a seventeenth century B.C. record of ancient Egyptian diagnostic techniques and herbal remedies [5]. Over millennia, scientific understanding of medicinal natural products has improved dramatically, firstly in the knowledge that extracts of natural products can improve the potency of medicinal properties and secondly that the medicinal qualities of natural product extracts are dependent on their molecular constituents. As such, modern research into natural medicines has had a significant focus on discovering biologically active natural extracts and isolating active components. In the past 30 years or so, this process of searching for natural products has become prevalent in the pharmaceutical industry, either for the purpose of developing plant based products for clinical use, or using active plant compounds as leads to discover new therapeutic products [6-9]. However, natural products often reach the market without a well characterised mechanism of action or human metabolism profile. Further characterisations of these areas can be beneficial to the development of therapeutic products, as well as being of scientific interest.

While they may come from a variety of sources and treat different conditions, natural medicines are ubiquitous across cultures and geographical regions of the world including Australia [10]. In traditional medicine systems, plants are often the most common source of medicines. One such Australian medicinal plant is *Dodonaea polyandra*, a plant of the Sapindaceae family, shown in Figure 1.1. This species is used by the indigenous Northern Kaanju (Kuuku I'yu) peoples, who refer to the plant as 'Uncha'. The traditional usage of the plant is to place the join of the stem and leaves of the plant in the oral cavity for the purpose of relieving inflammation and pain associated with toothache and infections in the mouth [11].

A  B 

Figure 1.1: Photographs of Dodonaea polyandra. *(A) Multiple Dodonaea polyandra ('Uncha') plants. (B) Close up of the leaves and fruit of the plant (Photographs taken by Nicholas M. Smith).*

A collaborative agreement between the Chuulangun Aboriginal Corporation, on behalf of the Kuuku I'yu peoples, and the University of South Australia was established in 2006 with the interest of investigating the medicinal activities of various plant species including *D. polyandra.* The purpose of the ongoing project is twofold: sharing indigenous medicinal knowledge and western scientific perspectives and to potentially develop therapeutic commercial products derived from plants.

Initial studies by Simpson et al. [11] confirmed the therapeutic actions of *D. polyandra* extracts in a mouse ear oedema model where acute skin inflammation is induced by 12-O-tetradecanoylphorbol-13-acetate (TPA). In this model, an ethanolic extract of the leaves and stems demonstrated an approximate 75% decrease in inflammation. Further investigation by Simpson et al. [12] led to the isolation of a series of clerodane diterpenoids that were found to be associated with anti-inflammatory activity. Clerodane diterpenoids are a subclass of diterpene structures derived from a 20-carbon framework consisting of a central 10-membered bicyclic structure with numerous alkyl extensions [13]. Two of these

compounds (see Figure 1.2) were found to possess significant anti-inflammatory activity, resulting in an approximate 70% decrease in inflammation in the same mouse ear oedema model previously used to screen *D. polyandra* extracts.

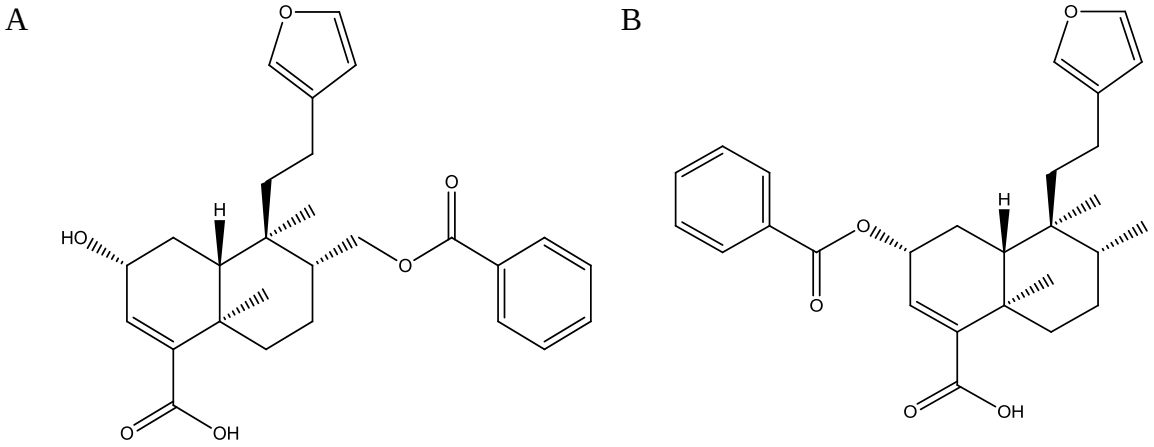

Figure 1.2: Structures of anti-inflammatory diterpenoids from D. polyandra. *(A) Polyandric acid A (PAA). (B) Polyandric acid B (PAB).*

Of the two leading anti-inflammatory constituents identified by the study, one compound, given the name polyandric acid A (PAA), was found to have a higher potency. PAA was also observed to have a standard monophasic dose-response curve with a maximal inhibition of inflammation (70.2 ± 10%, mean ± SEM) at a dose of 0.22 μmol/ear. This was considered to be a significant level of anti-inflammatory activity as the positive control used in this study, betamethasone-17-21-diproprionate (0.9 μmol/ear), a steroidal anti-inflammatory compound, inhibited inflammation by approximately 85%, which was within error of the maximal inhibition of PAA at the same dosage. The other compound, given the name polyandric acid B (PAB), was more unusual as it seemed to exhibit a biphasic dose-response curve with a U-shaped response curve observed over the range of 0.023 to 0.23 μmol/ear and a maximal response of 76.4 ± 7.3% (mean ± SEM) inhibition at 0.91 μmol/ear. While both PAA and PAB appeared to have similar anti-inflammatory responses at higher doses, the unusual kinetics of PAB, coupled with the higher potency of PAA resulted in further anti-inflammatory investigation being primarily focused on PAA.

As part of these further studies, Simpson et al. [14] determined that PAA (0.9 μmol/ear) was able to reduce mouse ear oedema by approximately 41% in a chronic model of mouse ear oedema. The effect was similar to the effect of betamethasone (0.9 μmol/ear) which produced a reduction in oedema of 54%. The compound was also tested for *in vitro* effects in cell lines stimulated with 12-*O*-tetradecanoylphorbo-13-acetate (TPA) and ionomycin, to instigate the production of pro-inflammatory cytokines. The effect of PAA against several pro-inflammatory markers was tested using human monocytic THP-1 and primary HFF-1 cells. From these experiments, it was determined that PAA reduced secretion of pro-inflammatory cytokines, including interleukin-1β, interleukin-6 and tumor necrosis factor alpha, which will be discussed in further depth in later sections of this thesis.

The studies of PAA to date, although promising, have yet to address the underlying question of how the observed effects are produced. It is well understood that for a compound to exert a pharmacological effect on a species it must interact with an enzyme or receptor to promote that pharmacological effect, but in the case of PAA the mechanism of anti-inflammatory effects is not yet understood. An unpublished study of the effects of PAA against cyclooxygenases 1 and 2 (COX-1 and COX-2), the enzymes targeted by many common anti-inflammatory drugs including aspirin and ibuprofen, found no binding activity [15]. Along with evidence from previous studies, this indicates that PAA is associated with anti-inflammatory activity by a mechanism different from many commercial anti-inflammatory drugs. Therefore, further study of the anti-inflammatory mechanism of PAA presents not just an academically interesting prospect, but may reveal promising therapeutic prospects as a lead compound acting by a novel mechanism of action.

1.2. Pathways of inflammation

1.2.1. Background of PAA and inflammation

As has been introduced in Section 1.1, the anti-inflammatory activity of *D. polyandra* is attributable to the actions of clerodane diterpenoid compounds, of which PAA is a chief constituent. A likely cause of these actions, as determined by Simpson et al. [14], is the inhibition of pro-inflammatory cytokine production, including interleukin-1β (IL-1β), interleukin-6 (IL-6) and tumor necrosis factor alpha (TNFα), although the precise target of PAA is unknown. Understanding the mechanism by which a drug functions is useful therapeutically as understanding a drug target can highlight potential disease states for which it can be applied, as well as potential undesirable effects. The following literature review is not intended to be an exhaustive description of the biology of inflammation, but instead primarily focuses on key mediators of inflammation, particularly IL-1β, IL-6 and TNFα, and the enzymes and receptors which interact with these mediators.

1.2.2. Characterisation of inflammation

The biology of inflammation is a highly complex web of protein and receptor interactions stemming from diverse stimuli that ultimately results in a few simple, observable outcomes: pain, redness, oedema and heat, ultimately resulting in loss of function [16]. These immediate symptoms of inflammation are attributable primarily to the effects of eicosanoids including prostaglandins (PGs) and leukotrienes (LTs) [17, 18]. Inflammation may be caused by numerous stimuli, both physical and chemical in nature, and can exist in different states of duration and severity, so an understanding of the different states of inflammation is important when considering an anti-inflammatory drug.

While unpleasant, inflammation plays a vital biological role, signalling to the organism that an injury or infection has occurred. These two categories of inflammation are referred to as sterile or non-sterile, respectively. In signalling this state to the organism,

measures can then be taken to allow the injury to heal, such as discontinuing activity of the inflamed area or limiting exposure to pathogens [19]. Typically, this type of inflammation is referred to as acute inflammation as it is short in duration and the tissues return to a normal state once the damage has been repaired. While the whole cascade of inflammation is engaged in acute inflammation, the action of eicosanoids, both PGs and LTs, are most commonly associated with this state [20]. Acute inflammation is not considered a disease state, but many drugs are available to relieve pain and discomfort associated with this form of inflammation. The key drug class used for this type of treatment are the Non-Steroidal Anti-Inflammatory Drugs (NSAIDs), which function primarily through the inhibition of COX enzymes to reduce expression of pro-inflammatory eicosanoids, and hence reduce inflammation [21, 22].

When inflammation persists for a long period of time, typically from months to years, the state is recognised as chronic inflammation and considered a disease state [23]. The same acute effects of inflammation may still be observed, but it is considered a more serious state as the persistent symptoms can become debilitating to the point of immobility or even depression [24, 25]. The causes of chronic inflammation can be straightforward, such as the result of a sustained serious injury, or more complex, such as the cases of rheumatoid arthritis or psoriasis. In the prior examples, the cause of inflammation is associated with a specific injury and the chronic nature of the inflammation may be directly tied to the time it takes for such an injury to heal. The latter examples, however, are the result of biochemical pathways causing an increase in pro-inflammatory cytokines resulting in a self-sustaining inflammatory cycle, referred to as autoimmune diseases (or disorders) [26]. Due to the varying causes and mechanisms underpinning chronic inflammation, treatments vary significantly, but corticosteroids and newer biological agents are commonly used in the treatment of many chronic inflammatory conditions [27].

As has been described thus far, the symptoms of inflammation are dependent on the actions of biochemical pathways with symptoms ultimately being controlled by the actions of eicosanoids. The treatment of inflammation is therefore typically related either directly or indirectly to reducing expression of these eicosanoids. The inflammatory cascade refers to

the biochemical pathways that facilitate the inflammatory response [28]. The central cell type associated with the inflammatory response is the macrophage, which initiates the release of numerous pro-inflammatory factors which propagate the inflammatory response [29]. These factors can be divided into upstream and downstream factors where downstream refers to the effectors of inflammation and upstream refers to the messengers that initiate release of the effectors.

1.2.3. Eicosanoids

The key downstream pro-inflammatory factors are eicosanoids, including prostaglandins (PGs) and leukotrienes (LTs) [30]. Of these two compound classes, PGs, particularly PGE_2, are most closely associated with the classical symptoms of inflammation [31], while LTs, particularly LTD_4, are most closely associated with specific inflammatory conditions such as asthma [32]. All eicosanoids are biosynthesised from arachidonic acid by a number of different enzymes, which will be briefly discussed. Given the distinct structures of PGs and LTs from arachidonic acid (see Figure 1.3), it is unsurprising that there are numerous steps in the biosynthesis of these compounds.

The synthesis of PGE_2 from arachidonic acid involves two key enzymes, COX-2 to produce PGH_2 from arachidonic acid, and PGE synthase to convert PGH_2 to PGE_2. The synthesis of LTD_4 involves two key enzymes, lipoxygenase (LOX) to produce arachidonic acid 5-hydroperoxide (5-HPETE) from arachidonic acid, and glutathione-S-transferase (GST) to convert HPETE, through a series of steps to LTD_4.

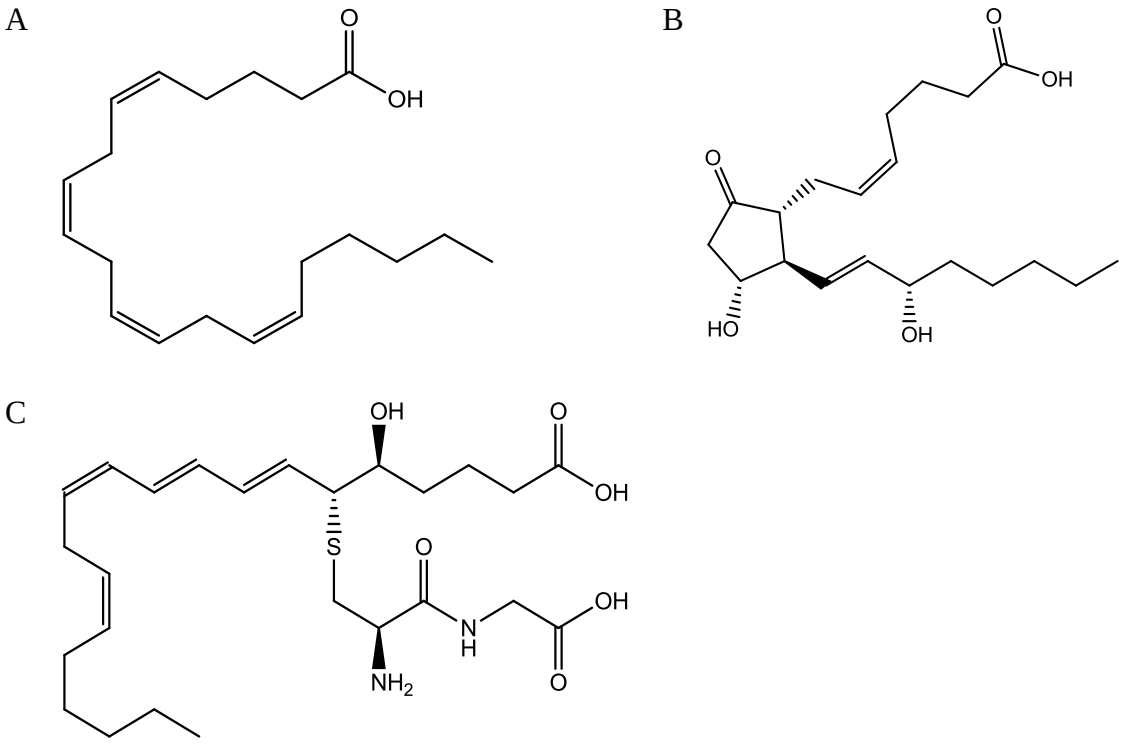

Figure 1.3: Structures of (A) arachidonic acid, (B) prostaglandin E_2, (C) leukotriene D_4.

The pro-inflammatory actions of PGE_2 are mediated by the type E prostanoid receptor family consisting of four subtypes (EP1, 2, 3 and 4). The varied symptoms of inflammation i.e. pain, redness, oedema and heat, are mediated by the actions of PGE_2 binding to specific EP receptors [33]. Briefly, activation of EP1 has been demonstrated to be coupled to an increase in intracellular Ca^{2+}, which increases pain perception through increased action potential signalling (discussed further in Section 1.3.3) [34]. Activation of EP2 is associated with the production of cAMP and innate immune responses including production of pro-inflammatory cytokines (discussed further in Sections 1.2.4-1.2.6) [35]. EP3 is associated with oedema and cellular infiltration, which facilitates the migration of various inflammatory cells into the vasculature and a "spreading" of the inflammatory response. EP4 has been demonstrated to regulate the stability of COX-2 mRNA and to be associated with immune responses in the skin, including redness [36]. Each of these receptors have been primarily characterised through animal models via the use of knock-out mice deficient in each receptor subtype, as well as the use of EP-specific agonists and antagonists [33]. Accordingly, the full human contribution of EP receptors may not be

completely understood, however their pro-inflammatory functions are well accepted and thus PGE_2 is rightly regarded as a significant mediator of inflammation.

For clinical applications, synthesis of PGE_2 (summarised in Figure 1.4) is typically inhibited at the stage of PGH_2 synthesis from arachidonic acid. This involves inhibition of COX enzymes which are the target of a number of marketed anti-inflammatory drugs including naproxen and diclofenac [37, 38]. Historically, inhibition of COX enzymes has been an effective method of treating inflammation, hence the longevity of the NSAID drug class, but it has not been without its issues, primarily involving gastric ulceration [39]. The cause of this ulceration is thought to be primarily due to inhibition of COX-1, which was determined to play a gastroprotective role rather than a significant anti-inflammatory role, and the non-selective nature of most typical NSAIDs in the inhibition of COX isoforms [40]. To this end, a series of COX-2 selective inhibitors were developed including celecoxib and rofecoxib which possessed a more favourable gastric safety profile, but were accompanied with adverse cardiovascular side effects which ultimately led to the retraction of rofecoxib from the market [37].

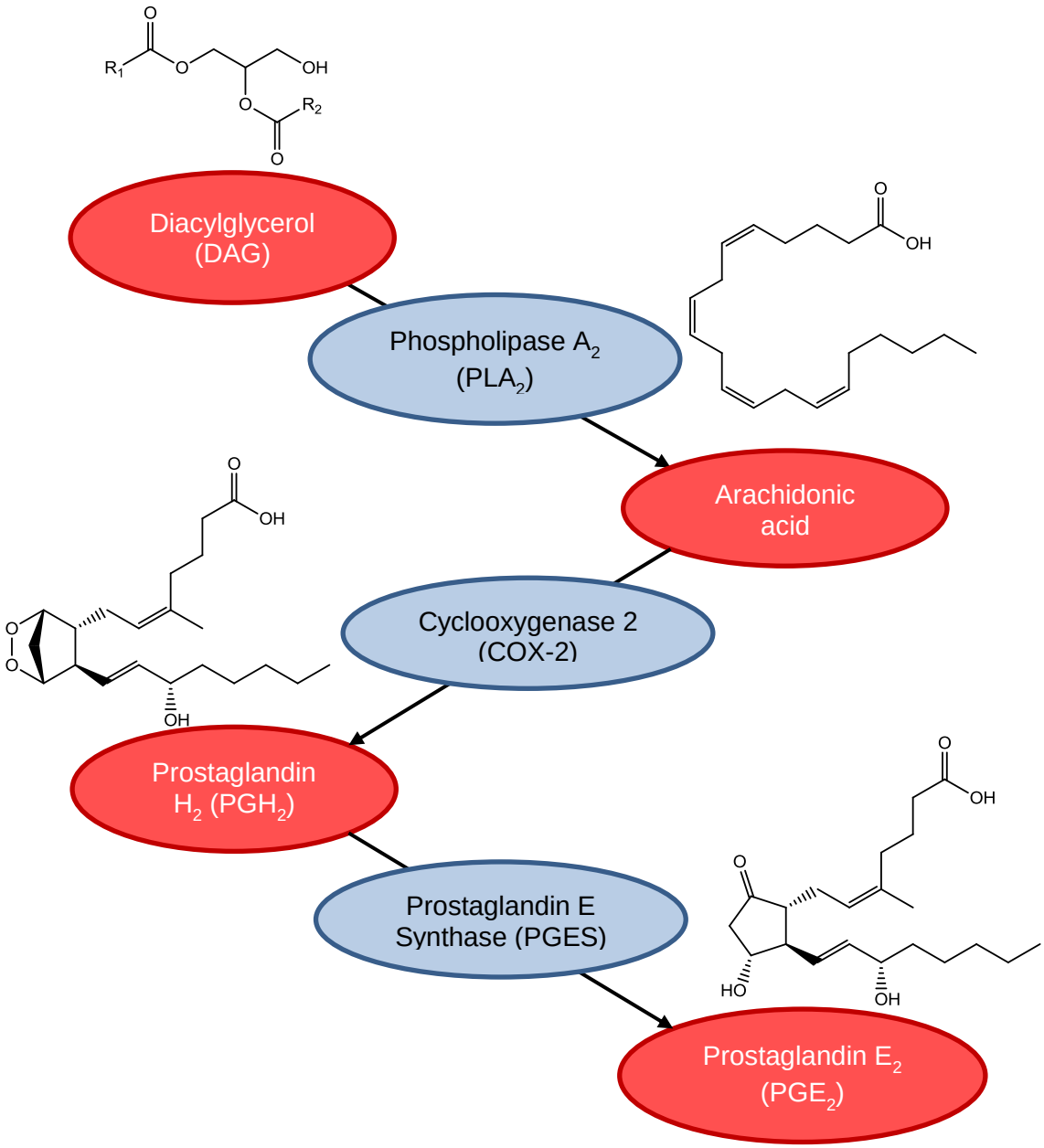

Figure 1.4: Production pathway of inflammatory prostaglandin PGE_2.

Beyond COX inhibition, inhibitors of both phospholipase A_2 (PLA_2) and prostaglandin E synthase (PGES) have been investigated for their anti-inflammatory potential. The rationale for each target is linked to COX inhibition in that they are involved in the synthesis of PGE_2 either indirectly through suppression of arachidonic acid by PLA_2 or indirectly through PGE_2 suppression of PGES [41, 42]. While these targets have been known for decades, little has been achieved in drug discovery. Multiple chemical scaffolds have been identified to inhibit PGES, but no commercial products have as yet emerged [43],

and development in PLA_2 inhibition is mostly confined to herbal supplement compounds and chemical probe molecules with minimal clinical potential [44, 45].

While PGE_2 is a primary agent involved in downstream inflammation, the upstream regulation of inflammation, by contrast, is a more complex web of protein agents, referred to as cytokines. There are a multitude of different cytokines involved in inflammatory processes, fulfilling roles that may be described as both pro- and anti-inflammatory. An exhaustive description of the network of inflammatory cytokines and their interactions is beyond the scope of this thesis, therefore this overview will focus on the three pro-inflammatory cytokines known to be modulated by PAA: IL-1β, IL-6 and TNFα. This is justifiable as these three cytokines are widely considered to be the primary pro-inflammatory cytokines in most inflammatory states [46, 47]. The specific functions of these cytokines are varied, but the common role of each cytokine is in intra- or extracellular signalling to further propagate the inflammatory cascade and promote the inflammatory process.

1.2.4. Interleukin-1β (IL-1β)

Of the IL-1 family, IL-1β is the most well categorised member, and a key pro-inflammatory cytokine. IL-1β is constitutively expressed by most cell types, but its overexpression is strongly associated with macrophages and especially with inflammatory processes. During inflammation, an inactive form of IL-1β (pro-IL-1β) is converted into its active form via cleavage by caspase-1, a cysteine protease enzyme [48]. Additionally, caspase-1 is involved in pyroptosis, an inflammation specific form of cell necrosis largely responsible for the release of IL-1β from macrophages [49]. Once produced and secreted, IL-1β can perform several tissue or cell specific functions but most relevant to the process of inflammation is the ability to induce expression of the COX-2 enzyme through activation of nuclear factor kappa B (NF-κB). As a result of COX-2 upregulation the production of pro-inflammatory prostaglandins, especially PGH_2 and PGE_2, is increased and thus the inflammatory process becomes promoted [50].

The signal cascade of IL-1β is depicted in Figure 1.5, and involves activation of the IL-1 receptor (IL-1R), by IL-1β and signal transduction by the intermediaries: TNF receptor

associated factor 6 (TRAF6), transforming growth factor-β-activated kinase (TAK) and its binding factor (TAB) and inhibitor of κB kinase (IKK) through to the nuclear factor κB complex (NF-κB). NF-κB is a heterodimer consisting of subunits, most commonly p65 (or RelA) and p50, but also potentially involving p52, RelB and c-Rel. Once the heterodimer is recruited by IκBα (nuclear factor of kappa light polypeptide gene enhancer in B-cells inhibitor, alpha), the IκBα unit is degraded, releasing the NF-κB heterodimer to be transported into the cell nucleus. Once the complex reaches the nucleus it binds with DNA at a given promoter region to produce mRNA which then goes on to be translated into proteins including COX-2 and inducible nitric oxide synthase (iNOS, discussed below), amplifying the inflammatory response [51, 52]. It is by this eventual production of pro-inflammatory proteins that IL-1β exerts its pro-inflammatory signalling actions.

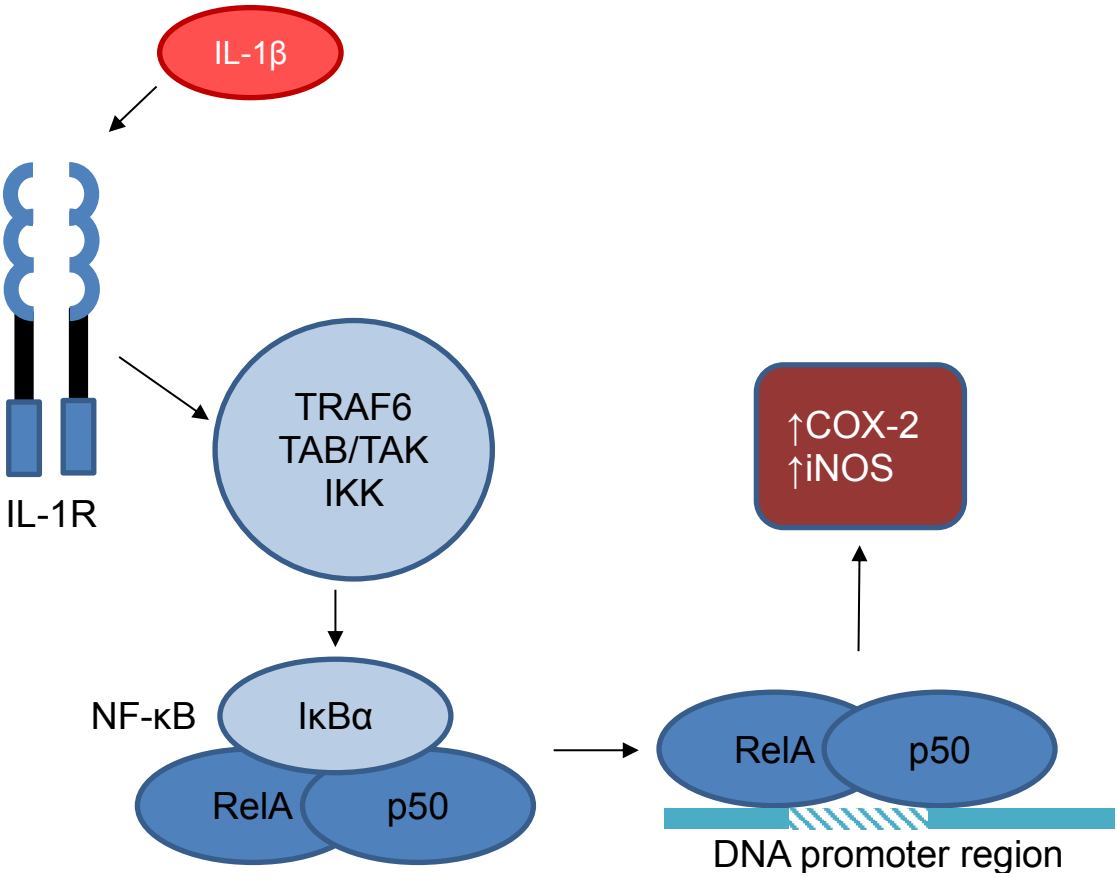

Figure 1.5: Condensed transduction cascade of IL-1β. *The figure condenses the transduction pathway between TRAF6, TAB/TAK and IKK to highlight the interaction between IL-1β and NF-κB. This figure has been adapted from Turner et al. [47].*

1.2.5. Tumor necrosis factor alpha (TNFα)

Like IL-1β, TNFα is a constitutively expressed protein and is responsible for several essential processes including apoptosis (programmed cell death) and inflammatory signalling. Increased concentrations of TNFα are strongly associated with a variety of inflammatory conditions, both acute and chronic, and inhibition of TNFα action or production has been proposed as a method of combating the development of numerous conditions including atherosclerosis and type 2 diabetes [53]. The actions of TNFα are primarily mediated by two distinct forms of the TNFα receptor, namely TNFα receptor 1 and 2 (TNF-R1 and TNF-R2), but TNF-R2 is more closely associated with inflammatory responses [54]. Once activated by TNFα, TNF-R2 follows a similar, but distinct, cascade to IL-1β via the activation of NF-κB through TRAF2, receptor interacting protein (RIP), IKK and regulatory subunit IKK-γ (NEMO). This signal transduction pathway is represented in Figure 1.6. While the activation of NF-κB by the TNFα pathway is distinct from IL-1β, the outcomes of NF-κB activation, namely increased expression of COX-2 and iNOS, are the same. Outside of interactions with TNF-R2, TNFα has also been reported to stimulate members of the protein kinase C (PKC) family.

The PKC family consists of at least 12 isozymes and associated signal transduction cascades for numerous important cell functions, including promotion of the inflammatory process [55]. This pro-inflammatory role is achieved through stimulation of a number of isozymes including PKCα, PKCδ and PKCγ which promote upregulation of pro-inflammatory genes and cytokines including COX-2 and IL-1β [56, 57].

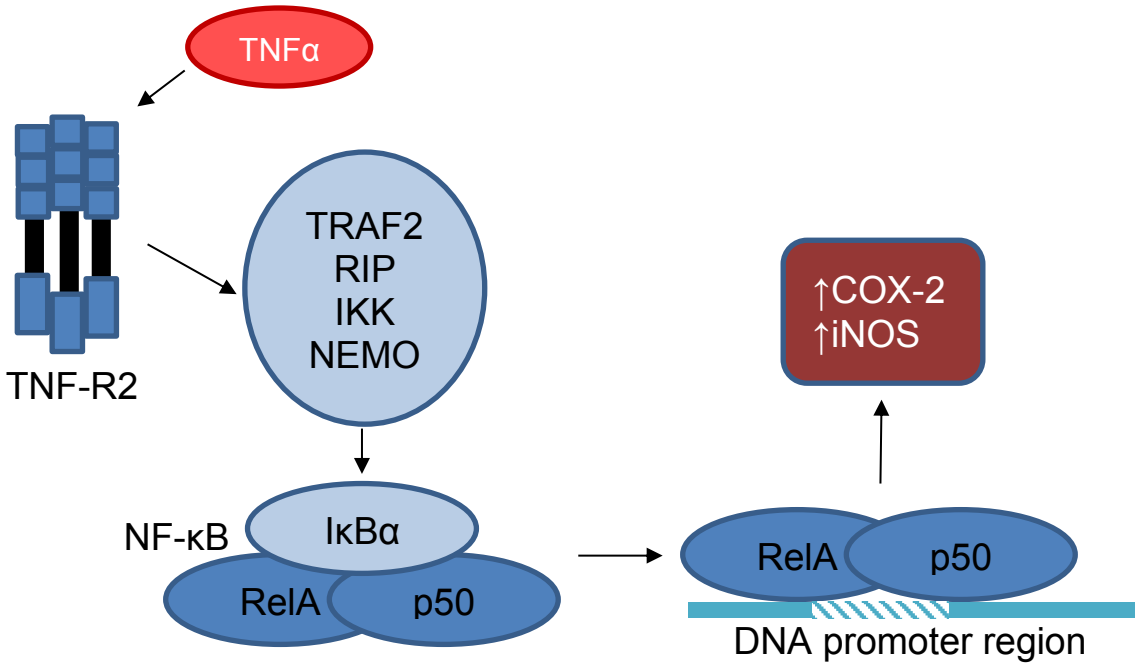

Figure 1.6: Condensed transduction cascade of TNFα. *The figure condenses the transduction pathway between TRAF2, RIP, IKK and NEMO to highlight the interaction between TNFα and NF-κB. This figure has been adapted from Turner et al. [47].*

1.2.6. Interleukin-6 (IL-6)

IL-6 is the most distinct of the three primary inflammatory cytokines as it exhibits its pro-inflammatory activity by upregulating production of pro-inflammatory cytokines, as well as prolonging the duration of the inflammatory state [58, 59]. This inflammatory activity is achieved through recruitment of Janus kinase (JAK) to the IL-6 receptor (IL-6R). Upon recruitment of JAK, a homodimer is formed from signal transducers and activators of transcription 3 (STAT3), which like the NF-κB complex enters the nucleus to promote transcription of genes of inflammatory proteins [60, 61]. This interaction is depicted in Figure 1.7.

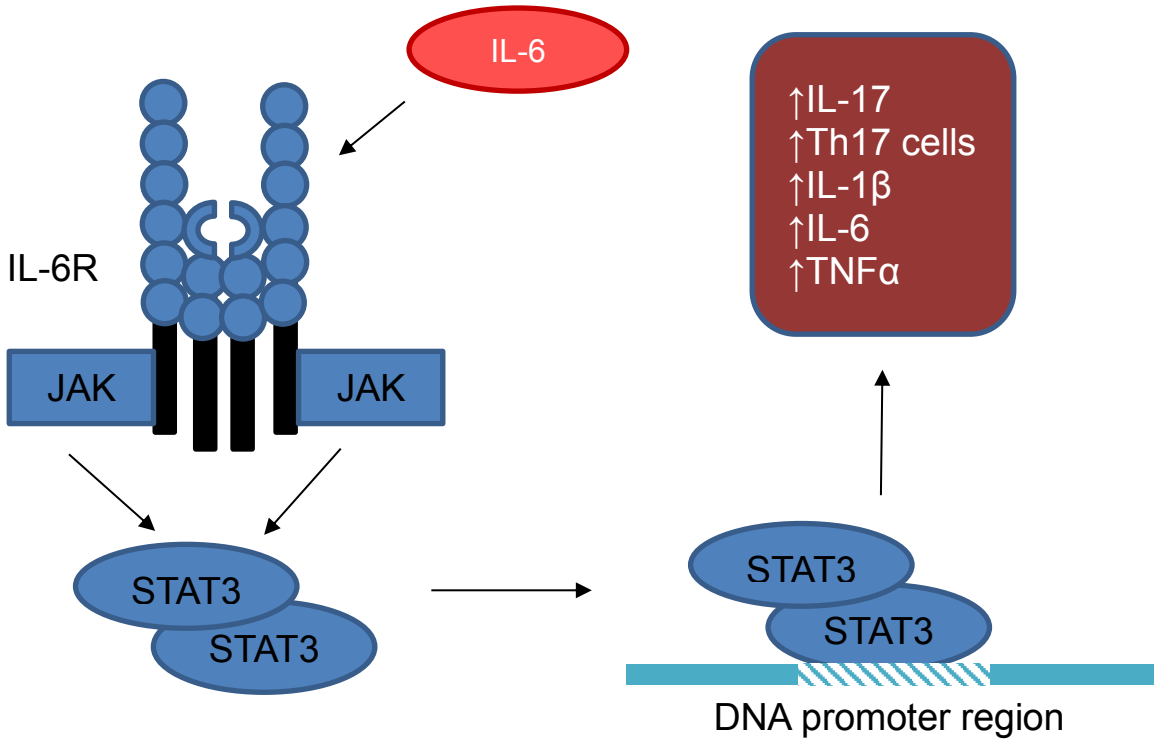

Figure 1.7: Signal transduction pathway of IL-6. *This figure has been adapted from Turner et al. [47].*

After activation, STAT3 upregulates the production of another interleukin, IL-17 which goes on to facilitate production of T helper 17 (Th17) cells, which in turn facilitate production of pro-inflammatory cytokines IL-1β, TNFα and IL-6 [62]. This enhanced production of IL-6, facilitated by activation of IL-6 is suggestive of a positive feedback loop. Additionally, IL-6 is understood to bind to the epidermal growth factor (EGF) receptor, which has been demonstrated to facilitate reactivation of STAT3, and hence to further prolong IL-6 activation, and therefore the duration of the inflammatory state [63].

1.2.7. Nitric oxide (NO)

As has been mentioned previously, the NF-κB pathway is involved in upregulation of the expression of iNOS, which produces the important pro-inflammatory chemical mediator nitric oxide (NO) [64, 65]. Produced by many types of cells including macrophages and neutrophils, NO is synthesised from L-arginine by a dimer of iNOS proteins and is a precursor to reactive nitrogen oxygen species (RNOS). This pathway is summarised in

Figure 1.8. Distinct from cytokines and eicosanoids, NO has no specific receptor target and instead exerts its effects via its role as a concentration dependent neurotransmitter [66]. At high concentrations NO is oxidised to RNOS, which goes on to activate several proteins including NF-κB, which leads to pro-inflammatory outcomes, as well as a feedback loop resulting in further production of NO [66, 67]. Furthermore, NO has been demonstrated to upregulate COX mRNA (both COX-1 and COX-2), which suggests that higher concentrations of NO lead to higher production of inflammatory PGs and therefore an enhanced inflammatory response [68].

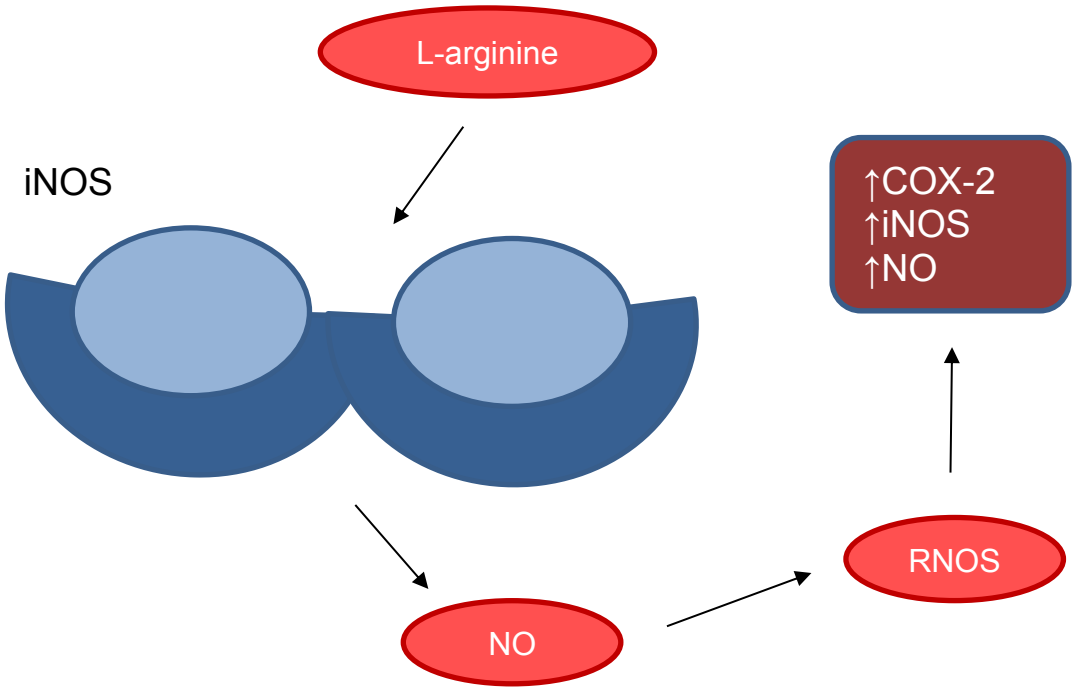

Figure 1.8: Production pathway of RNOS from L-arginine.

1.2.8. Glucocorticoid receptor

The glucocorticoid receptor system is often categorised as an anti-inflammatory protein due to its association with numerous inflammatory disease states (asthma, chronic obstructive pulmonary disease, rheumatoid arthritis) and pro-inflammatory cytokines (IL-1β, TNFα, IL-6) [69]. When a glucocorticoid agonist is bound to the cytoplasmic receptor, the glucocorticoid receptor becomes activated and is transported into the cell

nucleus where it binds to DNA at a specific promoter region and facilitates the transcription of genes, and therefore proteins, as summarised in Figure 1.9.

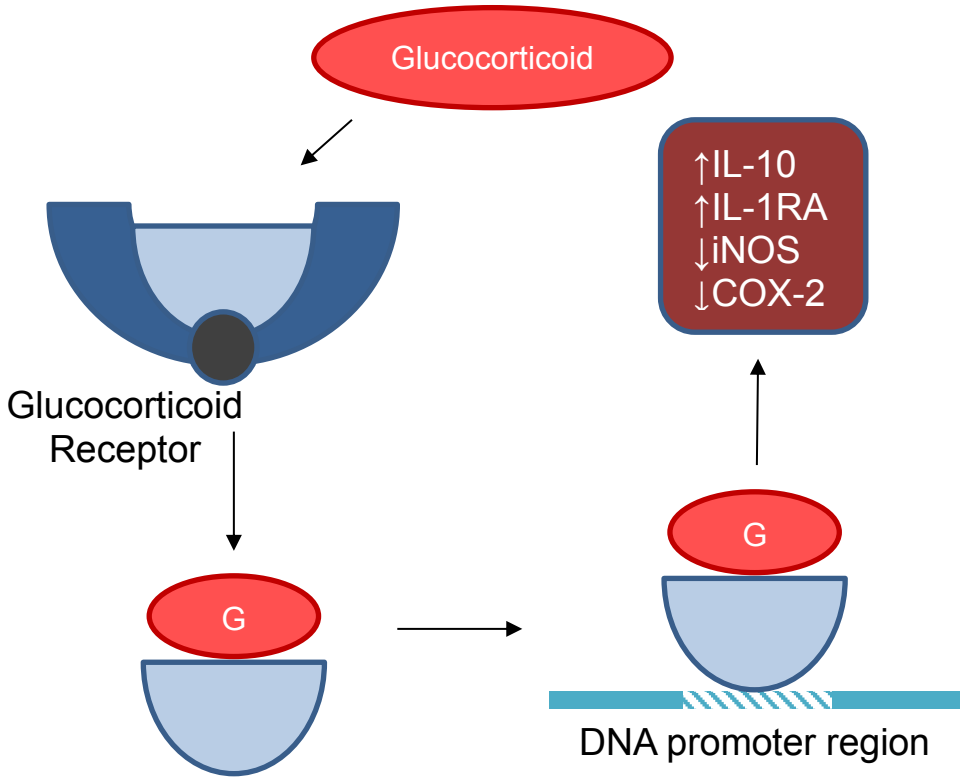

Figure 1.9: Signal transduction pathway of the glucocorticoid receptor.

The role of the glucocorticoid receptor is distinct from many other members of the inflammatory cascade, as it is neither involved in the production of pro-inflammatory cytokines, nor signalling to proteins, but instead exerts its effect via an inhibitory role [70, 71]. The inhibitory role of the glucocorticoid receptor is largely characterised by two interactions: the upregulation of anti-inflammatory cytokines IL-10 and IL-1 receptor antagonist (IL-1RA) and the inhibition of transcription factors including NF-κB and STAT3. Therefore, as a result of activation of the glucocorticoid receptor, the expression of pro-inflammatory cytokines (through NF-κB inhibition), eicosanoids (through COX-2 downregulation) and ROS (through iNOS downregulation) are all reduced and hence inflammation is reduced.

1.2.9. Summary of PAA and inflammation

As was previously highlighted, PAA has been demonstrated to significantly inhibit the symptoms of inflammation in a mouse ear oedema model, as well as decreasing the secretion of IL-1β, IL-6 and TNFα in cell lines. These findings indicate that PAA likely exhibits anti-inflammatory activity via interaction with an enzyme or protein complex target, or possibly multiple targets, involved in the production or secretion of these cytokines. Several enzymes and receptors related to these cytokines have been discussed thus far and what follows in Chapter 3 of the thesis focuses on a study of the potential interactions between PAA and four targets: caspase-1, for its role in IL-1β production and release; NF-κB, for its numerous roles in signalling and inflammatory gene production; PKC, for its roles in TNFα signalling and IL-1β production and the glucocorticoid receptor, for its association with NF-κB inhibition. Thus, one aim of this PhD study was to investigate these targets by *in silico* and *in vitro* means to determine the molecular target of PAA to further the understanding of the actions of the molecule.

1.3. Pain, analgesia and opioid receptors

1.3.1. Background of PAB and pain

As mentioned in Section 1.2.2, one of the primary symptoms of inflammation is pain. Treating inflammation is often associated with alleviation of pain, but there are also therapeutic pathways solely for the treatment of pain. In a previous honours study (conducted by this author) at the University of South Australia it was demonstrated through *in silico* investigations that *D. polyandra* compounds, particularly PAB, bore a strong structural resemblance to a series of novel opioid agonists [2] as further discussed below. As opioid receptors are traditionally associated with relief from serious pain, this finding led to a hypothesis that some part of the pain relief associated with the traditional use of *D. polyandra* may be attributable to actions of PAB at opioid receptors. This hypothesis was tested via *in vitro* screening of the μ- and κ-receptors but ultimately, no binding activity of PAB was observed at the opioid receptors. As such it was concluded that the pain relief associated with PAB was likely to be linked to its anti-inflammatory activity, or other pain pathways, rather than any opioid receptor modulation. Subsequently, a further hypothesis was suggested that structural analogues of PAB may have the capability of opioid receptor activity. The following sections present an overview of the biology of pain, an introduction to opioid receptors, and their agonists, and their relation to pain.

1.3.2. Characterisation of pain

Pain, both in conjunction with and distinct from inflammation, is an important biological process. Much like inflammation, a key role of pain in an organism is to communicate injury to the organism to promote relaxation of the injured tissue and facilitate healing. Pain is often characterised by the nature of its stimuli. ‘Minor pain’ is one such distinction, which occurs as the result of minor injury such as skin abrasion or stimulation of the ulnar nerve, colloquially referred to as the “funny bone”. Such pain is typically short lived, and the tissue is expected to return to a healthy state within minutes to hours of injury. A further distinction is ‘serious pain’ which is caused by more serious injuries such as bone

breakages or severe tissue damage. The strength of such pain is heightened in comparison to minor pains and can result in a pain state that may last from days to weeks, or even months, without significant relief. Both minor and serious pain can be considered as forms of acute pain where, as for inflammation, an injury is sustained and followed by healing. However, also like inflammation, a chronic state of pain may exist where pain is experienced seemingly in the absence of a stimulus. Such 'chronic pain' is most often experienced in tissues or joints that have previously experienced injury, but may also occur for seemingly no reason at all.

1.3.3. Action potentials and transmission of pain

Regardless of the type or severity of pain, however, the mechanism of pain is universal. In many ways also, the mechanism of pain is simpler than the mechanisms of inflammation, as while inflammation involves a large number of chemical mediators and receptors, at a biochemical level pain is mostly associated with two types of molecules: ions such as sodium (Na^+), potassium (K^+) and calcium (Ca^{2+}), which propagate signals along a nerve cell (depicted in Figure 1.10), and cyclic adenosine monophosphate (cAMP), which serves to propagate signals between nerve cells.

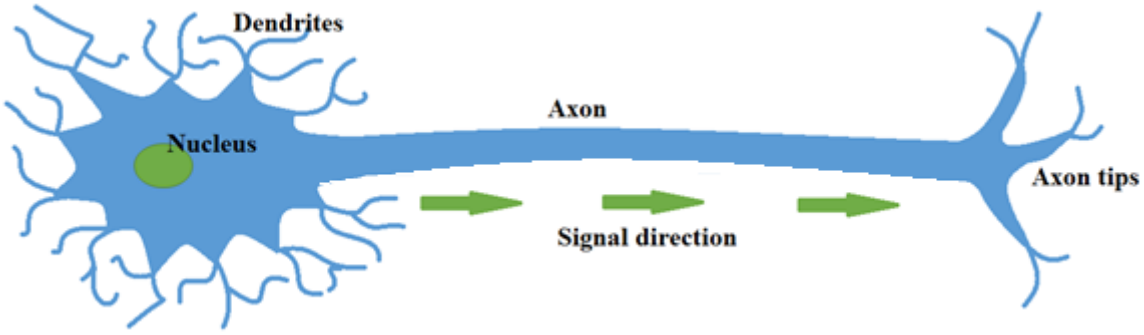

Figure 1.10: Structure of a nerve cell. *Signals are received by dendrites at the cell body and are transmitted along the axon towards the axon tips where the signal is carried to the next nerve cell.*

The mechanism of pain involves a stimulus to a tissue, such as an injury or disease state, which initiates a signalling cascade through sensory neurons, via action potentials, towards the cerebral cortex of the brain, which interprets the signal as pain. An action potential is the term given to the biochemical mechanism behind a nerve impulse. This nerve impulse is caused by neurotransmitter activated depolarisation of a neuron by Na^+ ion influx, followed by K^+ ion efflux to return the voltage to normal. This influx/efflux is a localised event that propagates in one direction along a neuron, until it reaches the terminal end of the cell [72]. Once the signal has reached the end of the cell, voltage-gated calcium channels (VGCCs) are opened, facilitating influx of Ca^{2+}, and adenylate cyclase is activated to produce cAMP [73, 74]. Both cAMP and Ca^{2+} then function to facilitate the release of neurotransmitters via vesicle formation and transport to the edge of the neuron, where the neurotransmitters are released to nearby neurons and the process repeats until the signal reaches the cerebral cortex [75].

1.3.4. Treatment of pain or analgesia

Pain management is typically controlled by three primary drug classes: NSAIDs and paracetamol (acetaminophen) for minor pain and opioids for more serious pain. NSAIDs have been previously mentioned for their anti-inflammatory actions, but in some cases they may be used exclusively for pain management. Largely this pain relief, or anti-nociception, is thought to be attributable to the anti-inflammatory actions of the drugs and as such NSAIDs are often recommended to treat pain associated with inflammatory injuries such as muscle or joint strain [76].

Paracetamol is an example of an anti-nociceptive (analgesic) drug widely used for pain management that is not traditionally associated with anti-inflammatory actions. For decades the mechanism of action of paracetamol was unclear, as it was found to be a useful analgesic drug in the central nervous system (CNS) but not in the peripheral nervous system (PNS). Paracetamol has since been determined to be a COX-2 selective inhibitor, but it was discovered that the presence of epoxides or other reactive oxygen species (ROS), such as in inflamed tissues, prevent this COX-2 inhibitory activity. Epoxides and ROS are found in

higher concentrations in the periphery than in the CNS, so this may explain why paracetamol exhibits systemic analgesia, without associated anti-inflammatory properties [77]. This inhibition of action in inflammatory states explains why anti-inflammatory activity is not associated with the drug [78]. As such, paracetamol is often associated with NSAID drugs, but is not classified as one.

Furthermore, some degree of pain management of paracetamol is thought to be attributed to an active metabolite, AM404, which functions as a modulator of cannabinoid activity by inhibition of anandamide uptake [79]. This modulation of the cannabinoid system results in reduced activation of pain receptors and, as such, reduced transmission of action potentials [80]. While the use of NSAIDs and paracetamol are considered as highly effective for the treatment of minor pain, they are considered ineffective in serious injuries and a stronger class of drugs, the opioids, are required for treatment of such ailments.

Opioids are a diverse class of drugs primarily associated with anti-nociceptive activity. The opioid class takes its name from the opium poppy (*Papaver somniferum*), the sap of which has had historical use as a natural analgesic medicine [81]. While the primary role of opioid drugs is analgesia, off target effects associated with euphoria, and a tendency towards drug addiction pathways, have led opioid drugs to be an abused class of drugs [82]. Numerous natural, synthetic and semi-synthetic variants of opioid molecules have since been developed, but the common feature of all opioid molecules is the modulation of opioid receptors.

1.3.5. Opioid receptors

Opioid receptors are a subfamily of G-protein coupled receptors (GPCRs) which are expressed widely throughout the CNS and PNS [83]. To date, four subtypes of opioid have been discovered: mu (μ), kappa (κ), delta (δ) and nociceptin or orphanin (NOP), with several other receptors, including zeta (ζ) and sigma (σ), being closely related but not necessarily classified as opioid receptors. The specific roles of each receptor are the subject of continued

research and scrutiny, but the general consensus is that the majority of anti-nociceptive activity is attributable to the actions of the μ, κ and δ receptors while the NOP receptor is associated with CNS effects including anxiety and depression [84, 85]. A further distinction among the three analgesic receptors are apparent euphoria associated with μ-receptors, dysphoria with κ-receptors and anti-depressant activity with δ-receptors [86, 87]. As euphoria is a useful side effect when treating serious pain, the μ-receptor is the most widespread clinically targeted opioid receptor, but each receptor is the subject of drug development for their own unique purposes.

Structurally, as GPCRs, the opioid receptors consist of seven α-helical domains around a central ligand-binding pocket. Until relatively recently, most structural information of opioid receptors was determined by inference, such as the development of homology models based on other characterised GPCRs, or by site directed mutagenesis (SDM) studies [88-90]. This approach has since been superseded as crystal structures of the four canonical opioid receptors have been determined and published for the first time [91-94]. These crystal structures have provided numerous structural insights into the receptors including important ligand binding residues, the structure of the binding pockets and water-ligand-protein binding interactions. Additionally, spatial analysis of all four crystal structures revealed the NOP receptor to be the most dissimilar, while the μ, κ and δ receptors bore strong spatial similarities, which may form a basis to explain why NOP is not associated with analgesia while the other three receptors are [95].

The anti-nociceptive functions of the μ, κ and δ receptors are largely similar and rely on interaction with two events in neuron signalling. The first of these events is related to neuron signalling through action potential transmission. Activation of an opioid receptor results in the inactivation of calcium channels and the activation of potassium channels. As was previously discussed, a key step of the action potential cycle is the opening of calcium channels to facilitate an influx of Ca^{2+} ions, leading to adenylate cyclase activation and neurotransmitter release. Therefore, inactivation of calcium channels prevents the propagation of nerve transmission and prevents pain signals from being received and

interpreted by the brain. Activation of potassium channels also contributes to this end by facilitating an influx of K^+ ions and "dampening" action potentials.

The second anti-nociceptive action of opioid receptors is specifically related to adenylate cyclase. As GPCRs, all opioid receptors are paired to adenylate cyclase. The activation of opioid receptors results in direct inhibitive activity against adenylate cyclase, and hence leads to decreased production of cAMP and decreased neurotransmitter signalling, further preventing propagation of nerve transmission [85]. Owing to these combined effects, the opioid receptors have strong anti-nociceptive effects and hence modulators of opioid receptors are widely used as analgesic drugs.

1.3.6. Opioid agonists

As previously mentioned, the origin of the opioid class is the sap, or latex, of *P. somniferum*, of which the primary active constituent is morphine. Morphine (see Figure 1.11) is widely considered as an archetypal opioid drug associated with strong analgesic activity through modulation of the opioid receptors, primarily the μ-receptor subtype [96]. In structural terms, most opioids, whether natural, synthetic or semi-synthetic, contain a simple pharmacophore, or reduced structural scaffold, that governs the opioid binding of the molecule. This pharmacophore is shown in Figure 1.11 and consists of an aromatic ring bound to a basic nitrogen by a three-carbon linker. Modifications to this scaffold can result in different opioid subtype affinities, for example μ- vs κ-selectivity, but the root scaffold is conserved in almost all opioid ligands. A noteworthy exception to this scaffold is the naturally occurring hallucinogen salvinorin A (shown in Figure 1.11).

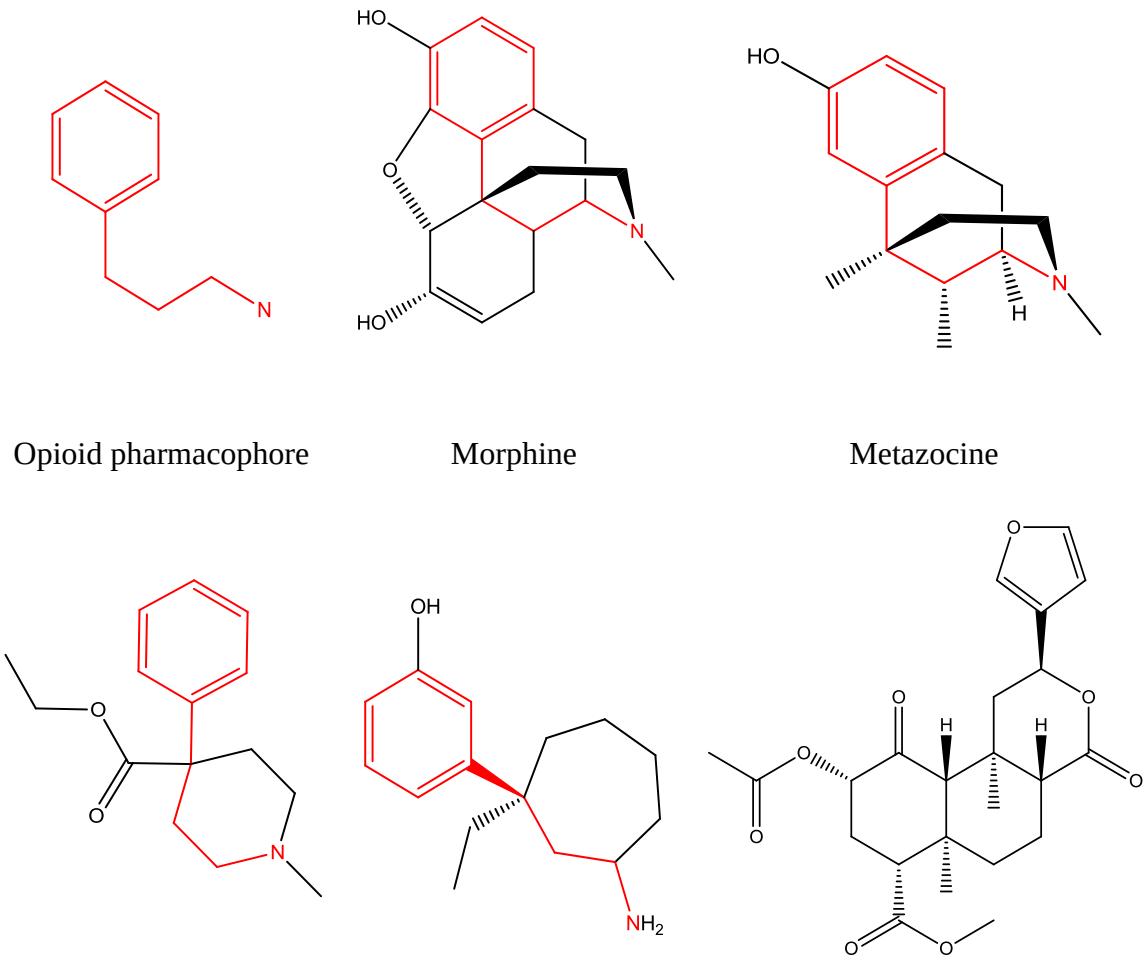

Opioid pharmacophore | Morphine | Metazocine

Pethidine | Meptazinol | Salvinorin A

Figure 1.11: Structures of opioid agonists. *The general opioid pharmacophore has been highlighted in red in all applicable structures.*

Salvinorin A, like PAA and PAB, is a clerodane diterpenoid and the primary active constituent of the Mexican psychotropic plant *Salvia divinorum* (Lamiaceae), from which it takes its name. Salvinorin A is atypical among opioids as it is primarily associated with psychotropic effects rather than analgesia, although analgesia has also been observed [97, 98]. The pharmacological activity of salvinorin A is primarily attributable to modulation of the κ-opioid subtype, and is regarded as the most potent naturally occurring hallucinogen and κ-opioid agonist [99]. Also of special interest is that, in addition to salvinorin A deviating from the "traditional" opioid pharmacophore, it is, along with salvinorin analogues, the only non-alkaloidal scaffold of an opioid molecule that has been identified.

1.3.7. Summary of PAB and pain

A previous honours study (conducted by this author) examined the receptor pharmacology of a diterpenoid constituent of *D. polyandra*, polyandric acid B (PAB). In this earlier study, PAB was identified by *in silico* methods to bear a close structural resemblance to salvinorin A [2]. The approach of this study involved ligand-based methods to establish structural similarity of PAB to other opioid agonists, including salvinorin A. This approach involved the use of a hit retrieval technique, where a set of opioid agonists was incorporated into a structurally diverse chemical library and chemical similarity techniques were used to compare the database to PAB. Molecules being ranked higher in the database would indicate a stronger chemical similarity to opioid molecules. It was determined that PAB bore stronger structural similarity to opioid agonists when compared to non-opioid chemical classes and it followed that PAB may also be an opioid receptor agonist. Some of the analgesia associated with *D. polyandra* may have therefore been attributable to opioid receptor activation. An *in vitro* receptor screening assay was used to screen PAB against the μ and κ opioid receptors, but no significant binding activity was observed at any tested concentration. Retrospective analysis of the hypothesis led to a conclusion that a key structural difference between PAB and salvinorin A, a carboxylic acid in PAB and a methyl ester in salvinorin A, may explain the disparity between the *in silico* and *in vitro* results.

As such, a new hypothesis was formed around the prospect that while PAB, and by extension *D. polyandra* plant extracts, may not modulate opioid activity, a structural analogue of PAB may potentially yield a molecule with opioid modulating abilities. This may have significance to drug development goals as there may be regulatory concerns regarding an anti-inflammatory drug that is able to be converted into an opioid drug by simple chemical modification. Furthermore, at the time of the honours study, the crystal structures of the opioid receptors had not yet been published and as such a significant tool in the *in silico* toolkit was not able to be used. As such, in addition to reasons of therapeutic potential and regulation, there are academic reasons to further explore potential interactions between *D. polyandra* and opioid receptors, either through PAB, or through chemical analogues.

1.4. Metabolism of drugs

1.4.1. Function and biology of metabolism

Metabolism is the biological process by which chemicals undergo structural modification. The two primary functions of metabolic processes are to transform compounds obtained through diet or environment into useful endogenous compounds and to assist in the elimination of such chemicals.

The transformation function may be found in many plants and animals, where compounds with a variety of physicochemical and pharmacological properties may be produced. The elimination function of metabolism, while ubiquitous in organisms, is most commonly regarded and studied in humans. Elimination is the ability to transform foreign (xenobiotic) molecules into a form that can be more easily eliminated from the organism to minimise external influence on the organism. While some metabolic processes may function spontaneously from environmental conditions, including heat, pH or mechanical churning, a majority of metabolism is carried out via specific chemical reactions mediated by enzymes [100].

In humans, there are numerous families of enzymes of vital importance to the metabolism of xenobiotics. Among these enzyme families are the cytochrome P450s (CYP), UDP-glucuronosyl transferases (UGT), carboxylesterases (hCE), sulfotransferases (SULT) and glutathione-S-transferases (GST). The total metabolism of any given xenobiotic is typically attributable to several enzyme families and as such, numerous metabolites may be expected to be formed. Some enzyme families can metabolise a wide range of substrates and are considered of general importance to many drugs, whilst others are only capable of metabolising a relatively narrow range of substrates. This specificity is in part due to the number of isoform members of the greater enzyme superfamily and in part due to the mechanisms performed by that enzyme family.

1.4.2. Cytochrome p450 (CYP) enzymes

The CYP superfamily of human enzymes consists of 57 subtypes and is widely regarded as the most important class of drug metabolising enzymes [101]. The primary metabolic function of the CYP enzymes is the oxidation of a substrate, usually by attaching an alcohol functional group to a hydrophobic centre. They may also participate in the cleavage of small functional groups such as short chain ethers. Examples of CYP metabolism are shown in Figure 1.12. With many structural isoforms in the superfamily, it is unsurprising that CYPs are responsible for the metabolism of an extensive range of substrates. Estimates indicate that CYPs may play a biotransformative role in as high as 70-80% of clinically used drugs [102].

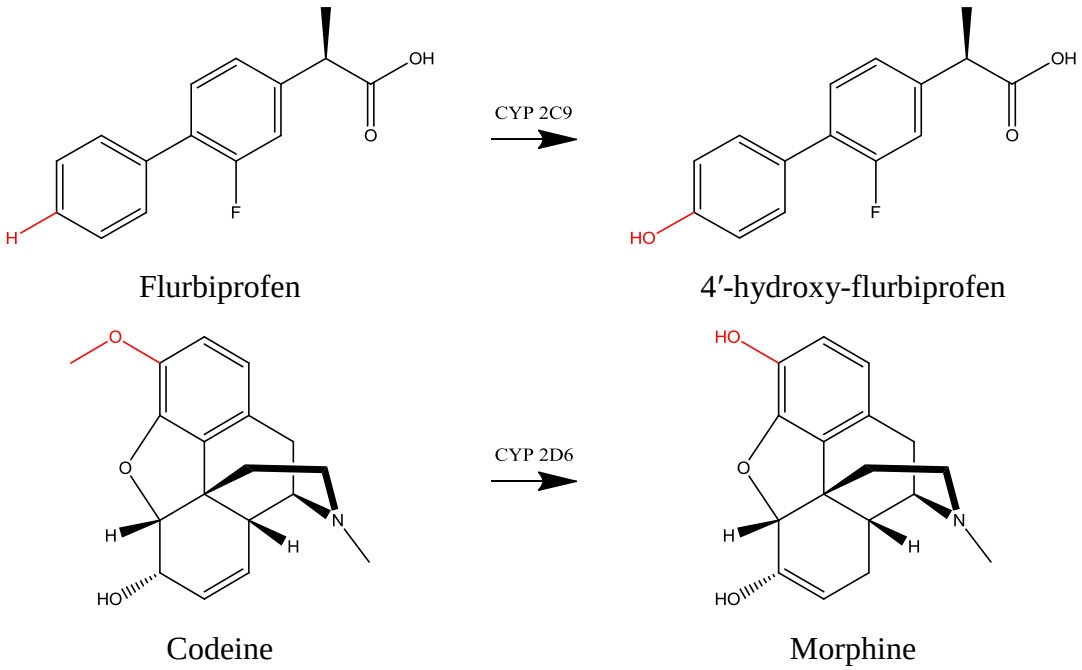

Figure 1.12: Examples of drug metabolites produced by CYP enzymes. *Sites of metabolism are highlighted in red with two separate forms of CYP metabolism depicted: hydroxylation and demethylation.*

1.4.3. UDP-glucuronosyltransferase (UGT) enzymes

The UGT superfamily of human enzymes consists of 22 proteins and follows the CYP family as the second most important class of drug metabolising enzymes [103]. The role of UGT enzymes is conjugative in nature, meaning their role is to attach a portion of a co-factor molecule to a substrate, typically to a hydroxyl, carboxylic acid or amine functional group. Examples of UGT glucuronidation in drug molecules are shown in Figure 1.13. The primary conjugate transferred by the UGT enzymes is glucuronic acid, which is transferred from UDP-glucuronic acid (UDPGA), but UGTs are also known to use other UDP-sugars such as UDP-glucose and UDP-xylose [104]. In transferring a highly polar head group such as glucuronic acid to a substrate molecule, the polarity of the resultant metabolite is increased relative to the substrate and accordingly, the substrate becomes more likely to be filtered through the kidneys and excreted. As UGTs are involved in the metabolism of a wide range of chemicals, UGT metabolism should be studied for new drug molecules containing appropriate functional groups.

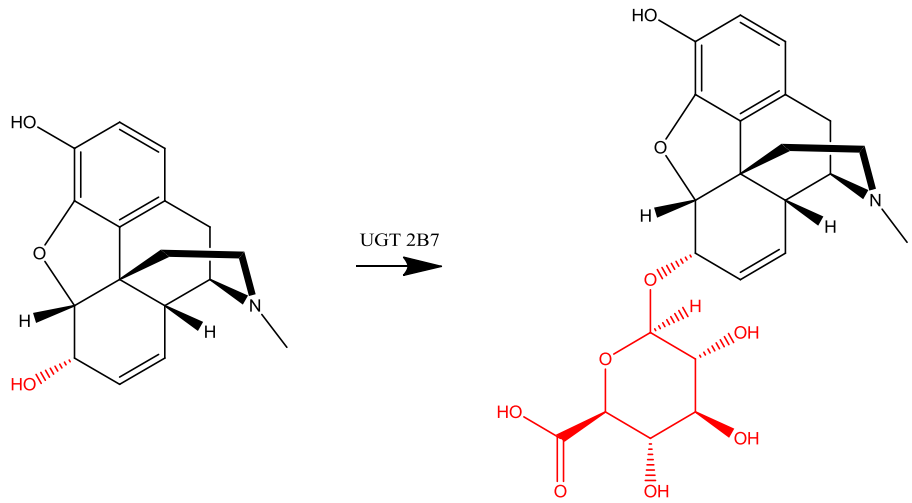

Morphine Morphine-6-glucuronide

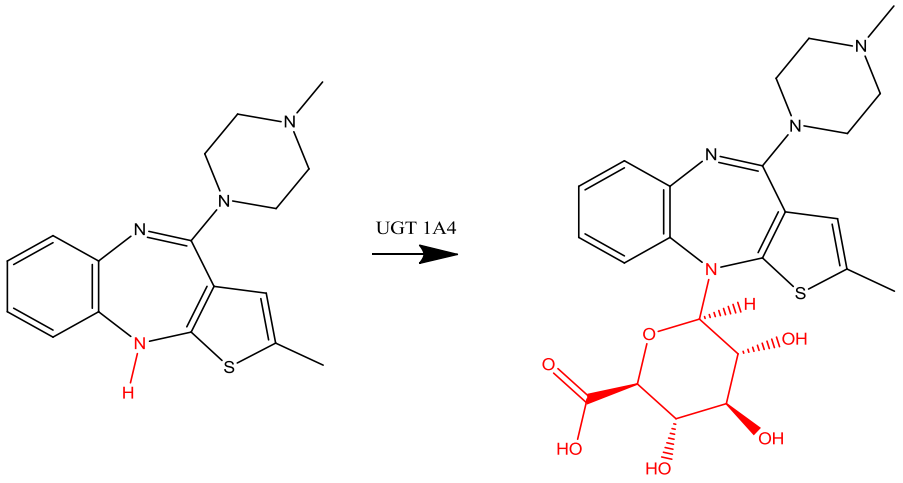

Olanzapine Olanzapine-N-glucuronide

Figure 1.13: Examples of drug metabolites produced by UGT enzymes. *Sites of metabolism are highlighted in red with two separate forms of UGT metabolism depicted: alcoholic (O) and amine (N) glucuronidation.*

1.4.4. Carboxylesterase (hCES) enzymes

The carboxylesterase family of human enzymes is a branch of the human esterase superfamily consisting of three primary isoforms; hCES1, hCES2 and hCES3 [105]. It fulfils a single specific but important metabolic function; the cleavage of ester functional groups to separate the component alcohol and carboxylic acid portions of the ester substrate [106]. This highly specific function tends to be quite efficient but limits the substrate specificity of the enzyme to substrates containing esters and certain ester-like functional groups such as

amides, thioesters and phosphates. Examples of esterase substrates are shown in Figure 1.14. In relation to xenobiotics, carboxylesterase metabolism often has the effect of deactivating the compound and assisting in the excretion of the compound, but in certain cases the opposite may occur and a previously inactive compound may be activated by the ester cleavage [107]. This process of molecular activation by esterases is commonly applied to molecules with desirable biological properties, but unfavourable solubility or pharmacokinetic properties. An example of a drug molecule undergoing this process is irinotecan, an inactive compound used in the treatment of colon and small cell lung cancers, that is converted by human carboxylesterases to SN-38, a topisomerase-1 inhibitor [108]. As carboxylesterases display high affinity to ester functional groups, the carboxylesterase activity of drugs containing esters should be investigated in new drug projects.

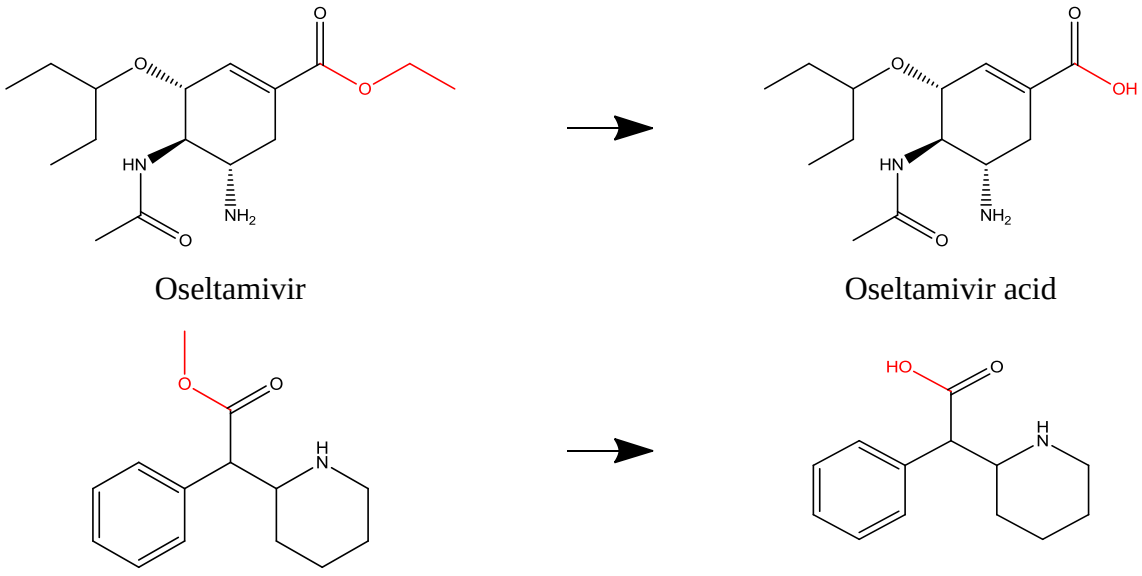

Figure 1.14: Examples of drug metabolites produced by hCES enzymes. *Sites of metabolism are highlighted in red.*

1.4.5. Other metabolising enzymes and their relative importance

Numerous other minor metabolising enzymatic families exist, but their roles tend to apply primarily to biological functions, and they have a lesser role in the metabolism of xenobiotic compounds. Such enzymes include sulfotransferases, which conjugate substrates

with sulphate groups [109], glutathione S-transferases, which conjugate substrates with glutathione groups [110] and monoamine oxidases, which deaminate monoamines [111]. Each of these enzyme families have vital biological roles, but tend not to play significant roles in xenobiotic metabolism, save for key examples.

The three most significant metabolising enzyme families of small molecule xenobiotics are widely reported to be CYPs, UGTs and esterases. Williams et al. [112] reported in 2004 that approximately 97% of the top 200 commercially marketed drugs were cleared primarily by CYPs, UGTs and esterases. Further to this, Cerny [113] analysed the literature of FDA approved small molecule drugs between 2006 to 2015 and determined that these three enzyme families accounted for the primary clearance of approximately 91% of new medicines. A depiction of the enzyme contributions determined by both studies is shown in Figure 1.15. The apparent difference between the two figures quoted by Williams et al. and Cerny may be a result of new attitudes towards drug design i.e. favouring molecules with a smaller extent of CYP metabolism, or by a targeted research focus towards molecules that favour alternative enzyme metabolism. Regardless of any differences between the figures, both studies conclusively show that the three enzyme families of CYPs, UGTs and esterases play a dominant role in the metabolism of drugs.

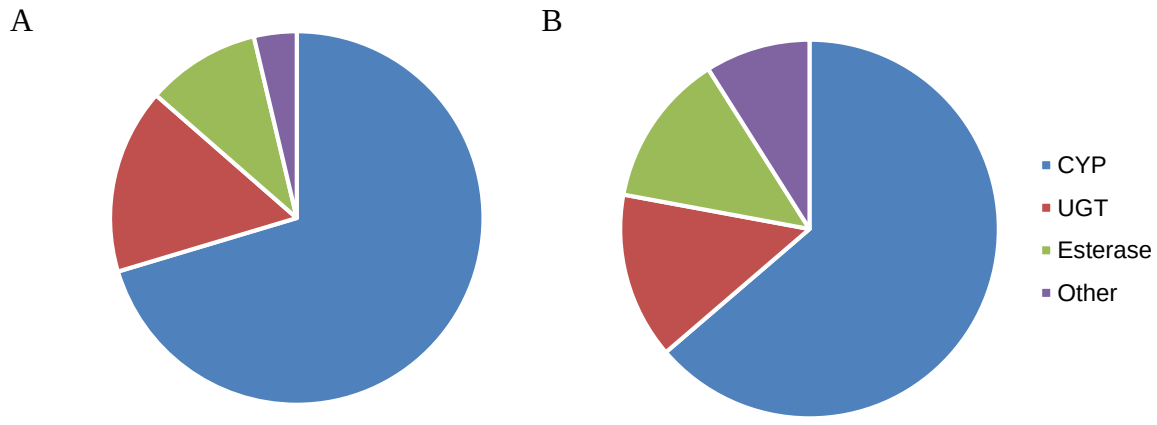

Figure 1.15: Contributions of enzyme families to the metabolism of marketed drugs. *(A) Figure adapted from data collected on top 200 commercially marketed drugs in 2004 by Williams et al. [112]. (B) Figure adapted from data collected on newly FDA approved small molecules entering the market between 2006-2015 by Cerny [113]. Data from both sources has been curated to reflect drugs that are primarily cleared through metabolic routes.*

Owing to the important biological role of metabolism from both a drug safety and activity perspective, it is unsurprising that drug metabolism has been proven to have a strong impact in drug discovery projects. A ten year study by Kola and Landis [114] was conducted over the period from 1991 to 2000 with the intention of assessing the rates of and reasons for drug discovery failures and successes. Among the key findings of this study was that in 1991 the single greatest cause of failure (~40%) in drug discovery projects was poor pharmacokinetic and bioavailability parameters, especially as a result of rate of metabolism. By 2000 however, the failure rate due to poor pharmacokinetic parameters was decreased to ~10%. This significant improvement in drug discovery attrition was brought about by two key innovations: commencing drug metabolism studies at an earlier period of the drug discovery process and improving the technologies used to define drug metabolism [115]. An industry trend of careful consideration towards drug metabolism has remained prevalent since the periods of the 1990s when attrition rates were improved. A 2014 study by Cook et al. [116] remarked that of the 2005 to 2010 product pipeline of the pharmaceutical company AstraZeneca, the attrition rate of drug discovery projects due to pharmacokinetic parameters was just 5%. This furthers the notion that studying the metabolism of a drug is important to the success of a drug discovery project.

1.5. *In vitro* and *in silico* approaches to studying molecules

1.5.1. *In vitro* techniques in the pharmaceutical industry

In the ancient world the process of drug discovery was conducted *in vivo*, involving human or animal sampling of natural products, observation of effects and, especially in the case of plant products, isolation of active extracts to improve medicinal qualities [117]. This process was largely trial and error, and had the disadvantage of posing significant danger to recipients of the products, given the considerable number of poisonous compounds in nature. One of the distinct shifts in drug discovery over history has been the development of *in vitro* techniques, which came about with improved knowledge of the natural sciences. The term *in vitro* literally means *in glass* and refers to experiments that take place external to a living organism. In pharmacology, the term usually reflects experiments performed with protein, cell or tissue samples. Each of these sample types represents a building unit of an organism and their use can allow greater insight into the actions of a drug by minimising external influence. The use of such *in vitro* techniques in preference to whole organism experiments reduces the risk of adverse drug events in drug discovery by limiting drug exposure to whole organisms until a basic level of drug safety is established. Additionally, without the need for whole organisms, experiments can be conducted more cheaply, faster and on a larger scale, which increases the efficiency of data collection.

While the use of *in vitro* techniques allows a safer and faster method of screening drugs, actions of a drug on a cell do not necessarily reflect the actions of drugs on a whole organism. To compensate for this, numerous strategies can be implemented to extrapolate *in vitro* data to better reflect *in vivo* outcomes. The first strategy of *in vitro – in vivo* extrapolation (IV-IVE) is to increase the complexity of the *in vitro* system, either through increased protein expression via DNA transfection, or by using more complex tissues in place of cells. This type of IV-IVE strategy is effective, but the increase in complexity of the system often leads to increased complexity in data analysis. This increase in complexity is a result of an increase in experimental variables, which adds to the difficulty when attempting to determine a precise cellular mechanism that has occurred. A second strategy for IV-IVE involves the use of mathematical models to "scale up" data and approximate a whole organism response from an *in vitro* model. For instance, the clearance of a drug from a whole

liver can be estimated from a microsomal clearance value by using average values of liver mass and microsomal concentration [118, 119]. The major benefit of this type of modelling is that the complexity of the experiment, and resultant analysis, is not increased. However, since the increased complexity of the results is estimated, it only reflects an idea of what the true *in vivo* results may be. As such, the accuracy of this type of strategy is dependent on high quality mathematical models and scaling factors.

Throughout this thesis *in vitro* techniques will be used for a range of purposes from receptor binding, to cellular function assays, to drug metabolism studies. The IV-IVE will be addressed as appropriate either by the use of whole-cell assays, or by mathematical modelling as appropriate.

1.5.2. *In silico* tools in the pharmaceutical industry

A modern approach in early phase drug discovery is to begin a project with many thousands or even millions of compounds and, through the process of high throughput screening, remove compounds from the pool until a small number of candidates remain and a single potential drug emerges. Numerous studies have been conducted on expenditure in the pharmaceutical industry. While the exact figure is disputed, there is general agreement that the cost to develop a new drug in the present market ranges from $1.8 to $2.6 billion (USD) [120]. This represents a significant economic barrier to drug development, and therefore technologies that can effectively reduce costs are of immense interest. This economic argument has proven to be a major motivating factor for the use of computational, or *in silico*, experiments in drug discovery and development. Since such techniques became commonly available in the late 1980s to early 1990s [121], *in silico* technologies have been developed and increasingly used throughout the pharmaceutical industry [122].

The ability for *in silico* technologies to influence costs in drug discovery is primarily tied to their ability to enrich available data. In a scenario where millions of compounds require screening, *in silico* technologies may be implemented to rule out, or promote, candidates without the need for any *in vitro* screening. This can prove to be of significant benefit as a computer simulation can be run in a fraction of the time and cost of a physical experiment, but can potentially yield comparable data [123]. This type of approach is

referred to as virtual high throughput screening, or just virtual screening, and exists as a powerful *in silico* tool, but is often complemented by other *in silico* methods [124]. Many specific technologies exist for this purpose, but they can generally be sorted into three categories: structure-, ligand- and knowledge-based methods.

1.5.3. Structure-based methods

Structure-based methods are a class of *in silico* methods that may be thought of as target centric methods. At the centre of structure-based methods is an emphasis on the structures of proteins and, in particular, the sites on these proteins to which drug molecules bind [125]. Typically, this involves a 3D structure of a protein which can then be analysed using a computer.

The gold standard method of obtaining a 3D structure of a protein is X-ray crystallography, an experimental method by which a protein is crystallised and analysed using X-ray diffraction. From this process, a set of cartesian coordinates denoting positions of atoms is generated and can then be visualised using appropriate computational tools [126]. The crystallography of proteins is a highly complex process. Of particular difficulty is the crystallisation of membrane bound proteins which are prone to denaturation during crystallisation. The opioid receptors, which have been discussed in Section 1.3.5, are examples of membrane bound receptors which were first discovered in 1973, but were not successfully crystallised until 2012 [127]. The UGT enzymes, discussed in Section 1.4.3, are also examples of membrane bound receptors that have been resistant to attempts at crystallisation as the only existing UGT crystal structure available in literature is a partial structure of the co-factor binding domain of UGT2B7, which was determined in 2010 [128]. Despite the difficulties in attaining these structures, crystallographers have been able to determine many thousands of structures, with more than 34,000 freely available online through the RCSB Protein Data Bank [129]. The protein structure of a substrate bound CYP2C9 receptor (PDB ID: 1R9O) is shown in Figure 1.16. This structure was used in this thesis for the purpose of rationalising CYP-mediated metabolism of a substrate molecule (see Chapter 2.2.15.1).

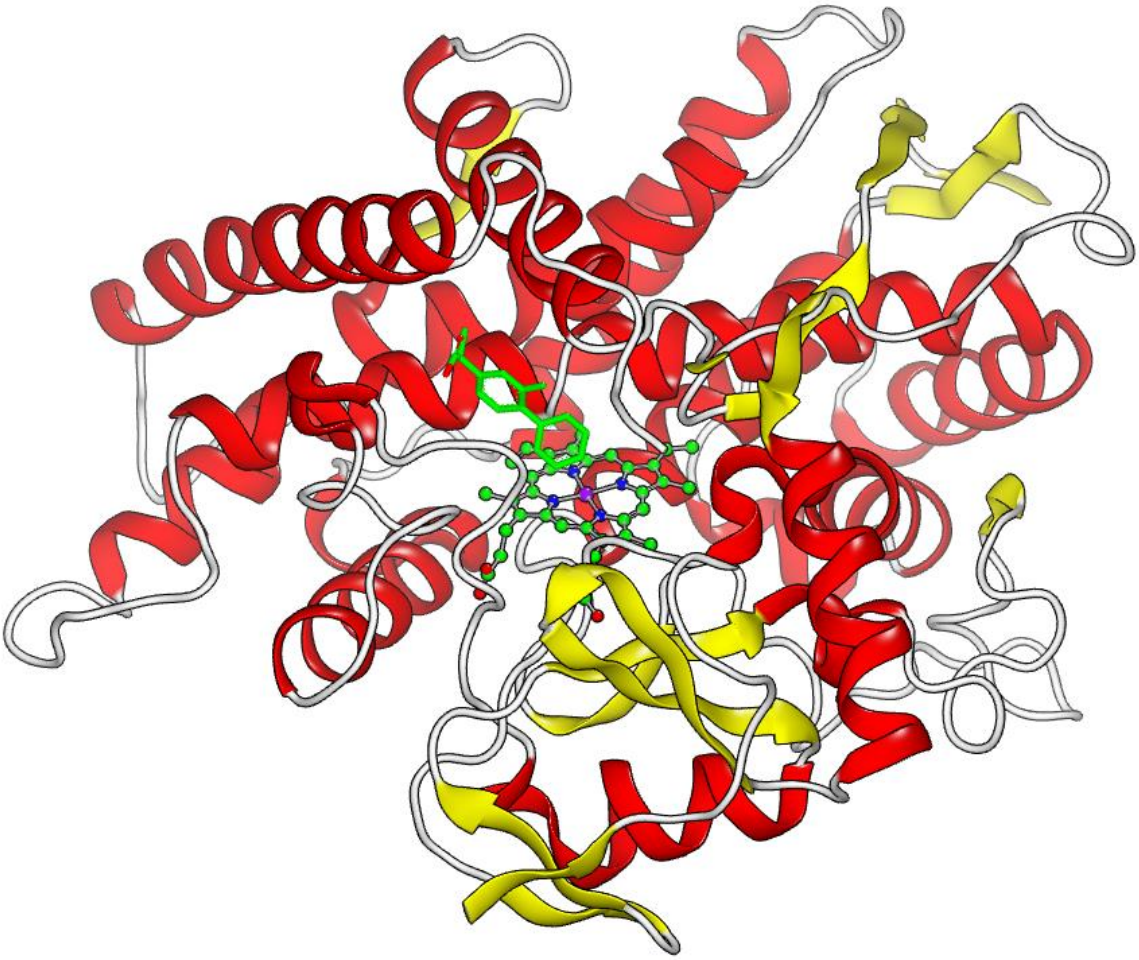

Figure 1.16: Crystal structure of the CYP2C9 enzyme (PDB ID: 1R9O). *Protein structure is displayed in ribbons. Central heme is displayed in ball and stick representation with green carbon atoms. Bound ligand (flurbiprofen) is displayed in stick representation with green carbon atoms.*

When crystallisation proves too difficult and a protein structure is sought, homology modelling is often the most pursued method. In homology modelling, the amino acid sequence of a protein is transposed and folded into a template structure to generate an estimated model of the protein. This template structure is typically a structure of a related protein that has been determined experimentally. As such, homology modelling is a process that is highly reliant on reliable structural information, and only serves as a usable extrapolation of data, rather than a set of absolute data. While homology models have been used successfully in the past, they are only recommended to be used when experimentally derived crystallographic data is unavailable [130].

Once a protein structure is available, structure-based methods typically involve simulations of how ligands may interact with the structure. Molecular docking, or just docking, is a widespread *in silico* tool used for this purpose. Docking involves simulations of how a molecule aligns itself within a defined region of a protein structure. Once simulated, these molecular conformations, or binding poses, are scored based on the calculated energy of the pose, with bias towards lower energy states as these states are considered closer to "natural" states of binding [131]. A crystal structure is essentially a 3D-snapshot of a protein in a fixed moment of time, and effectively a rigid structure. Similarly, 3D-structures of ligands used in docking are rigid structures also. In reality, both of these central components of docking are flexible and may be capable of adopting a number of conformational changes.

Computationally, it is possible to model this flexibility, but this comes at a significant cost of computational time. By using rigid structures it is possible to simulate this flexibility, without fully defining it. As ligands are typically smaller than receptors, it is generally easier to simulate their flexibility by defining conformational changes of a ligand. The 3D-structure generator Omega, by OpenEye [132], accomplishes this by identifying rotatable bonds in molecules and presenting conformations built around rotations of the bonds. These conformations are then ranked based on their energy, with bias towards lower energy conformers.

Flexibility of protein structures is more difficult to simulate due to the large amounts of computational time required to calculate energies of atoms and "allowed" flexible states in proteins. Some programs such as GOLD, by the Cambridge Crystallographic Data Centre, and Glide, by Schrödinger, are able to fulfil this function to some extent, but a different approach is used in OEDocking, by OpenEye [133]. In OEDocking a force field is defined at the active site of a protein. This force field can be biased towards the solvent or protein to influence the force field size and simulate increased or decreased flexibility of the protein. The combination of both Omega and OEDocking allows for a computationally inexpensive method of simulating flexibility in an inherently rigid docking process. OEDocking, through the FRED docking module, has been successfully used to identify ligands of numerous targets including MAPK, COX-2, thrombin, neuraminidase and numerous others [134].

A high-end structure-based method which allows fully flexible calculations of proteins and ligands is molecular dynamics (MD). In MD simulations, the flexible states of proteins and molecules can be modelled progressively over time such that the flexible nature of a protein can be modelled and progressive differences in structure can be observed. The progressive differences typically involve very small shifts in atoms and a great number of shifts, or slices, are required to simulate flexibility [135]. Accordingly, the computational time involved in an MD simulation is many times greater than docking and requires the use of very high end computational hardware to accomplish this simulation in a timely manner. Owing to this highly taxing requirement for computation, MD simulations are typically not used for prospective analyses or virtual screening, and are instead used retrospectively to analyse flexibility in proteins and rationalise the function of proteins.

In this project, docking was used as a structure-based approach for the investigation of potential targets of PAA and PAB, for the purposes of both predicting and rationalising experimental activity. As the combined use of Omega and OEDocking allows for an inexpensive approach to pursue pseudo-flexible docking of molecules, this approach was suitable in the present study, where multiple targets were able to be analysed while minimising computational expenditure.

1.5.4. Ligand-based methods

Ligand-based methods, in contrast to structure-based methods, are a class of *in silico* methods that are primarily concerned with the shape and electrostatic features of small molecules (that are usually drug-like in nature). The central philosophy that underpins these methods is that the action of a drug is primarily governed by the shape of a molecule and the electrostatic charge of its atoms. Ligand based analysis has lower entry requirements than structure based analysis as no protein structure information is required and analysis may be performed by simply using a library of molecules.

Pharmacophore modelling is a ligand based method that attempts to define a minimised set of structural features in a set of training molecules which can then be used to predict activity of other molecules [122]. The set of training molecules used typically incorporates a level of activity and structural diversity such that a broad range of binding

affinities are represented to compress the greatest amount of information into a minimised structural model. In other words, molecules of high and low activity are used to define a pharmacophore to help the model distinguish more potent molecules from less potent ones.

A test set will often be constructed similarly to the training set, consisting of a diversity of molecules intended to discern the ability of the developed model to predict high to low affinity molecules. The act of developing a pharmacophore model itself involves analysing the training set of molecules for common structural features, such as aromatic groups, hydrogen bond donors and acceptors, charged anionic and cationic groups and hydrophobic groups, and then developing hypotheses from these common features which best describe the activity of the training set molecules. The strength of a hypothesis is determined by the ability of the hypothesis to rank the test set of molecules from high to low activity. Ranking is determined by a root mean square deviation (RMSD) calculation which compares features in a test molecule to the features in the screened hypothesis, with closer matches resulting in a lower score, indicating low deviation and therefore better fit to the hypothesis [136].

When a pharmacophore of sufficient predictive power is developed, it can then be used to screen other molecules to predict potential activities. Numerous software packages exist to help facilitate pharmacophore modelling including Discovery Studio's Catalyst by BIOVIA/Accelrys and Phase, by Schrödinger. Figure 1.17 demonstrates a successful pharmacophore hypothesis formed to describe a series of non-steroidal glucocorticoid receptor agonists [137]. This glucocorticoid pharmacophore is used in this thesis for the purpose of testing the fit of a molecule to predict receptor binding activity (see Chapter 3.2.4.1).

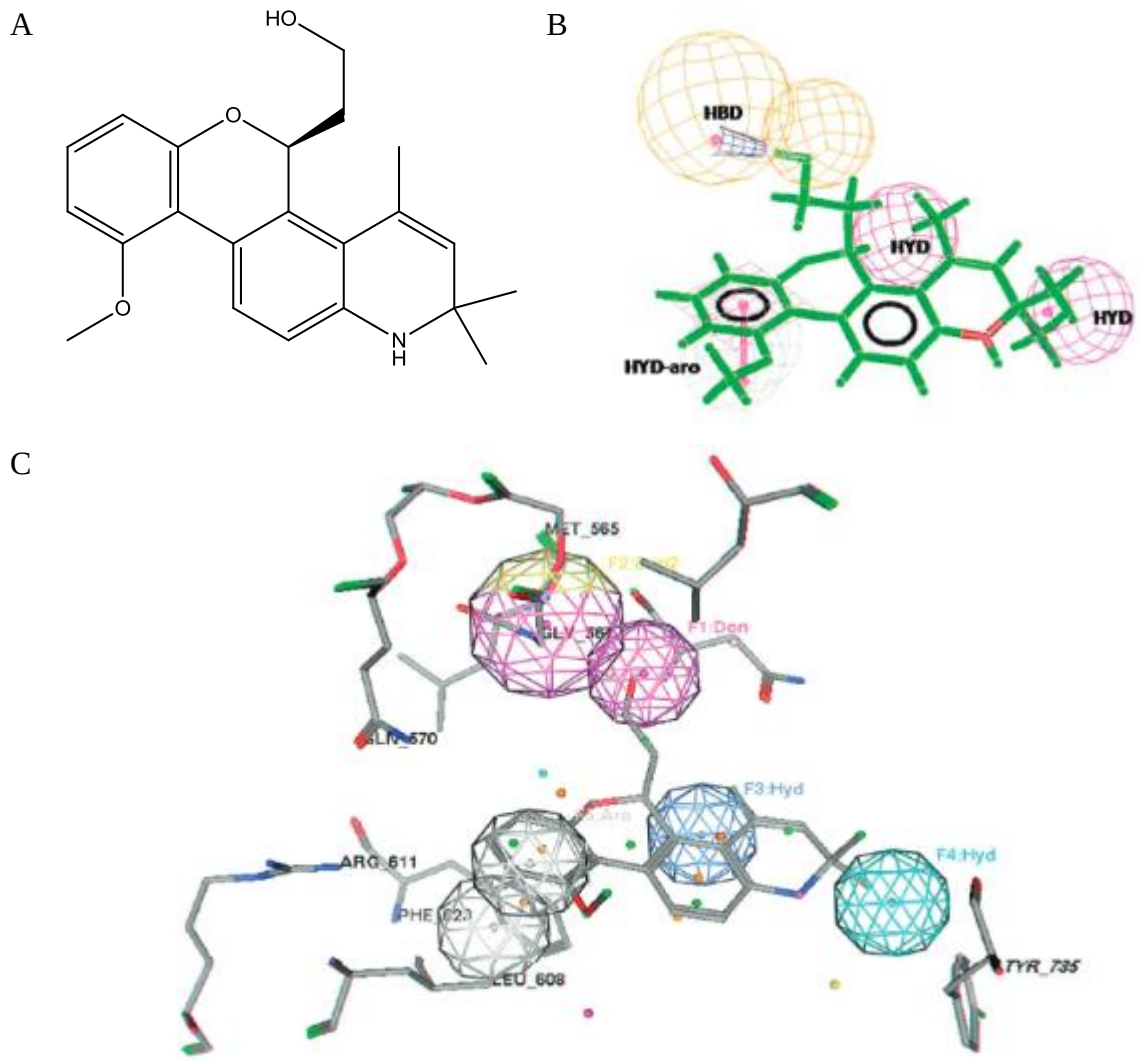

Figure 1.17: Pharmacophore mapping of compound ID 20 performed by a Catalyst Flexible Best Search. *(A) Structure of compound 20 (B) 3D overlay of pharmacophore hypothesis to compound 20. (C) Pharmacophore hypothesis superimposed to a docked conformation of compound 20 in the 1M2Z (glucocorticoid) crystal structure. (Adapted with permission from J Med Chem, 26 Mar 2010, volume 53, pages 3065-3074. Copyright 2010 American Chemical Society).*

The strength of pharmacophore modelling lies in its predictive power for a diverse range of applications. By catering the training set towards agonists, partial agonists, antagonists etc. distinct predictive models may be developed for each set to predict activity in other molecules. A weakness of the pharmacophore modelling approach is the time investment required to properly develop and validate a model. As there is no standard process to choosing a hypothesis to pursue, each hypothesis must be rigorously tested to

determine the most robust model. Additionally, as a pharmacophore model is built from a set of molecules, those molecules determine the hypotheses that can be formed. Structural diversity is encouraged in a pharmacophore training set, but inclusion of certain molecules may skew hypotheses towards a model that does not adequately describe the class of compounds being investigated. This is especially true if a set of molecules is included in the training set that bind to a target in a binding mode unique to other molecules in the set, and there is no structural information available to inform this.

Pharmacophore modelling is a strong approach for the investigation of a single target, but in a project where the target is unknown, focus may shift to new targets as additional experimental data is accrued. In the present study, a molecule with an unknown target is being investigated and as such, a number of targets are likely to be under consideration. Accordingly, the time investment to develop a robust pharmacophore model may be wasted if experimental data is collected that rules out that target. While there is still value in a robust pharmacophore model, it will not contribute to the aims of the project. As such, while there is value in utilising an existing pharmacophore, it may not be suitable to pursue development of models in the scope of this project.

While the pharmacophore modelling approach may not be suitable, there is likely to be value in pursuing a low-investment form of ligand-based modelling. ROCS, by OpenEye Scientific Software [138], is a form of ligand-based modelling that may be used as a pseudo-pharmacophore modelling approach. Like pharmacophore modelling, ROCS uses the approach of defining a structural fingerprint of a given molecule by its shape and electrostatic features (see Figure 1.18).

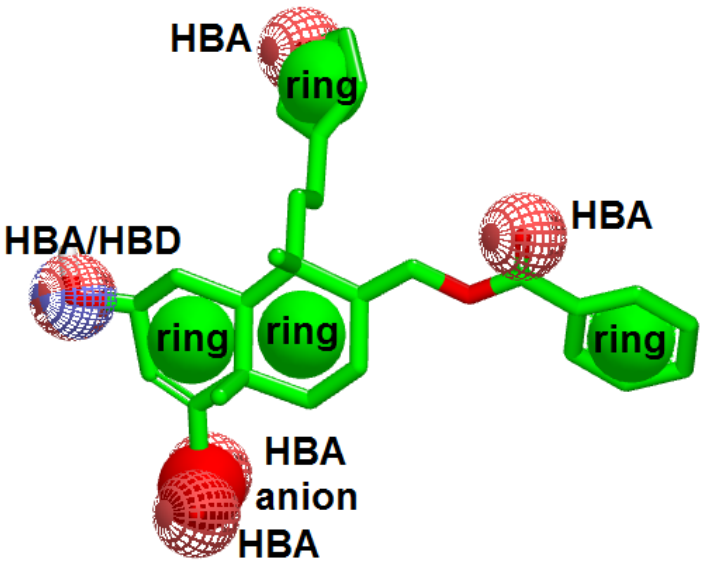

Figure 1.18: ROCS model of PAA displaying defined structural features. *'HBA' refers to a hydrogen bond acceptor and 'HBD' refers to a hydrogen bond donor. 'Ring' is a non-specific term encompassing both aromatic and non-aromatic ring structures.*

The two approaches of ROCS and pharmacophore modelling differ, however, in that while pharmacophore modelling uses a diverse range of ligands to condense the structural information to a reduced fingerprint, ROCS can use a single query molecule. The ROCS approach involves taking the chemical structure of a given query molecule and overlaying molecules against it to determine similarity based on shape and electrostatic features. ROCS may use multiple metrics to determine this similarity, but the default scoring function of ROCS is a Tanimoto based metric (TanimotoCombo) composed of two individual scoring functions which independently calculate shape and electrostatic similarity (color). A Tanimoto coefficient is scored in a range from 0 (entirely dissimilar) to 1 (entirely similar) [139]. The result of ROCS screening by the TanimotoCombo metric describes how similar (between 0 and 2) a molecule in a database is to a query molecule. An example of this type of overlay is shown in Figure 1.19.

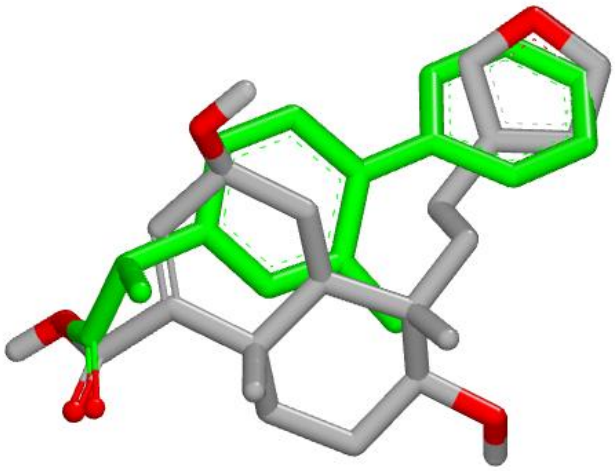

Figure 1.19: ROCS overlay of PAAH (grey) to flurbiprofen (green). *PAAH is the de-esterified alcohol form of PAA, which will be discussed in Chapter 2.*

Following the central tenet of ligand-based modelling, that the actions of molecules are determined by their shape and electrostatic features, it follows that a molecule with a high TanimotoCombo score (a value closer to 2) is more likely to exhibit similar activity to the molecule it was screened against. In other words, if a molecule displays a high TanimotoCombo score when compared to a query molecule known to be a strong inhibitor of an enzyme, it is more likely that the screened molecule may also be an inhibitor of that enzyme. A benefit to the usage of ROCS is that the computational power required is very low in comparison to other *in silico* methods i.e. docking, molecular dynamics, pharmacophore modelling etc. Accordingly, the ROCS method is comparatively very fast to set up and run, meaning that the use of ROCS is "low-commitment" and does not require a significant computational or time investment.

ROCS has previously been used successfully to search for new chemical scaffolds for targets [140, 141]. As mentioned previously, in this project a number of protein complexes and enzymes are to be investigated as potential targets of both PAA and PAB. This represents a similar approach to previous successful implementations of ROCS technology, however it involves the search for a target rather than a ligand. The use of ROCS, to screen for chemical similarity, represents a method to employ a ligand-based method that can be easily implemented for a range of targets.

1.5.5. Knowledge-based methods

Knowledge-based *in silico* methods are a diverse group of tools that rely on a systematic approach to discern metrics that can be used to predict properties of molecules. The uses of knowledge-based methods are varied and may include methods to predict drug metabolism, filter databases and predict drug-like molecules [142-144]. Knowledge-based methods may be thought of as algorithms, where a metric, or a number of metrics, are input and the results are then output for analysis. The prediction of molecular properties is a key component of many knowledge-based methods, as these properties often form the metrics that are used. The form of output data varies based on the purpose of the method and may involve a binary result i.e. yes/no for a given question, statistical output i.e. higher or lower probability, or a given value i.e. predicting a physicochemical property [145].

Knowledge-based methods may also be thought of as "rules-based" methods. These rules are derived from a systematic examination of experimental data to search for a set of metrics that can be used to reliably predict properties of new molecules. A famous example of a rules-based approach is the Lipinski 'rule of five' (RO5), which predicts that drug-like molecules should possess no more than 5 hydrogen bond donors, 10 hydrogen bond acceptors, a molecular mass less than 500 Da and a logP of less than 5 [146]. This set of rules was determined from systematic analysis of more than 2,000 molecules and determined that a molecule satisfying these metrics has a high probability of being a drug-like molecule and suitable for development. Since its publication, the RO5 has been subject to numerous additions and adjustments, but the rules remain a strong predictor of drug-like molecules and are an example of a knowledge-based approach to predicting properties of molecules [147].

Once defined, the usage of a knowledge-based method typically involves submission of a molecule, or database of molecules. The submission of the molecule may involve a 1-, 2- or 3-dimensional representation. Examples of each dimensional representation are presented in Table 1.1.

Table 1.1: Multidimensional representations of PAA. *1D structure consists of a SMILES string generated in PICTO by OpenEye. The 2D structure consists of a stick structure generated in ChemDraw by Cambridgesoft. The 3D structure consists of a stick representation generated in Omega by OpenEye.*

Dimension	Representation
1D	C[C@]12CC[C@@H]([C@@]([C@@H]1C[C@@H](C=C2C(=O)O)O)©CCc3ccoc3)COC(=O)c4ccccc4
2D	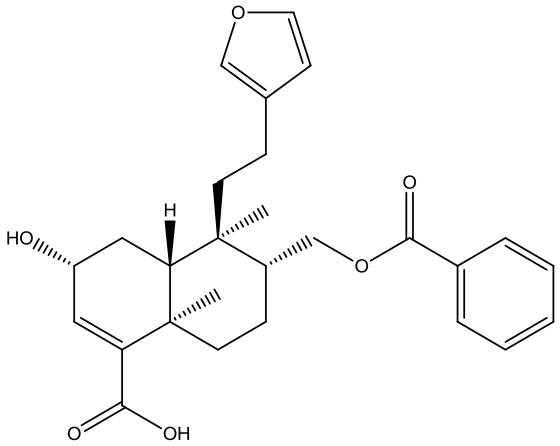
3D	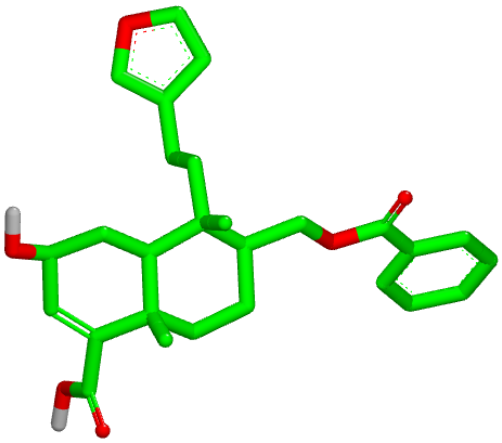

Representations of chemicals in 2- and 3-dimensions are reasonably intuitive to interpret, but 1D representations are typically more difficult to read and thus, are mostly handled by computational software. The most common 1D representation for chemical structures is the 'simplified molecular-input line-entry system' (SMILES) format. In brief, the SMILES language uses letters to represent atoms and the bonds between them are represented using symbols such as parentheses, to represent branching groups, 'equals' signs, to represent double bonds, and 'at' symbols to represent stereochemistry, as well as numerous other symbols. Single bonds and hydrogens are implicit in the language and are

not represented by symbols, except for special circumstances such as to denote stereochemical assignments of hydrogens.

An expanded form of the SMILES language, called the 'SMILES arbitrary target specification' (SMARTS) language is sometimes used for representing molecular substructures, and allows for precise definitions of groups. The primary use of SMARTS is in substructure searching, where it can be used to filter databases of molecules to retrieve, or discard, molecules containing a specific structural feature. The language is built from SMILES but uses additional notation and allows for logical operators to be embedded in the language. An example of the SMARTS language is: [$([NX3;H0])], which precisely describes an uncharged, tertiary amine where "NX3" refers to a nitrogen bound to three atoms, ";" refers to the logical argument of 'and', and "H0" refers to the number of hydrogen atoms being zero.

The success of utilising knowledge-based methods is dependent on the reliability of the model that has been produced. Typically a published knowledge-based tool will have been validated throughout the development of the model. Reliable online knowledge-based methods represent especially valuable tools in drug discovery projects as they provide a low-cost option to predicting molecular properties, without the need for specialised software or hardware. As reliable knowledge-based methods represent a valuable tool in drug discovery and development, they will be used throughout this present study.

1.6. Project aims

As has been outlined earlier, the Australian medicinal plant *D. polyandra* has been the subject of continued study for both academic and potential product development purposes. In this PhD project, a combination of *in silico* and *in vitro* tools have been utilised, as well as IV-IVE, for the purpose of exploring a low economic and computational cost approach to drug research. The studies in this thesis were conducted in three primary areas: metabolism, anti-inflammatory targets and pain. The specific aims in these areas were:

1. **Determination of the human liver metabolism of polyandric acid A (PAA) using *in vitro* and *in silico* approaches**

The general goal of metabolism research in this project was to determine how the human liver processes and biotransforms PAA. More specifically the goals of this portion of the project were to investigate the extent of metabolism by esterases, UGT and CYP enzyme families, calculate enzyme clearance parameters, determine the specific enzymes involved in metabolism and elucidate the structures of major metabolites. The study of the metabolism of PAA was primarily to be achieved through *in vitro* experiments using human enzymes and microsomes. *In silico* methods were also used, both prospectively and retrospectively, to formulate predictions of metabolism and rationalise observed results.

2. **Exploration of potential anti-inflammatory molecular targets of PAA using a combined *in silico* and *in vitro* approach**

The actions of *D. polyandra* as an anti-inflammatory medicinal plant were already understood from an ethnopharmacological perspective and through demonstration of anti-inflammatory effects in mice, although the specific mechanism of action of its constituent active compounds remained unknown. Thus, the focus of inflammatory research in this project was to identify possible molecular targets of PAA that could explain the anti-inflammatory mechanism of action of PAA. This was to be achieved by a feedback

approach utilising *in vitro* studies in cell lines and *in vivo* studies in animal models to formulate hypotheses about potential targets, investigating the hypotheses via *in silico* modelling and testing of hypotheses by *in vitro* screening methods. It had been established that PAA attenuates the cytokines IL-1β, IL-6 and TNFα, therefore protein targets associated with these cytokines were of primary interest. This aspect of the study also sought to examine the approach of integrating *in silico* with *in vitro* techniques for the purpose of identifying drug targets.

3. Examination of the interactions of polyandric acid B (PAB) and its methylated derivative with opioid receptors using *in silico* and *in vitro* approaches

While research into inflammatory targets was pursued as a result of ethnopharmacological evidence, the approach to studying pain, and opioid receptors in particular, came about solely through *in silico* investigations. The goal of this study was to further investigate the *in silico* led hypothesis of interactions between PAB and opioid receptors and draw a definitive conclusion through *in vitro* testing in a μ-opioid receptor assay.

Chapter Two: The enzymology of human PAA and PAAH metabolism

2.1. Introduction

It is well established that a drug metabolism and kinetic profile is an essential component in the development of new chemical entities. Major regulatory bodies such as the US Food and Drug Administration (FDA) and the European Medicines Agency (EMA) require, at a minimum, *in vitro* evaluation of drug metabolism for new chemical entities before they can receive approval for clinical use [148, 149]. Metabolic stability and reaction phenotyping represent powerful tools in the *in vitro* study of drug metabolism. The use of human liver microsomes (HLM) in the investigation of drug metabolic stability together with cDNA expressed enzymes and HLM in combination with selective inhibitors of cytochromes P450 (CYP) and UDP-glucuronosyl transferase (UGT) enzymes are now widely accepted approaches for the characterisation of key metabolic parameters of new chemical entities [150-153].

The study described in this chapter was undertaken to characterise the human hepatic metabolism of PAA *in silico* and *in vitro. In silico* experiments including site of metabolism prediction, structural overlay and protein docking experiments were used to make predictions regarding enzymes potentially involved in PAA metabolism and the types of metabolites that may be produced. *In vitro* reaction phenotyping experiments utilising HLM, human liver cytosol (HLC), selective UGT and CYP inhibitors and recombinant human CYP and UGT enzymes were used to elucidate the enzymology and kinetics of the metabolism of PAA and its de-esterified hydrolysis product PAAH (see Figure 2.1). Enzyme families of interest in this study included carboxylesterases (hCES), sulfotransferases (SULT), UGT and CYP enzymes. In addition to improving knowledge of human clerodane diterpenoid metabolism, this study represents the first such investigation of the human metabolism of an active constituent of an Australian Aboriginal traditional medicinal plant. Part of this chapter, specifically sections relating to *in vitro* investigations of PAA metabolism have been published as part of the paper *"In vitro metabolism of the anti-inflammatory clerodane diterpenoid polyandric acid A and its hydrolysis product by human liver microsomes and*

recombinant cytochrome P450 and UDP-glucuronosyltransferase enzymes" (provided at the end of this thesis). All methodology is described in Chapter 6.

A

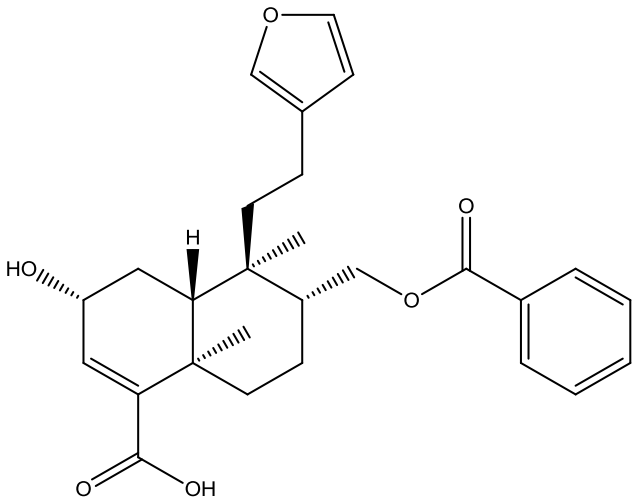

B

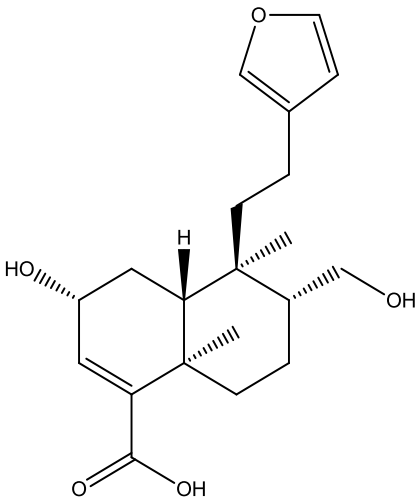

Figure 2.1: Structures of (A) PAA and (B) PAAH.

2.2. Results and Discussion

2.2.1. Incubation of PAA with standard media

The potential hydrolysis of PAA by phosphate buffer (0.1 M, pH 7.4) was investigated using the method described in Chapter 6.2.5.1. Analysis of samples was performed by HPLC according to the conditions given in Chapter 6.2.4. The results of the analysis are shown in Figure 2.2. Concentrations of PAA were quantified by reference to calibration curves prepared from authentic standards of each compound. The results are shown in Figure 2.2.

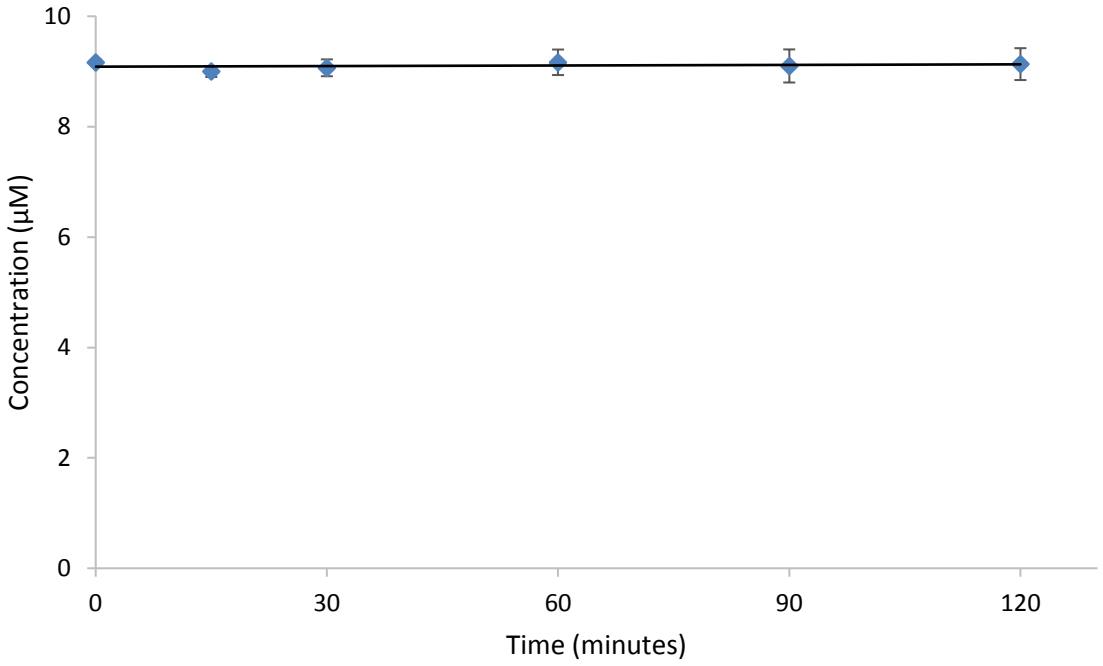

Figure 2.2: Incubation of PAA with standard media. *Incubation samples contained PAA (10 µM) and potassium phosphate buffer (0.1 M) at pH 7.4. Incubations were performed at 37 °C for 120 minutes. Results are presented as the mean ± SD (n=3).*

The concentration of PAA remained constant over the two hour incubation period, indicating that PAA is not hydrolysed by phosphate buffer at 37°C. This stable baseline could then be used to assess the effect of individual variables to this standard incubation

method such as the introduction of protein homogenates containing xenobiotic metabolising enzymes.

2.2.2. Incubation of PAA with HLM

The hydrolysis of PAA to the de-esterified compound PAAH by HLM was investigated by using the method described in Chapter 6.2.5.1. Pools of HLM from five donor livers were accessed from the Flinders University Department of Clinical Pharmacology human liver bank. Microsomal fractions were collected from the donor livers by the method described in Chapter 6.2.1 and pooled for use throughout this study. Analysis of samples was performed by HPLC using the conditions described in Chapter 6.2.4, and concentrations of PAA and PAAH in the incubation medium were quantified by reference to calibration curves prepared from authentic standards of each compound. The results are shown in Figure 2.3.

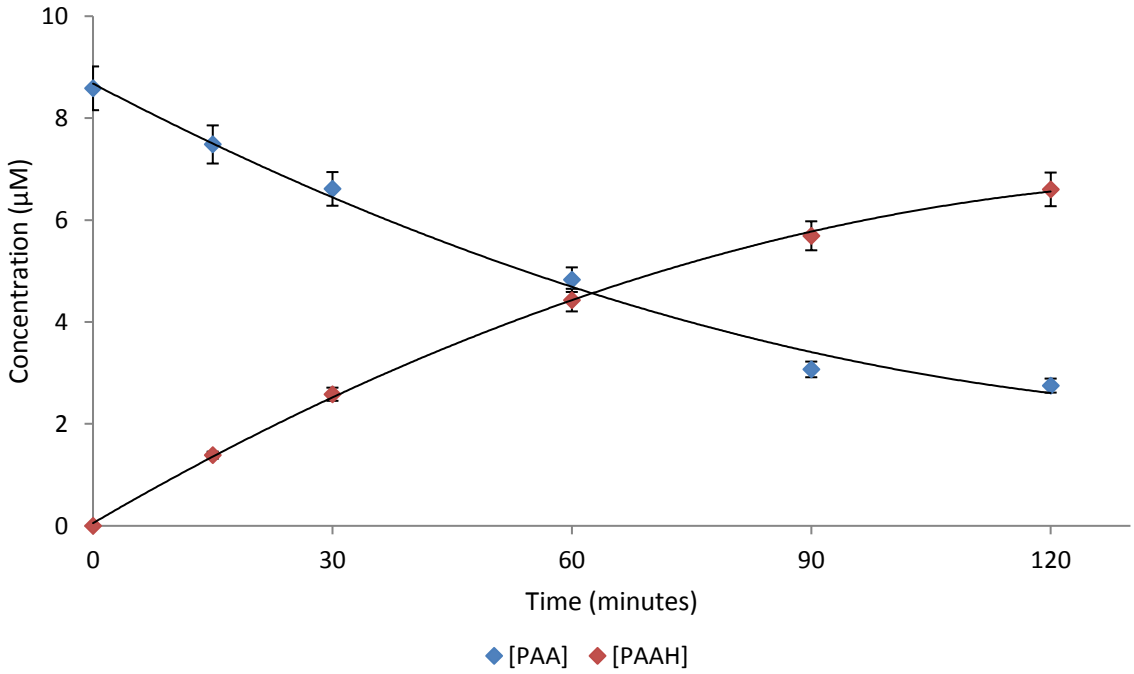

Figure 2.3: Incubation of PAA with HLM. *Incubation samples contained PAA (10 µM) and HLM (1 mg/mL) at pH 7.4. Incubations were performed at 37 °C for 120 minutes. Results are presented as the mean ± SD (n=3).*

There was a reciprocal relationship in the decline of PAA and the formation of PAAH, such that the sum of the concentrations of PAA and PAAH were approximately constant over the duration of the incubation. These data suggest that depletion of PAA corresponds to the generation of PAAH and that no further metabolic processing occurs beyond the hydrolysis of PAA to form PAAH.

Ester hydrolysis may occur spontaneously under either alkaline or acidic conditions but, as shown in Section 2.2.1, PAA hydrolysis was not observed in the absence of HLM. Enzyme catalysed hydrolysis of ester containing xenobiotics is mediated primarily by carboxylesterases, of which there are two primary isoforms (hCES1 and hCES2) in human liver [105]. Since PAA hydrolysis was linked to the presence of HLM, it is likely that the extensive hydrolysis shown in Figure 2.3 is catalysed by carboxylesterase(s). The enzyme hCES1 appears to preferentially hydrolyse substrates with a small alcohol but large acyl moiety, while the converse applies to hCES2 [154]. However, overlapping substrate specificity may occur with hCES1. As PAA contains a large alcohol and a small acyl moiety, hydrolysis by hCES2 seems likely although a contribution of hCES1 cannot be discounted. As noted above, both hCES1 and hCES2 are expressed in liver, while expression of hCES2 additionally occurs in the gastrointestinal tract and kidneys [107].

The hydrolysis of esters *in vivo* frequently occurs rapidly due to the involvement of hepatic, gastrointestinal, and blood esterases. It has been reported that salvinorin A, which is structurally similar to PAA and PAAH (Figure 2.4), is hydrolysed rapidly in blood *ex vivo* [155]. Thus, given the likely involvement of hepatic, gastrointestinal, renal and blood esterases in PAA hydrolysis, pre-systemic and systemic hydrolysis of PAA is expected to occur rapidly following oral administration and therefore PAAH is predicted to be the major circulating species in blood *in vivo.* Similarly, systemic hydrolysis would occur following dermal absorption. There is evidence that topically administered PAAH exhibits anti-inflammatory activity *in vivo.* However, the anti-inflammatory activity of topically applied PAAH in the mouse is lower than that of PAA, which may be the result of either a weaker interaction between ligand and target or improved membrane penetration of PAA due to the presence of the more hydrophobic ester group [12].

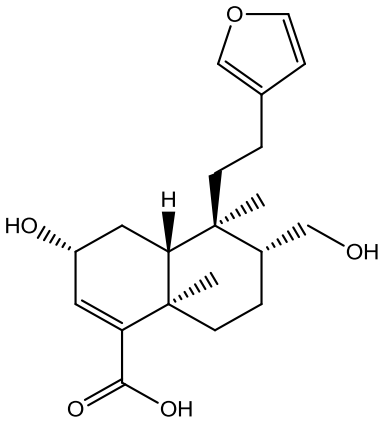

PAAH

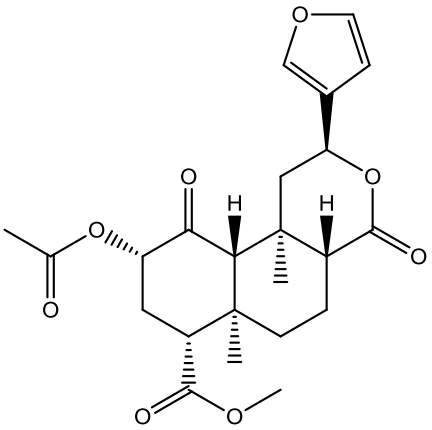

Salvinorin A

Figure 2.4: Structures of the diterpenoids PAAH and salvinorin A.

2.2.3. PAAH to substitute for PAA in further experiments

While metabolism of PAA by enzymes such as CYP and UGT cannot be discounted, significant non-hydrolytic biotransformation is unlikely given the rapid hydrolysis of esters that is normally observed *in vivo*. As such, it is more likely that the contribution of such enzymes will occur subsequently, rather than competitively to hydrolysis.

In practical terms it may be plausible to observe the contribution of non-hydrolytic enzymes to an ester drug, without the contribution of an esterase. This may be accomplished through the use of carboxylesterase inhibitors, as has been suggested by Hatfield and Potter [156] for both *in vivo* and *in vitro* applications. The issue of using selective carboxylesterase inhibitors has been addressed by Umehara et al. [157] who determined eserine (see Figure 2.5) to be a highly specific hCES2 inhibitor at a concentration of 10 μM, and as such is useful for determining subtype specificity of carboxylesterase substrates.

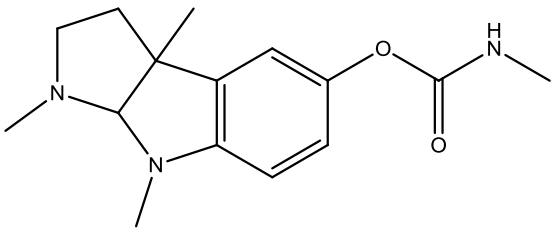

Figure 2.5: Molecular structure of eserine.

The use of eserine, or another such selective inhibitor, was not pursued in this study as the use of such an inhibitor would need to be performed with assurance that non-esterase enzymes were not inhibited by its presence. As this potential cross-inhibition was unknown, the further investigation of PAA metabolism with non-hydrolytic enzymes was performed using the hydrolysed PAAH form to simplify the analysis.

2.2.4. Cytochrome P450 mediated metabolism of PAAH

The extent of CYP-mediated metabolism of PAAH was investigated using incubations of HLM supplemented with an NADPH generating system according to the method described in Chapter 6.2.5.1. Analysis of samples was performed by HPLC using the conditions described in Chapter 6.2.4. Results are shown in Figure 2.6 as the percentage of control activity based on peak area.

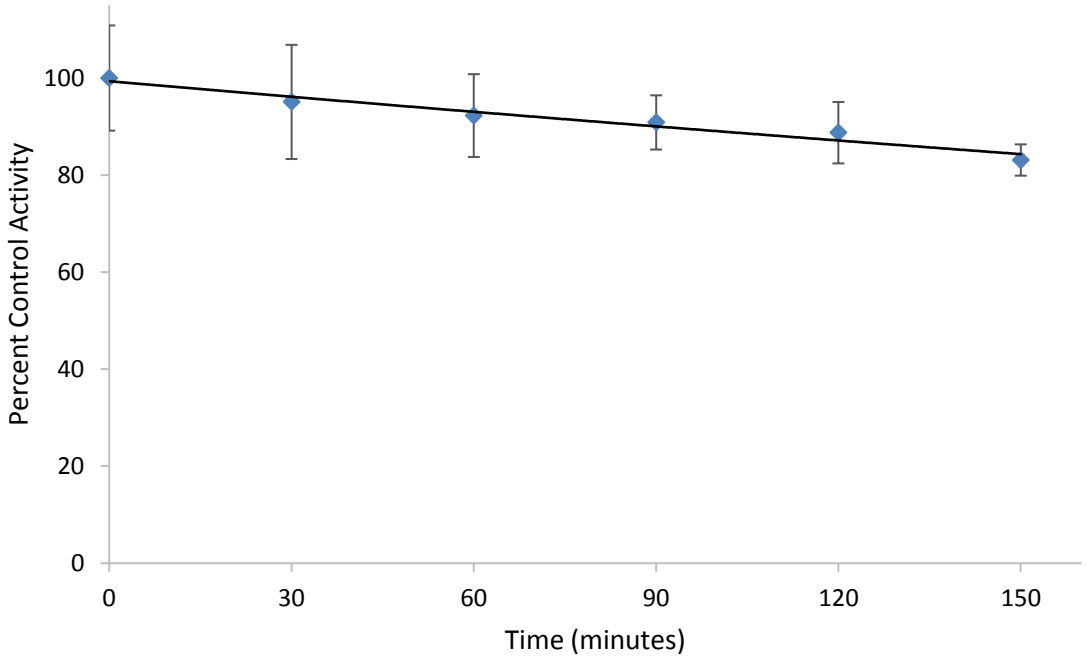

Figure 2.6: Incubation of PAAH with HLM and NADPH generating system. *Incubation samples contained PAAH (2 µM), HLM (1 mg/mL) and an NADPH generating system (50 µL) at pH 7.4. Incubations were performed at 37 °C for 150 minutes. Results are presented as the mean ± SD (n=4).*

On average, the peak area of PAAH was observed to decrease by approximately 15% over the incubation period. Given the relatively minor depletion observed, incubations were performed with a positive control to ensure the reaction conditions were conducive to CYP activity. Phenacetin was selected as a positive control as it is efficiently metabolised by CYP1A2 [158].

Human liver microsomal CYP-catalysed phenacetin depletion was investigated by incubation of HLM supplemented with an NADPH generating system, as described in Chapter 6.2.5.1. Analysis of samples was performed by HPLC using the conditions given in Chapter 6.2.4. Results of the analysis are shown in Figure 2.7 as the percentage of control activity based on peak area. Phenacetin was depleted by approximately 60% over the incubation period indicating that the reaction conditions were functional for CYP-catalysed metabolism.

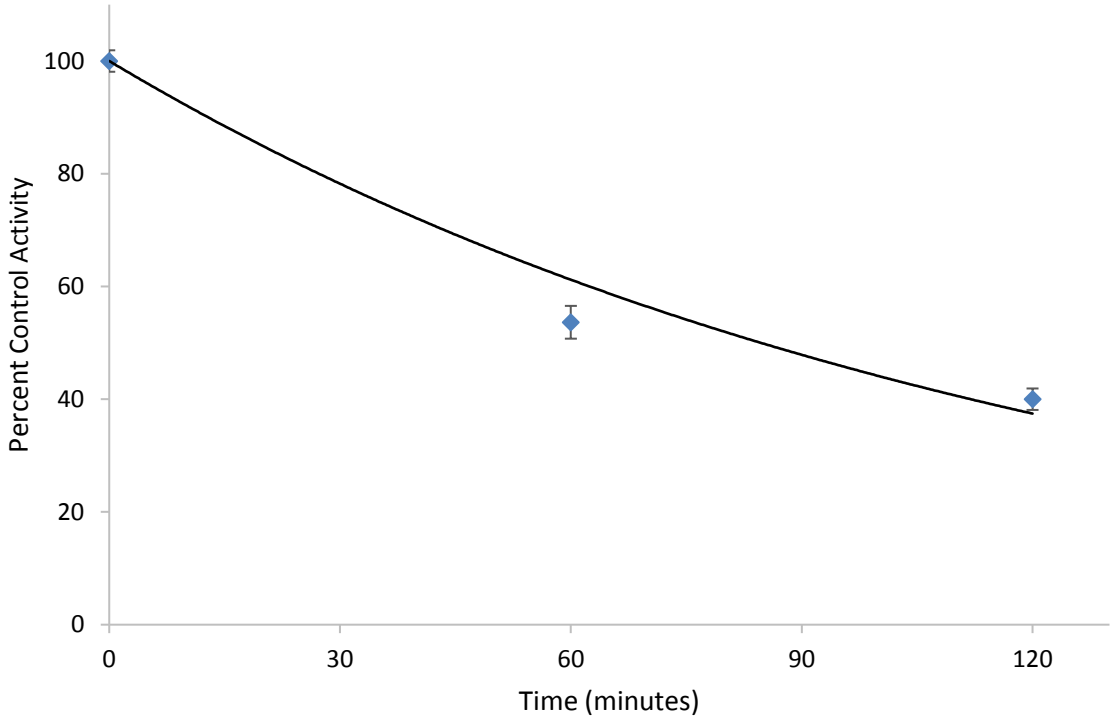

Figure 2.7: Incubation of phenacetin with HLM and NADPH generating system. *Incubation samples contained phenacetin (2 µM), HLM (1 mg/mL) and an NADPH generating system (50 µL) at pH 7.4. Incubations were performed at 37 °C for 150 minutes. Results are presented as the mean ± SD (n=4).*

Activation of HLM with alamethicin is required for the measurement of glucuronidation activities. It has been reported previously that alamethicin has no significant effect on human liver microsomal CYP enzyme activities [159]. Nevertheless, since subsequent experiments investigated the depletion of PAAH by microsomal incubations with both NADPH and UDPGA, the lack of effect of alamethicin pre-treatment was confirmed here by comparing PAAH depletion with and without alamethicin activation of microsomes.

CYP-catalysed metabolism of PAAH with alamethicin pre-treatment was assessed by incubation with HLM pre-treated for 30 minutes on ice with alamethicin (50 µg/mg) supplemented by NADPH generating system using the method described in Chapter 6.2.5.1. Incubation tubes contained PAAH (2 µM), pooled HLM (1 mg/mL) and NADPH generating system (50 µL) in a total volume of 200 µL. Analysis of samples was performed by HPLC using the conditions described in Chapter 6.2.4. The results are shown in Figure 2.8 as the percentage of control activity based on PAAH peak area.

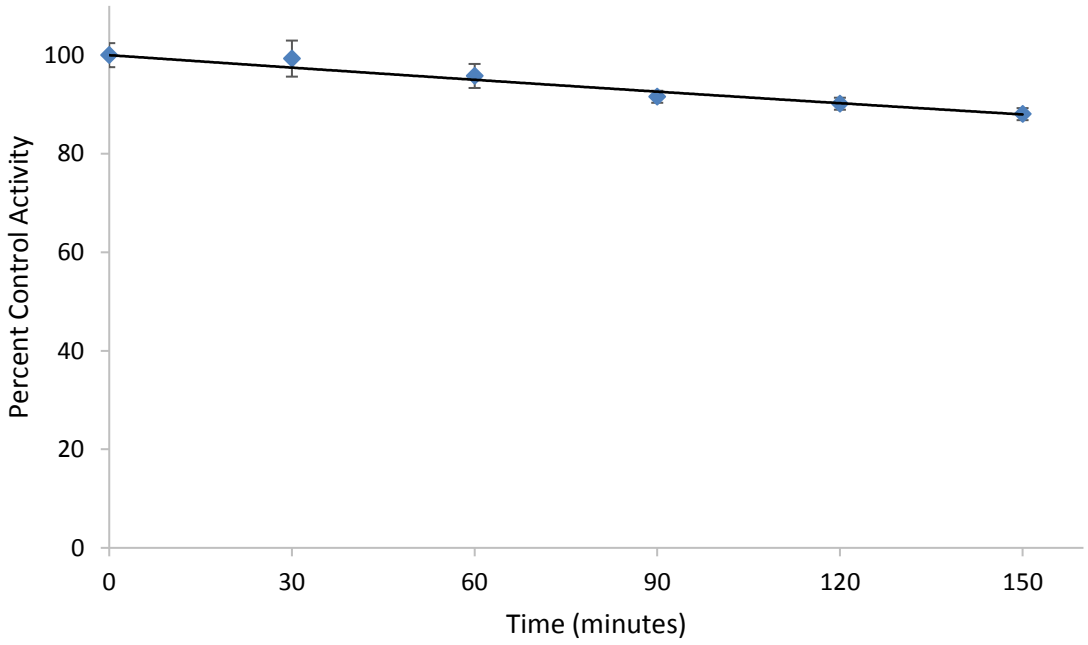

Figure 2.8: Incubation of PAAH with HLM, NADPH generating system and alamethicin. *Incubation samples contained PAAH (2 µM), HLM (1 mg/mL) pre-treated with alamethicin (50 µg/mg, for 30 mins on ice) and an NADPH generating system (50 µL) at pH 7.4. Incubations were performed at 37 °C for 150 minutes. Results are presented as the mean ± SD (n=4).*

Depletion of PAAH by incubations of HLM and NADPH, with (Figure 2.8) and without (Figure 2.6) alamethicin pre-treatment, were consistent with minor metabolism of PAAH by human liver microsomal CYP enzymes. Human liver microsomal CYPs depleted PAAH by approximately 10-15% over the 150 minute incubation period. Of note, there was less variability in the experiments, evidenced by lower standard deviation values, in the experiments with alamethicin-treated HLM.

2.2.5. UGT-mediated metabolism of PAAH

The extent of human liver microsomal UGT-catalysed PAAH glucuronidation was investigated by incubation in the presence of HLM supplemented with UDPGA using the method described in Chapter 6.2.5.1. Analysis of samples was performed by HPLC following the conditions described in Chapter 6.2.4. Results are shown in Figure 2.9 as the percentage of control activity based on PAAH peak area.

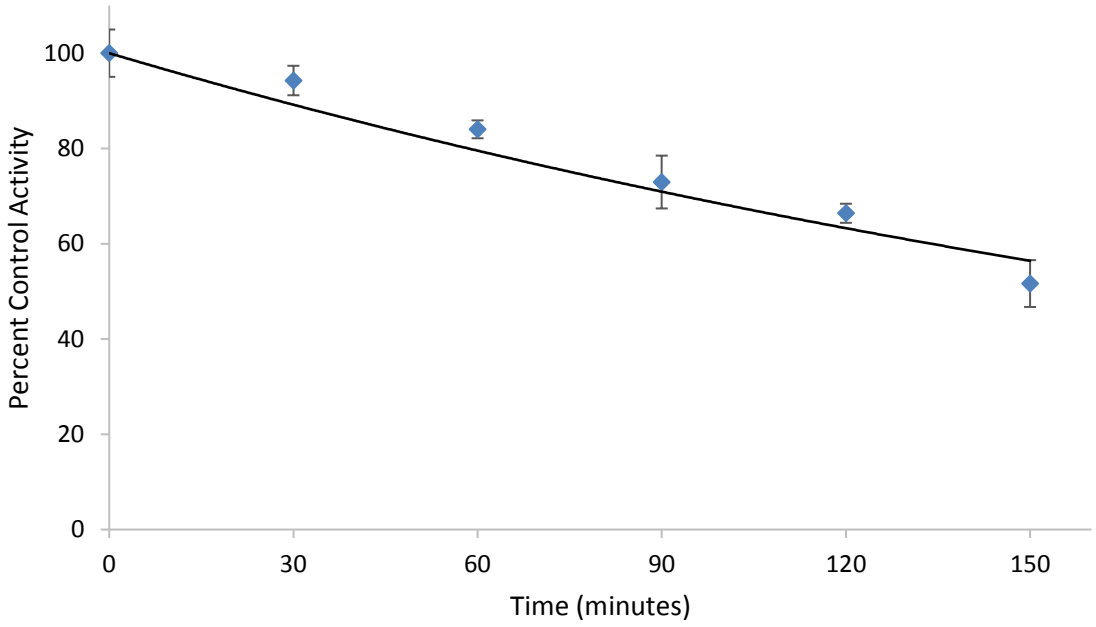

Figure 2.9: Incubation of PAAH with HLM and UDPGA. *Incubation samples contained PAAH (2 µM), HLM (1 mg/mL) pre-treated with alamethicin (50 µg/mg, for 30 mins on ice) and UDPGA (5 mM) at pH 7.4. Incubations were performed at 37 °C for 150 minutes. Results are presented as the mean ± SD (n=4).*

On average, the peak area of PAAH was observed to decrease by approximately 50% over the course of the experiment. Incubations were performed in quadruplicate and minor variance in the total substrate depletion was observed over time indicating reliability in the results. Compared to CYP metabolism, metabolism of PAAH by UGT enzymes was greater (described later in Section 2.2.9). Thus, it may be concluded that glucuronidation is likely to be a major metabolic pathway of PAAH.

2.2.6. Sulfotransferase (SULT) mediated metabolism of PAAH

The extent of sulfotransferase (SULT) mediated metabolism of PAAH was investigated using incubations of human liver cytosol (HLC) and 3'-phosphoadenosine 5'-phosphosulfate (PAPS), the co-factor required for sulfation, following the method described in Chapter 6.2.5.1. Analysis of samples was performed by HPLC using the conditions described in Chapter 6.2.4. Results are shown in Figure 2.10 as percentage of control activity based on PAAH peak area.

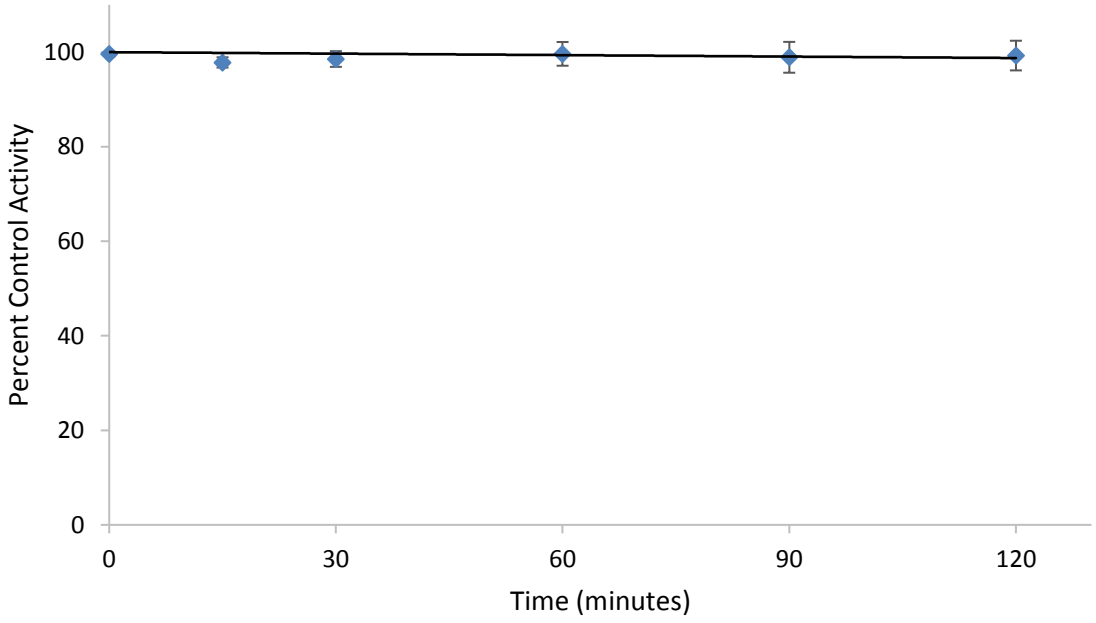

Figure 2.10: Incubation of PAAH with HLC and PAPS. *Incubation samples contained PAAH (2 μM), HLC (1 mg/mL) and PAPS (50 mM) at pH 7.4. Incubations were performed at 37 °C for 120 minutes. Results are presented as the mean ± SD (n=4).*

As demonstrated in Figure 2.10, no depletion of PAAH was observed by incubation with HLC and PAPS. HLC was used in place of HLM in these experiments as sulfotransferases are known to be more widely expressed in cytosolic fractions [109, 160] and as such were more suitable for experiments investigating SULT metabolism. Given that the concentration of PAAH was unchanged over the 120 minute incubation course it was concluded that sulfotransferases do not contribute significantly to the metabolism of PAAH.

Enzymes of the SULT family remain one of the least studied "major" enzyme families [109]. Part of the reason for this is that while SULT enzymes can sulfonate a broad range of substrates the extent of metabolism is typically far less than that of other enzyme families [160]. An *in vivo* examination of paracetamol metabolism by UGT and SULT enzymes by Reith et al. [161] reported that clearance of paracetamol by UGT enzymes occurred at approximately 70-times the rate of SULT clearance. Furthermore, the amount of SULT metabolite detected at 2 hours (the time course of the present study) was negligible compared to the amount of glucuronide metabolite. It is therefore possible that SULT metabolism of PAAH may occur, but the extent of metabolism is beyond the detection limits of the present experimental protocol.

2.2.7. Combined CYP and UGT mediated metabolism of PAAH

The effect of combined CYP- and UGT-catalysed PAAH depletion was investigated by incubation of HLM supplemented with both UDPGA and NADPH generating system using the method described in Chapter 6.2.5.1. Analysis of samples was performed by HPLC using the conditions as described in Chapter 6.2.4. Results are shown in Figure 2.11 as the percentage of control activity based on PAAH peak area.

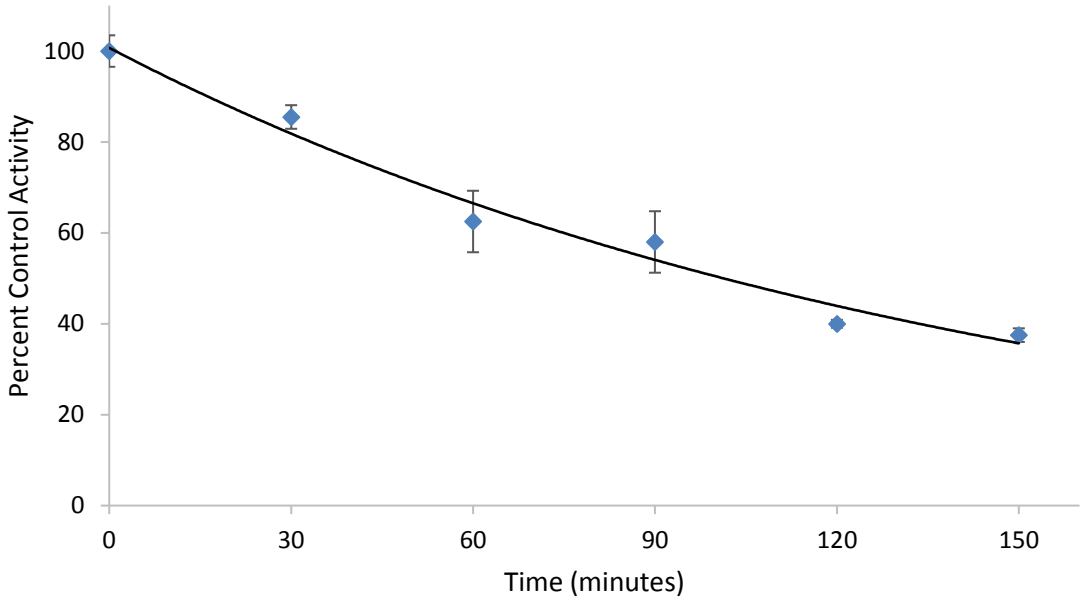

Figure 2.11: Depletion of PAAH with HLM, UDPGA and NADPH generating system. *Incubation samples contained PAAH (2 µM), HLM (1 mg/mL) pre-treated with alamethicin (50 µg/mg, for 30 mins on ice), UDPGA (5 mM) and an NADPH generating system (50 µL) at pH 7.4. Incubations were performed at 37 °C for 150 minutes. Results are presented as the mean ± SD (n=4).*

On average, the peak area of PAAH was observed to decrease by approximately 65% over the course of the experiment. As the depletion experiments were performed in the presence of both UDPGA and NADPH generating system, UGT and CYP enzymes are expected to be active in the system and as such higher depletion is expected. Comparison of the depletion observed in this experiment (~65% CYP+UGT) to those in the separate co-factor experiments (~15% CYP and ~50% UGT) revealed that the total depletion was approximately additive.

2.2.8. Summary of human hepatic enzyme depletion studies

The metabolism of PAAH by hepatic CYP, UGT and SULT enzymes, as the major xenobiotic metabolising enzyme families, were explored by incubations of PAAH with HLM and HLC in the presence of relevant enzyme cofactors. Substrate depletion was used to assess the contribution of CYP, UGT and SULT enzymes to PAAH metabolism. It was demonstrated that UGT-mediated glucuronidation is the major pathway of PAAH metabolism with HLM as the enzyme source, with a lesser contribution by CYP enzymes, and no observed contribution by SULT enzymes. The depletion observed with the combined CYP and UGT cofactors approximated the sum of the depletions determined in the presence of the individual cofactors. A summary of the total contributions of UGT and CYP enzymes is shown in Figure 2.12. As it was concluded that SULT enzymes had no observable role in PAAH metabolism the data from Section 2.2.6 was not included in this summary.

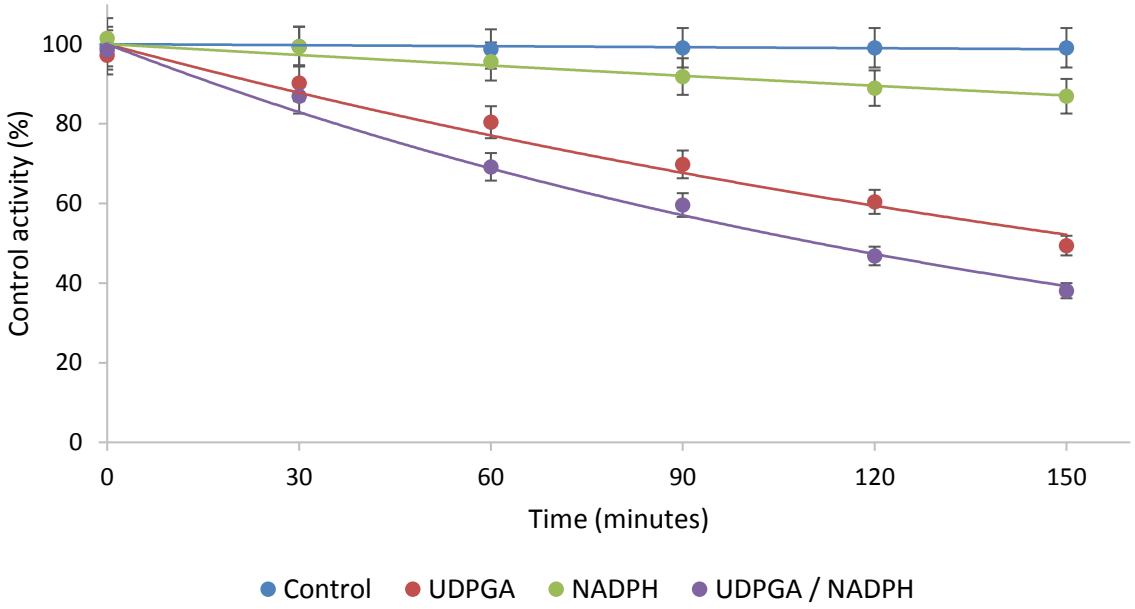

***Figure 2.12: Summary of PAAH depletion by HLM in the presence of enzyme cofactors**. The data was retrieved from Figure 2.2, Figure 2.8, Figure 2.9 and Figure 2.11. Results are presented as mean ± SD (n=4).*

2.2.9. Derived kinetic parameters and *in vitro* / *in vivo* extrapolation

Kinetic parameters for PAAH depletion in the presence of co-factors, including the elimination rate constant (k, minutes^{-1}), half-life ($t_{1/2}$, minutes) and intrinsic clearance (CL_{int}, µL/min.mg) were derived from depletion data reported in Sections 2.2.4, 2.2.5 and 2.2.7. These kinetic parameters, along with computationally derived physicochemical values and average values for physiological constants were then used to extrapolate *in vitro* findings to an *in vivo* parameter, hepatic clearance (CL_H) by application of the well-stirred model [162, 163].

Values of k were determined for each co-factor and used to calculate $t_{1/2}$ using Equation 2.1. Values of $t_{1/2}$ were then substituted into Equation 2.2 along with incubation volume (V_i, mL) and protein amount (M_p, mg) used in incubation experiments to determine CL_{int} values for depletion by HLM supplemented with each co-factor. The derived kinetic parameters are shown in Table 2.1.

Equation 2.1: Half-life

$$t_{1/2} = \frac{ln2}{k}$$

Equation 2.2: Intrinsic clearance

$$CL_{int} = \frac{ln2 \times V_i}{t_{1/2} \times M_p}$$

Table 2.1: Derived kinetic parameters for PAAH depletion by HLM and co-factors. *Results are reported as mean ± SD (n=4). Statistical significance is defined as *p or $^{\dagger}p < 0.05$ by Mann-Whitney U test.*

Co-factor	k (minutes^{-1})	$t_{1/2}$ (minutes)	CL_{int} (µL/min.mg)
UDPGA	0.0045 ± 0.0004	154 ± 12.2 †	4.51 ± 0.37 †
NADPH	0.0011 ± 0.0001	636 ± 41.6 *	1.09 ± 0.07 *
UDPGA / NADPH	0.0064 ± 0.0001	107 ± 2.12 * †	6.44 ± 0.13 * †

*p < 0.05 compared to UDPGA alone

†p < 0.05 compared to NADPH alone

CL_{int} was then scaled up from microsomal to whole hepatic clearance ($CL_{int,scaled}$) using average hepatic microsomal concentration (C_m, 32 mg/kg) [118] and average hepatic mass (M_H, 1,500 g) [119] using Equation 2.3. Derived parameters were obtained from Table 2.1. *In vitro - in vivo* extrapolation was performed by considering the case of metabolism by both CYP and UGT enzymes i.e. depletion with UDPGA and NADPH present, as major hepatic metabolising enzyme families. To achieve this, $CL_{int,scaled}$ was substituted into Equation 2.4 along with average hepatic blood flow (Q_H, 20.7 mL/min or 0.0207 L/min) and estimated fraction unbound of PAAH in blood (f_u, 0.03). The value of f_u for PAAH was estimated by SimCYP [164] with values of logP and pKa computationally determined by PhysChem History from ACD/Labs 12.0 [165]. By this method, the derived CL_H of PAAH was estimated as 1.25 L/hr.

Equation 2.3: Microsomal to hepatic scaling

$$CL_{int,scaled} = CL_{int} \times c_m \times M_H$$

Equation 2.4: Hepatic clearance

$$CL_H = \frac{Q_H \times f_u \times CL_{int,scaled}}{Q_H + f_u \times CL_{int,scaled}}$$

The *in vitro* CL_{int} for PAAH elimination by HLM in the presence of UDPGA was approximately 4-fold higher than the CL_{int} for HLM supplemented with NADPH. Taken together, these data indicate that the elimination of PAAH by glucuronidation accounts for approximately 80% of the total elimination resulting from glucuronidation plus CYP-catalysed oxidation. *In vitro-in vivo* extrapolation was employed to predict the hepatic clearance (CL_H) of PAAH. The mean microsomal CL_{int} for PAAH generated in the presence of UDPGA and NADPH (6.44 μL/min.mg, Table 2.1) was scaled to a whole liver CL_{int} using a human liver microsomal yield of 32 mg/kg [118] and a liver weight of 21.4 g/kg (i.e. 1500 g for a 70 kg person) [119]. The derived liver CL_{int} (309 mL/min, or 18.5 L/hr) was substituted into the equation for the well-stirred model of hepatic clearance to provide an *in vivo* CL_H of 1.25 L/hr. A contribution of enzymes other than CYP, UGT and SULT to PAAH metabolism cannot be discounted. Nevertheless, even a 10-fold underestimation of CL_H would still result in PAAH being classified as a "low" hepatic clearance compound (i.e. CL_H < 18 L/hr) [163].

2.2.10. Carboxylesterases involved in PAA hydrolysis

When considering which of the two major isoforms of carboxylesterases may be involved in the metabolism of an ester containing drug, there is a well-recognised pharmacophore that may be applied to predict the relevant isoform. The carboxylesterase pharmacophore simply relates to the ester moiety and considers the size of the acyl and alcohol portions of the ester [105, 107]. Figure 2.13 demonstrates how the acylic and alcoholic portions are defined.

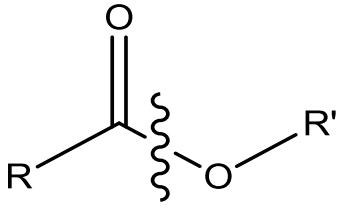

Figure 2.13: Scaffold of ester functional group. *Jagged line indicates the separation of acylic (left) and alcoholic (right) portions of the functional group.*

The carboxylesterase pharmacophore is such that hCES1 tends to favour substrates with a small alcoholic portion and larger acylic portion and hCES2 favours the converse situation. A number of carboxylesterase metabolised drugs are listed in Table 2.2 with their structures, highlighting the ester functionality and the carboxylesterase isoform known to preferentially hydrolyse the structure.

Table 2.2: Structures of human carboxylesterase substrates. *Ester functional groups are indicated by a dashed circle. Data was sourced from Parker et al. [166].*

Chemical name	Chemical structure	Major isoform
Oseltamivir	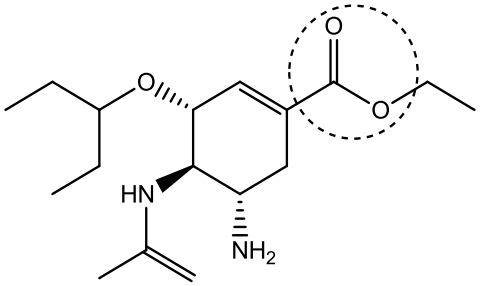	hCES1
Methylphenidate	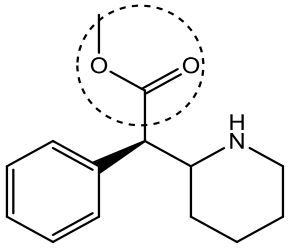	hCES1
Prasugrel	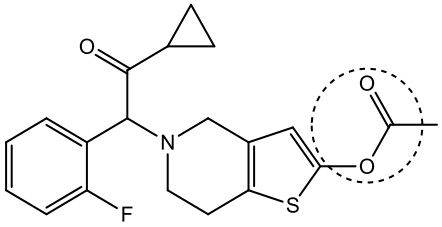	hCES2
Thebacon	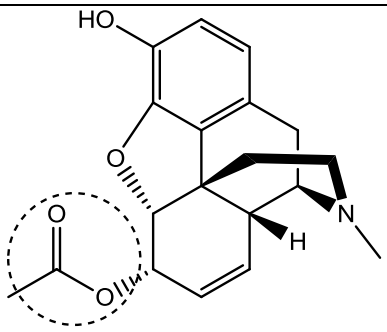	hCES2

The first two structures listed in Table 2.2, oseltamivir and methylphenidate are both hCES1 metabolised and contain smaller alcoholic portions, ethyl and methyl, respectively, compared to the rest of the molecule. The other two structures, prasugrel and thebacon however are preferentially metabolised by hCES2 and contain smaller ethyl acyl portions. The ester functionality in PAA is highlighted in Figure 2.14. It is evident that the smaller portion of the ester is the acyl portion, and it is therefore likely that PAA is metabolised by hCES2 in preference to hCES1.

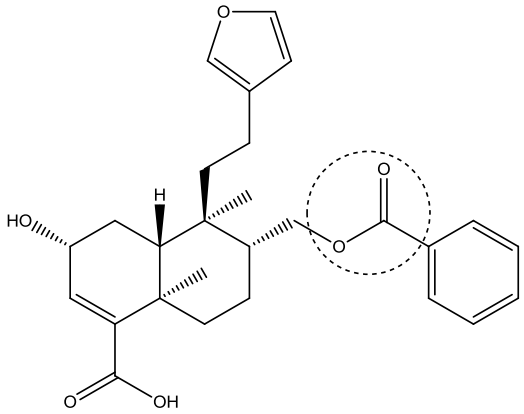

Figure 2.14: Structure of PAA with ester functionality highlighted.

2.2.11. CYP enzymes involved in PAAH metabolism

2.2.11.1. Reaction phenotyping using CYP enzyme selective inhibitors

Selective chemical inhibitors of CYP 1A2, 2B6/2C19, 2C8, 2C9, 2D6 and 3A4 were used to determine the CYP enzymes involved in the metabolism of PAAH by the method described in Chapter 6.2.6 followed by analysis of samples by HPLC using the conditions described in Chapter 6.2.4. The rationale for the use of selective chemical inhibitors is that addition of a selective enzyme inhibitor to an incubation of HLM mediated depletion of a drug will result in a reduction in depletion if the enzyme that is being inhibited is involved in metabolism of the drug. For example, the use of a selective CYP3A4 inhibitor will reduce the total depletion of a CYP3A4 substrate, but will have no effect on depletion of non-CYP3A4 substrates. If the enzyme is not involved in the metabolism of the drug, no significant difference will be observed between the incubation containing the specific inhibitor and the control.

Control experiments contained an equivalent volume of solvent used for dissolution of each inhibitor. The role of each enzyme in metabolism was established by significant ($*p < 0.05$) difference to control. Figure 2.15 shows the effect of a series of CYP selective inhibitors on the depletion of PAAH by HLM with NADPH present.

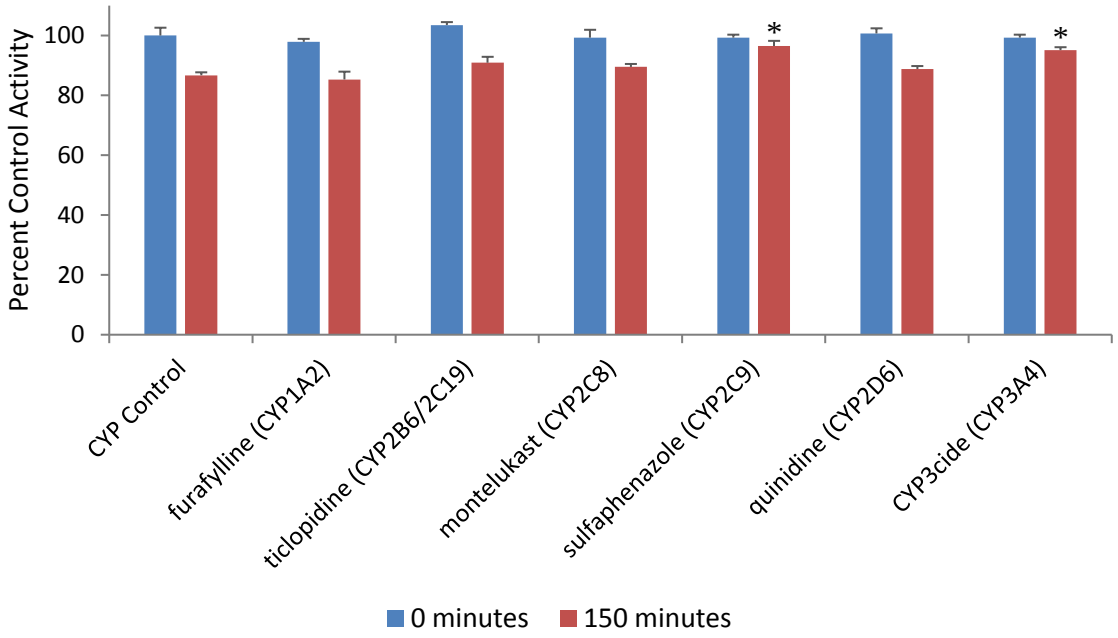

Figure 2.15: Effect of the use of enzyme inhibitors on total CYP depletion of PAAH. *Results are displayed as mean ± SD (n=4). Statistical significance is defined as *p < 0.05 as assessed by the Mann-Whitney U test.*

Of the chemical inhibitors used to assess PAAH depletion by CYP enzymes, two inhibitors were found to significantly inhibit PAAH metabolism, sulfaphenazole and CYP3cide. Sulfaphenazole (shown in Figure 2.16) is a selective inhibitor of CYP2C9 [167], therefore the significant inhibition of PAAH depletion by sulfaphenazole co-incubation suggested that CYP2C9 contributes to the total CYP-mediated metabolism of PAAH. CYP3cide (shown in Figure 2.16) is a selective inhibitor of CYP3A4 [168], therefore the significant inhibition of PAAH depletion by CYP3cide pre-incubation suggested that CYP3A4 also contributes to the total CYP-mediated metabolism of PAAH.

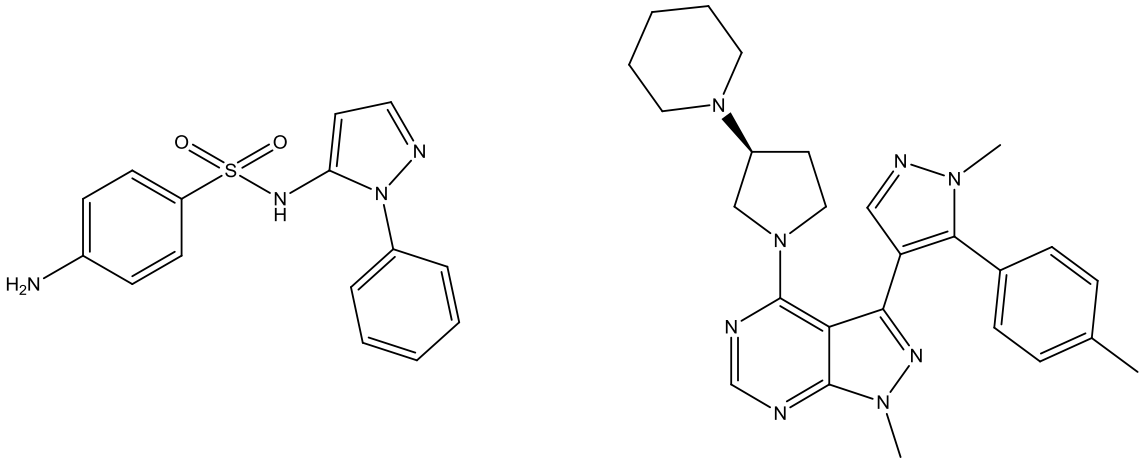

Figure 2.16: Structures of the selective CYP inhibitors sulfaphenazole (left) and CYP3cide (right).

2.2.11.2. Reaction phenotyping using recombinant CYP enzymes

Recombinant CYP 1A2, 2B6, 2C8, 2C9, 2C19, 2D6 and 3A4 were used to further assess the role of CYP enzymes in the metabolism of PAAH by the method described in Chapter 6.2.7 followed by analysis of samples by HPLC using the conditions described in Chapter 6.2.4. The rationale for using recombinant enzymes for this purpose was that any depletion of PAAH observed (versus control) would be attributable to the expressed enzymes present. Experiments were performed by incubation of PAAH with CYP enzyme transfected *E. coli*, prepared by the method of Elliot et al. [169]. Experiments were controlled by the use of untransfected *E. coli* membranes which resulted in no significant depletion after the incubation time period (See Figure 2.17). The role of each enzyme in metabolism was established by a significant ($*p < 0.05$) difference to control. Figure 2.17 shows the depletion of PAAH by seven CYP enzymes, as the percentage of control activity.

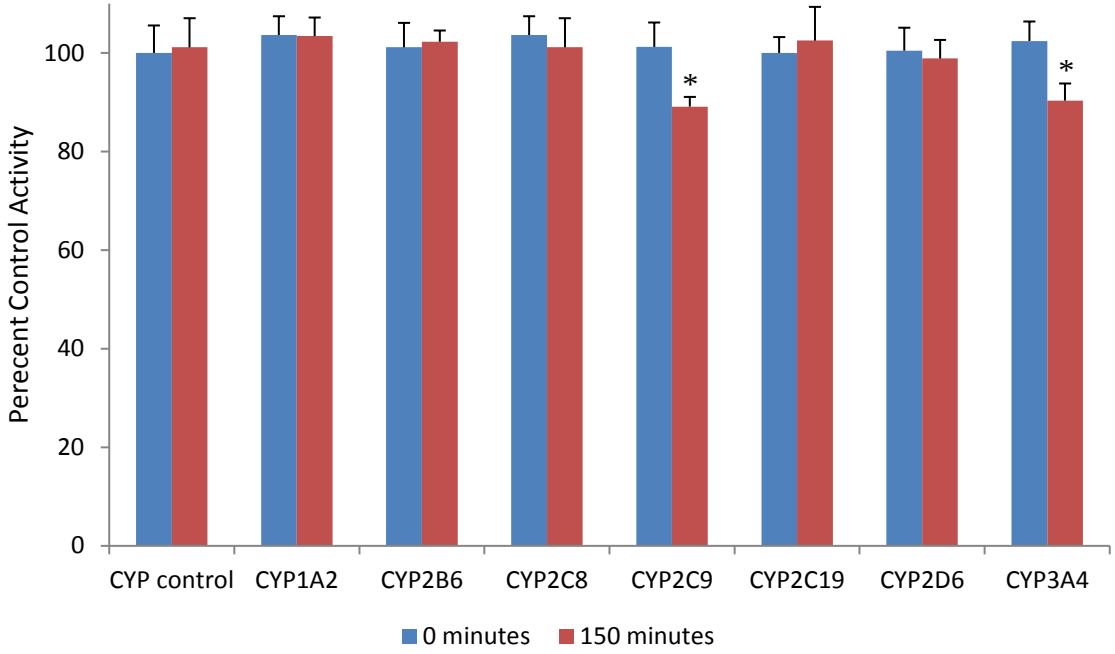

Figure 2.17: CYP mediated PAAH depletion attributed to recombinant CYP enzymes. *Results are displayed as mean ± SD (n=4). Statistical significance is defined as *p < 0.05 by Mann-Whitney U test.*

Of the recombinant enzymes used to assess CYP mediated metabolism of PAAH, two were found to possess significant metabolic activity by substrate depletion: CYP 2C9 and 3A4. Both of these enzymes are recognised to be widely expressed in hepatic tissues and are known to have an important role in the metabolism of many drugs and other xenobiotics [170-172]. While these enzymes have a significant abundance in various tissues, including the liver, and have been shown to be responsible for CYP-mediated PAAH depletion, the overall depletion of PAAH by CYP enzymes is relatively minor so their role may be concluded to be of less importance than other metabolic pathways.

2.2.12. UGT enzymes involved in PAAH metabolism

2.2.12.1. In silico examination of UGT enzymes

Prior to *in vitro* assessment, a knowledge-based *in silico* tool utilising physicochemical parameters was used to examine the UGT isoform selectivity (UGT 1A1, 1A9 and 2B7) of PAAH. This tool is based upon a set of physicochemical rules previously developed by Mr Steven Nguyen (as part of an honours thesis, described in Chapter 6.5.3, [173]). This tool was implemented with FILTER by OpenEye Scientific Software. Results of this analysis are summarised in Table 2.3.

Table 2.3: Knowledge-based predictions of PAAH metabolism by UGT enzymes.

UGT enzyme	Prediction*
UGT1A1	Pass
UGT1A4	Fail
UGT2B7	Pass

*based upon a ruleset developed by Mr Steven Nguyen [173].

Application of the FILTER rules suggested that PAAH may be a substrate of UGT 1A1 and 2B7. There are two sources of failure for PAAH in the UGT1A4 filter, specifically the rules:

RULE 0 carboxylic acid
RULE 1 phenol

PAAH fails this filter as the defined rules specify that there must be no carboxylic acids present, of which there is one in PAAH, and at least one phenol group, of which there are none in PAAH.

2.2.12.2. Selective UGT-enzyme inhibitor experiments

Chemical inhibitors of UGT 1A1, 1A4, 1A9 and 2B7 were used to determine the UGT enzymes involved in the metabolism of PAAH by the method described in Chapter 6.2.6 followed by analysis of samples by HPLC using the conditions described in Chapter 6.2.4. The rationale for the addition of a selective enzyme inhibitor to an incubation of HLM mediated depletion of a drug is that it will result in a reduction in depletion if the enzyme that is being inhibited is involved in metabolism of the drug. If the inhibited enzyme is not involved in metabolism of the drug, no significant difference will be observable between the inhibited incubation and control. Experiments were controlled by incubation of PAAH with HLM and a solvent vehicle analogous to the solvent vehicle used for each chemical inhibitor. The role of each enzyme in metabolism was established by significant (*$p < 0.05$) difference to control. Figure 2.18 shows the effect of a series of UGT selective inhibitors on the depletion of PAAH by HLM with UDPGA present.

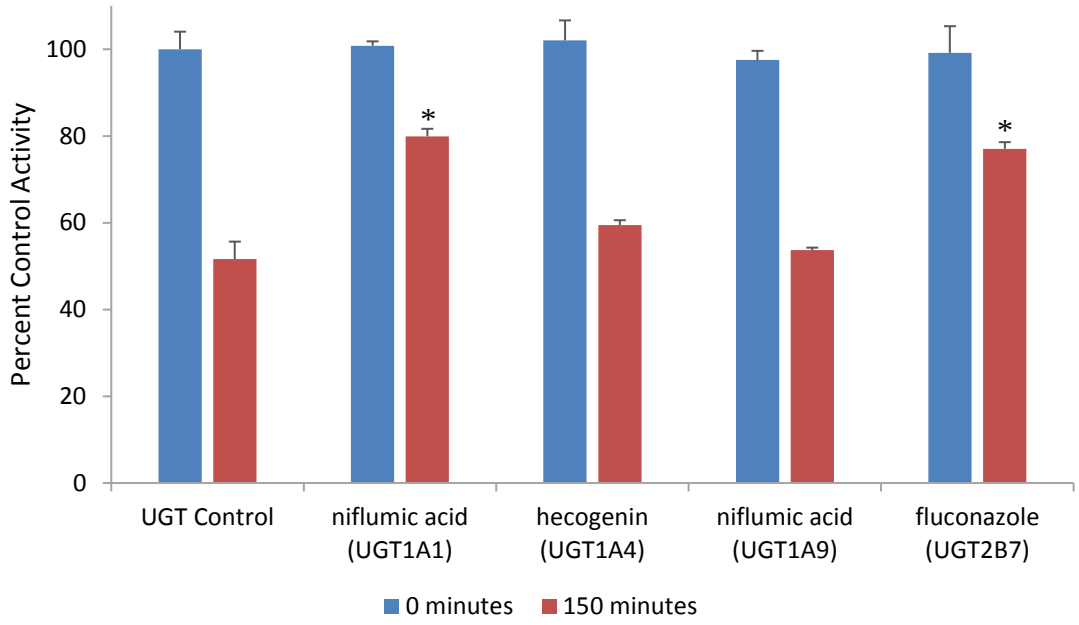

Figure 2.18: Effect of the use of enzyme inhibitors on total UGT depletion of PAAH. *Results are displayed as mean ± SD (n=4). Statistical significance is defined as *$p < 0.05$ by Mann-Whitney U test.*

Of the chemical inhibitors used to assess PAAH depletion by UGT enzymes, two inhibitors were found to significantly inhibit PAAH metabolism, niflumic acid (100 μM) and fluconazole. Niflumic acid (shown in Figure 2.19) is a selective inhibitor of UGT 1A1, 1A9 and 2B15 at a concentration of 100 μM [174], therefore the significant inhibition of PAAH depletion by HLM incubated with niflumic acid at this concentration suggested a potential role of any of these enzymes in the metabolism of PAAH. As niflumic acid only inhibits UGT1A9 at a concentration of 2.5 μM and no significant inhibition of depletion was observed after incubation of PAAH with niflumic acid at this concentration, it suggested that PAAH is likely not metabolised by UGT1A9. Fluconazole (shown in Figure 2.19) is a selective inhibitor of UGT2B7 [175], therefore the significant inhibition of PAAH depletion by HLM incubated with fluconazole suggested that both UGT 2B7 and 2B15 may fulfil a significant role in PAAH depletion.

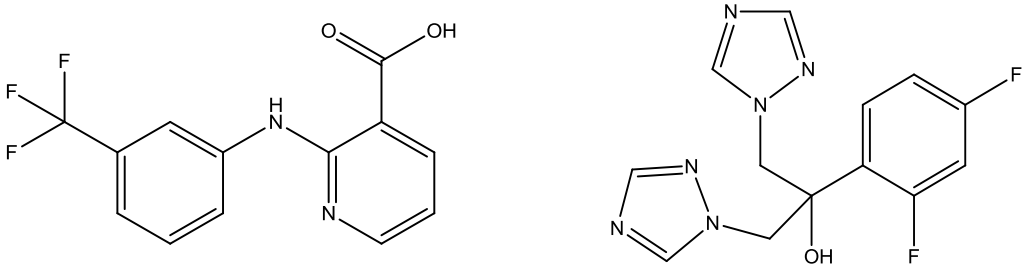

Figure 2.19: Structure of niflumic acid (left) and fluconazole (right).

2.2.12.3. Recombinant UGT-enzyme experiments

Recombinant enzymes of UGT 1A1, 1A3, 1A4, 1A6, 1A9, 2B4, 2B7, 2B9, 2B10, 2B15 and 2B17 were used to further assess the role of UGT enzymes in the metabolism of PAAH by the method described in Chapter 6.2.7 followed by analysis of samples by HPLC using the conditions described in Chapter 6.2.4. The UGT1A enzymes were expressed in human embryonic kidney (HEK293) cells using the method described by Bowalgaha et al. [176]. UGT2B enzymes expressed in HEK293 cells are known to possess lower metabolic activity *in vitro* [177] and as such supersomes of UGT2B enzymes were purchased from Corning Gentest (Clayton, Australia). Due to the different enzyme expression systems, separate control groups were used for UGT 1A and 2B enzymes, consisting of untransfected HEK293 cells and supersomes, respectively. Each control group resulted in no significant

depletion of PAAH as shown in Figure 2.20. The rationale for the use of recombinant enzymes for this purpose was that these individual recombinant UGT enzymes would be the only metabolic enzymes present in incubations, therefore any metabolic activity observed in the incubation would be attributed to the enzyme co-incubated with the drug. The role of each enzyme in metabolism was established by a significant (*$p < 0.05$) difference to control. Figure 2.20 shows the depletion of PAAH by five UGT1A enzymes and five UGT2B enzymes. The depletion is depicted as a percentage of control activity.

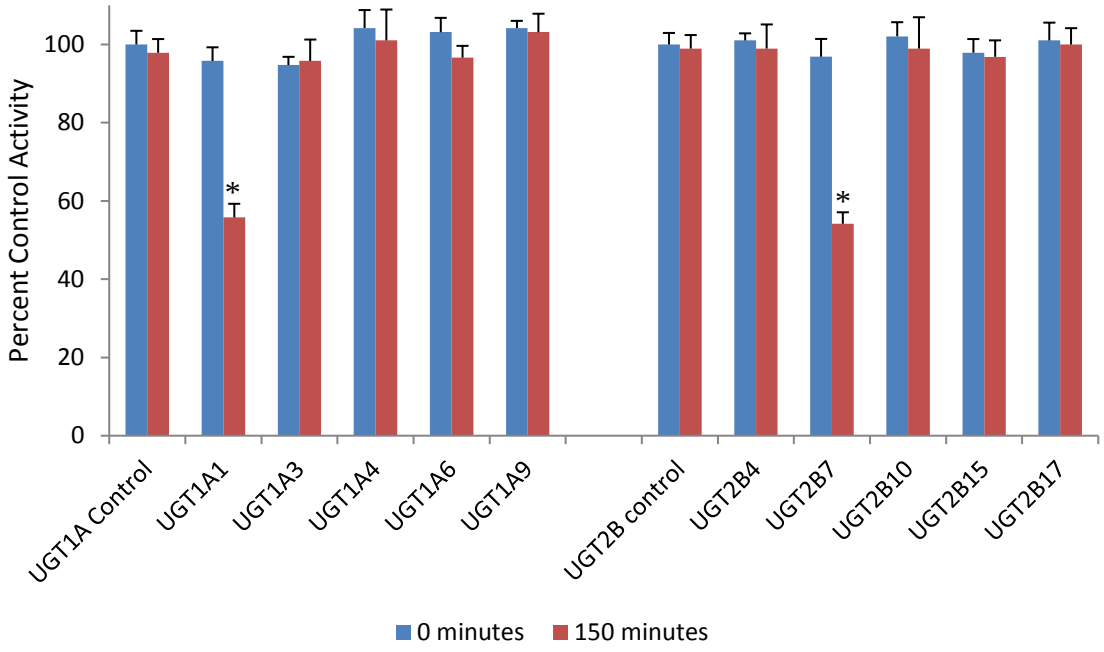

Figure 2.20: UGT mediated PAAH depletion attributed to recombinant UGT enzymes. *Results are displayed as mean ± SD (n=4). Statistical significance is defined as *$p < 0.05$ by Mann-Whitney U test.*

Of the recombinant enzymes used to assess UGT mediated metabolism of PAAH, two were found to possess significant metabolic activity by substrate depletion, UGT 1A1 and 2B7. Previously in Section 2.2.12.2 it was noted that the selective inhibitor fluconazole may indicate that UGT 2B7 and 2B15 are involved in metabolism of PAAH, but the use of recombinant UGT2B15 enzymes revealed no significant activity. Both, UGT 1A1 and 2B7 are recognised to be widely expressed in hepatic tissue and are known to possess an important role in the metabolism of many xenobiotics [170]. As both of these enzymes are

found in liver tissue in great abundance and have been demonstrated to significantly deplete PAAH, it is likely that UGT 1A1 and 2B7 may play a significant role in the human metabolism of PAAH.

2.2.13. Summary of specific enzyme contributions

The contribution of individual UGT and CYP enzymes was characterised using reaction phenotyping methods with enzyme selective inhibitors and recombinant enzymes. UGT mediated depletion of PAAH by HLM was inhibited by addition of the inhibitors fluconazole, a relatively selective inhibitor of UGT2B7 [175], and niflumic acid, an inhibitor of UGT1A9 that also exhibits inhibitory activity of UGT 1A1 and 2B15 at higher concentrations [178]. Significant inhibition of human liver microsomal PAAH glucuronidation occurred only at the higher niflumic acid concentration (100 μM), suggesting involvement of UGT 1A1 or 2B15 but not 1A9. Incubation of PAAH with recombinant enzymes provided further clarification of these data by demonstrating significant depletion of PAAH by recombinant UGT 1A1 and 2B7, but not UGT 1A9 and 2B15. Taken together, these data indicate that UGT 1A1 and 2B7 are responsible for human hepatic PAAH glucuronidation. Similarly to PAAH, belinostat, a histone deacetylase inhibitor, has been demonstrated to also exhibit glucuronidation by UGT 1A1 and 2B7, however while the extent of metabolism of PAAH was approximately equal between each enzyme, UGT1A1 has a major role in the glucuronidation of belinostat [179].

CYP mediated depletion of PAAH by HLM was inhibited by CYP3cide, a CYP3A4 selective inhibitor [168], and sulfaphenazole, a CYP2C9 selective inhibitor [167]. Incubation of PAAH with recombinant CYP enzymes provided further support for this observation, demonstrating significant depletion by CYP 3A4 and 2C9 but not by other CYP enzymes. Previous studies have demonstrated an important role of CYP3A4, and a trace role of CYP2C9, in the oxidation of furan rings in substrates [180, 181].

Given the contributions of UGT2B7 and CYP2C9 to hepatic PAAH metabolism, it is likely that the determined hepatic clearance value (1.25 L/hr) underestimates the true hepatic clearance due to the inhibitory effects of long-chain unsaturated fatty acids released

from the microsomal membrane during the course of an incubation [182, 183]. As a majority of total PAAH metabolism was conducted by just a few enzymes (UGT 1A1 and 2B7, and CYP 2C9 and 3A4), there may be a heightened risk of drug-drug interactions as a result of co-administration of other drugs and certain foods [170, 184, 185]. As CYP-mediated metabolism of PAAH was found to be a minor pathway compared to UGT-mediated metabolism there may be less impact by inhibitors of CYP 2C9 and 3A4, as a majority of metabolism is likely to be carried out by UGT enzymes. Conversely, this may raise the risk of interactions if co-administered with an inhibitor of UGT 1A1 or 2B7 as it may lower the total rate of PAAH metabolism and slow clearance of the drug. Coupled with the already slow hepatic clearance of PAAH as established previously this could pose risks to an individual and may require specific investigation prior to any clinical use.

2.2.14. Identity of UGT metabolites

2.2.14.1. In silico examination of glucuronide metabolites

Prior to *in vitro* investigations of PAAH glucuronide metabolites, various *in silico* methods were employed to predict the potential metabolites that may be detected. To investigate the potential structures of glucuronide metabolites of PAAH, three knowledge-based *in silico* models were employed, XenoSite, MetaPred and SomUGT [186-188].

XenoSite was used via an online webserver, by the method described in Chapter 6.5.2, as an *in silico* method of predicting sites of UGT-mediated metabolism. A SMILES string of PAAH, with specified stereochemistry, was submitted to XenoSite for analysis against predictive models of UGT enzymes. A graphical output of the results of the XenoSite analysis are shown in Figure 2.21.

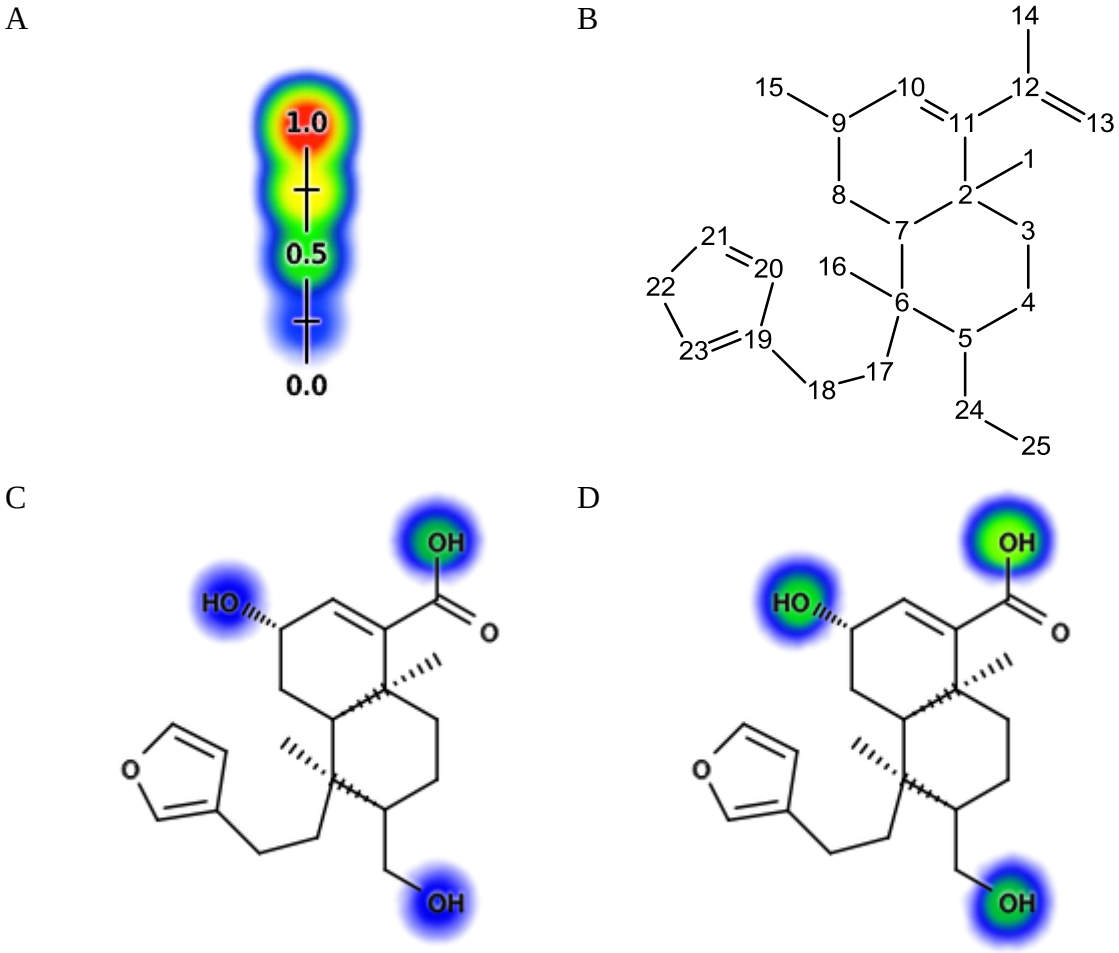

Figure 2.21: XenoSite predicted site of metabolism of PAAH by UGT enzymes in HLM. *(A) Colour scale denoting probability of metabolism. Colour scale ranges from high probability (red, 1) to low probability (uncoloured, 0) (B) XenoSite defined numbering system for PAAH. (C) Colour coded heuristic UGT prediction (D) Colour coded XenoSite UGT prediction.*

Based on the XenoSite output, shown in Figure 2.21, the sites most highly predicted to be subjected to glucuronidation by UGT enzymes were sites 14, 15 and 25 (s14, s15 and s25). The predictive values for each site were 0.44, 0.27 and 0.27 respectively for the heuristic model and 0.62, 0.47 and 0.46 respectively for the XenoSite model, with no other values of note. The heuristic model is defined by Dang et al. [186] as a simple model for identifying UGT substrates based on database statistics of known glucuronide substrates. The XenoSite UGT model is defined as an adaptation of the XenoSite CYP model and an

extension of the heuristic model providing higher precision predictions of UGT substrates, especially atypical glucuronide substructures formed from ketones, thiols and amides. The predictions of each mode resulted in three predicted metabolite structures; of the acyl group and both hydroxyl groups. The acyl group was highlighted as being a more probable site of metabolism than either hydroxyl group and furthermore, each hydroxyl was found to be approximately equivalent in both models. The probabilities of metabolism of each predicted site of metabolism were approximately 0.20 units higher for the XenoSite model of prediction than the heuristic model, in good agreement with the claim from Dang et al. [186] suggesting that XenoSite UGT offered higher predictive scores than the heuristic model. Based on this analysis by XenoSite UGT, it was predicted that up to three glucuronide metabolites may be formed and the acyl glucuronide was predicted most strongly, suggesting that the acyl glucuronide may form more readily than either hydroxyl glucuronide.

To perform site of metabolism analysis of PAAH by MetaPred, a SMILES string of PAAH, with specified stereochemistry, was submitted to the online webserver against a predictive model of UGT site of metabolism. The results of MetaPred analysis, including enumerated structure of PAAH and rankings of sites by ΔP, referring to a shift in probability from random, is shown in Figure 2.22.

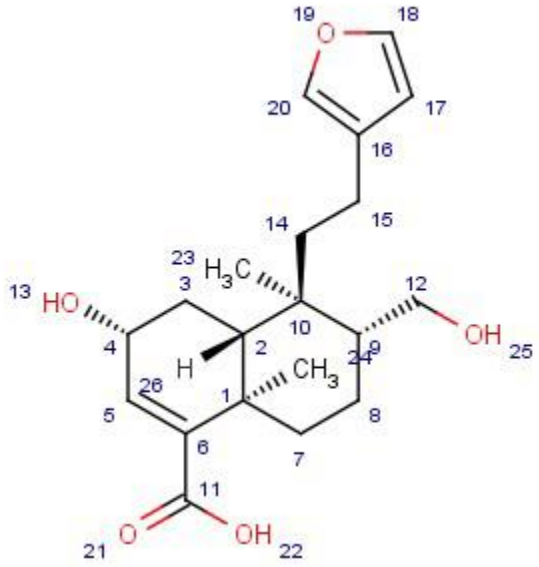

Rank	Atom Number	ΔP
1	13	0.180
2	22	0.135
3	25	0.134
4	10	-0.756
5	1	-0.710
6	9	-0.702
7	16	-0.644
8	17	-0.589
9	2	-0.581

Figure 2.22: MetaPred Web Server prediction results of PAAH metabolism by UGT enzymes. *Inset table shows ΔP values of the top 9 ranked sites predicted for metabolism.*

The value of ΔP is calculated from structural properties including constitutional and topological descriptors, eigenvalues, functional groups, and molecular properties. The ΔP value of an atom calculated in MetaPred specifies that a ΔP < 0.000 is essentially random, or not predicted to be metabolised while a ΔP > 0.000 – 1.000 is a predicted site of metabolism with ΔP = 1.000 representing a perfect prediction. Accordingly, a cut-off value of ΔP < 0.000 was used as a predictor of metabolism probability at enumerated sites of PAAH with higher values equating with stronger predictions. Of these sites, three were predicted as potential sites of glucuronidation by MetaPred, O13, O22 and O25. These sites correspond with the two hydroxyl groups in PAAH (O13, in proximity to the carboxyl group, and O25, in proximity to the furan ring) and the carboxyl group of PAAH (O22). While the ΔP values of each site are low, the values are still positive indicating some likelihood of metabolism. Furthermore, the low values of ΔP may not necessarily be caused by the sites having a low-probability of being sites of metabolism, but may be a characteristic of PAAH being structurally diverse in respect to the training set of molecules used to define the MetaPred scoring algorithm. Both hydroxyl and carboxyl groups are known to be vulnerable to glucuronidation by UGT enzymes, therefore the prediction that PAAH may undergo glucuronidation at the sites defined by MetaPred is not unreasonable.

The site of metabolism prediction software SomUGT was used to assess sites of metabolism in PAAH vulnerable to glucuronidation. As the output of SomUGT is a binary, non-graphical designation of positive/negative (i.e. 1, positive and 0, negative) indications for each heavy atom, the results have been summarised in Figure 2.23.

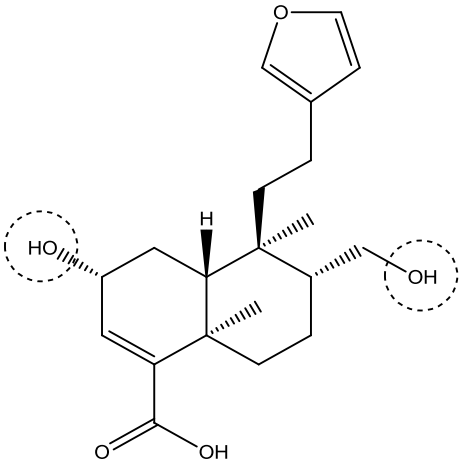

Figure 2.23: SomUGT prediction of glucuronidation sites in PAAH. *Predicted sites have been highlighted by dotted circles.*

SomUGT predicted two sites of metabolism in PAAH: the two hydroxyl moieties. In contrast to the output of XenoSite and MetaPred, the carboxylic acid of PAAH was not predicted as a site of metabolism by SomUGT.

The use of *in silico* techniques in this assessment involved three prediction algorithms: XenoSite, MetaPred and SomUGT. All three algorithms predicted the alcoholic functionalities of PAAH to be glucuronidated, but only XenoSite and MetaPred predicted the acyl functionality to be metabolised. While SomUGT only provided a binary value to distinguish predictions, XenoSite and MetaPred included a scoring metric to provide probabilistic context to the predictions. On this note, XenoSite scored the probability of functional groups in PAAH being glucuronidated higher than MetaPred, particularly in the case of the acyl group which was scored higher than the alcoholic groups of PAAH by XenoSite. The XenoSite model (2016) was built using almost 3,000 unique substrates containing over 4,000 glucuronidation reactions, which has been reported to use approximately 3-times more reactions than in any previously reported UGT metabolism

model [187], including MetaPred (2010). Further analysis of these scoring algorithms may be made following *in vitro* analysis of glucuronide metabolites of PAAH.

2.2.14.2. HPLC detection and characterisation of glucuronide metabolites

Initial *in vitro* investigation of glucuronide metabolites was performed by HPLC analysis of glucuronidated samples. Comparison of UDPGA co-incubated samples to control incubations revealed the presence of a peak at a retention time of 3.129 minutes predicted to be a glucuronide metabolite. Further HPLC analysis of this peak revealed that formation of the peak was both time and co-factor dependent, suggesting that the peak was representative of a glucuronide metabolite, as shown in Figure 2.24.

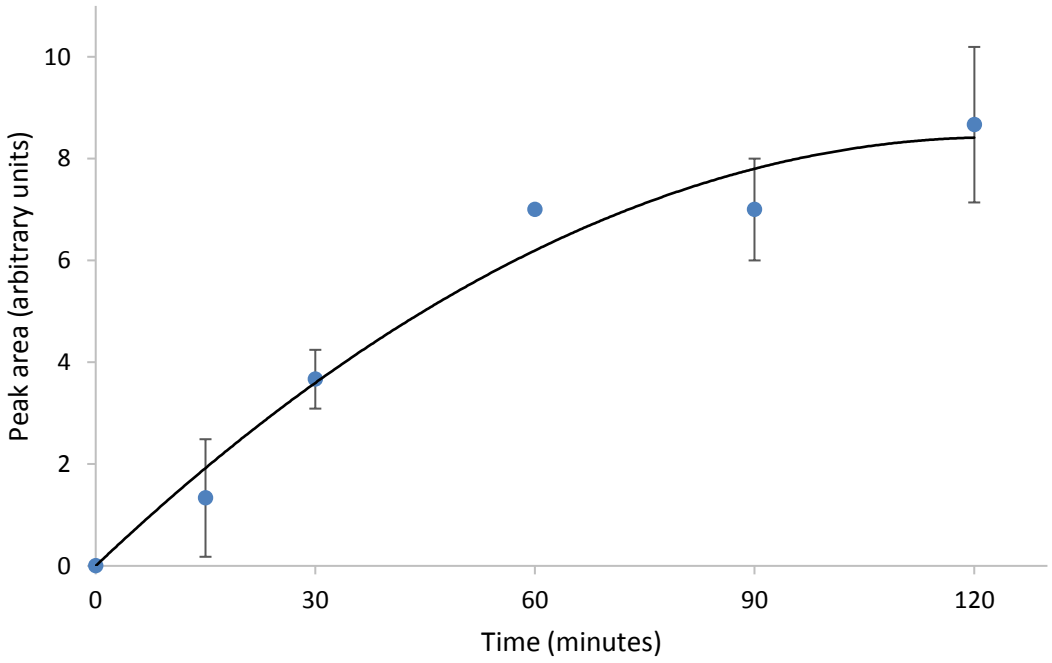

Figure 2.24: Formation of metabolite over time by incubation of PAAH with UDPGA. *Data was collected from HPLC analysis. Incubation samples contained PAAH (2 μM), HLM (1 mg/mL), alamethicin (50 μg/mg) and UDPGA (50 mM) at pH 7.4. Incubations were performed at 37 °C for 120 minutes. Results are presented as the mean ± SD (n=4).*

Additional *in vitro* analysis of this metabolite peak was pursued by secondary incubation of UDPGA-incubated samples with β-glucuronidase (2,000 IU), an enzyme

known to catalyse the hydrolysis of glucuronides both *in vitro* and *in vivo*, by the method described in Chapter 6.2.9.1. The predicted glucuronide metabolite peak was diminished entirely within 30-minutes of incubation with β-glucuronidase, and therefore it was concluded that the peak present after incubation of PAAH with UDPGA was representative of a glucuronide metabolite.

2.2.14.3. UPLC/MS detection and characterisation of glucuronide metabolites

Although it was determined by HPLC that PAAH was metabolised in the presence of UDPGA by HLM (Section 2.2.5), only a single metabolite was detected. As *in silico* analysis predicted that two, or perhaps three, glucuronide metabolites of PAAH may be produced (Section 2.2.14.2), further analysis utilising UPLC/MS was employed to determine the nature of the metabolite(s) and suggest a structure for the metabolite(s).

Analysis of samples analogous to those described in Section 2.2.14.2 was conducted by UPLC/MS using the system described in Chapter 6.2.10. Screening of the mass of PAAH (*m/z* 347.19) revealed two distinct peaks, one minor and one major, at retention times (RT) 1.46 and 2.75 minutes, respectively (Figure 2.25A). Screening of the mass of PAAH-glucuronide (*m/z* 523.22) revealed three distinct peaks, two minor and one major, at RT 0.99, 1.14 and 2.75 minutes (Figure 2.25B).

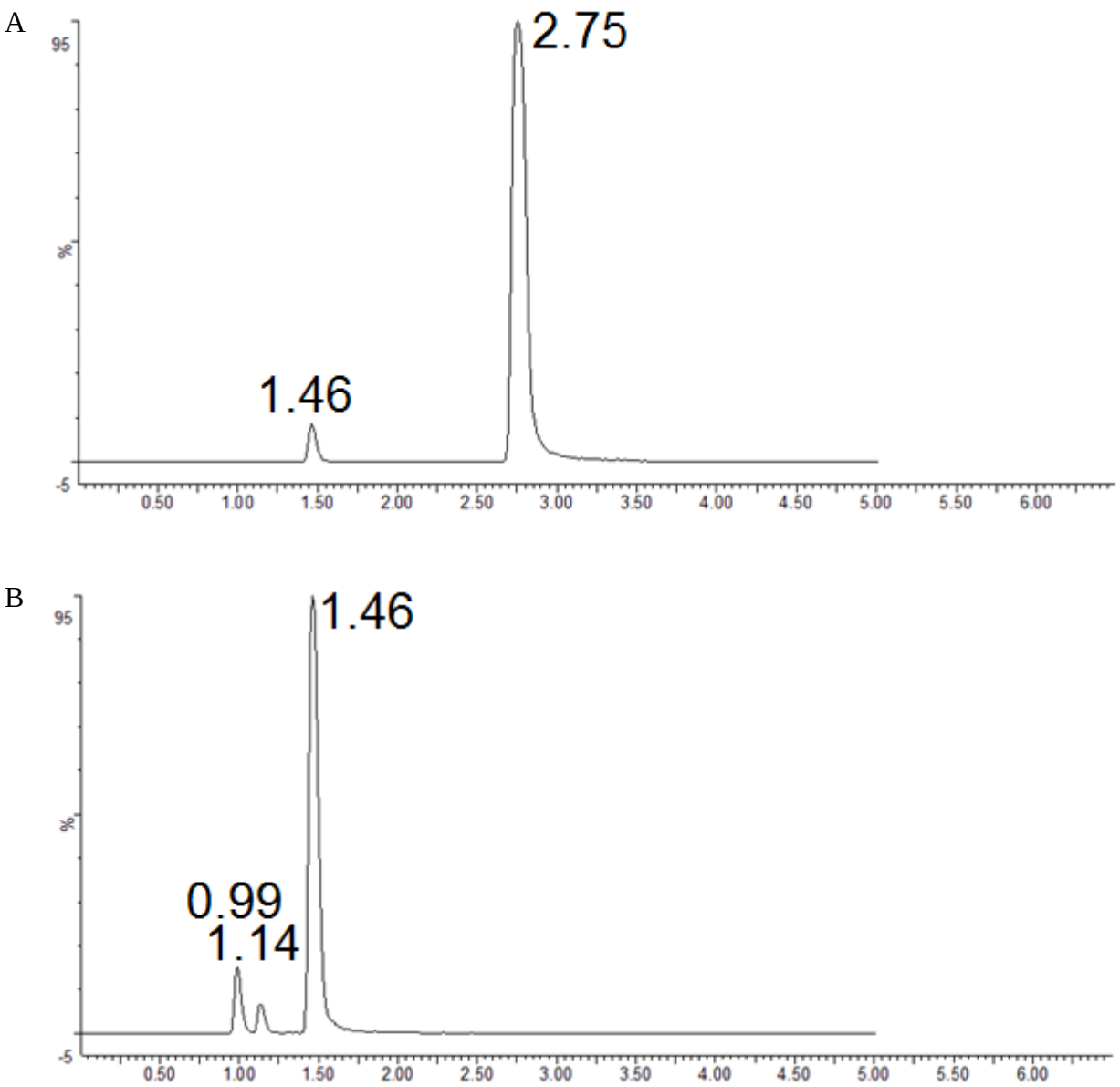

Figure 2.25: UPLC/MS chromatograms of (A) PAAH (m/z 347.19) and (B) PAAH-glucuronide (m/z 523.22). *Y-axis units are displayed as percentage of comparative abundance. X-axis units are displayed as time in minutes.*

The presence of two peaks in the "parent mass" chromatogram (Figure 2.25A) was unexpected, but as a larger peak appears at the same RT in the "glucuronide mass" chromatogram (Figure 2.25B), the presence of this second smaller peak may be a result of dissociation of the glucuronide moiety resulting in a secondary appearance of a "parent mass" peak. It is possible that small dissociation peaks may also be present at the RTs of 0.99 and 1.14 minutes, however as the peaks in the "glucuronide mass" chromatogram are

relatively minor, the associated peaks in the "parent mass" chromatogram may be too small to detect against background noise.

To further observe the proposed glucuronide metabolite peaks, UPLC conditions were altered (32.5% ACN, 0.1% formic acid and H_2O to 35% ACN, 0.1% formic acid and H_2O) to marginally increase the RT of PAAH-glucuronide metabolites, and provide greater resolution between the two minor peaks. The new RT of PAAH-glucuronide peaks are shown in Figure 2.26.

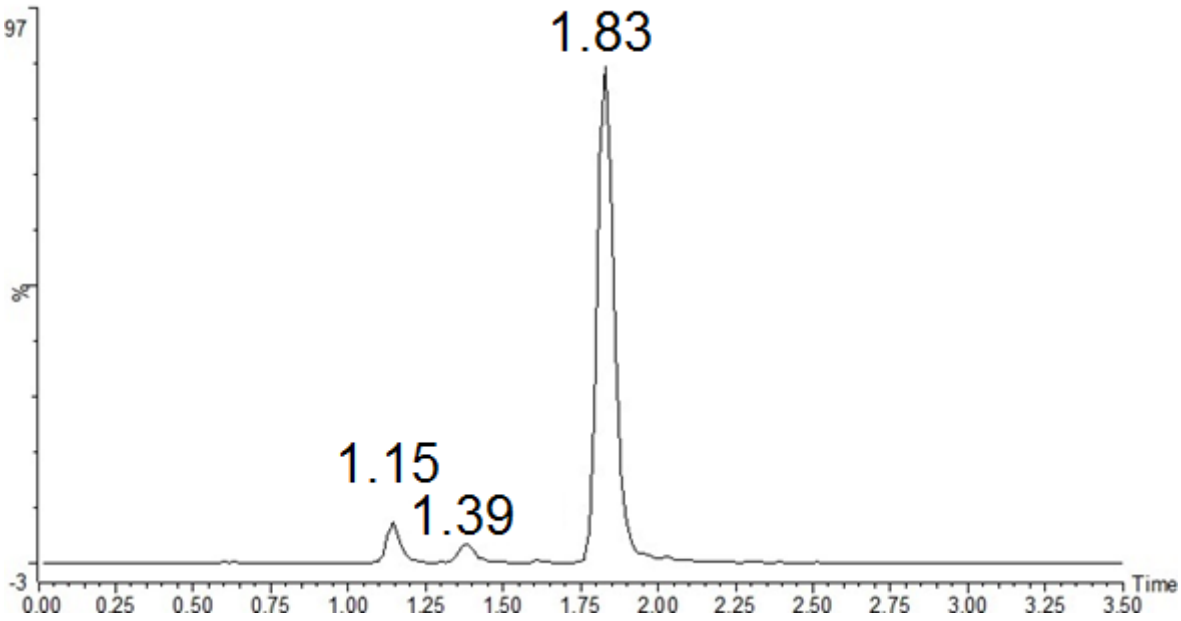

Figure 2.26: UPLC/MS chromatogram of PAAH-glucuronide metabolites filtered by mass at m/z 523.22. *Y-axis units are displayed as percentage of comparative abundance. X-axis units are displayed as time in minutes.*

Three metabolites were isolated by UPLC/MS in contrast to the singular peak observed by HPLC analysis, most likely as a result of the increased sensitivity and resolution of the UPLC/MS instrument. Further hydrolysis experiments were used to attempt to distinguish and characterise the peaks. Firstly, β-glucuronidase (2,000 IU) was used to hydrolyse glucuronidated samples analogous to the method of Section 2.5.1.2 to confirm that the three peaks isolated at mass *m/z* 523.22 are glucuronides. A chromatogram of this MS analysis is shown in Figure 2.27.

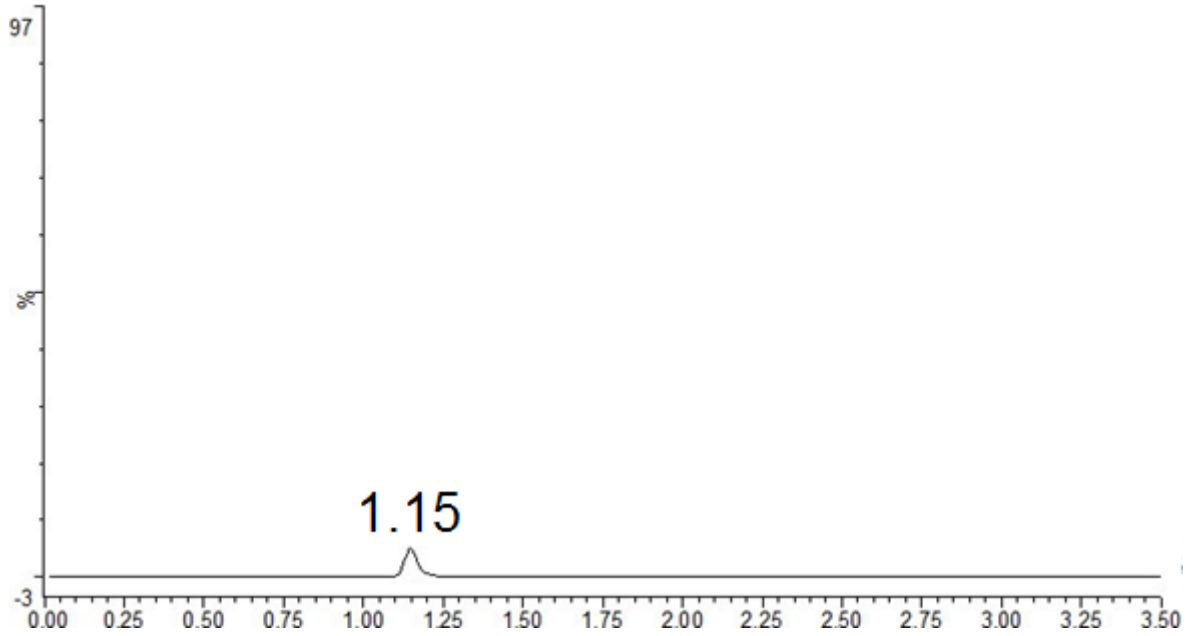

Figure 2.27: UPLC/MS chromatogram of PAAH-glucuronide metabolites filtered by mass at m/z 523.22 after incubation with β-glucuronidase. *Y-axis units are displayed as percentage of comparative abundance. X-axis units are displayed as time in minutes.*

Comparison of the chromatograms presented in Figure 2.26 and Figure 2.27, of the three peaks corresponding to the mass of PAAH-glucuronide, showed two were diminished entirely by β-glucuronidase incubation. These results suggested that at least two of the peaks (RT 1.39 and 1.83 minutes) were likely glucuronide metabolites, and the third peak (RT 1.15 minutes) was either not a glucuronide or was resistant to β-glucuronidase hydrolysis as is the case for some glucuronide drug metabolites [189].

Analysis of the MS fragmentation spectra for the two minor peaks (RT 1.15 and 1.39 minutes, see Appendix 1), revealed that the fragmentation patterns were nearly identical for both peaks and as such both peaks are likely to correspond to a similar molecule i.e. a glucuronide molecule, and therefore the latter case of β-glucuronidase resistance is more likely for the 1.15 minute peak. Furthermore, analysis of the MS fragmentation spectra of the major peak (RT 1.83 minutes, see Appendix 1) was significantly different to the spectra of the minor peaks, suggesting that of the three PAAH-glucuronide metabolites present, two of them are likely to be the same type of metabolite i.e. alcoholic glucuronides. This observation seemed to conform to the *in silico* predictions made in Section 2.2.14.1 that

PAAH may form up to three glucuronides metabolites, two alcoholic glucuronides and one acyl glucuronide. This analysis of spectra would suggest that the identity of the major metabolite (RT 1.83 minutes) corresponds to an acyl glucuronide, but further analysis would be required to confirm this.

To test the hypothesis that the major metabolite of PAAH was an acyl glucuronide a different method of chemical hydrolysis was employed utilising incubation with a weak base by the method described in Chapter 6.2.9.2. This method of hydrolysis is based on the well-recognised principle that acyl glucuronides are uniquely sensitive, amongst other types of glucuronide metabolites, to hydrolysis under weak alkaline conditions [190]. As such, glucuronidated samples of PAAH were subjected to incubation with 0.1 M NaOH and analysed by UPLC/MS at a specific mass of *m/z* 523.22. A chromatogram of these results is shown in Figure 2.28.

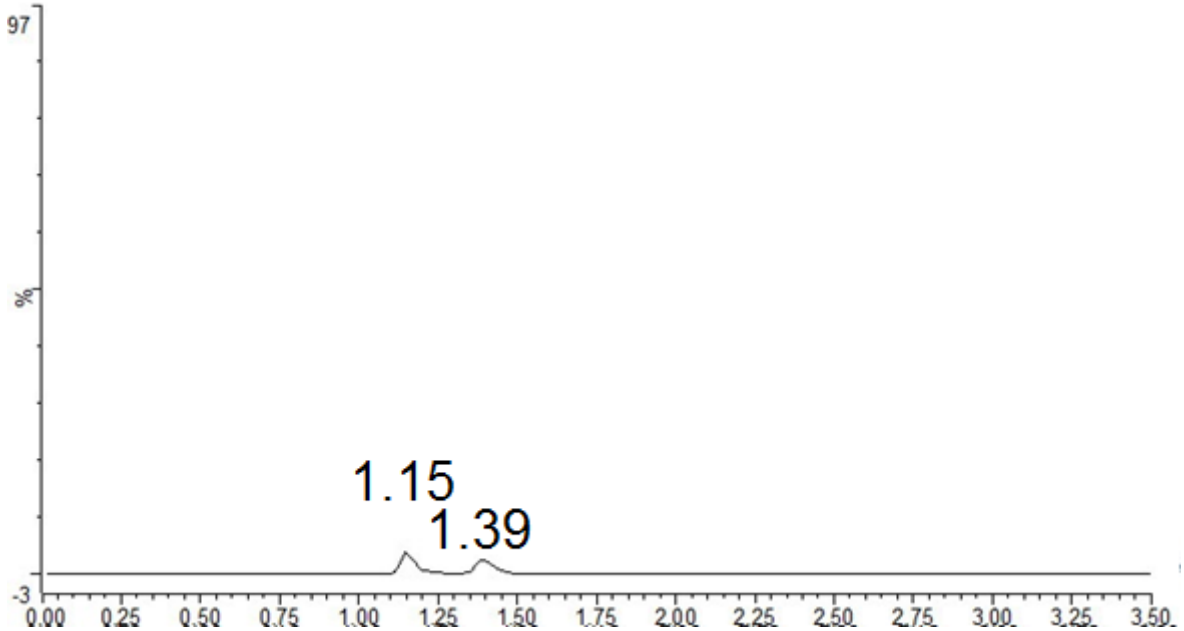

Figure 2.28: UPLC/MS chromatogram of PAAH-glucuronide metabolites filtered by mass at m/z 523.22 after incubation with weak base. *Y-axis units are displayed as percentage of comparative abundance. X-axis units are displayed as time in minutes.*

After incubation under weak alkaline conditions, the major peak (RT 1.83 minutes) was diminished entirely while the two minor peaks were not diminished (shown in Figure 2.28). Based on the previously mentioned propensity for acyl glucuronides to be

hydrolysed spontaneously in weak alkaline conditions, these results suggested that the identity of the major glucuronide metabolite of PAAH was that of an acyl glucuronide. This also suggested that the two remaining glucuronide metabolites detected in incubation samples were alcoholic glucuronides located at the C2 (marked as **2**) and C17 positions (marked as **3**) of PAAH (shown in Figure 2.29).

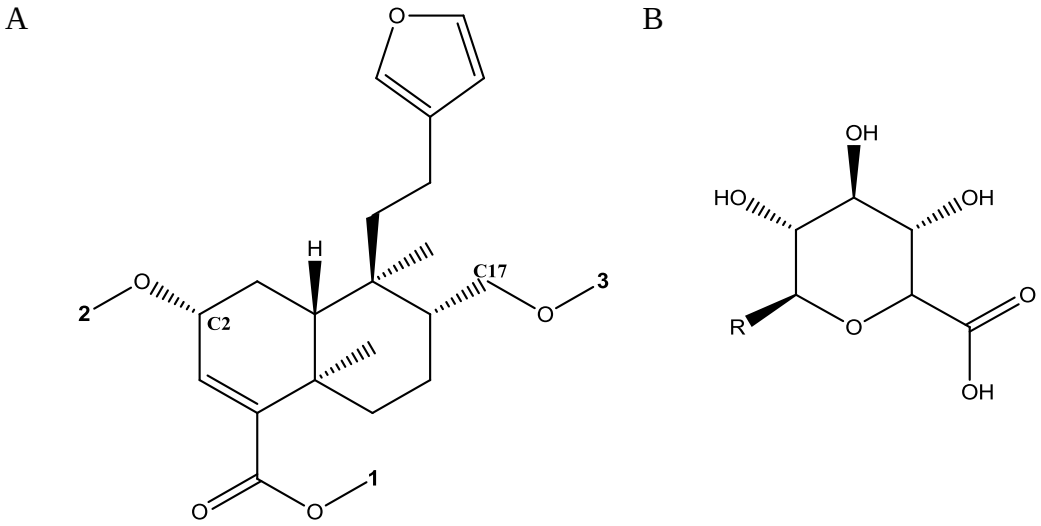

Figure 2.29: Structure of (A) proposed glucuronide metabolites and (B) glucuronide moiety. *Positions of the glucuronide moiety are denoted by enumerated positions: (1) PAAH-acyl glucuronide (PAAH-A-G), (2) PAAH-2-glucuronide (PAAH-2-G) and (3) PAAH-17-glucuronide (PAAH-17-G).*

In attempting to identify which of the two minor peaks correlates with the predicted C2 and C17 alcoholic glucuronides, it was not possible to conclude a definite identity of the peaks with the available techniques. Two techniques that may be employed to perform this identification include the use of chemical synthesis and NMR. The chemical synthesis approach would involve synthesising each alcoholic glucuronide and analysing pure samples of each with the same UPLC/MS technique, then using the retention times of the pure glucuronides to cross match with those in the PAAH incubation sample. The NMR approach would involve producing a large quantity of each metabolite, collecting and purifying the metabolites through chromatographic techniques and then performing NMR analysis, specifically 2D-NMR experiments, on the samples to determine the identity of the metabolites. Of the two methods, the chemical synthesis technique would likely be less technically difficult to achieve, but was not undertaken due to time and resource constraints.

2.2.14.4. Regioselectivity of glucuronide metabolites

Further investigation of the glucuronide metabolites of PAAH were investigated by replicating the experimental approach used in Section 2.2.14.3, but substituting HLM with recombinant enzymes. The purpose of this further experiment was to investigate regioselectivity of the enzymes in production of metabolites as it is understood that the overall metabolism of a drug in HLM, by UGT enzymes or otherwise, may constitute differing contributions of a number of enzymes [191]. As evidenced from selective inhibitor (Section 2.2.12.2) and recombinant enzyme (Section 2.2.12.3) experiments, UGT 1A1 and 2B7 were determined to be the major enzymes involved in the glucuronidation of PAAH so these enzymes were selected for further investigation.

Analysis of glucuronide metabolites produced by incubation with recombinant UGT 1A1 and 2B7 enzymes by UPLC/MS resulted in approximately equivalent proportions of all three metabolites formed by HLM as evidenced in Figure 2.30. This seems to indicate that there is no significant regioselectivity between UGT 1A1 and 2B7 in the production of PAAH glucuronide metabolites.

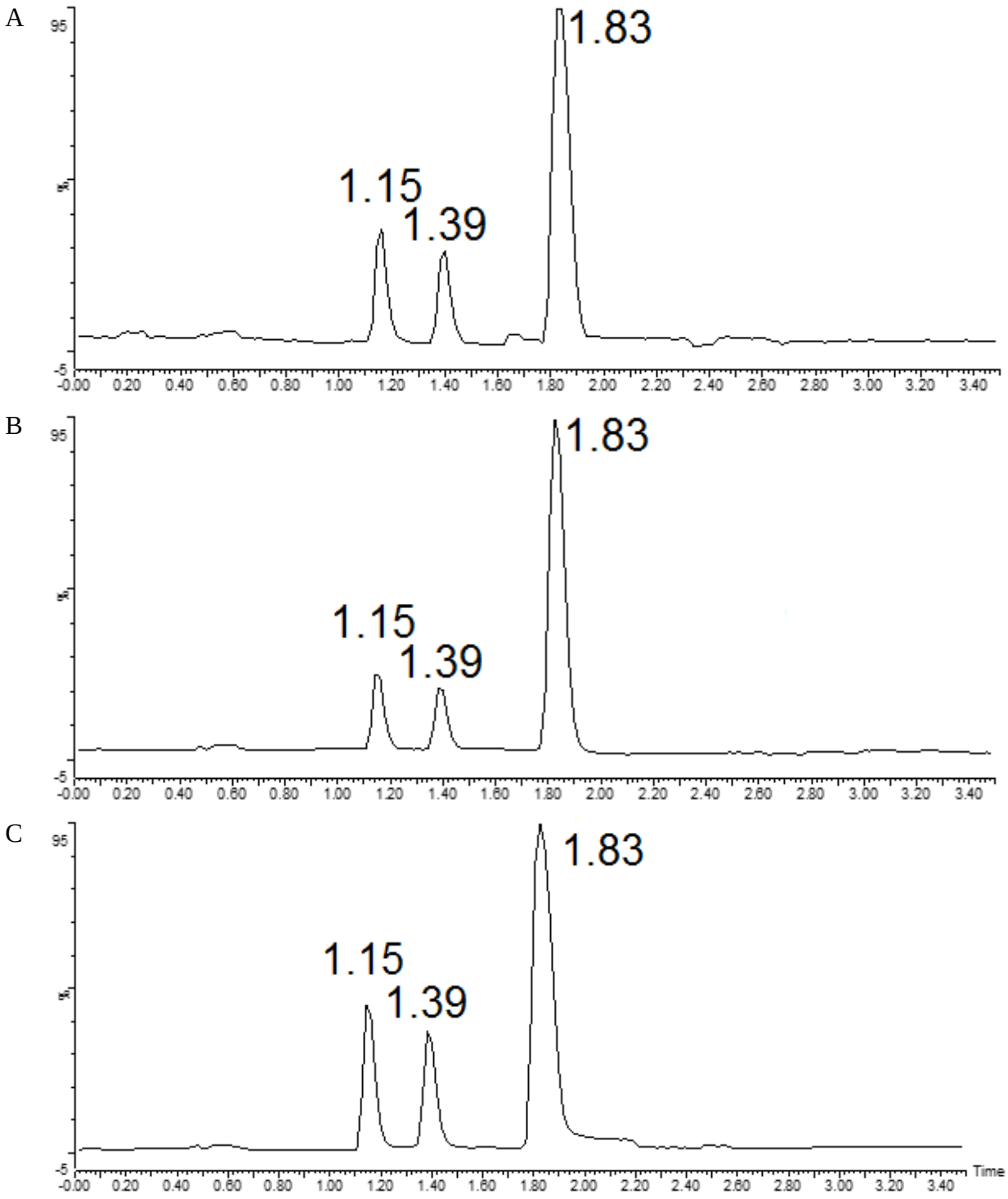

Figure 2.30: UPLC/MS chromatograms of PAAH-glucuronide metabolites produced by different enzyme preparations. *(A) Glucuronide metabolites produced by HLM. (B) Glucuronide metabolites produced by recombinant UGT1A1. (C) Glucuronide metabolites produced by UGT2B7.*

As seen previously in Section 2.2.14.3, the metabolites produced in this set of experiments broadly followed the same pattern, with a major metabolite and two minor metabolites being produced. Comparing the peak sizes in Figure 2.30 to those in Figure 2.26, it may appear that a larger proportion of minor peaks have been formed.

To further investigate this point the UV spectra of the samples was considered as MS spectra cannot be used to quantify samples without an internal standard to control fluctuation in sample response. A UV spectra, in contrast, can be analysed directly for quantification purposes. The UV spectra of data from Figure 2.30A is shown in Figure 2.31 and a full set of peak areas and percentages of metabolites of each spectra are shown in Table 2.4**.**

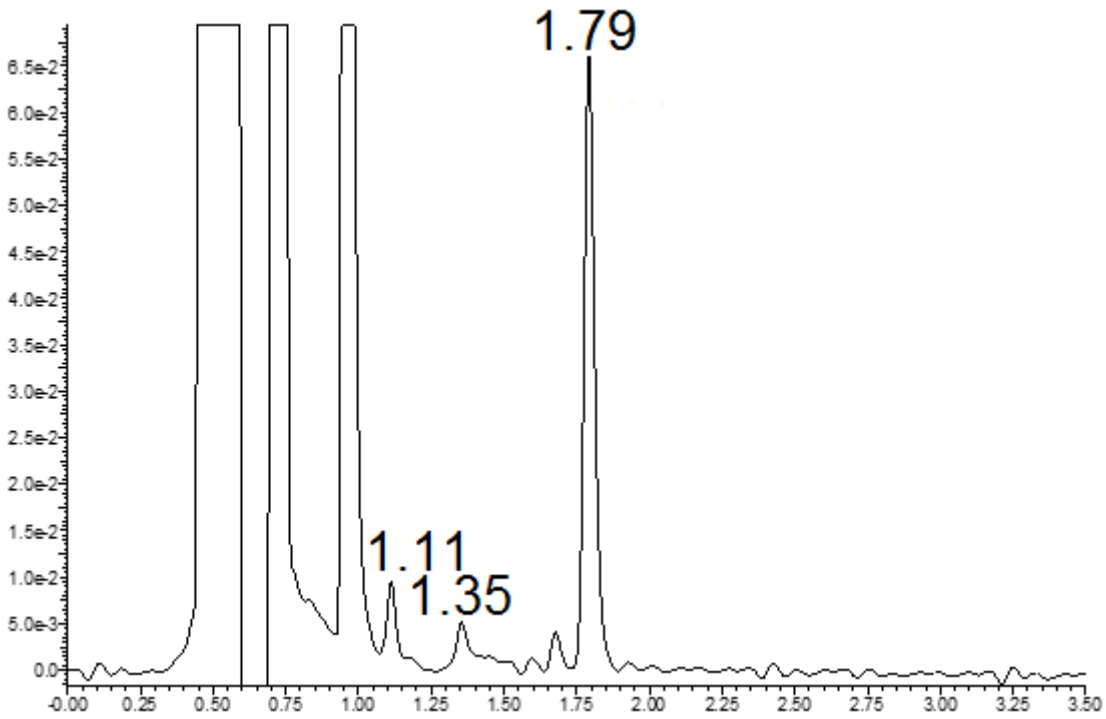

Figure 2.31: UPLC chromatogram of HLM/UDPGA incubated PAAH sample. *Sample was generated with 2 mg/mL HLM and analysed by UV at a wavelength of 225 nm.*

Table 2.4: Comparative quantitative analysis of glucuronide metabolites. *Data is taken from UV spectra of samples from Figure 2.30. Peak areas of each sample are shown on the left and corresponding percentages of each metabolite are shown on the right.*

Protein source	Peak 1	Peak 2	Peak 3	Peak area
HLM	260.6	166.3	2842.1	
UGT 1A1	148.8	127.3	1548.1	
UGT 2B7	450.4	277.2	6287.9	

Peak 1	Peak 2	Peak 3	Percentage
8.0	5.1	86.9	
8.1	7.0	84.9	
6.4	4.0	89.6	

Analysis of samples by UV spectrophotometry was able to detect all three metabolites previously identified by MS. Figure 2.31 shows the three peaks amongst others in the sample, which may correspond to other chemicals in the sample matrix such as UDPGA, solvent and long chain fatty acids released from cell membranes. There is an approximate 0.04 minute difference between the retention times from the UV analysis and MS analysis which is an artefact of the UV detector being approximately 0.04 minutes upstream of the MS detector in the UPLC/MS apparatus. The summary of the UV analysis in Table 2.4 shows that despite differences in peak areas, the percentages of each metabolite formed were approximately equivalent for all three metabolite peaks from each protein source. In addition to these findings providing evidence for the lack of regioselectivity in metabolite generation, the extent of metabolite production reported in Table 2.4 matched more closely with those reported in Section 2.2.14.3 compared to those in Figure 2.31.

Both UGT 1A1 and 2B7 are known to be involved in acyl glucuronidation with fluoroquinolone antibiotics, including levofloxacin and grepafloxacin, being metabolised by UGT1A1 (among other UGT1A family enzymes) [192] and naproxen and desmethylnaproxen being metabolised by UGT2B7 (among other UGT2B family enzymes) [176], so it is not necessarily surprising that there is no regioselectivity observed in PAAH. Potentially surprising, however, is that the extent of metabolism of each enzyme is approximately equal when considering the data reported in Figure 2.20. In the example of belinostat highlighted in Section 2.2.13, Dong et al. [179] reported that UGT1A1 was the dominant subtype of belinostat glucuronidation with a relatively minor contribution by UGT2B7.

2.2.14.5. Summary of glucuronide metabolite investigations

Structural identification of the glucuronide metabolites of PAAH was performed by HPLC, UPLC/MS and chemical hydrolysis. Inspection of the structure of PAAH reveals three positions amenable to glucuronidation: the hydroxyl groups located at C2 and C17 (Figure 2.29) and the carboxylic acid at C18. Use of various *in silico* techniques suggested that all three sites may be vulnerable to glucuronidation, with predictions made by XenoSite suggesting that the acyl position may be the most likely site. Three metabolites with *m/z* values corresponding to a PAAH-glucuronide metabolite were detected by UPLC/MS. There was no evidence of a diglucuronide metabolite as evidenced by selecting for its associated mass (*m/z* 700.26).

Mild alkaline hydrolysis is a well-recognised method for the selective hydrolysis of acyl glucuronides [193]. Mild alkaline hydrolysis resulted in almost complete loss of the major glucuronide formed by HLM, suggesting that this compound was the acyl glucuronide. The two remaining unassigned peaks were therefore likely to correspond to the (minor) hydroxy-glucuronides located at positions C2 (PAAH-2-G) and C17 (PAAH-17-G). Hydrolysis by β-glucuronidase resulted in complete loss of the peaks for the acyl glucuronide (RT 1.83 minutes), and one of the minor glucuronides (retention time 1.39 minutes). The resistance of the second hydroxyl-glucuronide to β-glucuronidase hydrolysis was likely a result of structural differences between PAAH-2-G and PAAH-17-G. An argument may be made that a key difference between the two glucuronides is proximity of the glucuronide moiety to the furan ring of PAAH which may result in reduced flexibility of PAAH-17-G due to steric hindrance. It may follow then, that owing to this reduced flexibility the glucuronide moiety may be less accessible by enzymes like β-glucuronidase, resulting in an apparent resistance to hydrolysis. A similar phenomenon has been reported for the differential effects of β-glucuronidase on the morphine 3- and 6-glucuronides whereby the 3-glucuronide is hydrolysed faster than the 6-glucuronide, presumably due to steric hindrance of the latter [189].

Investigation of UGT metabolism by *in silico* methods, while relatively underdeveloped in comparison to *in silico* CYP methods, performed quite well. Prediction of the site of metabolism of PAAH by UGT enzymes was performed using XenoSite,

MetaPred and SomUGT resulting in the prediction of three potential sites by XenoSite and MetaPred and two potential sites by SomUGT. As three glucuronide metabolites were ultimately discovered *in vitro,* it appears the predictions of XenoSite and MetaPred were more reliable than those of SomUGT. Further to this, SomUGT failed to predict the acyl glucuronide of PAAH, which was revealed after hydrolysis experiments to be the major metabolite of PAAH. In comparing XenoSite with MetaPred, XenoSite yielded a stronger preference for the acyl glucuronide, in agreement with the previously described UPLC/MS analysis. As discussed in Section 2.2.14.1, XenoSite represents a newer and more robust site of metabolism prediction model than previously reported models which is reflected in the results shown in this study.

Peng et al. [188] reported that SomUGT was capable of predicting the *in vitro* verified site of metabolism in a training set of 54 molecules with 84% accuracy. Of this training set, 11 contained acyl groups, 10 of which were known to form acyl glucuronides, and screening by SomUGT correctly predicted the acyl metabolism of all 11. The 11 acyl containing molecules in the training set represented a range of different positions of the carboxylic acid group including being in proximity to an alkyl chain, aromatic ring or amine, but none of the training set molecules matched the type of carboxylic acid present in PAAH, being part of a conjugation system with an alkene group. The false negative prediction of PAAH-A-G by SomUGT may be a result of this and may highlight a point of development for the software algorithms, despite its otherwise high performance for prediction of other glucuronides.

Further *in silico* predictions of UGT metabolism of PAAH performed by use of FILTER rules resulted in three predictions for specific enzymes involved in metabolism, of which all three were evaluated as accurate by *in vitro* screening. These predictions suggested that PAAH may be metabolised by UGT 1A1 and 2B7, but not by UGT 1A4. The simple rules, while limited to only three UGT enzymes, were successful in predicting metabolism of PAAH and may indicate there is the potential for further development and usage of the method for predictive purposes.

2.2.15. Identity of CYP metabolites

2.2.15.1. In silico prediction of CYP metabolite identity

To investigate the potential structures of CYP-mediated metabolites of PAAH, three *in silico* approaches were employed using XenoSite, MetaPred and ROCS/OEDocking by the methods described in Chapter 6.5.2. XenoSite was used via an online webserver as an *in silico* method of predicting sites of CYP-mediated metabolism. A SMILES string of PAAH, with specified stereochemistry, was submitted to XenoSite for analysis against predictive models of CYP metabolism. A graphical output of the results of the XenoSite analysis are shown in Figure 2.32.

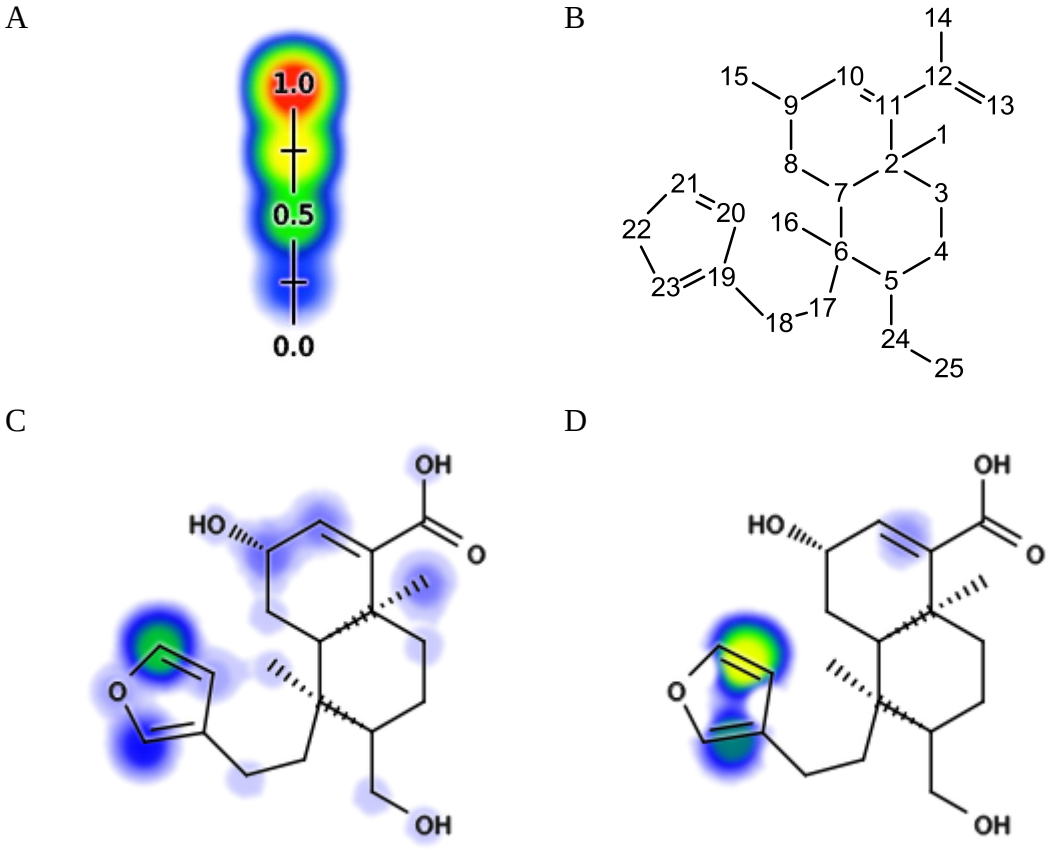

Figure 2.32: XenoSite predicted site of metabolism of PAAH by CYP enzymes in HLM. *(A) Colour scale denoting predictive value of activity. (B) XenoSite defined numbering system for PAAH. (C) Colour coded XenoSite CYP prediction (D) Colour coded XenoSite Epoxidation prediction.*

Based on the XenoSite output, shown in Figure 2.32, the sites most highly predicted to be subjected to CYP-mediated metabolism are sites 21 and 23 (s21 and s23) of the furan ring with the colour scale suggesting the s21 position to be more likely. The predictive values for each site were 0.45 and 0.24, respectively, with the next highest values being 0.16 and 0.13 for s9 and s10, respectively. Based on this analysis by XenoSite, it is predicted that the most likely site of potential metabolism in PAAH is at the furan ring at the s21. Further analysis by XenoSite Epoxidation, a subset of XenoSite dedicated to the prediction of sites of epoxidation, highlighted the alkene bridge between s20 and s21 of the furan ring as being highly vulnerable to epoxidation and as such an epoxide metabolite of PAAH may be predicted to be formed by CYP enzymes.

MetaPred was also used as an *in silico* method for predicting sites of CYP-mediated metabolism. A SMILES string of PAAH, with specified stereochemistry, was submitted to the online webserver for analysis against two predictive models of CYP site of metabolism specific to CYP 2C9 and 3A4 based on the *in vitro* results reported in Section 2.2.11. The results of the MetaPred analysis, including the enumerated structure of PAAH and rankings of sites by ΔP are shown in Figure 2.33 for CYP2C9 predicted metabolism and Figure 2.34 for CYP3A4 predicted metabolism.

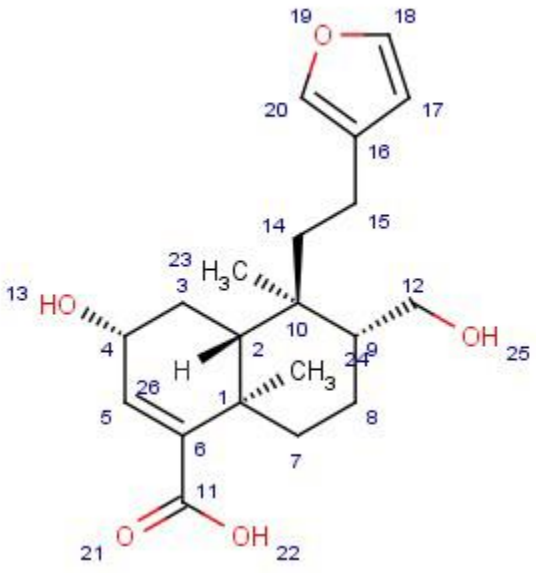

Rank	Atom Number	ΔP
1	12	0.61
2	20	0.07
3	18	0.05
4	22	-0.83
5	1	-0.79
6	6	-0.78
7	13	-0.75
8	21	-0.67
9	10	-0.66

Figure 2.33: MetaPred Web Server prediction results of PAAH metabolism by CYP2C9. *Inset table shows ΔP values of the top 9 ranked sites predicted for metabolism.*

As for the UGT predictions, the cut-off value of ΔP<0.000 was used as a predictor of metabolism probability at enumerated sites around PAAH. Of these sites, three were predicted as potential sites of CYP2C9 metabolism by MetaPred, C12, C20 and C18. The C12 position is already a hydrolysed centre of the molecule and as such further oxidation of the site by a CYP enzyme would likely result in formation of a carboxyl group such as an aldehyde or carboxylic acid. The C18 and C20 positions are also oxidated but the nature of their oxidation is significantly different to the C12 position as they share a mutually bonded oxygen as part of a ring system. Oxidation of either of these sites may potentially result in formation of a cyclic ester at either position, or possibly a ring opening to form a dialdehyde metabolite.

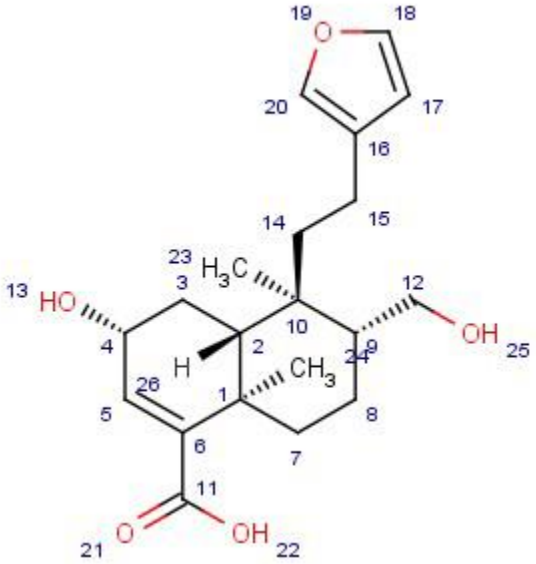

Rank	Atom Number	ΔP
1	4	0.33
2	12	0.20
3	18	0.13
4	13	-0.90
5	22	-0.87
6	6	-0.82
7	25	-0.79
8	21	-0.78
9	19	-0.69

Figure 2.34: MetaPred Web Server prediction results of PAAH metabolism by CYP3A4. *Inset table shows ΔP values of the top 9 ranked sites predicted for metabolism.*

Shown in Figure 2.34, three sites were predicted as potential sites for CYP3A4 metabolism by MetaPred, C4, C12 and C18. The C4 position is, as previously described for the C12 position, a hydrolysed centre of PAAH, so further metabolism by a CYP enzyme would likely result in a carboxyl group such as an aldehyde or carboxylic acid. The C12 and C18 positions were also predicted as potential sites of CYP2C9 metabolism for PAAH by MetaPred and as such there may be more weight to the predictions for these sites.

Owing to the predictions of MetaPred as well as the *in vitro* results reported in Section 2.2.11, CYP2C9 was considered for further in-depth *in silico* analysis by the method of Sykes et al. [194]. The Sykes method is a means of rapidly, and reasonably accurately, using overlay approaches to predict molecules that are likely to be substrates for CYP2C9, and further to use docking to suggest a binding mode that the substrate may adopt in the CYP2C9 enzyme. By this method, a 3D-structure of PAAH, defined by Omega 2.5.1.4, was analysed using the chemical similarity program ROCS 3.2.0.4 by comparison against a molecule of flurbiprofen taken from a crystal structure of CYP2C9 (PDB ID: 1R9O [195]). The ComboScore function was used as a scoring metric to judge the similarity of PAAH to flurbiprofen and a score of 0.99 was used as a reliability cut-off for molecules considered likely to be metabolised by CYP2C9. The ComboScore of PAAH in this analysis was 1.200, which comfortably exceeded the defined cut-off. A ROCS generated overlay of PAAH and flurbiprofen is shown in Figure 2.35.

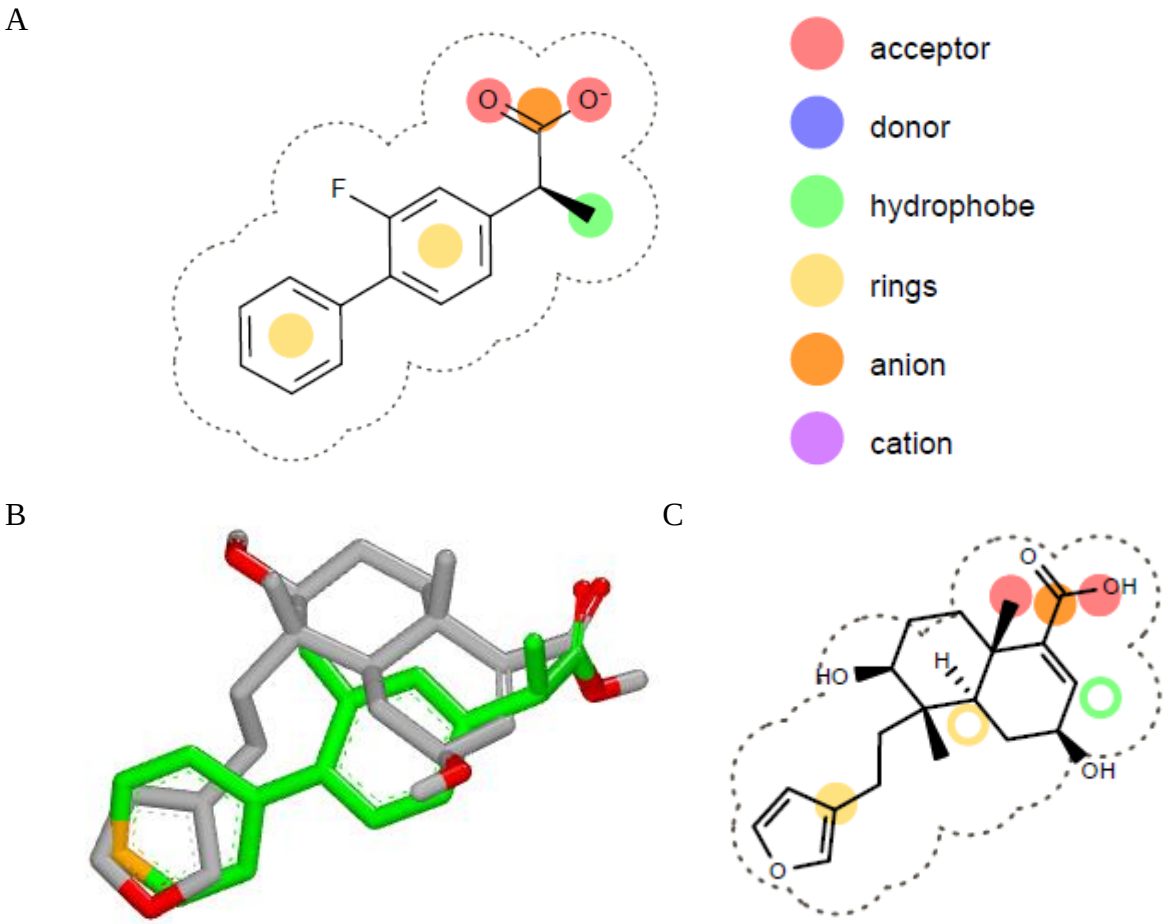

Figure 2.35: ROCS overlay of flurbiprofen (green) and PAAH (grey). *(A) ROCS report structure of flurbiprofen with legend of electrostatic features (B) 3D-representation of overlay presented by VIDA, flurbiprofen is featured in green with the primary site of CYP2C9 metabolism highlighted in orange and PAAH is featured in grey. (C) 2D-representation of overlay presented by ROCS_report, dashed outline and coloured circles represent shape and electrostatic features of flurbiprofen.*

From analysing the overlay of both structures it is readily apparent that two particular sites in each molecule contribute to the high ComboScore observed, the carboxylic acid of each molecule and an aromatic ring structure, a benzyl in flurbiprofen and a furan ring in PAAH. The central benzyl ring of flurbiprofen also approximately overlaps with the structure of PAAH suggesting reasonable alignment of both molecules in terms of both shape and electrostatic features. The site indicated in orange on flurbiprofen (see Figure 2.35B) is well characterised as the site of metabolism of flurbiprofen by CYP2C9 and the close

proximity of the C18 position of PAAH to this site in overlay suggests that the C18 position of PAAH may be metabolised by CYP2C9.

To further examine the potential interactions of PAAH with CYP2C9, PAAH was submitted to OEDocking using the previously acquired crystal structure of CYP2C9 (PDB ID: 1R9O [195]). An active site of CYP2C9 was defined around the flurbiprofen/heme complex and docking was performed using the Hybrid module of OEDocking 3.0.1 by the method described in Chapter 6.5.4. A docking pose of PAAH in the active site of 1R9O is shown in Figure 2.36.

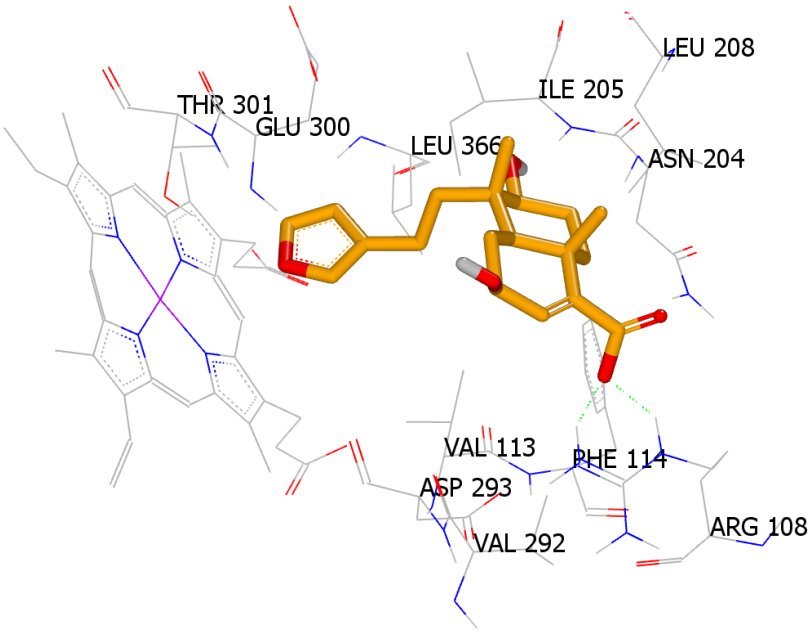

Figure 2.36: Docked structure of PAAH in the CYP2C9 receptor (PDB ID: 1R9O [195]). *Key surrounding residues and heme molecule are displayed by ball-and-stick representation and PAAH is displayed in orange by stick representation.*

The docking of PAAH in 1R9O suggests a binding pose with two key features; potential hydrogen bonding of the carboxylic acid to Arg 108 and proximity of the furan ring of PAAH to the heme portion of the active site. The Arg 108 residue of CYP2C9 is widely understood to be an integral feature of an anionic binding site in the enzyme [194, 196, 197], so the putative binding of PAAH with this specific feature may offer support to the predicted binding mode. The proximity of the furan ring (approximately 4.86 Å) to the heme portion of CYP2C9 is a significant feature as the heme is the site of CYP enzymes that facilitates

electron transfer and leads to the oxidation of the substrate, producing a metabolite. Since it has been previously shown that the average distance from the site of metabolism to the heme-iron in CYP2C9 is 5.21 ± 0.95 Å [194], the predicted distance of 4.86 Å is indicative of the furan ring being a likely site of metabolism for PAAH by CYP2C9.

2.2.15.2. *In vitro* investigation of CYP metabolites

Multiple attempts to use *in vitro* techniques to isolate and characterise CYP metabolites of PAAH were attempted, by the same HPLC method used for glucuronide metabolite detection (Section 2.2.14.2), but were ultimately unsuccessful. While glucuronide metabolites of PAAH were readily detectable by chromatography, no evidence for the formation of peaks was observed in incubations of PAAH with HLM in the presence of NADPH generating system, despite a depletion in the size of the peak corresponding to PAAH.

Multiple *in silico* screening methods in Section 2.2.15.1 predicted that the furan ring of PAAH was a likely site of CYP metabolism. Many CYP metabolites of furan containing chemicals are known to be reactive *in vivo* and may bind irreversibly to proteins [181]. Based on this, an attempt to "trap" any potential furan metabolites was implemented by performing a CYP metabolism incubation in the presence of glutathione, as glutathione has been used in numerous CYP metabolism studies to bind to furan metabolites [198, 199]. This approach was unsuccessful in producing any detectable metabolite however, and as CYP enzymes ultimately played a minor role in total PAAH metabolism, it was decided to focus further study on the detection of UGT metabolites.

2.2.15.3. Summary of CYP metabolite investigations

While *in vitro* methods of investigating CYP metabolism of PAAH were not successful in isolating specific metabolite structures, various *in silico* methods were employed to predict the types of metabolites that may be produced. All three of the applied

models (XenoSite, MetaPred and the Sykes ROCS model) provided consistent predictions that the furan ring of PAAH is most likely to be the site of CYP-mediated metabolism. Furan metabolism is well documented in the literature [181] and a summary of the types of metabolites that may be produced from furan rings is shown in Figure 2.37.

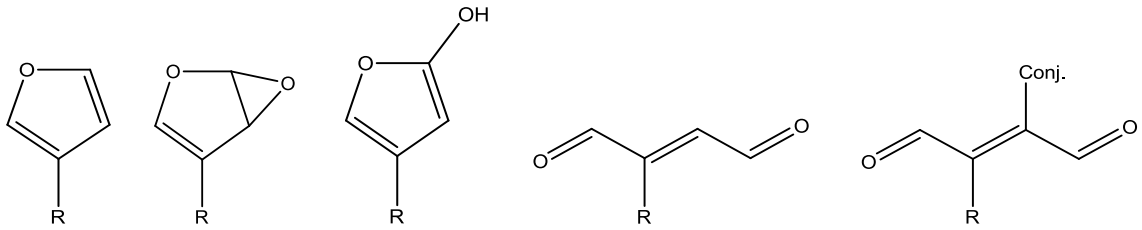

A B C D E

Figure 2.37: Structures of a furan ring and potential CYP-metabolites. *From left to right: (A) parent furan, (B) epoxide, (C) alcohol, (D) dialdehyde and (E) dialdehyde+conjugate.*

Based on *in silico* predictions of CYP metabolism of PAAH, and knowledge of CYP metabolites of furans, it can be hypothesised that the CYP metabolites of PAAH may feature these types of structures, but the lack of *in vitro* data to support this leaves the data purely speculative. Conjugates of the furan dialdehyde metabolite most commonly include glutathione but can also include semicarbazide and DNA adducts such as N-acetylcysteine and N-acetyllysine, resulting in a range of further metabolites through conjugation [181].

Investigation of CYP-mediated PAAH metabolism by *in silico* methods produced relatively consistent results. Prediction of the site of metabolism of PAAH by CYP enzymes was performed using MetaPred and XenoSite, resulting in a number of predicted sites of metabolism by CYP enzymes, but one particular site was highlighted in particular by consensus, the C15 site of the furan ring. XenoSite predicted this site as the only potential site of metabolism while MetaPred made a number of additional predictions around the molecule with the site being ranked 3rd highest in the list. The additional sites predicted by MetaPred consisted of already hydroxylated sites in PAAH, and while CYP enzymes are capable of further oxidising hydroxylated sites i.e. forming acyls from alcohols, oxidation of non-hydrolysed carbons is more commonly seen [200]. While validation of these predictions could not be made due to issues with metabolite detection, the models used have

been validated and published with reported accuracies of approximately 89% for XenoSite [201] and 86% for MetaPred [202], therefore the predictions made are realistically grounded.

As part of a retrospective *in silico* analysis after *in vitro* determination of CYP enzymes involved in PAAH metabolism, specific investigation of CYP2C9 was performed using the model of Sykes et al. [194]. The Sykes model presented data in good agreement with the observed *in vitro* results that PAAH was able to be metabolised by CYP2C9. Both ROCS alignments and OEDocking results highlighted the C15 position of the furan ring of PAAH as the most likely site of metabolism, in good agreement with the results of MetaPred and XenoSite.

2.3. Conclusions and future directions

In this study, the metabolism of PAA and PAAH was investigated by a combination of *in vitro* and *in silico* methods. PAA was demonstrated to be hydrolysed in the presence of HLM suggesting a potential role of carboxylesterase enzymes to produce the de-esterified alcohol, PAAH. Following this first step, significant depletion of PAAH was observed by HLM incubated in the presence of UPDGA, suggesting a major metabolic role of UGT enzymes. Using the "well stirred model" [162, 163, 203] and appropriate scaling factors, *in vitro* data was extrapolated to derive *in vivo* kinetic parameters which suggested that *in vivo* clearance of PAAH may be slow. Use of selective inhibitors and recombinant enzymes highlighted two UGT enzymes as having significant importance in the metabolism of PAAH, UGT 1A1 and 2B7, in agreement with *in silico* predictions.

In vitro and *in silico* screening methods were used to investigate glucuronide metabolites of PAAH and three were discovered, one major acyl metabolite and two minor alcohol metabolites. Additional depletion, although minor, was observed in incubations of PAAH with HLM and NADPH generating system, suggesting a minor role of CYP enzymes in total PAAH metabolism. Selective inhibitors and recombinant enzymes were also used to investigate CYP enzymes involved in PAAH metabolism and CYP 2C9 and 3A4 were found to play a role, in agreement with *in silico* predictions. No CYP metabolites were able to be discovered by *in vitro* methods, but *in silico* screening of PAAH by various methods resulted in predictions that the furan ring of PAAH was the most vulnerable site of metabolism and from this, structures of predicted metabolites could be hypothesised. A full summary of the metabolism of PAA as evidenced by this study is depicted in Figure 2.38.

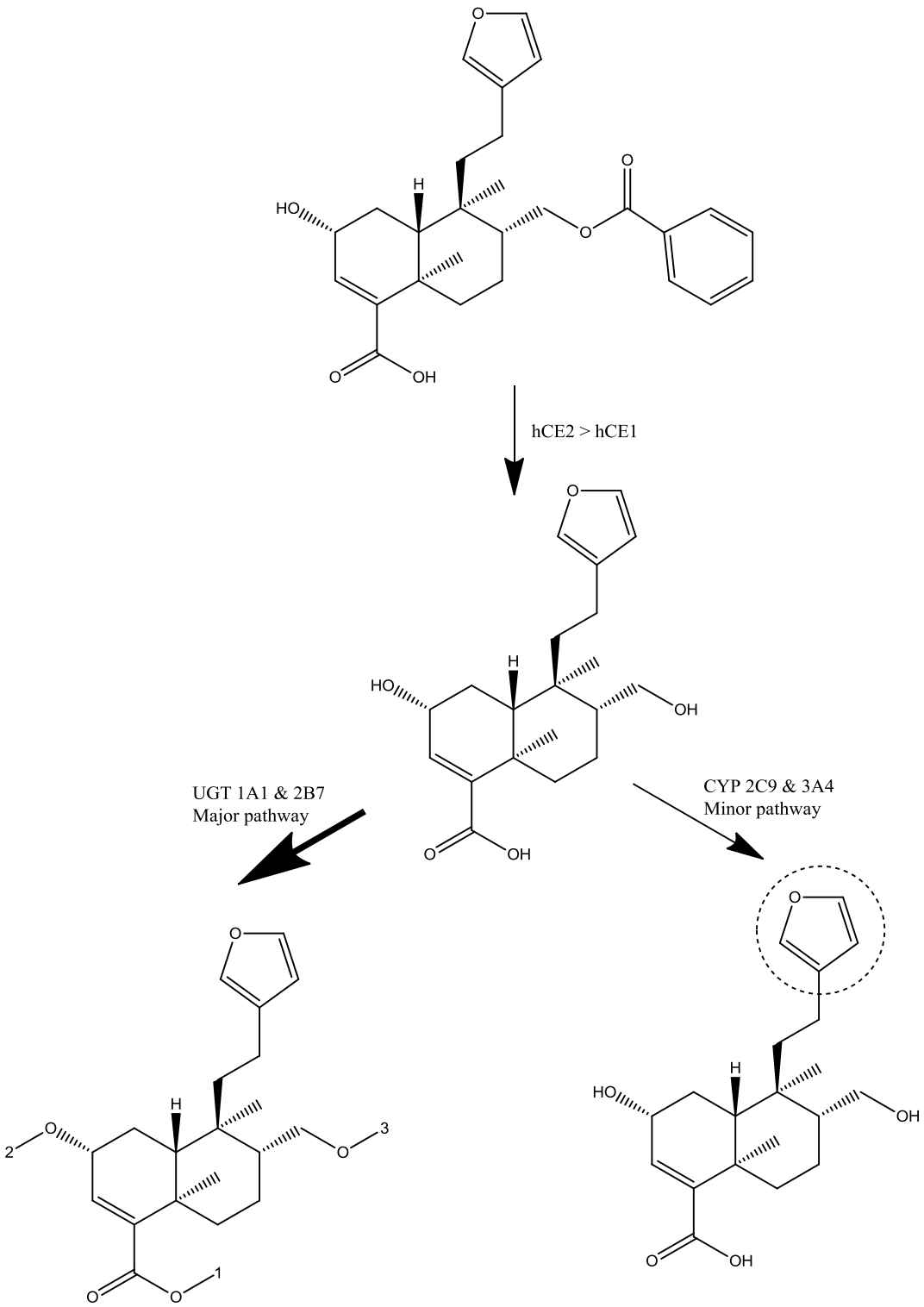

Figure 2.38: Proposed in vitro metabolic pathway of PAAH. *Initial carboxylesterase metabolism is followed by major contribution by UGT enzymes and minor contribution by CYP enzymes. Designations of 1, 2 and 3 refer to locations of glucuronides. The dashed circle around the furan ring refers to in silico predictions for CYP-mediated furan metabolites.*

Further investigations into the metabolism of PAA and PAAH may be warranted for the continued development of a therapeutic product. Areas that may be investigated include a conclusive summary of CYP metabolites of PAAH, as the identity of CYP metabolites, despite being minor metabolites, were not successfully elucidated. Investigations of enzyme inhibition, specifically related to drug-drug interactions by UGT or CYP enzyme inhibition, may also warrant further investigation due to the clinical implications that may be posed by inhibition. While the extent of *in vivo* metabolism was extrapolated from *in vitro* data by kinetic parameters, there may still be a need to quantify the *in vivo* metabolism of PAA as these data may be important to consider in the future for clinical dosing. Each of these areas are also of academic interest due to the scarcity of published material regarding diterpenoid metabolism, but also, as highlighted, there are numerous clinical perspectives to consider. In addition to the significance of the study in the space of clerodane diterpenoid pharmacology, this study represents the first such metabolism study of an Australian medicinal plant compound.

Chapter Three: Anti-inflammatory investigation of PAA

3.1. Introduction

While understanding the physiological actions of a xenobiotic is important, an understanding of how those physiological actions are achieved is also of considerable interest. Understanding the enzymes and receptors a drug may interact with is important from a drug safety perspective. Knowledge of these pathways is vital in avoiding side effects that may arise from sources such as off target effects and drug-drug interactions [204]. *In vitro* methods utilising specialised cell lines or free receptors have long been used for such studies to investigate drug-target interactions and their use may widely be considered non-controversial. The use of *in silico* methods for this purpose, by contrast, is a far newer innovation and one still very open to new developments and improvement [205, 206]. Protein docking and 3D-chemical similarity methods have been employed in the past to predict drug activities and there is evidence to suggest that a complementary approach of *in silico* and *in vitro* screening can improve pharmacological investigations above that of either approach alone [207, 208].

The study described in this chapter was undertaken to further understand and characterise, by combined *in silico* and *in vitro* means, the anti-inflammatory activity of PAA [12]. Prior to this study, the cyclooxygenase (COX) enzyme was the only target in an inflammatory pathway which had been investigated [15] and thus, this study sought to extend this work to a number of other targets and determine a biomolecular mechanism for the anti-inflammatory actions of PAA and PAAH. *In silico* experiments including 3D-chemical similarity by the ROCS approach and protein docking were used to explore anti-inflammatory targets and form hypotheses regarding potential interactions by PAA or PAAH. PAAH was also investigated in these experiments due to the previous findings described in Chapter 2 (Chapter 2.2.2) that PAA is readily hydrolysed by human liver microsomes, likely through carboxylesterase-mediated hydrolysis to PAAH. This was based on the conclusion that the hydrolysed form was the dominant species in physiological conditions and thus, likely responsible for drug activity. Both *in silico* and *in vitro*

investigation of targets was performed alongside experiments from Chapter 2, and accordingly PAA was primarily considered in experiments described in Sections 3.2.1 and 3.2.2, but after the extent of hydrolysis of PAA was better understood, PAAH was used primarily thereafter.

In addition to examining aspects of drug action and drug safety of PAA and PAAH, this study was also undertaken to improve knowledge of other clerodane diterpenoids such as hautriwaic acid and hardwickiic acid which, like PAA, have been demonstrated to possess anti-inflammatory activity [209, 210]. Like PAA, these diterpenoids have not had their mechanisms determined and it follows that elucidating the mechanism of action of any one clerodane diterpenoid may lead to a breakthrough in other molecular investigations [211, 212]. The sections in the results and discussion portion of this chapter are presented according to the target investigated and all methodology is described in Chapter 6.

3.2. Results and discussion

3.2.1. Caspase-1

Caspase-1, also referred to as interleukin-1 converting enzyme (ICE) is an enzyme that cleaves proteins, including interleukin-1β and -18. This cleavage process activates the interleukins and, accordingly, caspase-1 is considered a key functional protein of the inflammatory cascade [48]. As PAA was already established to have some inhibitory effects on production of IL-1β [14], and given the importance of the target in the pro-inflammatory cycle, caspase-1 was considered as a potential target. PAA was examined for caspase-1 inhibition activity both *in silico* and *in vitro.*

3.2.1.1. ROCS investigation of caspase-1 as a target

A list of caspase-1 inhibitors was constructed by retrieving crystal structures from the RCSB Protein Data Bank. In total 27 structures were retrieved from the databank, as listed in Table 3.1. The 2D-representations of the structures are listed in Appendix 2. Suitability criteria of structures were limited to proteins sourced from *Homo sapiens* with a maximum allowable resolution of 3.00 Å.

Table 3.1: List of PDB crystal structures of caspase-1. *Names of bound inhibitors are enumerated for simplicity. Protein symmetry, resolution and associated citations are listed as described by the PDB. Structures can be viewed in Appendix 2, or through the RCSB.*

PDB ID	Enzyme state	Bound ligand	Symmetry	Resolution (Å)	Citation
1BMQ	Wild type	**1**	Asymmetric	2.50	[213]
1IBC	Wild type	**-**	Cyclic – C2	2.73	[214]
1ICE	Wild type	**2**	Cyclic – C2	2.60	[215]
1RWK	Wild type	**3**	Cyclic – C2	2.30	[216]
1RWM	Wild type	**4**	Cyclic – C2	2.70	[216]
1RWN	Wild type	**5**	Cyclic – C2	2.00	[216]

Continued on following page

Table 3.1: Continued from previous page.

PDB ID	Enzyme state	Bound ligand	Symmetry	Resolution (Å)	Citation
1RWO	Wild type	**6**	Cyclic – C2	2.10	[216]
1RWP	Wild type	**7**	Cyclic – C2	2.20	[216]
1RWV	Wild type	**8**	Cyclic – C2	2.10	[216]
1RWW	Wild type	**9**	Cyclic – C2	2.80	[216]
1RWX	Wild type	**10**	Cyclic – C2	1.85	[216]
1SC1	Cys285 → Ala	**-**	Asymmetric	2.60	[217]
1SC3	Cys285 → Ala	**11**	Asymmetric	1.80	[217]
1SC4	Cys285 → Ala	**-**	Asymmetric	2.10	[217]
2H48	Cys285 → Ala Cys364 → Ala Cys397 → Ala	**12**	Cyclic – C2	2.20	[218]
2H4W	Glu390 → Asp	**12**	Cyclic – C2	2.00	[219]
2H4Y	Arg286 → Lys	**12**	Cyclic – C2	1.90	[219]
2H51	Glu390 → Asp Arg286 → Lys	**12**	Cyclic – C2	2.10	[219]
2H54	Thr388 → Ala	**12**	Cyclic – C2	1.80	[219]
2HBQ	Wild type	**12**	Cyclic – C2	1.80	[218]
2HBR	Arg286 → Ala	**12**	Cyclic – C2	2.20	[218]
2HBY	Glu390 → Ala	**12**	Cyclic – C2	2.10	[218]
2HBZ	Arg286 → Ala Glu390 → Ala	**12**	Cyclic – C2	1.90	[218]
3D6F	Arg240 → Gln	**12**	Cyclic – C2	1.90	[220]
3D6H	Asn263 → Ser	**12**	Cyclic – C2	2.00	[220]
3D6M	Lys319 → Arg	**12**	Cyclic – C2	1.80	[220]
3NS7	Wild type	**13**	Asymmetric	2.60	[221]

Co-crystallised inhibitor coordinates were retrieved from crystals containing bound ligands for the purpose of creating a small library for ROCS similarity studies with PAA. Duplicate ligand entries of compound **12** were culled to a single entry taken from 2HBQ, the wildtype form of caspase-1, to form a final list of 13 ligands. Structures of 10 caspase-1 inhibitors featuring identical symmetry (cyclic – C2) were retrieved from the library and analysed for common structural features in VIDA 4.3.0.4 by overlaying each structure and removing the surrounding protein residues. This overlay is shown in Figure 3.1.

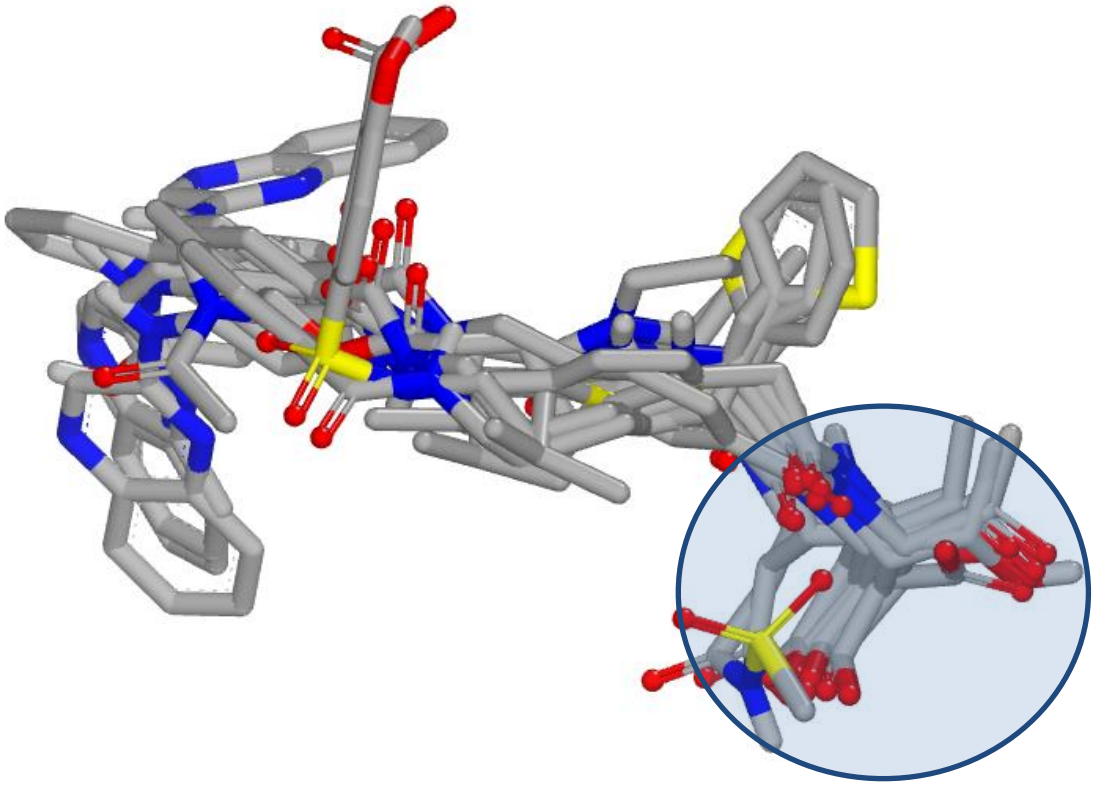

Figure 3.1: Overlay of 10 caspase-1 crystallised ligands. *Blue circle highlights the most highly conserved region of all ligands. Ligand structures are taken from crystals with identical cyclic - C2 symmetry.*

Analysis of the caspase-1 inhibitors showed that a region (highlighted by a blue circle in the figure) was conserved in all crystal structures, and the remaining portion of the structures was more variable. The conserved region consists of two key features: a hydrogen bond donor, typically a carboxyl or sulfonyl group, which forms hydrogen, or ionic, bonds with arginine residues (Arg 179 and Arg 341), and a group capable of forming covalent bonds, most commonly an aldehyde, with a Cys 285 residue. However some structures i.e. 1RWO, 1RWP, appear to also form hydrogen bonds with His 237 and Gly 238 residues. The mean distance between the two features in each caspase-1 ligand was determined to be 4.04 ± 0.28 Å (mean ± SD, n = 13, see Table 3.2). The remainder of each caspase-1 ligand is more highly variable and involves numerous peptide and peptidomimetic variations.

To assess structural similarities between the caspase-1 inhibitors and PAA, the ROCS approach was utilised as described in Chapter 6.5.5. PAA was used as a query molecule against the database of caspase-1 inhibitors retrieved from the PDB caspase-1

structures described earlier. Results of the ROCS analysis including scoring functions are shown in Table 3.2 and examples of the four highest ranked overlays are shown in Figure 3.2.

Table 3.2: ROCS scores of caspase-1 inhibitors with PAA as the query. *Compounds are ranked by TanimotoCombo score. 'Distance between features' denotes the distance between the hydrogen bond donor and covalent bonding group (described in the text).*

ROCS ligand	PDB ID	Distance between features (Å)	Tanimoto Combo	Shape Tanimoto	Color Tanimoto
3	1RWK	3.97	0.825	0.248	0.577
11	1SC3	3.25	0.685	0.220	0.465
13	3NS7	4.37	0.571	0.363	0.208
1	1BMQ	3.91	0.548	0.261	0.287
7	1RWP	4.07	0.502	0.323	0.179
8	1RWV	4.09	0.499	0.193	0.307
12	2HBQ	3.75	0.496	0.446	0.050
10	1RWX	4.10	0.486	0.320	0.166
4	1RWM	4.19	0.474	0.370	0.104
2	1ICE	4.27	0.472	0.196	0.276
9	1RWW	4.20	0.447	0.309	0.138
6	1RWO	4.10	0.445	0.366	0.079
5	1RWN	4.19	0.413	0.274	0.138

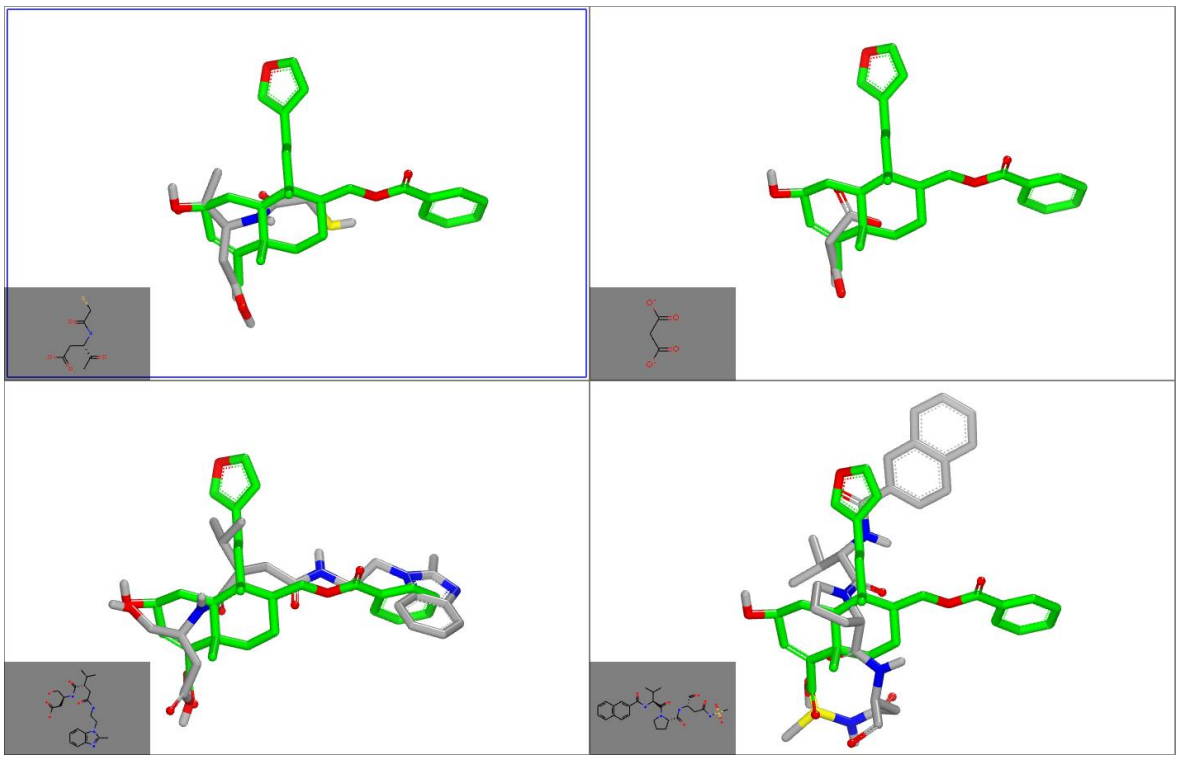

Figure 3.2: ROCS overlays of PAA with the four highest ranked caspase-1 inhibitors. *PAA is displayed in green, while each caspase-1 inhibitor is displayed in grey. Caspase-1 ligands are **3** (top left, indicated by blue box), **11** (top right), **13** (bottom left) and **1** (bottom right). Compounds have been ranked by TanimotoCombo score and 2D representations of the ligands are inset.*

TanimotoCombo scores were quite low for PAA with the highest score being 0.825 for **3** (PDB ID: 1RWK) and over half of all compounds having scores between 0.400 and 0.500. Breaking the TanimotoCombo score down to its constituent color and shape components further revealed that PAA was considered quite dissimilar in both shape and electrostatic features to the known inhibitors. Molecules **3** and **11** exhibited somewhat higher color scores (0.577 and 0.465 respectively) than the rest of the known inhibitors. These higher scores are likely an artefact of the smaller size of **3** and **11** in that when there are fewer molecular features in a molecule, a small number of matches can represent a higher ratio of overall matches. Interestingly, however, two of the top posed structures (**3** and **13**) are overlaid to PAA in a manner where the highly conserved region of caspase-1 ligands (mentioned earlier) are closely overlaid with the carboxylic acid and hydroxyl of PAA. It should be noted that PAA does not contain a group such as an aldehyde which is capable of forming covalent bonds with a protein residue (such as cysteine), but as mentioned

previously, certain hydrogen bond interactions may possibly take the place of a covalent bond in binding to caspase-1. The distance between the carboxylic acid and hydroxyl in PAA is 4.24 Å, which is similar to the distance between features in caspase-1 ligands. Additionally, the overlay of PAA and **13** demonstrated that the two molecules occupy a similar volume of space lengthwise, with some additional structural features in PAA (furan ring and decalin ring structure) making PAA a more spatially extended structure.

While the scoring metrics did not indicate significant structural similarity between PAA and caspase-1 ligands, key structural similarities understood to contribute highly to caspase-1 activity were observed. Therefore, while the results of the ROCS analysis were only moderately indicative of structural similarity, it was decided that further *in silico* analysis by docking was warranted.

3.2.1.2. Docking investigation of caspase-1 as a target

As many caspase-1 crystal structures were available to perform docking with, a selection process was employed to choose a suitable docking structure using the methods described in Chapter 6.5.4. To select a model docking site, the enzyme state of each protein was assessed as either being a wild type or mutant protein (see Table 3.1), with wild type proteins being considered as more suitable for docking analysis. TanimotoCombo scores from ROCS alignments in Section 3.2.1.1 were then used to select a structure as a model site for docking based on the understanding that docking results may be considered more reliable *a priori* when there is higher structural similarity between docked molecules and bound ligands. This concept, proposed by Tuccinardi et al. [222] will be discussed further in Section 3.2.6.

ROCS analysis of caspase-1 ligands with PAA as the query revealed **3**, **11**, **13** and **1** as the top scoring molecules. Ligands **3** and **11**, corresponding to the crystal structures 1RWK and 1SC3, are smaller molecules than most other caspase-1 inhibitors and as such the ROCS scores may be considered less reliable, as previously mentioned [223]. Additionally, crystal structures of smaller bound molecules often have smaller active sites, and may be less able to accommodate larger molecules, which may lead to such molecules being unable to dock in an optimum pose or even fit into the active site at all. Due to this,

the crystal structure corresponding to the third highest ROCS ranked molecule, **13** (PDB ID: 3NS7), was selected for docking studies. Also, it was previously established (Section 3.2.1.1) that PAA and **13** were of comparable size, and hence suitable for docking. Docking was performed by the method described in Chapter 6.5.4 using the Hybrid module of OEDocking 3.2.0.2. The top scoring pose for PAA in the 3NS7 receptor is shown in Figure 3.3.

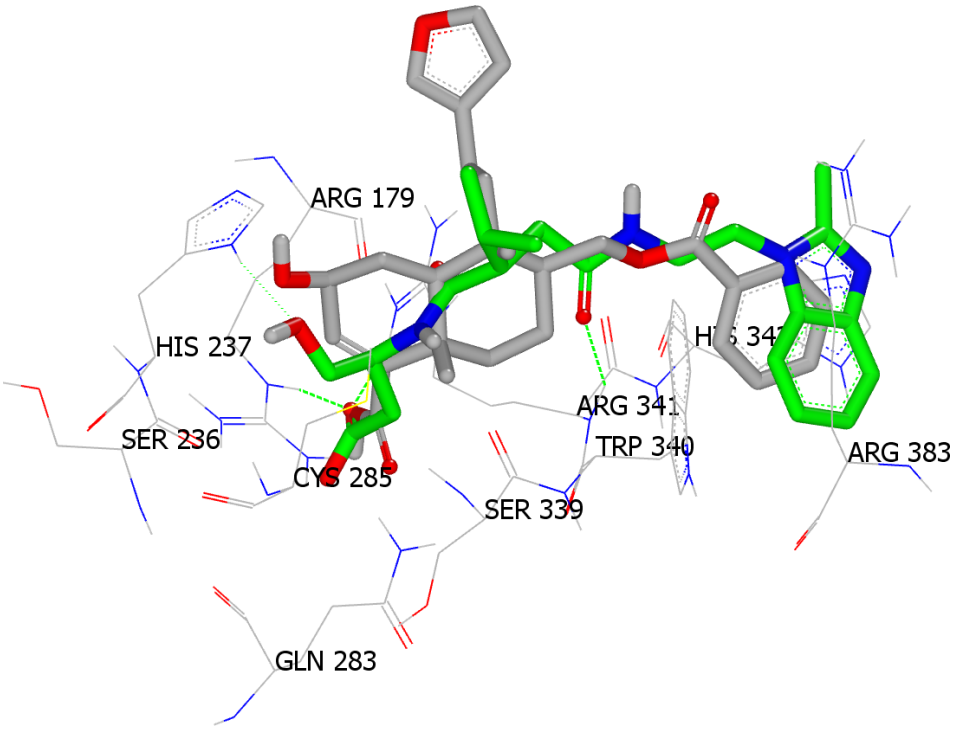

Figure 3.3: Docking pose of PAA (grey) and bound ligand, 13 (green), in the active site of caspase-1 (PDB ID: 3NS7). *Ligands are displayed as stick representations with residues presented as wireframe.*

From the docking of PAA to 3NS7, the lowest energy binding pose indicated that a number of key binding features of the co-crystallised ligand, **13**, may be replicated by PAA, including ionic interactions between the carboxylic acid and Arg 179 and Arg 341 and the hydroxyl group and His 237, and π-π stacking with the aromatic ring of the benzyl ester and His 342 and Trp 340 residues. The two hydrophilic binding features (carboxylic acid and hydroxyl group) are of particular note as these two features have been shown previously (Section 3.2.1.1) to be highly conserved in caspase-1 inhibitors.

A hydrogen bond interaction between **13** and Arg 383, which is facilitated by the benzimidazole ring of **13,** is not present in PAA. This may be an important interaction to the binding of **13** to the caspase-1 receptor, as a structural study by Galatsis et al. [221] determined that a benzyl group in place of a benzimidazole resulted in a significant decline in binding affinity (K_i value, 115 nM versus 4.68 nM, respectively). The two structures of PAA and **13** also occupy a similar spatial volume in the binding site with the key difference being a furan ring, which extends out of the active site into void space and as such is incapable of forming interactions with the 3NS7 crystal structure.

In summary, docking revealed conservation of key binding interactions of caspase-1 ligands, namely interactions with Arg 179, Arg 341 and His 237, as well as a π-π stacking interaction between the aromatic ring of PAA and His 342. This analysis seemed to support a hypothesis that PAA may have some of the necessary molecular features to bind to the caspase-1 receptor. As an interaction with Arg 383 analogous to that in **13** was not observed with PAA, and this type of interaction has been shown to be important for binding of caspase-1 inhibitors it is likely that if PAA binds to the receptor, it will likely bind with a lower affinity than that of **13**. In order to test this hypothesis, *in vitro* testing of PAA for activity against the caspase-1 was performed using a cell based ELISA test.

3.2.1.3. *In vitro* testing of PAA for caspase-1 inhibition

PAA was tested *in vitro* for inhibition of caspase-1 via an in-direct process. The role of caspase-1 in the inflammatory cascade, briefly summarised from Chapter 1.2.4, is to activate the pro-inflammatory cytokines IL-1β and IL-18 by cleaving inactive pro-IL-1β and pro-IL-18 cytoplasmic precursors. As such, an inhibitor of caspase-1 would decrease production of IL-1β, but not pro-IL-1β, which would remain constant, or potentially increase in concentration. Thus, determination of concentrations of pro-IL-1β and IL-1β is an indirect method for testing caspase-1 activity.

To determine the effect of PAA on intracellular levels of pro-IL-1β and IL-1β, an *in vitro* cell based assay was carried out by Dr Brad Simpson using a human monocytic cell line (THP-1 cells). In brief, the assay consisted of preincubation of THP-1 cells with PAA or Bay-11-7082 (as a positive control). Inflammatory pathways were stimulated with TPA

and cells were incubated for 24 hours. After incubation, the supernatant was separated and cells were washed and lysed. Lysates of samples were then centrifuged and analysed by an ELISA method. Further details can be found in Chapter 6.3.1. The collected data of intracellular pro-IL-1β and IL-1β are shown in Figure 3.4.

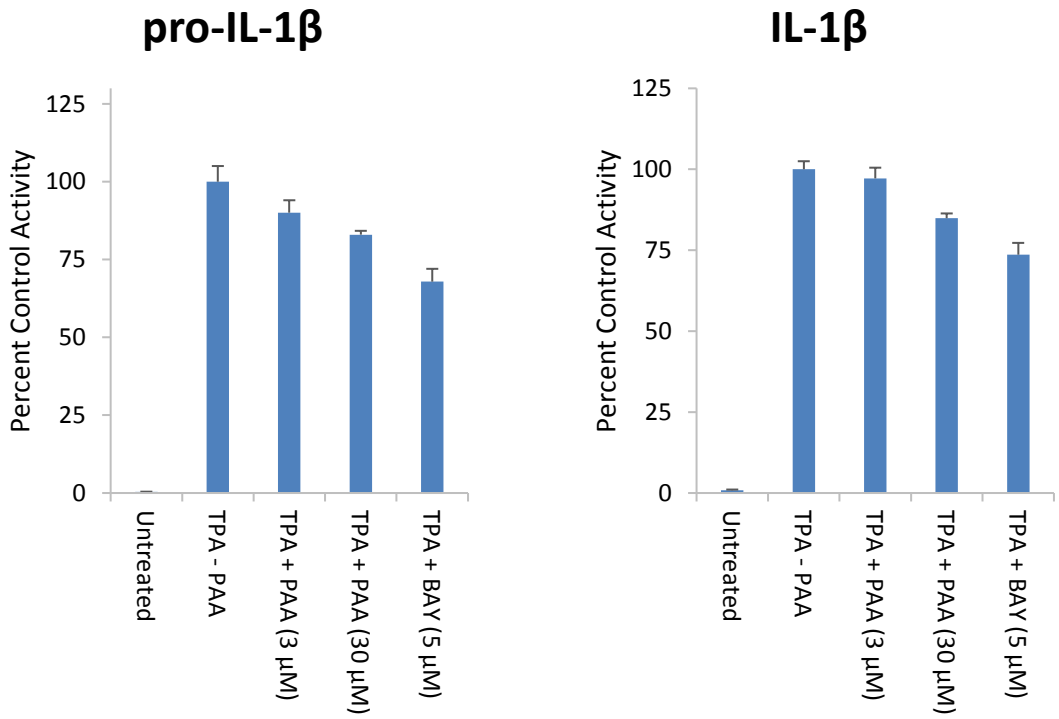

Figure 3.4: Effects of PAA on pro-IL-1β (left) and IL-1β (right) intracellular production by THP-1 cells. *Experiments are controlled by the presence of a NF-κB inhibitor (BAY 11-7082, positive control) and absence of inhibitor (negative control). Data are presented as means ± SEM (n = 8). Experiments were performed by Dr Brad Simpson.*

It was observed that PAA inhibited production of both pro-IL-1β (17% by 30 µM PAA) and IL-1β (15% by 30 µM PAA) to approximately equivalent extents at similar concentrations. In affecting both the inactive and active forms of the cytokine, this observation suggested that PAA is unlikely to be an inhibitor of caspase-1. As the method used to assess caspase-1 activity was indirect, it is possible that PAA may still bind to the receptor, however the evidence collected suggests that this is either not the case, or PAA binding to caspase-1 does not result in significant inhibition.

3.2.1.4. Caspase-1 discussion

Caspase-1 was investigated as a target of interest as it is well understood that caspase-1 activates the pro-inflammatory cytokines IL-1β and IL-18 from their inactive forms [224]. While caspase-1 is recognised for its involvement in the inflammasome and has previously been highlighted in the literature for its potential as an anti-inflammatory target [225], only one inhibitor of caspase-1, pralnacasan, has been developed for the treatment of anti-inflammatory disorders, specifically rheumatoid arthritis [226]. Development of pralnacasan was ultimately terminated in phase II after a long-term animal toxicology study discovered liver abnormalities, although no such abnormalities were observed in humans involved in trials [227, 228]. As PAA had been demonstrated to downregulate expression of IL-1β, caspase-1 was considered as a potential inhibitory target of PAA.

Initial investigation of caspase-1 was performed with *in silico* techniques, utilising ROCS overlays and docking to probe the potential of caspase-1 as a target of PAA. ROCS overlays were performed against a set of caspase-1 inhibitors retrieved from appropriate PDB crystal structures. The results showed that ROCS similarity was weak between PAA and the known inhibitors of caspase-1 for both the shape and color scoring components, although two small caspase-1 ligands showed stronger color scores than all other ligands. Owing to the availability of crystal structure data, docking of PAA to caspase-1 enzymes was also pursued and revealed several promising findings. Docking of PAA to a crystal structure of caspase-1 (PDB ID: 3NS7) suggested that PAA binds in a similar mode to the bound ligand (**13**) by forming interactions with key residues including Arg 179, Arg 341 and His 352. Despite weak ROCS alignment results, results from docking indicated potential of PAA as a caspase-1 inhibitor and *in vitro* techniques were used to screen PAA against caspase-1. As caspase-1 initiates the cleavage of pro-IL-1β to form IL-1β, an inhibitor of caspase-1 would be expected to lower the production of IL-1β but leave production of pro-IL-1β unchanged. Hence, screening of the production of both of these compounds was used to determine if there was any inhibitory activity towards caspase-1.

As shown in Figure 3.4, production of both pro-IL-1β and IL-1β by THP-1 cells were reduced to a similar extent by dose dependent exposure to PAA suggesting that while PAA is involved in the downregulation of IL-1β, the mechanism of this down-regulation is likely

to occur independent of the caspase-1 mechanism. It is possible that further *in vitro* analysis using direct receptor binding studies, or gene transcription via western blot studies, could further elucidate potential interactions of PAA and caspase-1, however based on the data collected further investigation into caspase-1 as a target of PAA was discontinued.

3.2.2. Protein kinase C (PKC)

Protein kinases are a large and diverse family of enzymes that phosphorylate other proteins to either alter their function or activate them [229]. The biological functions of kinases are extensive and diverse, including many aspects of cell function, regulation and proliferation, but the focus in this section will be devoted to the inflammatory functions of a specific subset of protein kinases, namely the subgroup referred to as protein kinase C (PKC) [230]. Primarily, PKC was considered as a target because of its role in TPA-induced inflammation [56]. As TPA-induced inflammation has previously been demonstrated to be attenuated by PAA [14], it was examined for inhibitory activity against PKC using both *in silico* and *in vitro* methods.

3.2.2.1. ROCS investigation of PKC as a target

A list of PKC inhibitors was constructed by searching through commercial databases. In total, 15 compounds were retrieved from the Tocris Bioscience PKC inhibitor catalogue [231] and stored as SMILES strings, with stereochemical information retained in structures. This catalogue of inhibitors was used as the compounds consisted of a diverse range of structural scaffolds. The 2D-representations of the structures are listed in Appendix 3. The 3D-structures of the PKC inhibitors were generated by Omega 2.5.1.4 using the default maximum number of conformers for each structure (200 conformers). Overlay analysis was then performed using ROCS 3.2.0.4 by the methods described in Chapter 6.5.5. PAA was used as a query for ROCS analysis against the prepared 3D-structural library of PKC inhibitors. A scoring breakdown of the ROCS analysis is shown in Table 3.3.

Table 3.3: ROCS scores of PAA as a query to PKC inhibitors. *Compounds are ranked by TanimotoCombo score.*

VIDA Name	Tanimoto Combo	Shape Tanimoto	Color Tanimoto	Shape/Color ratio
Chelerythrine	0.697	0.483	0.214	2.3
Go 6976	0.670	0.470	0.200	2.4
CGP 53353	0.629	0.487	0.143	3.4
C-1	0.619	0.470	0.148	3.2
PKC 412	0.614	0.469	0.145	3.2
K-252c	0.598	0.498	0.100	5.0
Bisindolylmaleimide II	0.597	0.427	0.170	2.5
LY 333531	0.566	0.469	0.097	4.8
Ro 32-0432	0.558	0.449	0.108	4.2
Rottlerin	0.554	0.449	0.106	4.2
TCS 21311	0.543	0.338	0.205	1.7
Go 6983	0.520	0.443	0.077	5.8
Calphostin C	0.517	0.352	0.165	2.1
GF 109203X	0.503	0.453	0.050	9.1
D-erythro-sphingosine	0.480	0.330	0.150	2.2

TanimotoCombo scores were low across the inhibitors screened, with the highest ranked compound, chelerythrine scoring 0.697 and the lowest ranked compound, D-erythro-sphingosine scoring 0.480. Breaking the TanimotoCombo score down to its component shape and color scores, revealed that a significant proportion of each combo score was due to contribution of shape similarity. The ShapeTanimoto scores described moderate similarity in some molecules (K-252c, 0.498; CGP 53353, 0.487; chelerythrine, 0.483) and, over all molecules, an average score of ~0.440. ColorTanimoto scores, by comparison, were uniformly low with the highest scoring compound, chelerythrine, scoring just 0.214 and the mean of all scores being ~0.145. As a simple means of comparing the two scoring functions, the ratio of shape to color scoring was determined and it was found that shape scored universally higher with most compounds scoring 2- to 4-fold higher, with the most extreme example (GF 109203X) being 9-fold higher. This finding suggested that PAA bore some structural similarity in its size and shape to PKC inhibitors, but its electrostatic

features were vastly different. ROCS aligned poses of the four highest ranked compounds are shown in Figure 3.5.

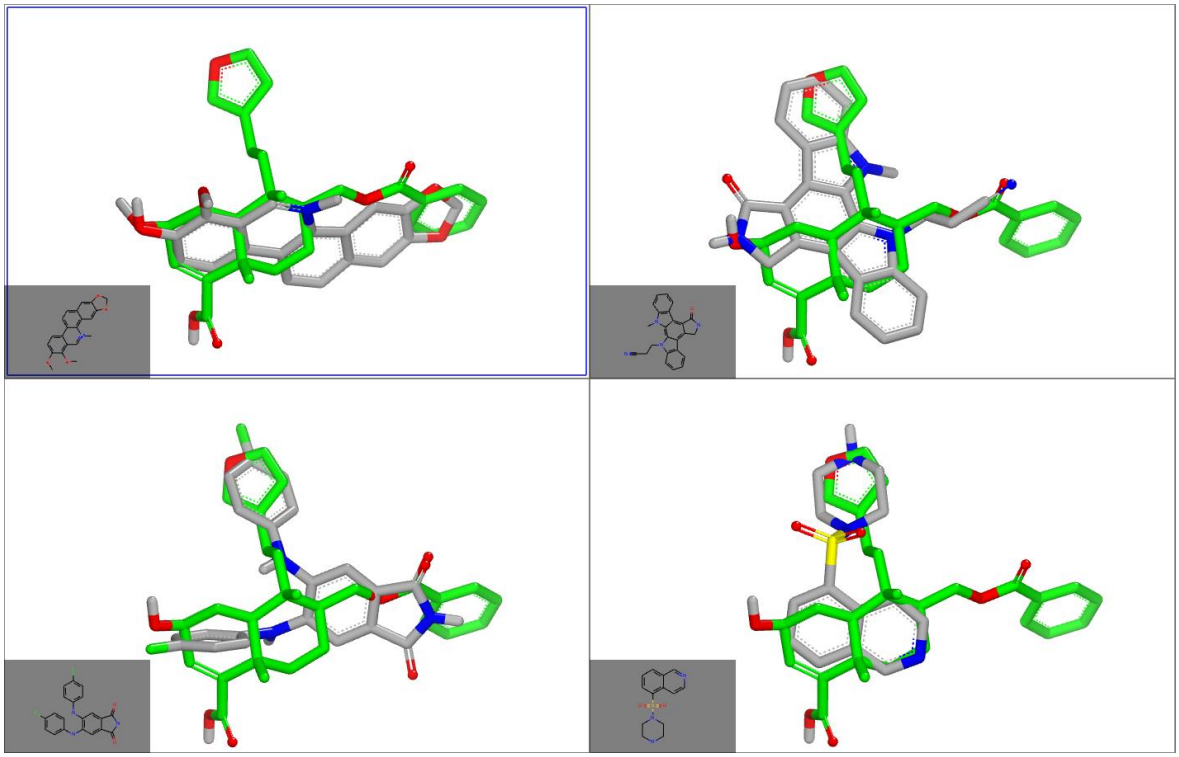

Figure 3.5: ROCS overlays of PAA (green) to the four highest ranked PKC inhibitors (grey). *PKC inhibitors are chelerythrine (top left, indicated by blue box), Go 6976 (top right), CGP 53353 (bottom left) and C-1 (bottom right). Compounds have been ranked by TanimotoCombo score and 2D representations of the inhibitors are inset.*

Of the top four ROCS aligned compounds, the highest scoring alignments did not appear to reveal any significant structural similarities between PAA and the compounds. While the PKC inhibitors appear to occupy a similar volume to PAA and the shapes of the structures broadly overlap, there are few observable electrostatic matches. The central ring structure of PAA overlapped with rings in three of the molecules (chelerythrine, Go 6976 and C-1) and the furan ring also overlapped with ring structures in three molecules (Go 6976, CGP 53353 and C-1), but the nature of these ring overlaps was quite different. For example, the furan ring of PAA overlapped with a piperazine ring in C-1. Amongst the hydrophilic features of the molecules, the only noteworthy overlaps were the hydroxyl groups in PAA and chelerythrine. According to these observations it is predictable that in the

TanimotoCombo metric, shape features will contribute more strongly to the aggregate score than color features.

A pharmacophore map to describe small molecule inhibitors of PKC was developed by McGregor [232]. This study consisted of mapping 220 PKC inhibitors superimposed over the bound ligand of a kinase crystal structure (PDB ID: 1ATP [233]) by least-squares fitting. The electrostatic features of each molecule were then characterised (hydrogen-bond acceptors/donors, hydrophobes, positive and negative charges, aromatic rings and "non-specific", or X), represented by a coloured dot and plotted on the crystal structure. The complete pharmacophore map of all PKC inhibitors is shown in Figure 3.6.

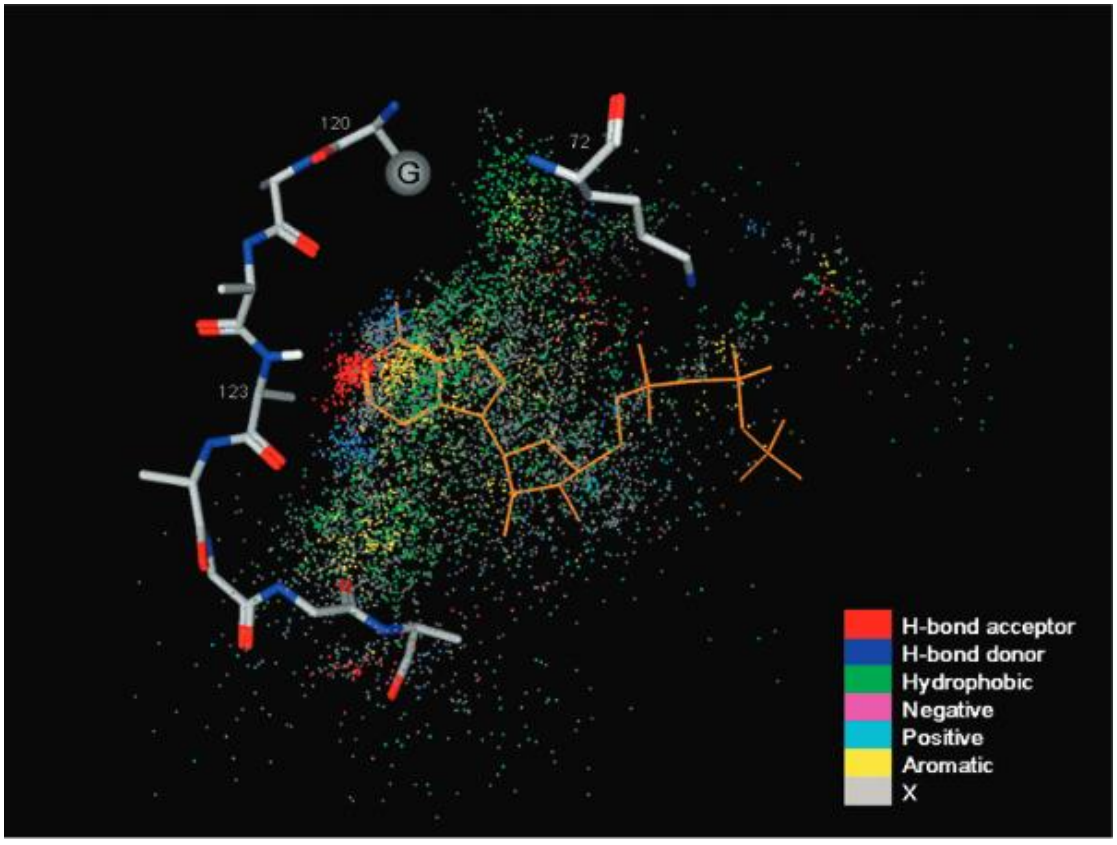

Figure 3.6: Complete pharmacophore map for PKC inhibitors. *Residues of the reference protein (PDB ID: 1ATP) are displayed along with reference ligand (ATP). The sphere 'G' represents the 'gatekeeper' residue of the structure. (Adapted with permission from J Chem Inf Model, 1 Nov 2007, volume 47, pages 2374-2382. Copyright 2007 American Chemical Society).*

In summary, it was determined that the most abundant electrostatic features of PKC inhibitors were hydrophobes, including rings and alkyl chains, followed by aromatic rings [232]. More hydrophilic features such as hydrogen-bonding groups or formal charges were far less abundant. This suggested that PKC inhibitors, in general, are more hydrophobic in nature, and hydrophilic features, especially formal charges, are rarer. In the case of PAA, which has a prominent formal charge because of its carboxylic acid group, the findings of McGregor would suggest that there is a low likelihood of PAA being an inhibitor of PKC. However, the presence of the charged acid group does not necessarily preclude PAA from having this activity.

While there are a number of PKC crystal structures available for analysis by docking [234-236], since there was no strong indication of similarity between PAA and PKC inhibitors from ligand-based *in silico* methods, it was decided that there was likely little value in pursuing structure-based methods. Additionally, as there are 15 subtypes of PKC receptors, prospective docking is not a suitable approach as selecting any given receptor subtype for docking without prior indications of binding information is an irrational approach. According to the results of the ROCS analysis, PAA was screened *in vitro* against a battery of PKC receptors to test the hypothesis that PAA would not be an inhibitor of PKC.

3.2.2.2. *In vitro* screening of PKC by PAA

A number of PKC subtypes were screened *in vitro* via a binding inhibition study. The binding study was performed externally by a Life Technologies SelectScreen Biochemical Kinase Profiling Services assay. In brief, the assay protocol involved combining a kinase receptor with PAA in buffer and ATP solution as a kinase co-factor, followed by incubation at room temperature. Upon incubation a reagent solution was added and followed by a further incubation period, plates were then analysed using a fluorescence plate reader. Screening results of PAA against PKC subtypes are shown in Table 3.4.

Table 3.4: Screening results of PAA against various PKC subtypes. *PKC screening is determined by binding inhibition of a labelled inhibitor (staurosporine). Data are presented as percentage inhibition of two replicate assays and the mean.*

Kinase tested	Replicate 1 (%)	Replicate 2 (%)	Mean inhibition (%)	Z' factor
PKCα	3	6	4	0.81
PKCβI	-1	1	0	0.74
PKCβII	-14	-21	-18	0.53
PKCδ	3	3	3	0.87
PKCϵ	-3	-6	-4	0.70
PKCγ	11	8	9	0.64
PKCη	2	8	5	0.54
PKCι	0	-14	-7	0.85
PKCν	-9	-7	-8	0.76
PKCθ	0	3	1	0.92
PKCζ	-11	-12	-11	0.79
PKCμ	10	6	8	0.64

Screening of PAA against a battery of PKC subtypes revealed no significant inhibitory activity by PAA. Perhaps the most significant observed result from screening was binding to PKCβII, which had a negative inhibition, or activation, of 18%. This weak PKC activation by PAA may be reflected in cellular responses associated with PKC activation, but in terms of inflammation, it would run counter to the observed anti-inflammatory actions of PAA. The reliability of each assay was assessed by the Z' factor, which is a ratio between positive and negative controls. In general, a Z' factor of >0.5 is considered reliable. In this assay, Z' factor was established by the difference in signal between staurosporine binding with no inhibitor (positive control) and no staurosporine binding (negative control). Since all Z' factor scores in these assays were above this threshold, the results may be considered reliable. Thus, it is unlikely that the data is indicative of interactions between PAA and PKC and the anti-inflammatory activity of PAA is likely attributed to a different target (or targets).

3.2.2.3. Protein kinase C discussion

The term protein kinase refers to a family of enzymes that phosphorylate other proteins to instigate a functional change [237]. The kinase receptors of the protein kinase C (PKC) subfamily have been highlighted in numerous studies as potential anti-inflammatory targets as the activation of PKC has been suggested to mediate activity of pro-inflammatory proteins and cytokines such as NF-κB, TNFα and various interleukins [55]. The use of phorbol esters, such as TPA, to initiate inflammation *in vivo* and *in vitro* is typical in inflammatory research and it is well understood that the primary pathway of phorbol ester inflammation involves PKC activation [238, 239]. For this reason, the PKC family was initially considered as a potential target of PAA as TPA had been used in mice to initiate inflammation and, furthermore, that PAA was demonstrated to significantly inhibit this inflammation [12].

By way of initial exploration, *in silico* screening utilising the ROCS method was employed to investigate structural similarities between commercial PKC inhibitors and PAA. Overall, structural similarity was poor with color similarity being low while shape scoring provided only moderate indications of similarity. Additionally, analysis of a published pharmacophore map describing PKC inhibitors showed that as formal charges on molecules are quite rare in typical PKC inhibitors, it was predicted that PAA was not likely to be an inhibitor of PKC. According to these findings PAA was screened against a battery of PKC subtypes to determine receptor binding. As shown in Table 3.4, no significant binding was observed suggesting no interaction between PAA and the protein kinases screened and it was concluded that PAA is unlikely to produce an anti-inflammatory response by PKC inhibition.

3.2.3. Nuclear factor-κB (NF-κB)

Nuclear factor-κB (NF-κB) is a protein complex that is associated with the production of pro-inflammatory cytokines including IL-1β, IL-6 and tumor necrosis factor alpha (TNFα), through upregulation of proteins associated with production of cytokines [240]. As it had been demonstrated that PAA is capable of attenuating these same cytokines, NF-κB was considered as a potential target of PAA. It was thought that PAA was likely to

be extensively hydrolysed *in vitro* (refer to Chapter 2.2.2), particularly in cell based assays where hydrolysis may occur enzymatically, or otherwise, and PAAH was likely to be the primary active compound. As such *in vitro* experiments continued to be carried out with PAA, but the focus of *in silico* experiments shifted to PAAH.

3.2.3.1. ROCS investigation of NF-κB as a target

A list of NF-κB inhibitors was constructed by searching through commercial databases. In total 31 compounds were retrieved from the Tocris Bioscience NF-κB and IκB inhibitors catalogue [241] and stored as SMILES strings, with stereochemical information retained in the structures. The 2D-representations of the structures are listed in Appendix 4. The 3D-structures of the NF-κB inhibitors were generated by Omega 2.5.1.4 using a default maximum number of conformers for each structure (200 conformers). Overlay analysis was then performed using ROCS 3.2.0.4 by the methods described in Chapter 6.5.5. A scoring breakdown of the ROCS analysis is shown in Table 3.5.

Table 3.5: ROCS scores of PAAH as a query to NF-κB inhibitors. *Compounds are ranked by TanimotoCombo score.*

VIDA Name	Tanimoto Combo	Shape Tanimoto	Color Tanimoto	Shape/Color ratio
Andrographolide	0.973	0.764	0.209	3.7
Cardamonin	0.926	0.623	0.303	2.1
Caffeic acid phenethyl ester	0.861	0.556	0.304	1.8
ML 120B	0.849	0.633	0.216	3.0
PS 114	0.842	0.614	0.228	2.7
Arctigenin	0.804	0.556	0.248	2.2
Tanshinone IIA	0.802	0.588	0.215	2.7
ML 130	0.799	0.653	0.146	4.5
Ro 106-9920	0.789	0.614	0.175	3.5
Honokiol	0.754	0.574	0.18	3.2
Bay 11-7085	0.751	0.559	0.191	2.9

Continued on following page

Table 3.5: Continued from previous page

VIDA Name	Tanimoto Combo	Shape Tanimoto	Color Tanimoto	Shape/Color ratio
HU 211	0.745	0.654	0.091	7.2
Gliotoxin	0.731	0.531	0.200	2.7
10Z-Hymenialdisine	0.708	0.607	0.101	6.0
Bay 11-7821	0.698	0.551	0.147	3.8
Amlexanox	0.697	0.49	0.208	2.4
ACHP	0.694	0.571	0.123	4.6
TPCA-1	0.694	0.526	0.168	3.1
Luteolin	0.688	0.484	0.204	2.4
SC 514	0.687	0.462	0.225	2.1
IMD 0354	0.673	0.547	0.126	4.3
CID 2858522	0.672	0.481	0.191	2.5
Sulfasalazine	0.667	0.516	0.151	3.4
SP 100030	0.667	0.484	0.182	2.7
BMS 345541	0.662	0.488	0.173	2.8
Piceatannol	0.628	0.527	0.101	5.2
Celastrol	0.628	0.509	0.119	4.3
Pristimerin	0.628	0.509	0.119	4.3
IKK_16	0.577	0.45	0.127	3.5
PF_184	0.530	0.398	0.132	3.0
Bengamide_B	0.436	0.309	0.127	2.4

Based on the TanimotoCombo metric, moderate similarity between PAAH and NF-κB inhibitors was observed. When considering the Tanimoto metric, there is no standard for determining whether any given value is significant, although a score of 0.5 or higher (1.0 for the TanimotoCombo scoring function) is often considered interesting [242]. The highest ROCS scored molecule was andrographolide with a combo score of 0.973, which is slightly lower than the previously described level of interest. Splitting the combo score into its component shape and color scores however made the ROCS analysis more informative as it revealed a fairly strong relationship between PAAH and NF-κB inhibitors based on shape scoring. The average ShapeTanimoto score for the set of NF-κB ligands was 0.543, with a maximum score of 0.764 for andrographolide and with a few other high scoring

examples (HU 211, 0.654 and ML 130, 0.653). Color scores, by comparison, were much lower, with a mean score of 0.175 and maximum of 0.304, lower than the lowest shape scored compound (bengamide B, 0.309). By measuring the ratio of shape to color scoring for each molecule, it is apparent that shape scored significantly higher in all molecules with a mean ratio for all molecules of 3.4. This analysis found that PAAH bore many similarities in shape to NF-κB inhibitors, but little overlap of electrostatic features was observed. Overlay poses of the highest ranked NF-κB inhibitors and PAAH are shown in Figure 3.7.

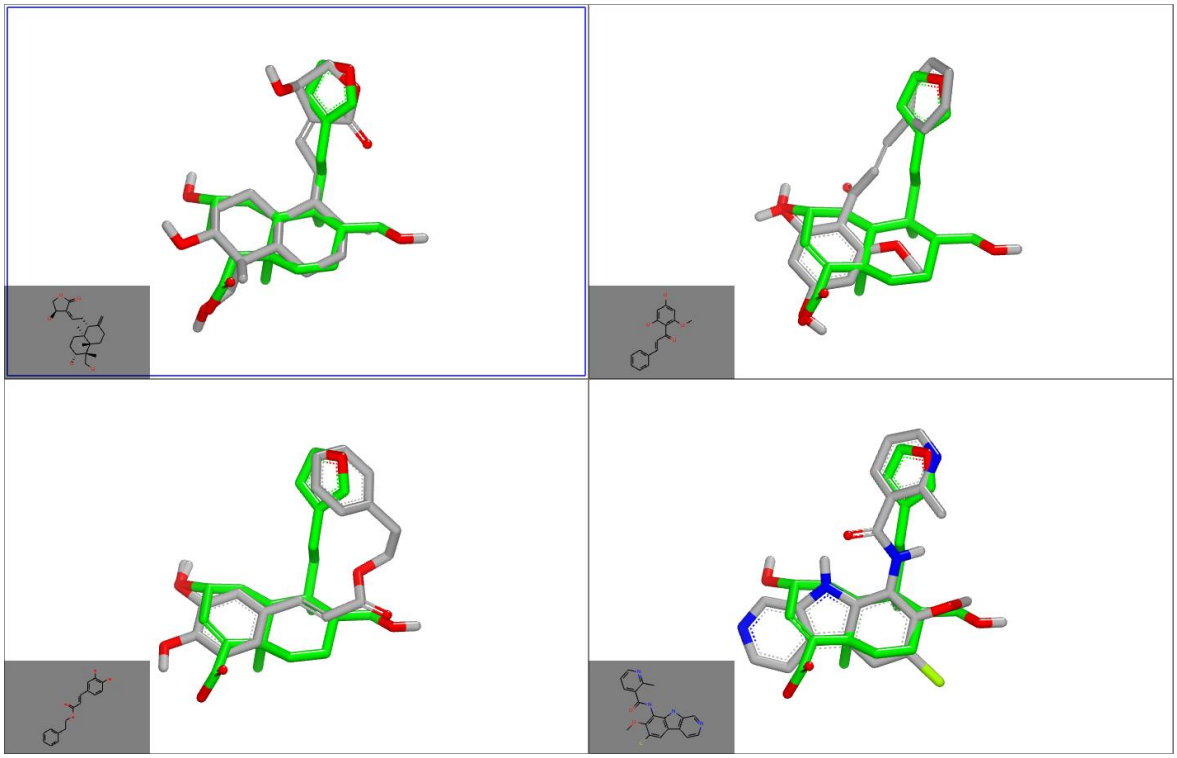

Figure 3.7: ROCS overlays of PAAH (green) to the four highest ranked NF-κB inhibitors (grey). *NF-κB inhibitors are andrographolide (top left, indicated by blue box), cardamonin (top right), caffeic acid phenethyl ester (bottom left) and ML 120B (bottom right). Compounds have been ranked by TanimotoCombo score and 2D representations of the inhibitors are inset.*

Based on analysis of the ROCS poses of the top four ranked compounds (by TanimotoCombo), there are obvious shape similarities apparent in the molecules. The occupied volume of each molecule quite closely matches the structure of PAAH, especially in the top ranked compound, andrographolide. Andrographolide is a naturally occurring diterpenoid, isolated from *Andrographis paniculata* (Acanthaceae), and has been

demonstrated to possess anti-inflammatory and anti-malarial activity [243]. As the two molecules come from the same structural class it is unsurprising that the scaffolds of both molecules are highly similar, however there are some key differences in electrostatic features. Two key differences between the molecules are a lactone ring in andrographolide, in place of a furan ring in PAAH, and a hydroxyl group in andrographolide, in place of a carboxylate in PAAH. These differences explain why the overlay of the two molecules has a low color score, while the shape scores are much higher. In all four of the top ranked molecules, a ring feature of each molecule is overlaid to the furan ring of PAAH by a flexible linking chain. Additionally, ring overlaps are observable in each of the molecules with the central decalin structure of PAAH. Hydrophilic features of the molecules did not appear to overlap well with PAAH. None of the top scoring molecules contained an anionic group and hydroxyl overlaps were only evident in two structures (cardmonin and caffeic acid phenethyl ester). These observations reflect the previous findings in the scoring metrics that the shape of the molecules matched well with PAAH, but the color features matched poorly.

While crystal structures of NF-κB are available [244, 245], no crystal structure containing a bound inhibitor i.e. in its inactive state, has been characterised. This complicates the process of docking as a protein may change shape significantly between active and inactive forms. Additionally, there is evidence that NF-κB inhibitors may bind to multiple sites of the receptor complex, including indications of an allosteric site [246]. As such, a docking approach would not be suitable without prior knowledge of how the molecule is thought to bind to the receptor complex. Accordingly, docking was not pursued, but based on the shape similarities noted between PAAH and NF-κB inhibitors from ROCS analysis, an *in vitro* experiment was used to determine if any biological activity followed the observed shape similarity.

3.2.3.2. *In vitro* screening of NF-κB by PAA

The ability for PAAH to inhibit NF-κB activity was tested *in vitro* via an in-direct process. Summarised from Chapter 1.2.7, a common marker of NF-κB activity is nitric oxide (NO) production via NF-κB-mediated iNOS activation [64]. NF-κB inhibitors are known to inhibit production of NO and accordingly, screening of nitrite, via the Griess assay, can be used as a marker of NO production, and hence, NF-κB activity [247]. The experiment,

performed in rodent macrophage cells (RAW 264.7), used PAA as a test molecule and not PAAH. It was considered acceptable to use PAA for this purpose as it had been previously established that PAA is metabolised to PAAH by esterases (see Chapter 2.2.2), and RAW 264.7 cells express esterases, and have previously been used to screen esterase-sensitive anti-inflammatory prodrugs [248].

To determine the effect of PAA on nitrite production, an *in vitro* cell based assay was carried out by Dr Brad Simpson using RAW 264.7 cells. In brief, the assay involved preincubating RAW 264.7 cells with PAA or Bay-11-7082 (as a positive control). Bay-11-7082 is an inhibitor of cytokine induced Iκβ-α phosphorylation, and hence an inhibitor of NF-κB translocation to the nucleus [249]. The use of RAW 264.7 cells, as murine cells, is justifiable for this testing as PAA has previously been demonstrated to attenuate inflammation in mice [12]. An inflammatory response in the cells was then stimulated via addition of lipopolysaccharide (LPS) and incubated for 24 hours. Nitrite was detected by the Griess assay and absorbance was measured using a plate reader. Further details can be found in Chapter 6.3.1. Results of NO screening in RAW 264.7 cells are shown in Figure 3.8.

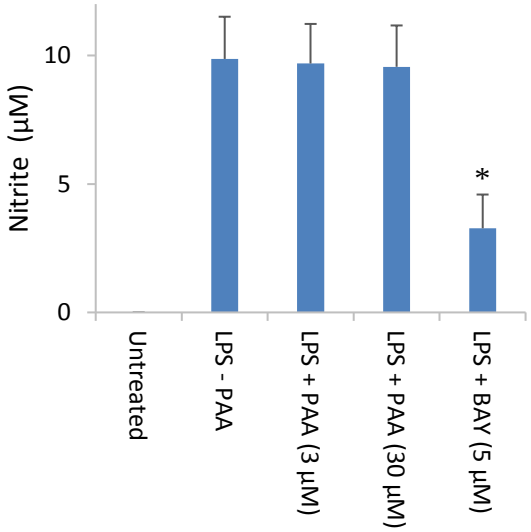

Figure 3.8: Screening results of PAA effects on nitrite production by RAW 264.7 cells as measured colorimetrically using the Griess assay. *Experiments are controlled by the presence of the NF-κB inhibitor BAY 11-7082 (positive control, LPS + BAY) and absence of inhibitor (negative control, LPS – PAA). Data are presented as means ± SEM (n = 8). *p < 0.05, significant difference was observed between LPS – PAA (control) and LPS + BAY as determined by Dunnett's post hoc test. Experiments were performed by Dr Brad Simpson.*

Screening of the effects of PAA on NO production in cells revealed no significant inhibition (*$p < 0.05$) after treatment by PAA at concentrations up to 30 μM. In contrast, treatment by BAY-11-7082, a known NF-κB inhibitor, resulted in a significant decrease of nitrite versus control (*$p < 0.05$). These findings are suggestive that PAA, and by extension PAAH, is not an inhibitor of NF-κB. Western blot studies could be used to conclusively state that PAA does not interact with NF-κB via determination of NF-κB gene expression, but this was not pursued based on the indications from the Griess assay.

3.2.3.3. NF-κB discussion

NF-κB, like caspase-1, is a nuclear factor that is well understood to be involved in the expression of a number of pro-inflammatory cytokines including interleukins and TNFα [240]. NF-κB has been highlighted in numerous studies as a potential anti-inflammatory target [250, 251] and many natural products, including andrographolide, bengamide B and cardamonin, are known to inhibit the function of NF-κB in inflammatory states [252-254]. Testing for inhibition of NF-κB by PAA was undertaken as a result of cytokine screening suggesting a decrease in IL-1β and TNFα, both cytokines of which are known to be regulated by NF-κB [255].

Inhibitors of NF-κB are known to function by a number of mechanisms [256, 257], for instance, andrographolide exhibits NF-κB inhibition via MAPK inhibition [258] and sulfasalazine is known to suppress NF-κB activity via IKKβ inhibition [259]. For this reason, low structural similarity to certain NF-κB inhibitors may not be a strict impediment to predictive activity if other molecules have a higher similarity, since low similarity may just indicate that a particular mechanism of inhibition is unlikely. Reasonably high shape based similarity was observed with many NF-κB inhibitors, especially between PAAH and andrographolide, another natural diterpenoid [260], but color based similarity was approximately 3.5-fold lower. This suggested that while PAAH had some structural similarity to NF-κB inhibitors, the differences in electrostatic features may mean that PAAH is not suitable for binding to the NF-κB receptor complex. Potential activity of PAA was investigated *in vitro* by screening of NO secretion in RAW 264.7 cells as NF-κB activation is known to induce NO expression and therefore inhibition of NF-κB can reduce secretion of NO [261].

As shown in Figure 3.8, PAA was ineffective at all drug concentrations in reducing NO production as measured indirectly as nitrite concentration using the Griess assay. In comparison, BAY-11-7082, a known inhibitor of NF-κB function, reduced the nitrite concentration significantly [262]. These findings suggested that NF-κB was likely not inhibited by PAA, and therefore the anti-inflammatory activity of PAA was concluded to operate independently of NF-κB.

3.2.4. Glucocorticoid receptor

Glucocorticoid receptors are a type of nuclear receptor associated with homeostasis, metabolism and immune responses [161, 162]. It has been demonstrated that activation of the glucocorticoid receptor results in inhibition of NF-κB [163] and accordingly glucocorticoid drugs have been used widely for the treatment of inflammatory disorders [263]. As PAA had been demonstrated to operate independently of the NF-κB receptor, but seemed to be associated with actions common to the NF-κB receptor i.e. TNFα and interleukin suppression, the glucocorticoid receptor was considered for investigation. PAAH was used as the investigative molecule for the glucocorticoid receptor for *in silico* analysis and both PAA and PAAH were screened *in vitro.*

3.2.4.1. ROCS investigation of the glucocorticoid receptor

In a study by Onnis et al. [137], a pharmacophore was developed to describe glucocorticoid agonists. Many traditional glucocorticoid agonists, such as dexamethasone and betamethasone, adhere to a steroidal scaffold (see Figure 3.9), although there are some known glucocorticoid agonists which do not follow this scaffold. One of the key advantages of the study by Onnis et al. was that the pharmacophore generated was created from a number of steroidal and non-steroidal agonists.

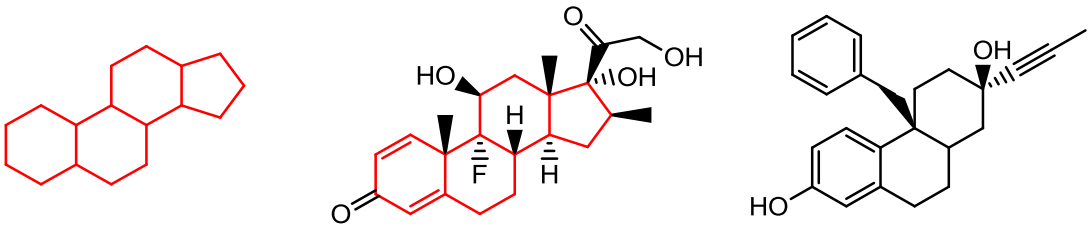

Steroid scaffold Betamethasone CP-409069

Figure 3.9: Structures of glucocorticoid agonists. *Structures include a steroidal (betamethasone) and non-steroidal (CP-409069) glucocorticoid receptor agonist, with a steroid scaffold (indicated in red) for reference.*

The pharmacophore of Onnis et al. was developed from a training set of 19 molecules consisting of 5 steroidal structures and 14 non-steroidal structures of diverse scaffolds. The most successful pharmacophore hypothesis (see Figure 3.10) consisted of four-spheres: two hydrophobes (HYD), one hydrogen-bond donor (HBD) and one aromatic sphere (HYD-aro). Robustness of the model was established through analysis of the correlation coefficient of binding affinity data (R^2 = 0.92), which indicated strong correlation between predicted and experimental values, thus validating the model. Additionally, RMSD analysis was used to assess the fit of the pharmacophore hypothesis to the training molecules, with a good fit obtained RMSD = 1.18 Å (where between 0 and 2 Å is considered low deviation [264]).

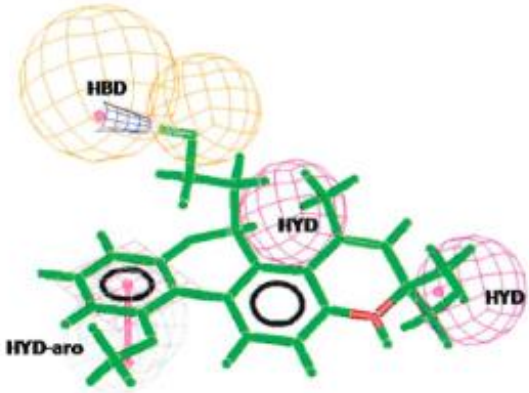

Figure 3.10: Pharmacophore of glucocorticoid receptor agonists. *'HBD' refers to a hydrogen bond donor, 'HYD' refers to a hydrophobe and 'HYD-aro' refers to an aromatic ring. (Reprinted with permission from J Med Chem, 26 Mar 2010, volume 53, pages 3065-3074. Copyright 2010 American Chemical Society).*

As the pharmacophore of glucocorticoids was demonstrated to be effective in describing both steroidal and non-steroidal glucocorticoid receptor agonists, both the pharmacophore and the training set used to develop the pharmacophore were utilised to determine the similarity of PAAH to glucocorticoid agonists. This was accomplished, as previously, through the use of the ROCS approach. The 19 compounds from the pharmacophore training set of Onnis et al. were retrieved and stored as SMILES strings, with stereochemical information retained. The 2D-representations of structures are listed in Appendix 5. Conformers of the molecules (200) were generated by Omega 2.5.1 and overlay analysis was then performed using ROCS 3.2.0.4 by the methods described in Chapter 6.5.5. PAAH was used as a query for ROCS analysis against the prepared 3D-structural library of glucocorticoid agonists. A scoring breakdown of the ROCS analysis is shown in Table 3.6.

Table 3.6: ROCS scores of PAAH as a query to glucocorticoid modulators. *Modulators have been defined as steroidal or non-steroidal modulators based on conformity to the traditional steroid scaffold. Compounds are ranked by TanimotoCombo score.*

VIDA Name	Steroidal/Non-steroidal	Tanimoto Combo	Shape Tanimoto	Color Tanimoto	Shape/Color ratio
GR9	Non-steroidal	0.779	0.619	0.160	3.9
GR7	Steroidal	0.764	0.552	0.212	2.6
GR19	Non-steroidal	0.762	0.633	0.130	4.9
GR13	Steroidal	0.759	0.540	0.219	2.5
GR10	Steroidal	0.749	0.594	0.155	3.8
GR17	Non-steroidal	0.707	0.534	0.173	3.1
GR5	Non-steroidal	0.705	0.561	0.144	3.9
GR8	Non-steroidal	0.694	0.561	0.133	4.2
GR16	Non-steroidal	0.693	0.508	0.185	2.8
GR14	Non-steroidal	0.693	0.560	0.133	4.2
GR12	Non-steroidal	0.687	0.577	0.110	5.3
GR2	Non-steroidal	0.677	0.431	0.246	1.8
GR18	Non-steroidal	0.677	0.524	0.153	3.4
GR15	Non-steroidal	0.671	0.508	0.163	3.1
GR3	Steroidal	0.662	0.550	0.112	4.9

Continued on following page

Table 3.6: Continued from previous page

VIDA Name	Steroidal/Non-steroidal	Tanimoto Combo	Shape Tanimoto	Color Tanimoto	Shape/Color ratio
GR4	Non-steroidal	0.654	0.431	0.223	1.9
GR11	Non-steroidal	0.630	0.484	0.146	3.3
GR6	Steroidal	0.605	0.464	0.141	3.3
GR1	Non-steroidal	0.594	0.484	0.110	4.4

From the ROCS analysis of PAAH with glucocorticoid agonists, there are moderate indications of similarity. The highest ranked compound, GR9, scored 0.779 in the TanimotoCombo metric, which was highly favourable towards the shape scoring function over color scoring (0.619 to 0.160). The shape-to-color ratio of each ROCS assessment was similar in all molecules with the mean of all values being 3.5. This indicates that of the glucocorticoid ligands, while the shapes of each ligand are similar to that of PAAH, there are larger differences in their electrostatic features. These apparent differences in electrostatic features may indicate a low possibility of similarity in binding activity, however further analysis can be conducted based on the pharmacophore developed by Onnis et al. A structure overlay of the highest ranked glucocorticoid modulator, GR9, and PAAH is shown in Figure 3.11.

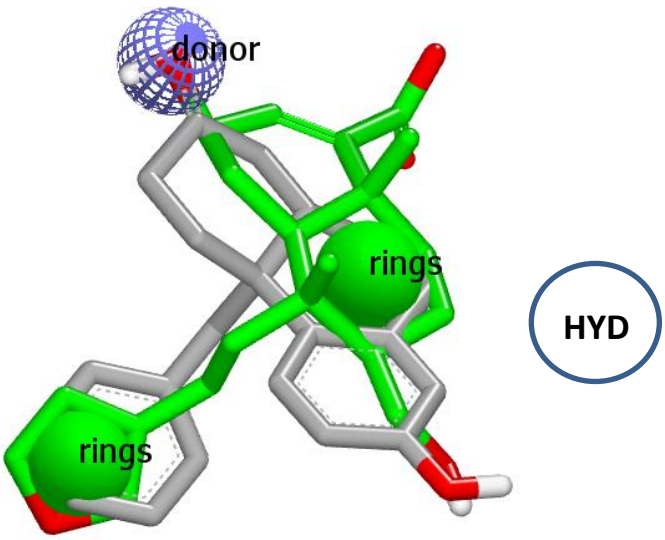

Figure 3.11: ROCS overlay of PAAH (green) and GR9 (grey). *ROCS generated spheres are indicated where significant pharmacophore overlaps are present. A blue circle represents the approximate position of a hydrophobic sphere not present in either molecule. Structures have been orientated to the pharmacophore presented in Figure 3.10.*

From the ROCS overlay of PAAH to GR9, it appears that three of the four spheres generated in the Onnis et al. pharmacophore hypothesis have strong alignment with analogous electrostatic features in PAAH. The four spheres in the original hypothesis include two hydrophobes, an aromatic sphere and a hydrogen bond donor. In the ROCS alignment there is strong overlap between one of the hydrophobic spheres, the aromatic sphere and the hydrogen bond donor sphere. The two methyl groups and carboxylate features of PAAH are not represented in GR9 with analogous structural features. This may explain why the Color Tanimoto score of the compounds is quite low (0.160). In most cases, a low color score may indicate that the possibility of an activity relationship between the two molecules is also quite low. However, in this example the key matches in structural features occur in positions which have been identified in a pharmacophore model to be predictive of glucocorticoid agonists. Therefore, while there may be electrostatic disparity elsewhere in the molecules, the matching of PAAH to three out of the four spheres in the pharmacophore hypothesis of Onnis et al. may be of potential interest. Additionally, the pharmacophore sphere not filled by PAAH, the second hydrophobic sphere, is also unoccupied by GR9.

The K_i value of GR9 as a glucocorticoid modulator was reported as 6 nM (binding affinities are listed in Table 3.9). GR2, which is an analogue of GR9, contains an alkyne group which is hypothesised to occupy the second hydrophobic sphere of the glucocorticoid pharmacophore (see Figure 3.12), and thus fill all four spheres of the hypothesis.

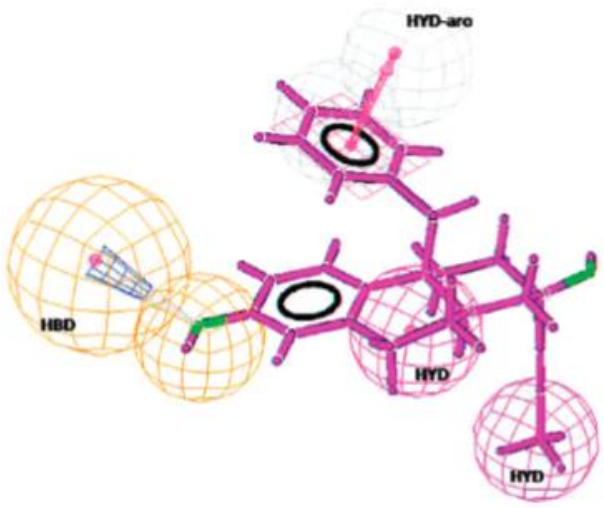

Figure 3.12: Pharmacophore of glucocorticoid agonists overlaid to GR2. *'HBD' refers to a hydrogen bond donor, 'HYD' refers to a hydrophobe and 'HYD-aro' refers to an aromatic ring. (Reprinted with permission from J Med Chem, 26 Mar 2010, volume 53, pages 3065-3074. Copyright 2010 American Chemical Society).*

The reported K_i value of GR2 as a glucocorticoid modulator is 0.17 nM (35-fold more potent than GR9, see Table 3.9), and as such it appears that not occupying all spheres of the pharmacophore is tolerated, but it may come at a cost of binding affinity. In the case of PAAH, which may be predicted to occupy three of the pharmacophore spheres, it may follow that its binding affinity will be lower than modulators which occupy all spheres. Additionally, the presence of the carboxylate group in PAAH, which does not have an analogous presence in GR2 or GR9, may further lower binding activity if the electrostatics of the receptor are incompatible with the feature.

To further investigate the usage of ROCS, an experiment utilising the same methodology as above was performed but instead using GR1 as a query and inserting PAAH in the screening library. GR1 was chosen as a query molecule firstly as it was the most dissimilar glucocorticoid modulator to PAAH as defined by the previous ROCS analysis and

secondly as GR1 had potent binding affinity to the glucocorticoid receptor (K_i 0.1 nm, see Table 3.9). The purpose of this analysis as such was two-fold, to compare how PAAH overlays with a known, potent modulator of glucocorticoid activity and to also compare how PAAH ranks amongst a pool of glucocorticoid modulators. The results of this analysis are shown in Table 3.7.

Table 3.7: ROCS scores of GR1 as a query to glucocorticoid modulators and PAAH. *Compounds are ranked by TanimotoCombo score. PAAH has been highlighted in bold.*

Position	VIDA Name	Tanimoto Combo	Shape Tanimoto	Color Tanimoto
1	GR1	2.000	1.000	1.000
2	GR2	1.888	0.999	0.889
3	GR9	1.665	0.901	0.763
4	GR4	1.245	0.746	0.499
5	GR6	1.164	0.721	0.442
6	GR3	1.062	0.605	0.458
7	GR19	0.885	0.626	0.259
8	GR11	0.882	0.592	0.289
9	GR10	0.874	0.517	0.357
10	GR8	0.873	0.659	0.214
11	**PAAH**	**0.837**	**0.591**	**0.246**
12	GR16	0.794	0.556	0.238
13	GR12	0.781	0.497	0.284
14	GR5	0.774	0.512	0.262
15	GR15	0.773	0.528	0.245
16	GR17	0.768	0.545	0.223
17	GR4	0.767	0.567	0.200
18	GR7	0.757	0.545	0.212
19	GR18	0.750	0.519	0.231
20	GR13	0.743	0.514	0.228

The structural scaffold of GR1 is highly similar to GR2 and GR9 (mentioned previously), and it is therefore unsurprising that both of these non-steroidal glucocorticoid agonists are ranked at the top of the list. The highest ranked steroidal structures are GR6 and

GR3 at rank 5 and 6, respectively. This suggests that, as a query molecule in a ROCS experiment, GR1 can successfully retrieve both steroidal and non-steroidal agonists successfully. There is, however, a large tanimoto difference between the rankings of the compounds: 1.888 (GR2) and 1.665 (GR9) for non-steroidal compounds and 1.164 (GR6) and 1.062 (GR3) for steroidal compounds. PAAH was ranked in position 11 with a Tanimoto Combo score of 0.837 (shape factor = 0.591, color factor = 0.246). These scores improved from the previous ROCS alignment scores reported earlier where GR1 scored a Tanimoto Combo of 0.594 (shape factor = 0.484, color factor = 0.110), with PAAH as a query. The likely reason for this apparent increase in shape similarity is due to the number of chemical features in the query molecule. When a query with a smaller number of features is used for ROCS analysis, the same number of feature matches can result in a higher ratio of matches, and hence a higher similarity score. This is analogous to the situation previously described in Section 3.2.1.1. It is notable from this ROCS analysis that between ranks 7 to 20, the Tanimoto Combo score only changed from 0.885 to 0.743, a shift of 0.142. The Tanimoto Combo of PAAH at 0.837 ranked in the middle of this cluster of glucocorticoid agonists. What this implies is that, from the perspective of GR1 as a query molecule, GR1 does not appear to distinguish PAAH as significantly different from a range of other glucocorticoid agonists, both from a steroidal and non-steroidal scaffold.

3.2.4.2. Docking investigation of the glucocorticoid receptor

Crystal structures of glucocorticoid receptors have been solved both with and without bound ligands, and so further *in silico* investigation by docking was applied. Crystal structures were retrieved from the RCSB Protein Data Bank and filtered by protein source (*Homo sapiens*), presence of a bound ligand and resolution (<3.00 Å). A list of glucocorticoid receptor structures satisfying these rules was constructed and is shown in Table 3.8. The 2D-representations of bound ligands from the list are provided in Appendix 6.

Table 3.8: List of PDB crystal structures of glucocorticoid receptors. *Names of bound ligands, structure resolutions and associated citations are also included.*

PDB ID	Bound ligand	Resolution (Å)	Citation
4UDC	Dexamethasone	2.50	[265]
4UDD	Desisobutyrylciclesonide	1.80	[265]
4CSJ	NN7	2.30	[265]
4P6W	Mometasone furoate	1.95	[266]
4P6X	Cortisol	2.50	[266]
4LSJ	Dibenzoxapine sulfonamide	2.35	[267]
3K22	Alaninamide	2.10	[268]
3K23	D-prolinamide	3.00	[268]
3E7C	GSK866	2.15	[269]
3CLD	Fluticasone furoate	2.84	[270]
3BQD	Deaxylcortivazol	2.50	[271]
1M2Z	Dexamethasone	2.50	[272]
1P93	Dexamethasone	2.70	[273]

Of the list of glucocorticoid receptor crystal structures available through the RCSB PDB, 4P6W and 3CLD stood out due to their furan-containing co-crystallised ligands, mometasone furoate and fluticasone furoate, respectively. This feature was considered especially interesting due to the presence of a furan ring in PAAH. The resolution of 4P6W was almost 1.00 Å higher at 1.95 Å compared to 2.84 Å for 3CLD, suggesting that the resolved crystal structure of 4P6W may be more reliable than that for 3CLD, and as such 4P6W was selected for docking experiments.

The crystal structure 4P6W was processed with Make Receptor 3.2.0.2 to define the active site. The active site was defined as the cavity around the co-crystallised ligand (mometasone furoate), as calculated using the molecular probe function of Make Receptor. A binding contour pocket was defined using the 'extend towards protein' function to maximise the binding area, resulting in a pocket size of 2839 $Å^3$. Docking was performed by the FRED module of OEDocking 3.0.1, using the method described in Chapter 6.5.4. The set of glucocorticoid ligands collated from Onnis et al. and PAAH, were submitted for

docking. Docking scores and binding affinities (as reported by Onnis et al.) are included in Table 3.9.

Table 3.9: Docking table of Chemgauss4 scores. PAAH and GR9, the highest ROCS scoring compound from Section 3.2.4.1, are highlighted in bold.

Position	VIDA Name	Chemgauss4 score	Activity, K_i (nM)
1	GR6	-17.0949	0.1
2	GR7	-15.7108	2.4
3	GR13	-15.4704	30
4	GR10	-15.1507	1.1
5	GR2	-14.3996	0.17
6	GR1	-14.0708	0.1
7	**GR9**	**-13.4163**	**6**
8	GR8	-13.3943	6.9
9	GR15	-13.3803	1,036
10	GR11	-13.2566	18
11	GR4	-12.9447	2
12	GR19	-12.8926	4,109
13	**PAAH**	**-12.7009**	**-**
14	GR17	-12.6439	2,465
15	GR16	-12.4692	1,766
16	GR18	-12.4371	3,210
17	GR14	-11.7796	2.8
18	GR3	-11.7105	0.24
19	GR12	-11.219	4.2
20	GR5	-10.9852	51

As shown in Table 3.9, FRED docking scored PAAH with a Chemgauss4 score of -12.7009, which placed it in position 13 amongst the glucocorticoid agonist list. The docking procedure appeared to moderately discriminate the agonists based on activity order as weaker agonists (K_i >1000 nM), appeared lower on the list and stronger agonists (K_i <10 nM), appeared higher on the list, but several quite strong agonists, such as GR3 (0.24 nM) and GR18 (2.8 nM) appeared near the end of the list at positions 18 and 17

respectively. The lowest energy docking pose for PAAH in the 4P6W receptor is shown in Figure 3.13.

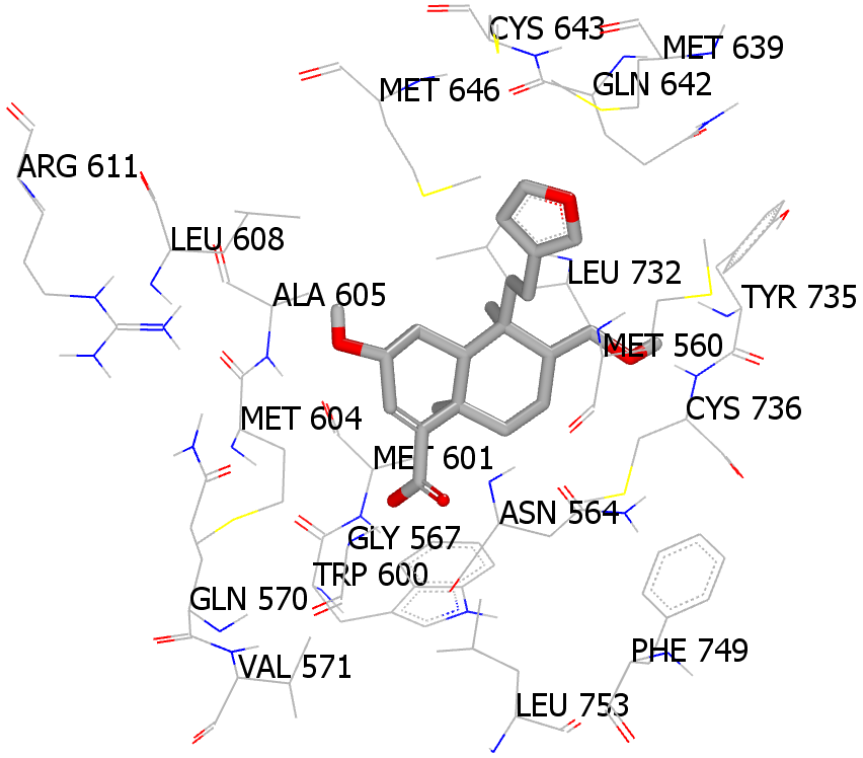

Figure 3.13: Docked pose of PAAH in the active site of the glucocorticoid receptor (PDB ID: 4P6W).

Figure 3.13 shows a proposed docking pose of PAAH in the glucocorticoid receptor active site. A number of hydrophilic and hydrophobic interactions can be observed between the docked PAAH and surrounding amino acid residues. Hydrophilic interactions include ion-dipole interactions between the carboxylic acid and Asn 564, and hydrogen bonding between the C2 alcohol (alcohol adjacent to the carboxylic acid) and Arg 611 and C17 alcohol (alcohol adjacent to the furan ring) and the amide backbone of Cys 736. The hydrogen bond between the C17 alcohol and Cys 736 is analogous to one formed by a hydroxyl group in mometasone. Hydrophobic interactions are observed between the furan ring and a number of residues forming a hydrophobic pocket including Met 639, Cys 643, Met 560 and Phe 623. The hydrophobic pocket occupied by the furan ring of PAAH is analogous to that occupied by the furan ring of mometasone furoate, the co-crystallised ligand of 4P6W (see Figure 3.14).

Based on previous ROCS analysis (Section 3.2.4.1), it was noted that numerous features in PAAH adhered to a pharmacophore of glucocorticoid agonists, however the carboxylate group in PAAH fell outside of the volume of this defined pharmacophore. The docking pose of PAAH in the glucocorticoid receptor placed the carboxylate group of PAAH into a weakly hydrophobic pocket of the binding cavity formed by residues including Trp 600, Met 601 and Leu 753, which would not be expected to accommodate a carboxylic acid group. The docking position of PAAH in this cavity places the carboxylic acid approximately equidistant (3.02 and 3.07 Å, respectively) between two residues: the hydrophobic Trp 600 and the hydrophilic Asn 564. The presence of the Asn 564 residue allows for ion-dipole interactions with the carboxylic acid, which could offset some of the unfavourable electrostatic interactions with Trp 600. A comparison of co-crystallised mometasone furoate to the docked structure of PAAH (without protein residues) is shown in Figure 3.14.

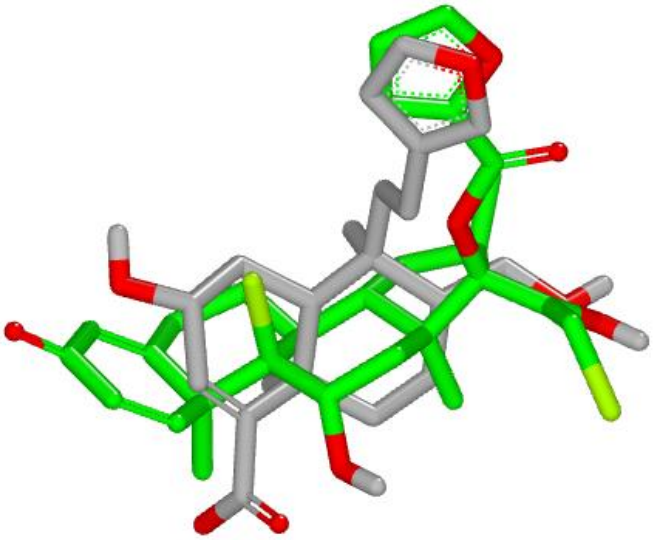

Figure 3.14: Overlay of docked PAAH to co-crystallised mometasone furoate. *PAAH is depicted in grey, mometasone furoate is depicted in green. Structure of mometasone furoate is that of the co-crystallised ligand of the glucocorticoid receptor (PDB ID: 4P6W). Amino acid residues from the crystal structure have been hidden.*

There is significant spatial overlap between PAAH and mometasone furoate, especially in the furan ring and central ring structure of both molecules. The C17 alcohol of PAAH and a hydroxyl of mometasone furoate are also in close proximity, suggesting that

analogous binding interactions of mometasone furoate may occur with PAAH, as mentioned previously. There are some differences in electrostatic features of the two molecules along the steroid-scaffold portion of mometasone furoate, with the C2 alcohol and carboxylic acid groups of PAAH not being particularly analogous to any feature of mometasone furoate. The distance between the C2 alcohol and the carbonyl group of mometasone furoate is approximately 3 Å, and the interactions observed between the receptor and mometasone furoate are not analogous between the receptor and PAAH.

Based on this docking study of PAAH with the glucocorticoid receptor there was some evidence to suggest that PAAH may be able to form binding interactions with the receptor. Due to the charge state of PAAH potentially interfering with the hydrophobic Trp 600 residue of the glucocorticoid receptor, it is possible that this interaction could result in either reduction or abolition of binding activity. Some of the interactions observed in the lowest energy docking pose of PAAH are common with mometasone furoate, a known modulator of glucocorticoid activity. Taking these docking results, along with the established structural relationship with the glucocorticoid agonist pharmacophore discussed in Section 3.2.4.1, *in vitro* investigation of PAAH as a glucocorticoid receptor modulator was conducted via a receptor binding assay.

3.2.4.3. *In vitro* screening of PAA and PAAH activation of the glucocorticoid receptor

The glucocorticoid receptor was screened *in vitro* by a direct process of receptor binding utilising a LanthaScreen TR-FRET (time-resolved fluorescence energy transfer) Glucocorticoid Receptor Coactivator assay. The glucocorticoid receptor increases the transcription of numerous anti-inflammatory proteins including IL-10 and IL-1 receptor antagonist as well as causing inhibitory functions on pro-inflammatory proteins such as NF-κB. As such, modulators of glucocorticoid receptor activity are known to possess anti-inflammatory activity.

A full description of the TR-FRET assay can be found in Chapter 6.3.3. In brief, the TR-FRET assay consisted of pre-incubating glucocorticoid receptors with PAA or PAAH, then adding a binding fluorophore and measuring fluorescence by TR-FRET. Addition of

the fluorophore results in fluorescence when bound to the receptor, therefore inhibition of fluorophore binding via a competitive ligand will result in diminished fluorescence. Screening results of glucocorticoid fluorophore displacement by PAA and PAAH are shown in Figure 3.15.

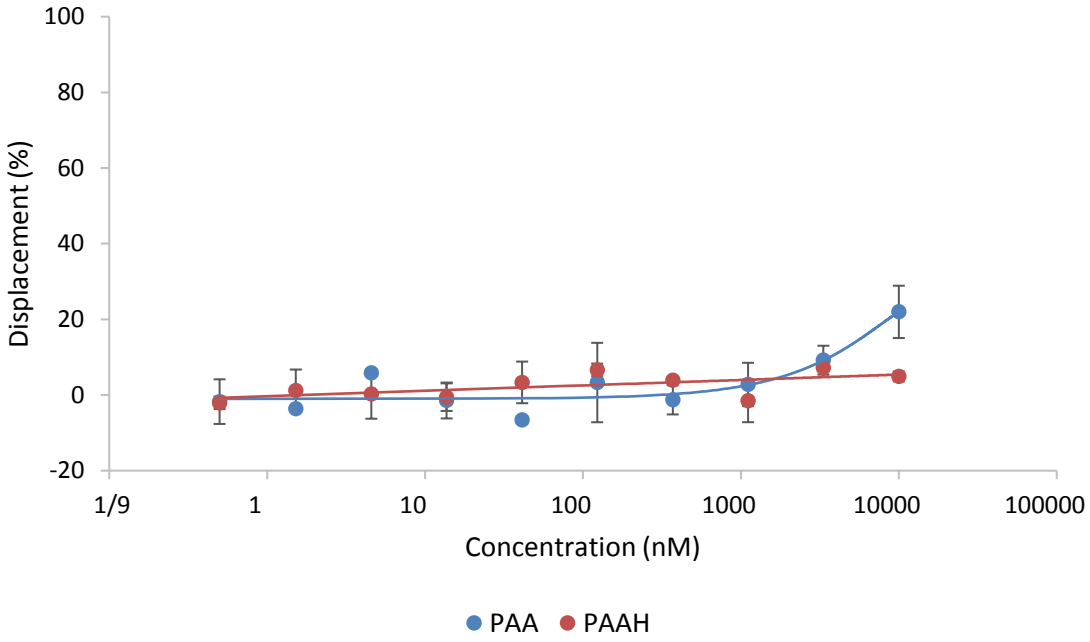

Figure 3.15: Measurement of PAAH and PAA binding to the glucocorticoid receptor. *Binding activity was determined by displacement of Fluormone GS1 Green in the LanthaScreen TR-FRET glucocorticoid receptor coactivator assay.*

In vitro screening of PAA and PAAH as a modulator of the glucocorticoid receptor revealed no significant activity up to a concentration of 3,333 nM (3.33 µM). At a concentration of 10,000 nM (10 µM) there was some evidence of weak activity by PAA, but with a displacement of just 22% at such a comparatively high concentration of drug it seems unlikely that this activity could translate beyond an *in vitro* receptor assay.

3.2.4.4. Glucocorticoid receptor discussion

The glucocorticoid system is a subset of nuclear receptors associated with regulation of homeostasis, metabolism and immune responses [69, 274]. Relevant to this study, activation of the glucocorticoid receptor has been associated with anti-inflammatory

responses via inhibitory activity on pro-inflammatory factors including NF-κB and activator protein-1 (AP-1) and as such was considered as a potential target to explore for the anti-inflammatory properties of PAA and PAAH [263]. As in the previous sections, *in silico* techniques were initially employed to investigate structural similarity between PAAH and glucocorticoid modulators retrieved from the literature [137].

The ROCS method suggested weak to moderate structural similarity between PAAH and glucocorticoid modulators, with higher shape similarity than color. Furthermore, highlighted in the study by Onnis et al. [137] was a pharmacophore hypothesis defining glucocorticoid modulators. When comparing the ROCS overlayed structures of PAAH to GR9, significant overlap between the structures was observed, with overlaps seen with three of the four spheres of the pharmacophore hypothesis. This suggested that despite the differences between the structures, PAAH seemed to possess a number of structural features hypothesised to be involved in the definition of glucocorticoid modulators. As numerous crystal structures of the glucocorticoid receptor were available through the RCSB Protein Data Bank, docking was also employed to investigate potential interactions. Docking of PAAH to the glucocorticoid receptor (PDB ID: 4P6W [266]) suggested a number of hydrophilic and hydrophobic interactions between PAAH and the glucocorticoid receptor that were common to those observed in the crystal structure of the receptor and its bound ligand, mometasone furoate. Analysis by docking suggested a potential clash between the carboxylic acid of PAAH and the Trp 600 residue of the glucocorticoid receptor. This electrostatic clash between PAAH and the glucocorticoid receptor was predicted to result in a penalty to binding affinity.

Based on *in silico* findings suggesting some similarities between PAAH and glucocorticoid modulators, *in vitro* techniques were employed to further investigate the glucocorticoid receptor as an anti-inflammatory target of PAAH. In a TR-FRET displacement assay both PAA and PAAH were found to display no significant binding to the glucocorticoid receptor over concentrations relevant to the anti-inflammatory activity previously observed in animal and cell-based assays. This suggests that despite some positive *in silico* indications of potential activity, these failed to translate into *in vitro* activity and the mechanisms of PAA/PAAH action were not attributable to direct binding to this receptor.

3.2.5. Additional pathways investigated using an *in silico* approach

In addition to the pathways described in earlier sections that were investigated both *in silico* and *in vitro*, several pathways were investigated *in silico* only due to time and availability constraints. These pathways included phospholipase A_2 (PLA_2) and enoyl-acyl carrier protein reductase (enoyl ACP reductase).

3.2.5.1. Phospholipase A_2 (PLA_2)

Phospholipase A_2 is a member of a family of enzymes that catalyses the release of fatty acids, particularly arachidonic acid, from glycerol [275]. As arachidonic acid is the precursor to inflammatory eicosanoids such as prostaglandin E_2 (PGE_2) and leukotriene B_4 (LKB_4), PLA_2 plays a key role in the inflammatory cascade, and inhibition of PLA2 may accordingly have therapeutic anti-inflammatory potential [45]. PLA_2 was identified as a potential target via screening of PAAH through the ZINC database [276] by a knowledge-based screening method described in Chapter 6.5.2. Screening of the ZINC database retrieved a clerodane diterpenoid, isolated from a sea sponge *(Cacospongia mollior)* described as cacospongiolide E (see Figure 3.16) [277]. Searching cacospongiolide E through the Similarity Ensemble Approach (SEA) webserver [278] using the World of Molecular Bioactivity (WOMBAT) database revealed an association to PLA_2 [279].

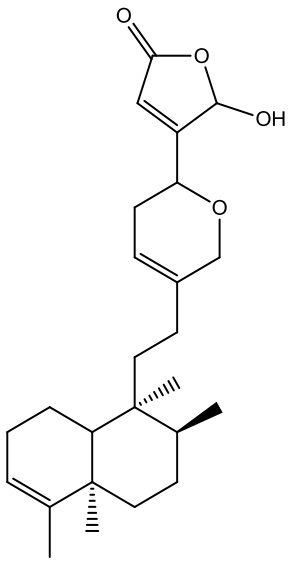

Cacospongiolide E

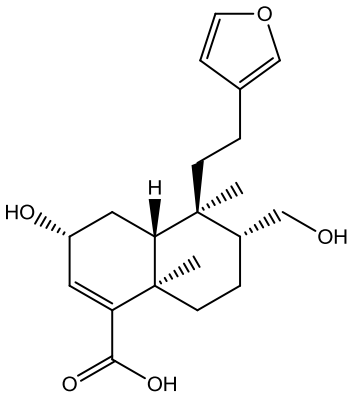

PAAH

Figure 3.16: Structures of cacospongiolide E and PAAH.

As both structures are clerodane diterpenoids, there are a number of common structural features between the molecules, but also several key differences. The central decalin moiety, including connected methyl groups and a branching alkyl chain leading to a cyclic ether group (dihydro pyran in cacospongiolide E, furan in PAAH) is conserved between the two molecules, but cacospongiolide E contains a hydroxy furanone group attached to the dihydro pyran, and the decalin moiety contains no oxygenated features whereas the analogous structure in PAAH contains two hydroxyl groups and an acyl feature. For this reason it may be expected that comparison of the structures may reveal stronger shape similarity than color similiarity and analysis by ROCS, using the method described in Chapter 6.5.5, supported this hypothesis by scoring the compounds with a ShapeTanimoto of 0.495 and ColorTanimoto of 0.200.

3.2.5.2. Enoyl-ACP reductase

Enoyl-ACP reductase is an enzyme involved in the type II fatty acid synthesis system in bacteria and is of specific interest in the development of antibiotics [280]. While it is not usually associated with inflammation, Sharma et al. [281] reported that inhibition of enoyl ACP reductase by triclosan in a mouse model infected with an acute *E. coli* infection was associated with a reduction in TNFα, but as a secondary effect caused by reduction in bacterial load. Screening of PAAH by TargetHunter, a webserver which functions by matching query molecules to a database of molecules with biological activity, retrieved a clerodane diterpenoid compound (a closed ring form of hautriwaic acid referred to as Compound 6, see Figure 3.17) associated with weak inhibition of enoyl-ACP reductase [282].

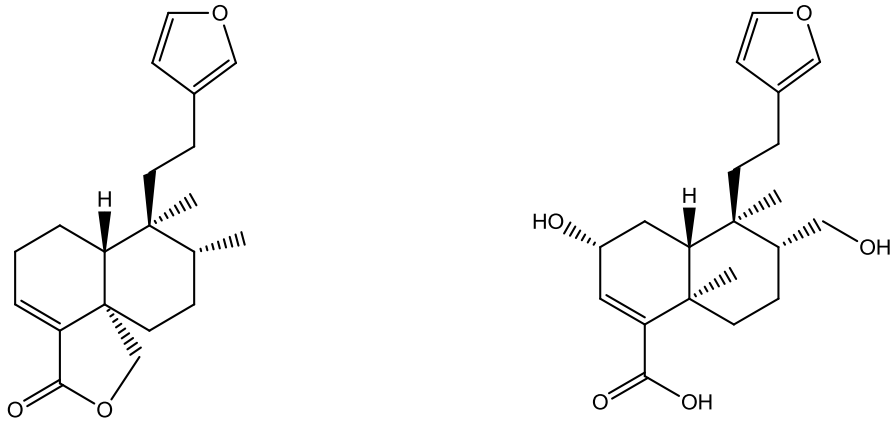

Compound 6 PAAH

Figure 3.17: Structures of compound 6 and PAAH.

There are extensive structural similarities between Compound 6 and PAAH including the central decalin structure, alkyl chain linking to a furan ring and acyl groups. Key differences, however, include the number of oxygenated centres, and the acyl group of Compound 6 being a closed ring ester (butyrolactone) instead of a carboxylic acid. Precursory investigation by ROCS (method described in Chapter 6.5.5) determined reasonable structural similarity between the two structures with a TanimotoCombo score of 1.111, consisting of a shape contribution of 0.71 and color contribution of 0.401. The high shape score is unsurprising, given that both molecules are clerodane diterpenoids, and the stereochemistry of each molecule is identical. The lower color score is also intuitive given

the disparity between electrostatic features mentioned previously, especially the difference in acyl groups. It is worth noting that the color score observed between PAAH and Compound 6 was higher than almost all other examples seen in earlier sections of this chapter. Owing to the structural similarities between Compound 6 and PAAH, it may be of interest to further examine enoyl-ACP reductase in the future, however since the target is not traditionally associated with anti-inflammatory activity it was not further investigated in this study.

3.2.6. Discussion of *in silico* implementation

In silico methods were used in this study in tandem with *in vitro* methods to examine possible targets of PAA. In part these methods were employed to enrich *in vitro* explorations and to rationalise determined activities, but also to investigate the implementation of *in silico* methods in prospective target prediction. In this study, such an implementation did not result in the elucidation of a protein target for PAA or PAAH. A number of targets were investigated computationally, and as noted in relevant sections of this chapter, interesting structural relationships were determined and pursued *in vitro* but did not ultimately result in a confirmed protein target.

The use of ROCS was favoured as an *in silico* method in this study due to its low computational investment requirements compared to alternative methods such as docking. Due to reasons described further in depth in Chapter 1.5.3, docking has a larger list of requirements for successful implementation such as the availability of protein structures and receptor binding data. As such, docking could only be applied to certain targets explored in this study, such as caspase-1 and the glucocorticoid receptor. By contrast, ROCS merely requires the 3D-structural information of a series of compounds, which can be derived either from crystallographic or *in silico* methods. For these reasons, ROCS was used in the analysis of each protein target while docking was only used for a few appropriate targets.

In review of the results of *in silico* analysis, ROCS as a ligand based method did not strongly indicate structural relationships between PAA/PAAH and ligands relevant to a range of targets. Typically, shape screening scored higher than color screening across all targets with shape screening typically scoring in a range of 0.400-0.600 and color screening

typically scoring in a range of 0.100-0.300 to form a combined score in the range of 0.500-0.900 with some exceptions on either end of the scale. Decisions to pursue *in vitro* screening of targets despite relatively weak *in silico* predictions were made on the basis of one score, typically shape, making stronger predictions. The results generated by this approach may serve to highlight the necessity of considering both aspects of scoring and not to bias one at the expense of the other.

Since its initial description in 1957 by Tanimoto [283], the Tanimoto system of mathematically defined similarity has been adapted to the field of molecular modelling and cheminformatics to great effect [139, 284]. The Tanimoto system has been used to describe similarities in both molecular shape and electrostatic charge with significant discussion over each element and their relative importance in defining molecular similarity [285, 286]. The consensus opinion seems to be that each element can be considered of greater or lesser importance in different situations and both should be considered carefully before reaching conclusions. In analysis of a wide range of virtual screening methods and scoring functions, McGaughey et al. [287] determined that ROCS-color, an early ROCS scoring function that added a color force field to shape based tanimoto scoring (later surpassed by TanimotoColor), was superior to the shape-only scoring function. This study followed another by Hawkins et al. [288] which demonstrated that ROCS-color was at least as effective, and in the case of several targets more effective than a shape-only scoring function. These findings seem to agree with the results of this study in that utilising one scoring component, primarily shape, to define structural relationships did not effectively establish an activity relationship and that considering both shape and color provided better predictive modelling.

Where applicable, protein docking was used to complement ROCS and while docking protocols were able to postulate binding modes of PAA/PAAH in protein structures, the results of *in vitro* screening did not support the hypotheses posed by docking. Docking poses of PAA in the caspase-1 receptor and PAAH in the glucocorticoid receptor were considered intriguing given the observation of potential interactions between ligand and protein that were common to co-crystallised ligands in respective crystal structures. The scoring system used for docking in this study was the Chemgauss4 algorithm, which is a modification of the Chemgauss3 scoring function with improved hydrogen bonding

designation [289]. While use of docking seemingly provided positive indications of interactions between PAA/PAAH and protein structures the analyses did not translate to *in vitro* evidence of biomolecular interactions.

A study by Tuccinardi et al. [222] comparing docking programs, including FRED, in the docking of ligands to protein kinases found that docking reliability improved when the compounds being docked were more similar to bound ligands. This was established by docking a diverse chemical library (TanimotoCombo ranging from 0.0 to 1.9) to protein kinase crystal structures with bound ligands attached and calculating the root-mean-square deviation (RMSD) of docked poses to the bound ligands with an RMSD value <2.0 Å considered significant. The findings of this study are shown in Figure 3.18.

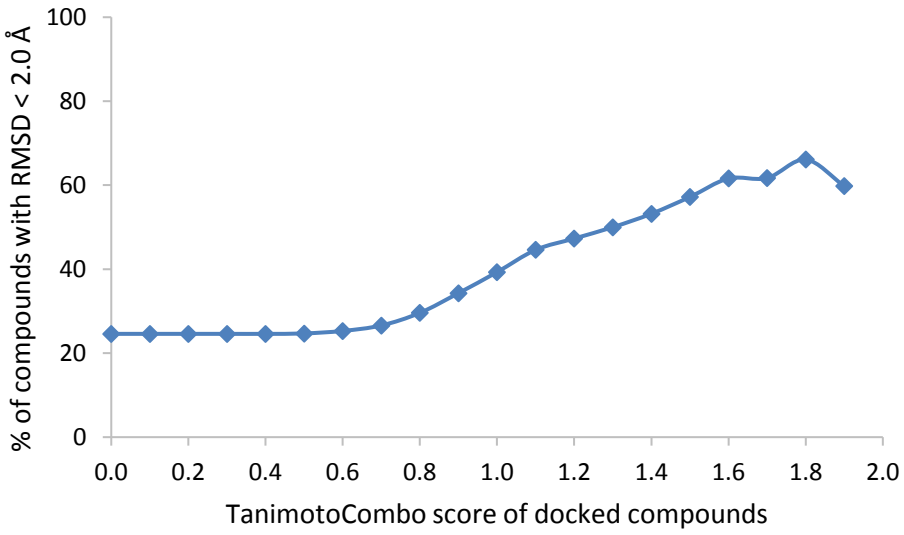

Figure 3.18: Compounds docked by FRED into protein kinases. *TanimotoScore and RMSD values were calculated comparing docked compounds to bound ligands. Figure has been adapted from data published by Tuccinardi et al. [222].*

The outcomes of this study are intuitive, especially in regard to rigid-docking methods, as these methods are reliant on structural information provided by a protein crystal structure, and a protein crystal structure bound with a ligand will adopt a conformer suitable for docking other high Tanimoto scoring ligands. Based on the findings in the study, it is evident that the reliability of pose prediction by FRED improved dramatically when docked ligands were more similar to the bound ligand. While this data was drawn specifically from

docking studies of protein kinases, it is not unreasonable to presume that the underlying principle can be extrapolated to other docking targets. Considering the use of docking in the present study for caspase-1 (see Section 3.2.1.2), a TanimotoCombo score of 0.571 was calculated between PAA and the bound ligand (3NS) of the crystal structure used for docking (3NS7). Considering also the use of docking in the investigation of the glucocorticoid receptor (see Section 3.2.4.2), the TanimotoCombo score of PAAH and the bound ligand (mometasone furoate) was 0.708. In applying the findings of Tuccinardi et al. to these TanimotoCombo scores, it is reasonable to conclude that the docking results are likely to be less reliable.

The approach of using both ROCS and docking in this study is similar to the approach reported by Kruger and Evers [290] where multiple screening protocols including ROCS, Glide (docking) and Feature Trees (FTrees) were used in tandem to improve data enrichment. The findings of the study indicated that for a number of enzyme targets it was beneficial to use multiple *in silico* approaches to form a consensus hypothesis. The results of the present study appear to, in part, support the findings of Kruger and Evers as in cases where multiple *in silico* approaches were used, hypotheses were often drawn from single results rather than a consensus approach, resulting in hypotheses that did not reach agreement with *in vitro* data. In Section 3.2.1, both ROCS and docking were used to examine the caspase-1 receptor as a potential target of PAA. From this analysis, ROCS indicated low structural similarity between PAA and caspase-1 inhibitors, save for a conserved substructure, however docking results suggested PAA may bind in a mode similar to numerous caspase-1 inhibitors. Ultimately a hypothesis that PAA may inhibit caspase-1 activity was formed based largely on docking results, which was not supported by *in vitro* results. Based on the *in silico* results, taking a consensus approach to forming a hypothesis may lead to the conclusion that caspase-1 inhibition was unlikely, which is in better agreement with *in vitro* data.

Analysis by the ROCS approach has been demonstrated in both prospective and retrospective analyses to possess predictive power [291]. Coupled with the predictive power of ROCS, the relatively low computational power and entry requirements necessary to perform analyses make it a very useful tool in drug discovery projects. Docking too has been used for the purpose of predicting protein-ligand interactions, however opinions on the

validity of this method have been divided [292, 293]. Primarily, the dissent towards the use of docking as a predictive tool has focused on the issue of false positive / true positive discernment, or in other words, it is difficult to distinguish if a given docking pose reflects the biological reality or if it merely generates a simulated pose.

Detailed in this study are several instances where docking seemed to produce predictive binding modes that were not reflected by the results *in vitro*. This seems to reflect the conclusions of Enyedy and Egan [293] that while docking can provide predictive contributions, results should be scrutinised carefully to remove misleading docking results. For these reasons, it might be concluded that ligand-based methods, such as ROCS, may be more suitable for prospective analyses, such as drug target prediction, than structure-based methods. Docking is still a powerful *in silico* tool, however the results from this study suggest that its use is better suited to retrospective analyses such as predicting or rationalising binding modes.

3.3. Conclusions and future directions

In this study, PAA and PAAH were investigated against a number of enzyme and receptor targets using an integrated *in vitro* and *in silico* approach with the intention of elucidating a mechanism of action for the anti-inflammatory properties of PAA based on effects observed in previous *in vivo* and *in vitro* studies. Prior to this study, COX enzymes (both 1 and 2 subtypes) were screened both *in silico* and *in vitro* and it was determined that there were no significant interactions between PAA and COX enzymes and therefore the anti-inflammatory activity of PAA was likely not attributable to this enzyme pathway. In this study, *in silico* and *in vitro* investigations were made into four further targets known to influence the production of pro-inflammatory factors including caspase-1, NF-κB, PKC and the glucocorticoid receptor. Furthermore, *in silico* methods were used to look at PLA_2 and enoyl ACP reductase as potential targets.

While the implementation of *in silico* technologies were not successful in determining a target by which PAA or PAAH exert their effects, numerous insights were gained in the usage of *in silico* technologies. It was concluded that ligand-based methods such as ROCS are more likely to be effective than structure-based docking methods when considering prospective analyses of drug targets. Additionally, it was concluded that the use of both methods is likely to be more effective than the use of either method alone, in agreement with previous findings [290]. Evidence was also found in support of a previous finding that the use of docking is more reliable when a protein structure containing a closely structurally related bound ligand is used [222].

As it was not ultimately determined by which mechanism, or mechanisms, PAA exerts its anti-inflammatory properties, there is room for further investigation. Future directions may include investigation of other protein targets known to be associated with inflammatory activities including PLA_2, which was briefly highlighted in *in silico* studies, and Toll-like receptor (TLR) proteins, which are known to be associated with NF-κB activation. Studies could also be broadened to include transporters of cytokines to investigate if PAA can exert effects in this way. Also, while PAA has been demonstrated to possess a number of anti-inflammatory activities, it is merely a single constituent of *D. polyandra* and

therefore there is potential for anti-inflammatory contributions or even synergistic effects to exist between PAA and other *D. polyandra* constituents.

Chapter Four: Opioid investigation of PAB

4.1. Introduction

It had been noted in a previous honours study by the candidate [2] that PAA bore numerous structural similarities to the κ-opioid agonist, salvinorin A. Furthermore, it was determined that PAB, another constituent of *D. polyandra*, bore a closer structural resemblance to salvinorin A than PAA (see Figure 4.1).

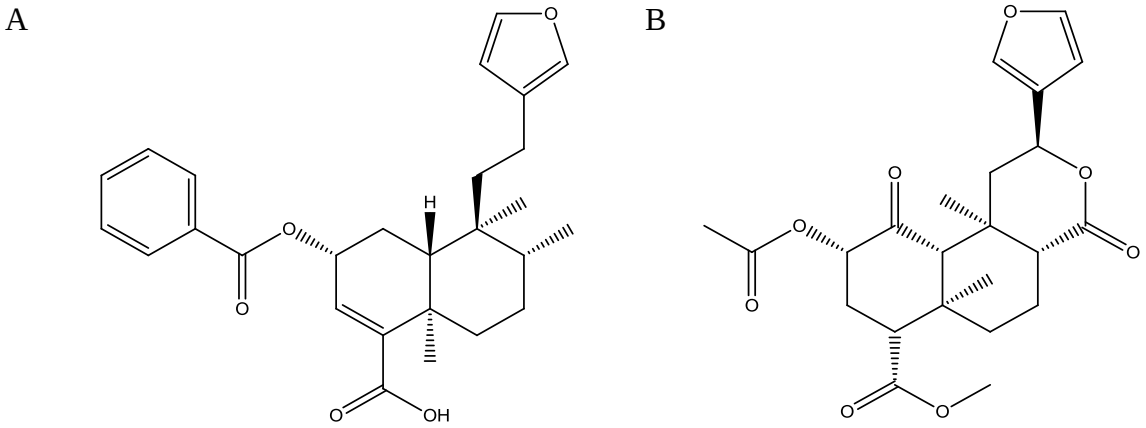

Figure 4.1: Chemical structures of (A) polyandric acid B and (B) salvinorin A.

While it has not been established that *D. polyandra* or its extracts may be associated with opioid activity, the structural similarities observed were considered of sufficient interest to warrant further analysis. Briefly, the findings of the aforementioned honours study determined, through the use of the ROCS method, that PAB bore significant structural similarity to salvinorin A as well as minor structural similarity to other known opioid structures. According to these findings, *in vitro* receptor screening of PAB against the μ and κ-opioid receptors was pursued but no significant receptor binding activity was observed. Post-screening analysis of the modelling, and further review of the literature, determined that the presence of a methyl ester in salvinorin A may be crucial to its opioid activity. As such, it was concluded that while PAB yielded no activity with the μ or κ-opioid receptors, a methyl ester transformation of the carboxylic acid of PAB would increase the similarity with salvinorin A, and hence increase the likelihood of binding to opioid receptors.

In recent years a significant development in opioid research was achieved when a set of four crystal structures of opioid receptors, including the μ, κ, δ and NOP receptors, were characterised and published for the first time [91-94]. These published structures set a new precedent for opioid research by allowing, for the first time, reliable structural analysis of the receptors and the first opportunity for docking with an opioid receptor, without the need for homology modelling.

The study described in this chapter was undertaken to further the previous honours investigation into opioid structural relationships between PAB and opioid agonists, by continuing the previous uses of combined *in silico* (primarily the use of docking) and *in vitro* investigations. Following *in silico* analyses, chemical modification was pursued along with *in vitro* techniques involving cell-based receptor assays. Chronologically, the studies performed in this chapter occurred before those in Chapter 2 and, as such, the role of hydrolysis in metabolism of compounds was not closely considered. The subchapters in the results and discussion portion of this chapter are arranged in a logical order from *in silico* investigations, chemical synthesis and *in vitro* analysis and on to final discussions and conclusions. All methodology relevant to this chapter is described in Chapter 6.

4.2. Results and discussion

4.2.1. *In silico* investigations and structure-activity relationships

4.2.1.1. Crystal structures

Following on from the previous honours study which sought to investigate a potential activity relationship between PAB and known opioid agonists, there was interest in rationalising why the predicted κ-opioid binding activity was not observed *in vitro.* Publication of opioid crystal structures facilitated an opportunity to better understand interactions between ligands and receptors.

Crystallographic data of the κ-opioid receptor was retrieved from the RCSB protein data bank (PDB ID: 4DJH) and processed with Make Receptor 3.0.0 to remove co-crystallised ligands and solvent molecules to provide a clearer view of the protein structure of the receptor. The processed receptor was then viewed with VIDA 4.1.0.2 and a molecular surface was created to view the electrostatic potential. The calculated molecular surface is shown in Figure 4.2.

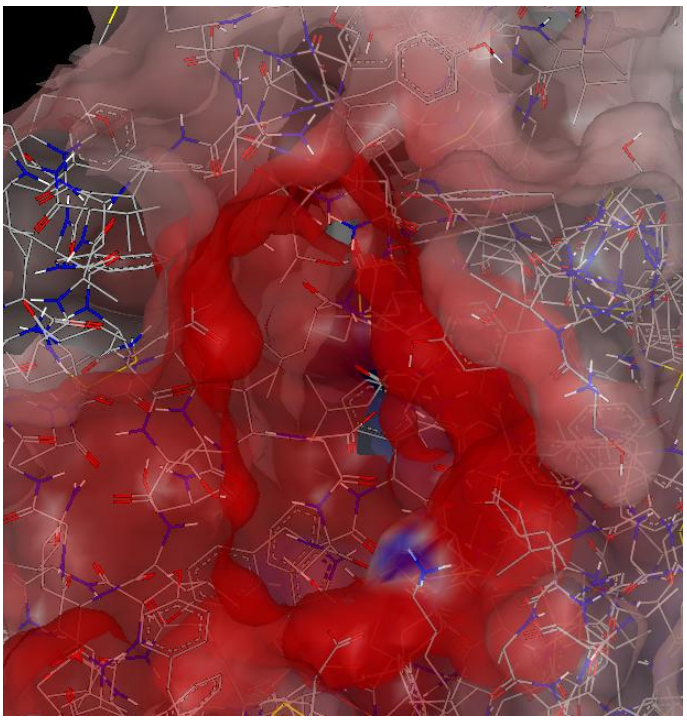

Figure 4.2: Molecular surface of the active site of the κ-opioid receptor (PDB ID: 4DJH). *Molecular surface is colour coded based on electrostatic potential (Red = negative, grey = neutral, blue = positive). View of the surface is presented from above, looking in towards the active site of the protein.*

Shown in Figure 4.2 is a view of the active site of the κ-opioid receptor with surface electrostatic potential depicted by colour. At the centre of the figure is a view down into the active site through an access channel. The bright red colour in this region is indicative of the contribution of numerous aspartic acid and glutamic acid residues to the electrostatic surface potential. Based on the surface electrostatic potential of the protein in this region, it is not unreasonable to conclude that the net local electrostatic potential of this access channel is strongly negative. From this conclusion, it follows that anionic molecules may be less favoured and the access channel of the active site may play a gatekeeping role in selecting for opioid ligands. It should be noted that the active sites of the μ and δ-opioid receptors were also examined by the same process and similar electrostatic trends were observed.

The concept of an access channel playing a role in substrate specificity is found in several other enzymes. It has been proposed by Urban et al. [294] that substrate specificity of CYP1A enzymes is mediated, to some extent, by the active site access channel, which

filters molecules by size. The cyclooxygenase (COX) enzymes have also been thought to engage in some degree of size-based substrate selectivity due to access channel architecture [295]. In the present example of opioid receptors it has been proposed that the access channels of opioid receptors may play a role in selecting for binding molecules by physicochemical properties beyond size, namely electrostatic charge. This follows the proposition made by Kingsley and Lill [296] that the same principles of shape and electrostatic matching that govern active site binding should also apply to access channels. An established example of such an effect taking place occurs in Fms1, an enzyme found in yeast responsible for conversion of spermine into spermidine, which contains a largely hydrophobic access channel. The hydrophobic nature of this channel has been proposed to facilitate its substrate unique access to the catalytic site [297].

In the chemical space of opioid ligands there are numerous distinct chemical scaffolds, however a common linking characteristic in almost all scaffolds is the presence of an ionisable nitrogen feature making most opioid ligands cationic at physiological pH. The only known exception to this commonality is the scaffold belonging to salvinorin A and its analogues (discussed in further depth in Section 4.2.1.2), which contains no ionisable nitrogen feature and exists as a neutral structure at physiological pH. As has been previously established, since PAB and salvinorin A come from the same diterpenoid class, they share many common structural features. The two molecules bear some key structural differences however, and potentially the most important of these differences is the presence of a carboxylic acid in PAB in place of a methyl ester in salvinorin A. This makes PAB anionic at physiological pH.

It therefore follows that since PAB exists as an anion at physiological pH, and salvinorin A is neutral, that significant differences in activity may be observed. Dramatic changes in activity stemming from minor changes in structure are referred to in medicinal chemistry as activity cliffs, and may provide important shape and electrostatic information regarding structure-activity relationships (SAR) [298, 299]. As PAB and salvinorin A differ by more than a simple carboxyl/ester transformation it is not reasonable to conclude that this structural feature is the only resultant factor in structure-activity disparity. Taking into account the aforementioned hypothesis that the access channel of the opioid receptors plays a gatekeeping role by preferentially selecting neutral or cationic ligands, it is reasonable to

conclude that the presence of a carboxylic acid in PAB plays a key role in the structure-activity disparity. This warranted further *in silico* and *in vitro* investigations.

4.2.1.2. Salvinorin structure activity relationship

A large amount of information regarding salvinorin A SAR studies is available, in large part from studies by Tidgewell et al. [300], Prisinzano and Rothman [301] and Riley et al. [302]. The studies by Tidgewell et al. [302] and Prisinzano and Rothman [303] covered a large array of structural modifications, while the study by Riley et al. [304] focused primarily on replacements to the furan ring. Figure 4.3 shows a consensus diagram of the three studies regarding structural features of salvinorin A that may be substituted to retain opioid activity.

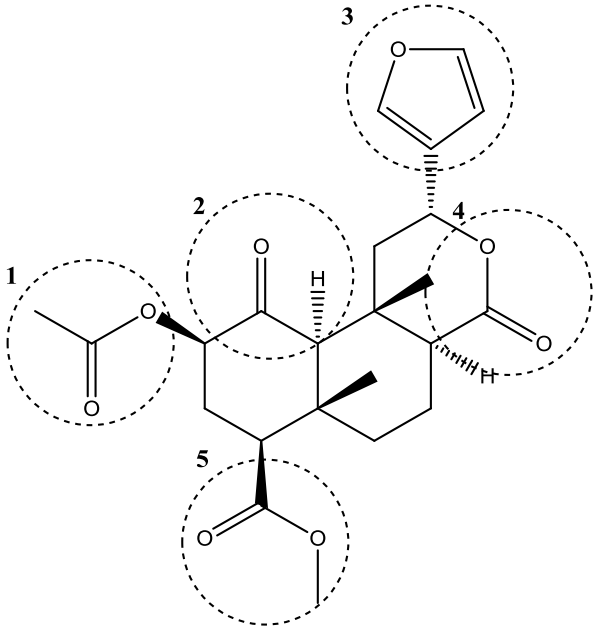

Figure 4.3: Consensus of three SAR studies into salvinorin A. *(1) Replacement of ester with bioisosteres is tolerated, small alkyl esters favour the κ-opioid receptor, aromatic esters favour the μ-opioid receptor. (2) Removal of carbonyl is tolerated. (3) Removal of furan decreases affinity, replacement and modification is tolerated. (4) Reduction and removal of lactone is tolerated. (5) Hydrolysis of ester significantly reduces affinity, replacement of methyl group with small alkyl groups is tolerated.*

Of particular note in the SAR studies are the importance of the furan ring, acetyl ester and methyl ester functionalities. In the study by Prisinzano and Rothman [303] it was shown that modification of the furan ring was tolerated, but removal diminished binding activity. Further study by Riley et al. [304] investigated, in greater depth, the types of furan modifications that were tolerated and determined some furan substitutions of greater potency than the original species. From studies by Tidgewell et al. [302] and Prisinzano and Rothman [303] it is evident that substitution of the methyl ester to other small alkyl esters is tolerated, but at a detriment to potency. Perhaps most importantly, de-esterification of the methyl ester was found to diminish activity almost entirely. This finding supports the aforementioned notion that PAB may not display opioid activity due to its carboxylic acid group.

Studies by both Tidgewell et al. [302] and Prisinzano and Rothman [303] showed that substitutions of the acetyl group were tolerated and could alter activity in surprising ways. Both studies demonstrated that substitution of the acetyl ester with aromatic esters diminished the κ-opioid selectivity of the compound and modified them into μ-opioid selective ligands. One particular salvinorin A analogue, referred to as herkinorin, is identical to the salvinorin A structure save for the replacement of the acetyl ester with a benzyl ester. Herkinorin has been established as a potent μ-selective opioid agonist in multiple studies [303, 304]. In addition to this receptor selectivity, it has also been demonstrated that herkinorin is not associated with β-arrestin recruitment, leading to a reduction in receptor internalisation [305]. This is significant as receptor internalisation has been suggested as a key mechanism in the development of *in vivo* opioid desensitisation and tolerance [306]. The proclivity towards μ-selectivity is of specific interest to the present study as PAB, like herkinorin, has a benzyl ester in place of an acetyl ester and this may suggest that if PAB, or a related compound, were to exhibit opioid binding activity, it may be more likely to be selective for the μ-opioid receptor subtype.

Previously, PAB had been screened against both κ and μ-opioid receptor subtypes but no binding activity was determined at either receptor [2]. Based on the findings of the SAR analysis and inspection of opioid crystal structures, there seems to be an indication that the carboxylic acid present in PAB may be a key factor in the negative screening results and furthermore that the presence of a benzyl ester in PAB may influence the molecule to have a stronger binding potential for the μ-opioid receptor. As such it was concluded that PAB

was an unlikely candidate for opioid binding, however there may be good prospects to investigate binding of a methyl ester form of PAB to the μ-opioid receptor.

4.2.1.3. Docking of MPB to the μ-opioid receptor

To investigate the potential binding of a methyl ester of PAB (methyl polyandrate B, MPB) to the μ-opioid receptor, a structure of the μ-opioid receptor was obtained to postulate a potential binding mode by the use of docking, via the methods described in Chapter 6.5.4. To perform docking, a crystal structure of the μ-opioid receptor (PDB ID: 4DKL [307]) in a binding mode with an opioid morphinan antagonist (β-FNA) was used. The 4DKL structure was processed with Make Receptor 3.2.0.2. The crystal was first processed by removing the bound ligand, water molecules and co-crystallised salts and solubilising agents (i.e. sulfate, chloride, short-chain fatty acids). An active site was defined as the area surrounding the bound ligand using the molecular cavity detection tool of Make Receptor. Site shape was calculated with a bias towards extension towards protein, meaning the binding site defined by Make Receptor was larger to offer more freedom to the docking program to find a suitable pose. The calculated shape was defined with a volume of 1631 $Å^3$ and no binding constraints were defined. The prepared protein was then exported for use with the FRED module of OEDocking 3.2.0.2 by the method described in Chapter 6.5.4. Herkinorin and MPB were docked independently in the active site of 4DKL and visualised using VIDA 4.3.0.4. An overlay of the docked poses is shown in Figure 4.4.

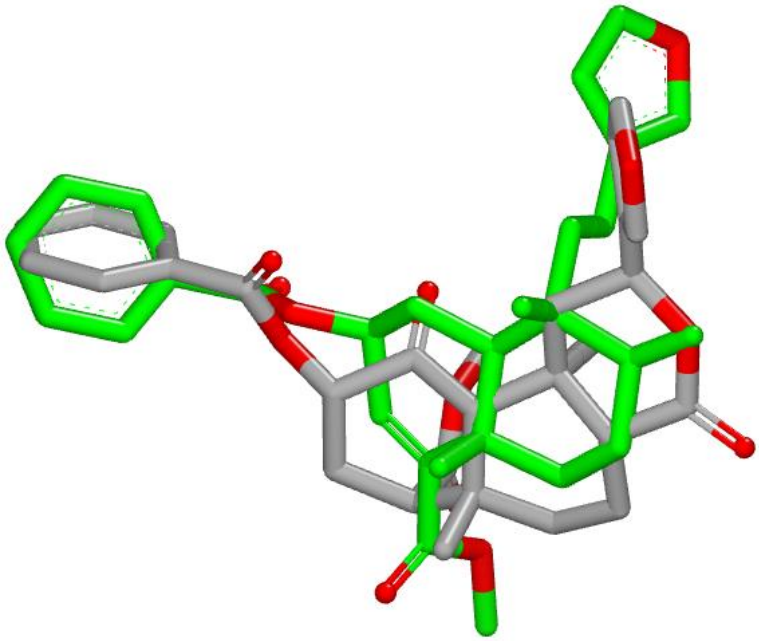

Figure 4.4: Overlay of the docked poses of MPB and herkinorin in the μ-opioid structure 4DKL. *MPB is displayed in green, while herkinorin is shown in grey. Structural overlap of the benzyl esters, central ring structures and furan rings is visible. Residues from the surrounding protein structure have been removed.*

The use of homology modelling and docking, as well as *in vitro* evidence through site directed mutagenesis studies, have provided structural insights into the binding of salvinorin A to the κ-opioid receptor [308], however at the time of this docking study no such information was available regarding the binding of herkinorin to the μ-opioid receptor. A key finding from analysis into salvinorin A binding has been that the structure is thought to adopt a binding mode distinct from traditional opioid modulators.

In summary, traditional opioid modulators of all three analgesic opioid receptors involve a significant binding interaction with an aspartic acid (Asp) residue in the active site of the receptor. This is evidenced in the available crystal structures with interactions between Asp147 and β-FNA in the μ-opioid receptor (4DKL [91]), Asp138 and JDTic in the κ-opioid receptor (4DJH [92]), and Asp128 and naltrindole in the δ-opioid receptor (4EJ4 [93]). Each of these interactions are characterised by an ionic interaction between the acidic portion of the aspartic acid residues and a basic nitrogen of the ligands.

Salvinorin A, lacking a basic nitrogen in its structure, is incapable of forming an ionic interaction with aspartic acid residues, and therefore must adopt a unique binding mode. As previously indicated, no specific structural information was available regarding herkinorin binding to the μ-opioid receptor at the time of this analysis, therefore it is not unreasonable to postulate that herkinorin also adopts a binding mode that is dissimilar to traditional opioids. As such, the use of traditional models of opioid binding are more likely to be misleading. Accordingly, since any binding mode generated through docking is largely speculative there is unlikely to be significant value in describing the specific residues proposed to interact with MPB/herkinorin. The value of this docking approach is instead in highlighting that the active site of the μ-opioid receptor is able to accommodate both MPB and herkinorin in a similar binding mode.

4.2.2. Chemical synthesis of methyl polyandrate B

Following on from the previous findings that the presence of a carboxylic acid moiety may have deleterious effects on opioid activity due to its negative charge, a decision was made to subject PAB to synthetic procedures and generate a methyl ester to investigate this effect. Two synthetic methods were implemented in an effort to produce the methyl ester: synthesis by thionyl chloride and synthesis by methyl iodide.

4.2.2.1. Thionyl chloride procedure

The synthesis of MPB by reflux with thionyl chloride was performed by the method described in Chapter 6.4.1, following the reaction pathway proposed in Figure 4.5.

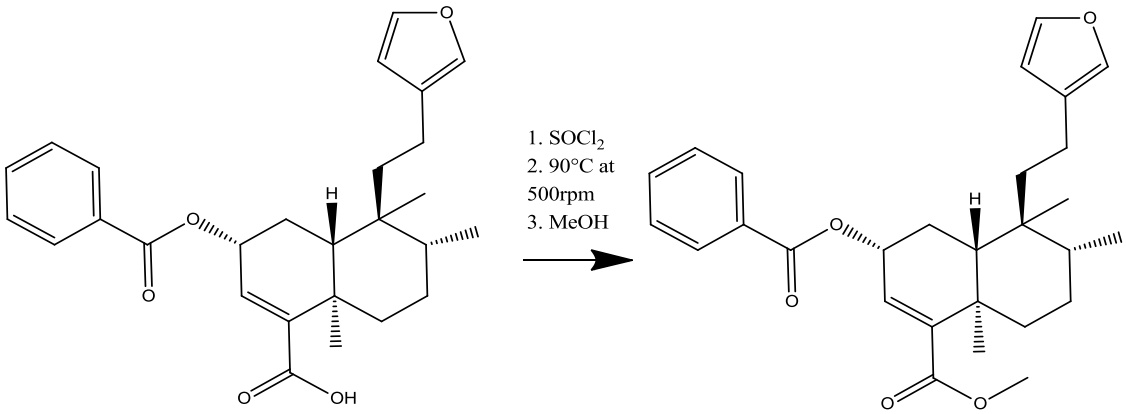

Figure 4.5: Proposed reaction pathway of MPB synthesis by reflux with thionyl chloride.

Analysis of the reaction product was performed by ToF-MS in negative-ion mode which revealed two peaks in the mass range of *m/z* 100 to 1000. The major $[M-H]^-$ peak was located at *m/z* 329.1967 and the minor $[M-H]^-$ peak was located at *m/z* 657.3786. The MS spectra of the reaction product is included as Appendix 7.

The observed mass of *m/z* 329.1967 was in agreement with the theoretical mass of PABH (330.1988 Da), the de-esterified alcohol form of PAB. This suggested that rather than the expected methyl ester synthesis, ester hydrolysis occurred at the existing ester functional group, yielding the de-esterified alcohol of PAB (PABH) rather than MPB. The probable cause of this unplanned reaction was unsuitable conditions for PAB in the reaction media; perhaps most notably the temperature of the reaction (90 °C). It has been noted that the extraction yields of benzyl ester diterpenoids from the leaves and stems of *D. polyandra* are improved when the temperature of the extraction solvent is kept below 40 °C, when compared to higher temperatures [309]. For this reason, the temperature of the reaction may have provided unstable conditions for PAB, resulting in the ester degradation and formation of PABH.

The $[M-H]^-$ mass of *m/z* 657.3786 was in agreement with the theoretical mass of a dimer of PAB (658.3976 Da). This may be suggestive of dimerization caused by an artefact of mass spectrometry where two molecules of PABH have coordinated together to give the signal of the observed mass of *m/z* 657.3786, or it might also suggest that an esterification reaction occurred between two molecules of PABH rather than between PAB and methanol as intended. The latter case might conceivably occur as the reaction conditions were

conducive to an esterification reaction, but given the considerable excess in concentration of methanol it seems unlikely that the dimerization reaction would occur in preference to PAB-methanol esterification, the intended product of which was not detected by mass spectrometry. For this reason, it is likely that the minor peak determined at *m/z* 657.3786 was formed as an artefact of the mass spectrometry process and less likely to be formed in a chemical process. In conclusion, it was determined that the conditions of the thionyl chloride procedure resulted in the reaction pathway summarised in Figure 4.6.

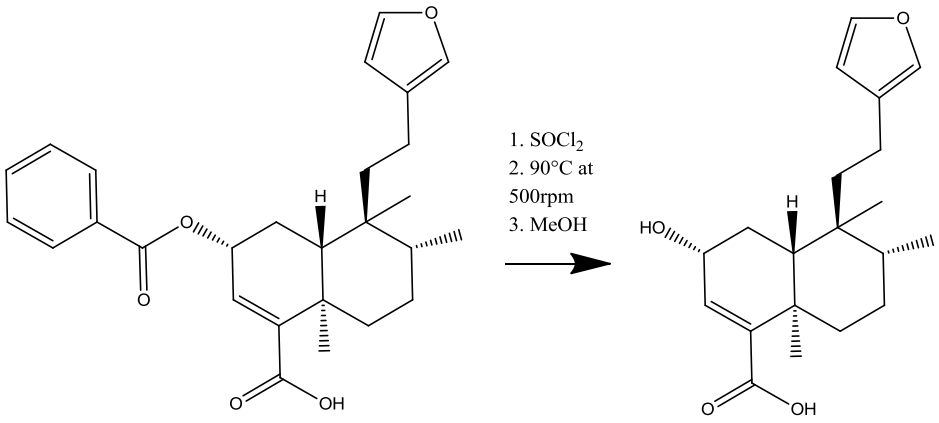

Figure 4.6: Likely reaction pathway that occurred during reflux with thionyl chloride.

4.2.2.2. Methyl iodide procedure

The synthesis of MPB by reflux with thionyl chloride was performed by the method described in Chapter 6.4.2, following the intended reaction pathway summarised in Figure 4.7.

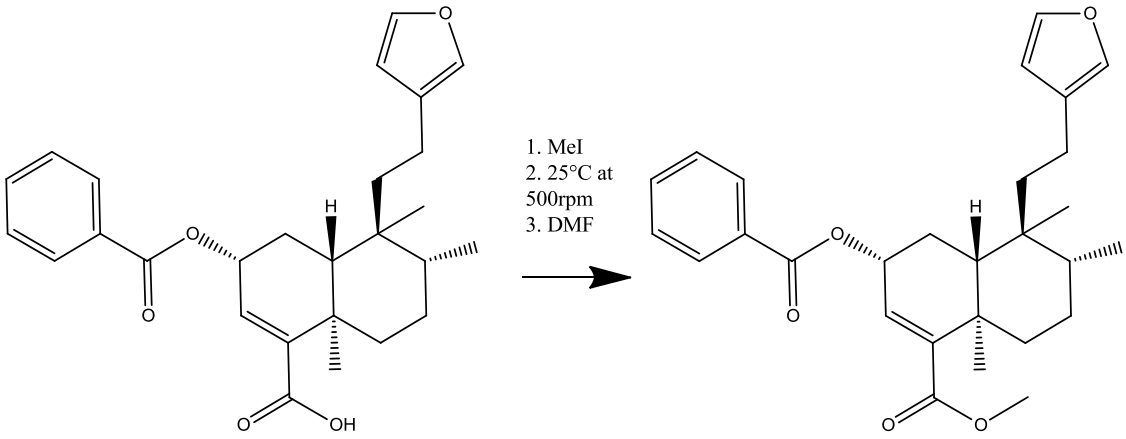

Figure 4.7: Intended reaction pathway of MPB synthesis by reflux with methyl iodide.

Analysis of the reaction product was performed by ToF-MS in negative-ion mode which revealed a number of peaks in the range of 100 to 1000 *m/z* including two major $[M-H]^-$ peaks at *m/z* 329.2084 and *m/z* 473.2243. The MS spectra of the reaction product is included as Appendix 8.

The $[M-H]^-$ mass of *m/z* 329.2084 was in agreement with the theoretical mass of PABH (330.1988 Da), the de-esterified alcohol form of PAB. Previous mass spectrometric analysis of products from the thionyl chloride reaction method also produced the undesirable peak of *m/z* 329.20. In the previous analysis fragmentation energy was lower so detection of a peak at *m/z* 329.20 indicated that the reaction did not proceed as intended. In this analysis however, collision energy was higher and a peak at *m/z* 329.21 may indicate the breakdown product as a major artefact of mass spectrometric analysis.

The $[M-H]^-$ mass of *m/z* 473.2243 was in agreement with the theoretical mass of the expected product in complex with a sodium ion (473.2304 Da). Sodium carbonate was incorporated in the reaction process to keep the reaction dry and as such was concluded that sodium ions could coordinate with MPB, detectable by mass spectrometry analysis. A full ^{1}H NMR and ^{13}C NMR summary is recorded in Table 4.1.

Table 4.1: ^{1}H (500 MHz) and ^{13}C (125 MHz) NMR spectral data of MPB in MeOD-d_4.

Carbon number	δ_C	δ_H	Carbon number	δ_C	δ_H
Primary structure					
1	24.9, CH_2	1.90	11	38.3, CH_2	2.14
2	67.8, CH	5.56	12	17.8, CH_2	1.57
3	133.1, CH	6.48	13	125.1, C	-
4	147.6, C	-	14	110.7, CH	5.95
5	38.0, C	-	15	142.5, CH	7.19
6	35.3, CH_2	2.16	16	138.3, CH	6.71
7	27.1, CH_2	1.53	17	15.8, CH_3	0.82
8	36.2, CH	1.69	18	167.5, C	-
9	38.5, C	-	19	19.1, CH_3	1.21
10	42.0, CH	1.87	20	18.0, CH_3	0.78
Benzyl ester					
1′	165.9, C	-	5′	130.1, CH	7.47
2′	130.0, C	-	6′	128.4, CH	7.30
3′	129.7, CH	7.93	7′	129.7, CH	7.93
4′	128.4, CH	7.30			
Methyl ester					
1*	51.56, CH_3	3.65			

Instrument: Bruker Avance III 500 MHz spectrometer

Solvent: Methanol-d_4

Connectivity of the ester groups to the structure of MPB was confirmed by HMBC-NMR experiments. The HMBC showed ^{3}J correlations between δ_H 5.56 (H2) and 7.93 (H3′/H7′) with δ_C 165.9 (C1′), indicating that the benzyl ester remained intact in the reaction product. Furthermore, HMBC showed ^{3}J correlations between δ_H 6.48 (H3) and 3.65 (H1*) with δ_C 167.5 (C18), confirming that the methyl ester had been formed in the reaction, and was present in the reaction product. A summary of the HMBC correlations is depicted in Figure 4.8.

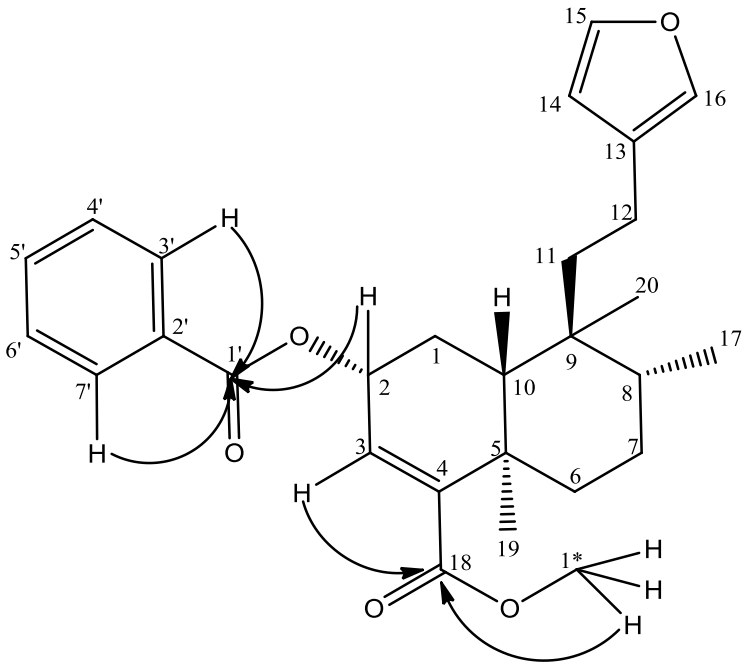

Figure 4.8: Key correlations observed in the HMBC spectrum of MPB.

It was demonstrated through MS experiments that the predicted mass of product was detectable, suggesting that the intended reaction had been successful. Further analysis by NMR, especially utilising HMBC experiments, demonstrated the presence of the intended methyl ester and retention of the benzyl ester, further suggesting the reaction was successful and the intended product had been synthesised.

4.2.3. *In vitro* opioid screening

A 3.19 mg portion of dry MPB (3.19 mg, 7.01 mM) was submitted for screening in a μ-opioid assay. Screening was performed by Ricerca Biosciences using cell-based assays. The opioid assay was performed using Chinese Hamster Ovary (CHO-K1) cells expressing the μ-opioid receptor and tested against DAMGO, a μ-opioid specific peptide agonist, as a positive control. Special requests were made to limit water and light exposure to prevent potential breakdown of the compound from hydrolysis and photolysis. The results of the screening process are shown in Table 4.2.

Table 4.2: In vitro binding of MPB to the μ-opioid receptor. *All screening was performed in duplicate using human opioid receptor expressed in CHO-K1 cells.*

Assay name	Concentration (μM)	% Inhibition	IC_{50}
Opiate, μ (OP3, MOP)	10	4	>10μM
	1	-5	
	0.1	9	

As shown, the results for the screening suggested no significant activity of the compound at the μ-opioid receptor even at the highest concentration (10 μM). Furthermore, there was no evidence for a dose-response relationship. Therefore, it was unlikely that any biologically relevant activity could be observed at a higher concentration.

4.2.4. Post screening *in silico* analysis

As no binding was observed between MPB and the μ-opioid receptor, this finding ran counter to the docking results generated in Section 4.2.1.3. The previous docking results suggested that MPB may be capable of adopting a similar binding mode to herkinorin in the active site of a crystal structure of the μ-opioid receptor. The crystal structure used for this docking analysis (PDB ID: 4DKL) was the only crystal structure of the μ-receptor available at the time, and as such was the most suitable structure available without generating, or utilising, a homology model. However, since the completion of the *in vitro* binding study, a new μ-opioid crystal structure had been published [307]. This new crystal structure (PDB ID: 5C1M) provides an opportunity to revisit the previous docking approach with additional structural information. A summarised list of comparative parameters is presented in Table 4.3.

Table 4.3: Parameters of μ-opioid crystal structures.

Structure	4DKL	5C1M
Published date	March 2012	August 2015
Expression system	*Spodoptera frugiperda*	*Spodoptera frugiperda*
Binding mode	Antagonist	Agonist
Co-crystallised ligand	β-FNA	BU72
Method	X-ray diffraction	X-ray diffraction
Resolution	2.8 Å	2.1 Å

A key difference between the two crystal structures is that 4DKL contains a bound antagonist, and is therefore in its inactive state, while 5C1M contains a bound agonist, and is therefore in its active state. As MPB was hypothesised to function as an agonist towards the μ-opioid receptor, it follows that 5C1M would be a superior choice to investigate by *in silico* docking. Additionally, there is an improvement in resolution between the two crystal structures of 0.7 Å, with 5C1M offering a higher resolution, and therefore a more reliable crystal structure.

To investigate the structural insights offered by this new μ-opioid crystal structure, the same docking procedure described in Section 4.2.1.3 was utilised. To perform docking, a crystal structure of the μ-opioid receptor (PDB ID: 5C1M [307]) in binding mode with an opioid agonist (BU72) was used. The 5C1M structure was processed with Make Receptor 3.2.0.2. The crystal was initially processed by removal of the bound ligand, water molecules, co-crystallised salts and solubilising agents i.e. phosphate and short-chain fatty acids. An active site was defined as the area surrounding the bound ligand using the molecular cavity detection tool of Make Receptor. Site shape was calculated with a bias for extension towards protein, meaning the binding site defined by Make Receptor was larger to offer more freedom to the docking program to find a suitable pose. The calculated shape was defined with a volume of 581 $Å^3$ and no binding constraints were defined. The prepared protein was then exported for use with the FRED module of OEDocking 3.2.0.2 by the method described in Chapter 6.5.4. Herkinorin and MPB were docked independently in the active site of 5C1M and visualised using VIDA 4.3.0.4. An overlay of the docked poses is shown in Figure 4.9.

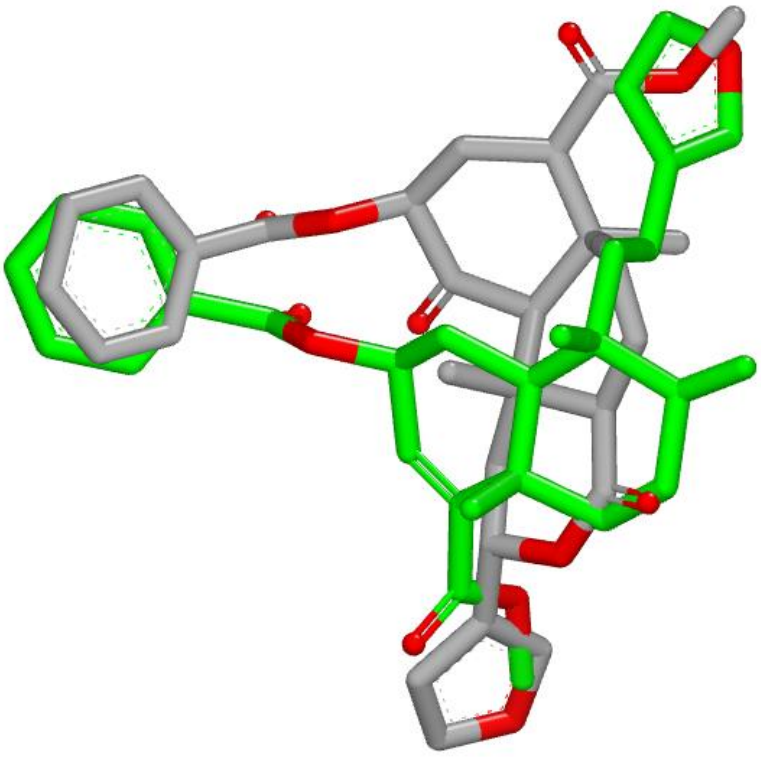

Figure 4.9: Overlay of docked structures of MPB and herkinorin in the μ-opioid structure 5C1M. *MPB is displayed in green, while herkinorin is shown in grey. Reasonable structural overlap is evident with the benzyl esters, but other key functional groups are poorly matched.*

The overlaid pose of MPB and herkinorin shows generally poor overlap similarity with the closest structural matches evident in the benzyl esters. Surprisingly, the furan rings and methyl esters do not overlap to their analogous structural features in each molecule in the poses produced by docking analysis. The poor overlap of features between these two structures suggest that they are unlikely to adopt a similar binding pose in the same receptor, and as such are unlikely to display similar biological activity.

These findings seem to better reflect the receptor screening described in Section 4.2.3 in contrast to the previous *in silico* findings detailed in Section 4.2.1.3. The key difference between the two docking methods used was nature of the crystal structure. Previously the structure of 4DKL, as an antagonist bound structure, was used while this docking method utilised 5C1M, as an agonist bound structure. A significant difference between the two structures is the volume of the active sites. The area of the active site of 4DKL, as defined by Make Receptor, was 1,631 $Å^3$ while the active site of 5C1M was

defined as 581 Å^3. This difference of 1,050 Å^3 (approximately 3-fold) is significant as the allowable docking poses of the molecules are more highly restricted in the 5C1M structure compared to the 4DKL structure. This may indicate that the active site of the μ-opioid receptor has a degree of flexibility between the agonist and antagonist bound (active and inactive) forms, that allows the structure to fold-inwards when an agonist is bound, resulting in a smaller active site. The co-crystallised ligands of each respective structure are shown in Figure 4.10.

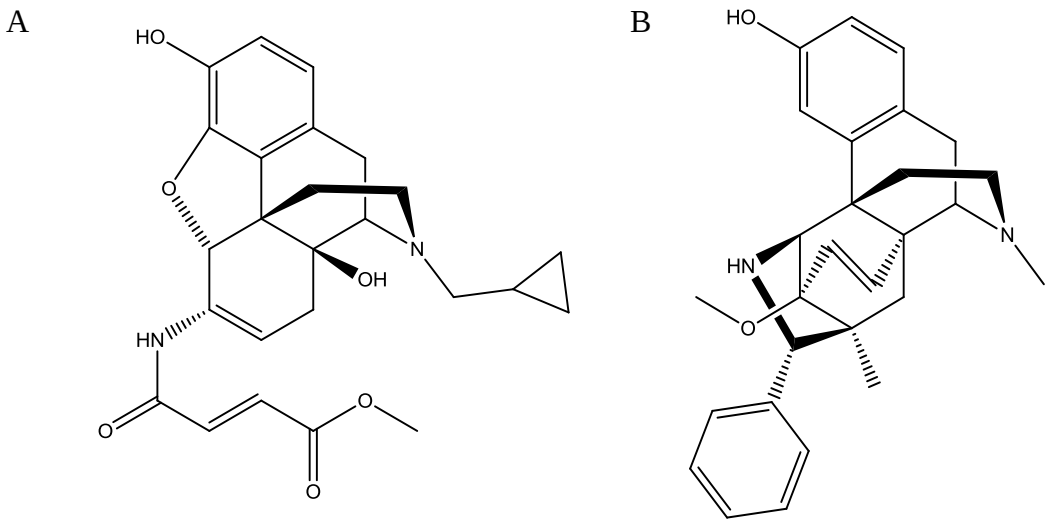

Figure 4.10: Chemical structures of co-crystallised opioid ligands. *(A) Opioid antagonist β-FNA from PDB structure 4DKL. (B) Opioid agonist BU72 from PDB structure 5C1M.*

The antagonist, β-FNA, occupies a slightly larger spatial volume in 3D space due to an extended cyclopropane group and flexible chain (featuring amide and ester groups), while the agonist, BU72, has additional ring structures. Despite a small difference in spatial volume between the two structures, the difference in binding site areas is quite significant, presumably as a result of different levels of protein folding influenced by the respective ligands. This may mean that exploring agonists using an antagonist bound structure is inadvisable due to significant differences between active sites.

Additionally, as indicated, an increased active site area comes with increased entropy as a larger number of binding poses may be achieved by a molecule due to the increased degrees of freedom. As the only set of poses that may be considered valid are those that fall within an RMSD range of a validated (usually biological) pose (1.5-2.0 Å as reported by

Hevener et al. [310]), a greater number of available binding modes raises the possibility of generating false positive results. In this study, two docking approaches were used, which generated conflicting results. As *in vitro* screening of MPB showed no indication of binding with the μ-opioid receptor, this may suggest that an increased active site size during initial *in silico* analysis was detrimental to the predictivity of the experimental outcome.

4.2.5. Discussion of findings

Reflecting on the findings of the *in vitro* analysis, there is an opportunity to discuss the disparity between predictions made due to an *in silico* led hypothesis and the results of receptor screening. Firstly, there is a possibility that instability of MPB contributed to receptor binding failure. The structure of MPB was positively confirmed by MS and NMR techniques, however these techniques were applied prior to transporting the compound to an overseas facility for screening. Additionally, the stability of MPB was unknown, since only a small amount of compound was able to be produced owing to the scarcity of sufficiently pure PAB. It therefore cannot be known if the compound arrived in an undiminished form at the screening facility, and thus if the compound was screened accurately. Furthermore, there is a possibility that esterase activity may contribute to a deleterious effect on binding. The assay used to assess μ-opioid binding (OP3 assay) was performed in CHO-K1 cells, which are known to express esterase enzymes [311].

In Chapter 2 the metabolism of PAA by esterase enzymes was assessed (Chapter 2.2.2) and it was hypothesised that the hCES2 enzyme may be responsible (Chapter 2.2.10). MPB differs to PAA in two key ways, firstly the benzyl ester is positioned on the opposite side of the molecule with respect to the diterpenoid structure, and secondly the methyl ester is present in place of a carboxylic acid. It was previously discussed that both esters found in herkinorin are of importance to activity and while replacement of either may be tolerated, complete removal, such as may be encountered by esterase activity, is deleterious to activity. The OP3 assay involves a 60-minute incubation before samples are analysed. While the structures of PAA and MPB are distinct, it would not be unreasonable to presume that MPB would also be vulnerable to esterase mediated hydrolysis. As such, it may be feasible that MPB is inherently unstable in this assay and undergoes hydrolysis before it can bind with the opioid receptors. This may not be the case however as

salvinorin A and its analogues were also screened in CHO-K1 cells using a similar technique to the one detailed in this study [302]. The same arguments of structural similarity between MPB and salvinorin A analogues that led to investigating the opioid receptors would also apply to other targets of salvinorin A analogues, including esterases. It would therefore be predicted that MPB would have similar susceptibility to esterase activity as salvinorin A analogues and the observed difference in activity would likely be attributable to binding differences, rather than differences in ester stability.

Docking algorithms are 3D methods, highly dependent on available structural information. Previously, in Chapter 1.5.3, the importance of high quality protein structures was highlighted, but perhaps of equal importance are the structures of the compounds being docked. Structural conformers were generated in these experiments by Omega (OpenEye Scientific Software), a conformer generation tool optimised to generate biologically relevant molecular structures. An issue that may occur with the use of conformer generation software is representation of stereochemistry, as stereochemistry can have drastic effects on pharmacological effects. Thus, an inaccurate stereochemical assignment can negatively impact *in silico* studies, by offering misleading results.

The structure of PAB presented and utilised in this study was determined by Simpson et al. [12] using the method of Rotating Frame Nuclear Overhauser Effect (ROESY) NMR spectroscopy to assign a relative stereochemical assignment. The vulnerability of this assignment method is that, while not necessarily inaccurate in itself, the stereochemical assignment is based on relative signals in NMR spectra and is not an absolute assignment of stereochemistry, thus there is potential for error.

The absolute stereochemical assignment of *D. polyandra* compounds was pursued by the use of X-ray crystallography but was ultimately unsuccessful. Multiple attempts were made to produce crystals of PAA and PAB suitable for X-ray analysis using a two-chamber approach. In brief, this involved dissolving a small amount of PAA or PAB in solvent in an unsealed vial and placing this vial in a larger container solvent in which the compound was less soluble and leaving the two chambers for several days. The expectation of this method was that over time vaporisation of each solvent would distribute the solvents between both vials and lead to precipitation of the compound and the formation of crystals. Multiple

attempts, with a number of modifications to the methodology, were made initially by Dr Bradley Simpson, and later in the present study, and while crystals were produced in each attempt, the crystals were of generally poor quality (size, uniformity, cloudiness) and were unsuitable for X-ray crystallography. A more complex approach was briefly investigated in collaboration with Associate Professor Christopher Sumby at the University of Adelaide utilising the novel "crystalline sponge" method of Inokuma et al. [312] but this was not ultimately pursued experimentally due to the complexity of the method and time constraints. As a result, the absolute stereochemistry of PAB and MPB remain unknown, and the relative stereochemical assignments are the most reliable structures available.

Given that, to a large extent, interactions between MPB and the μ-opioid receptor were investigated as a result of structural similarity between herkinorin and MPB, there is value in reviewing the similarity of the structures. Primarily it was sought to assess the shape similarity of MPB and herkinorin using a similar methodology to that employed in a previous honours study where PAB was compared to salvinorin A. An overlay of MPB and herkinorin was generated using ROCS by the method described in Chapter 6.5.5. Furthermore, the ROCS output was visualised in 2D and 3D using ROCS_report and VIDA respectively. Overlays in 2D and 3D are depicted in Figure 4.11.

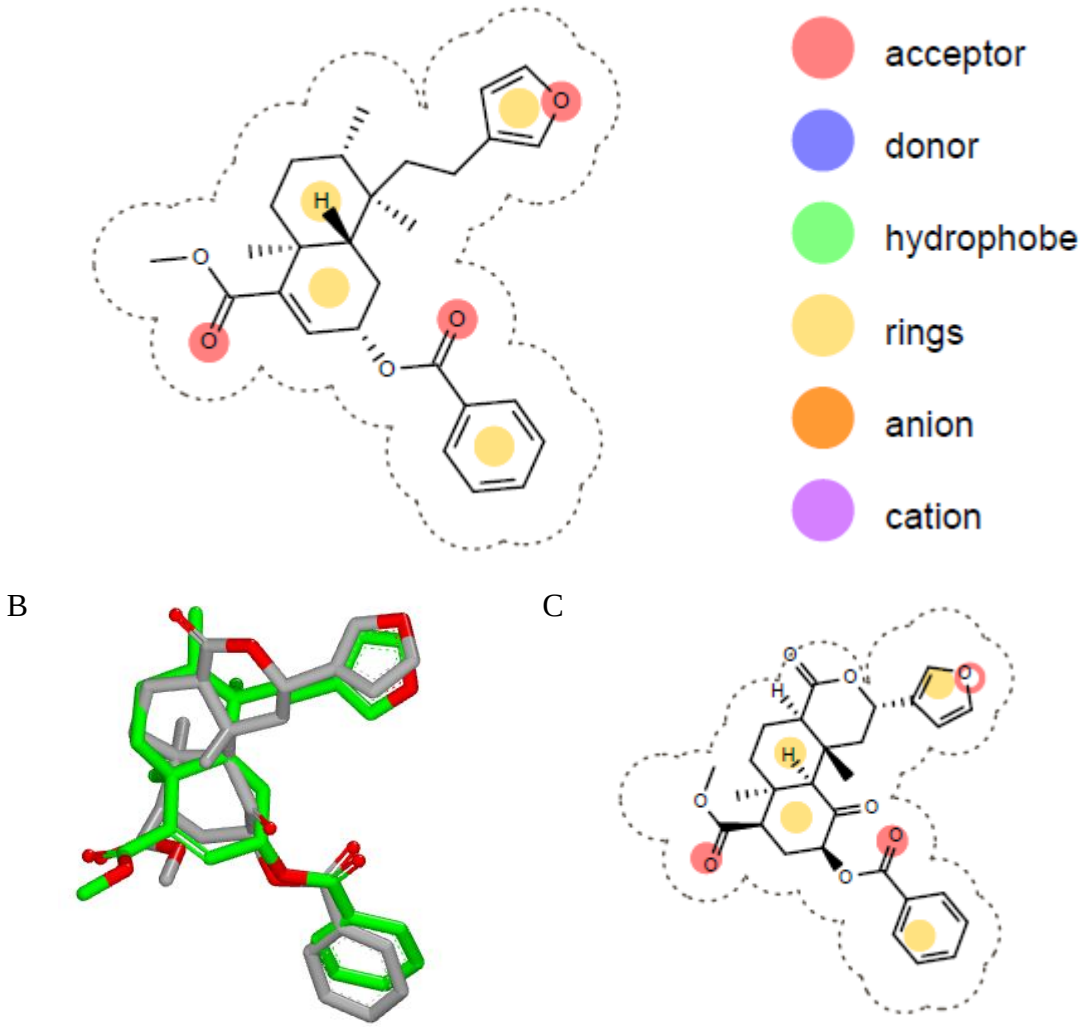

Figure 4.11: ROCS overlay of herkinorin to MPB. *(A) ROCS report structure of MPB including a legend of electrostatic features. The dashed outline represents the shape of MPB. Coloured circles represent electrostatic features. (B) 3D-representation of overlay presented by VIDA, MPB is featured in green and herkinorin is featured in grey. (C) 2D-representation of overlay presented by ROCS_report, dashed outline and coloured circles represent shape and electrostatic features of MPB. A 'full' circle represents a match while a 'hollow' circle represents a mismatch.*

The overlay of herkinorin to MPB shows that both molecules share a similar shape and have many common electrostatic features. It is readily apparent in the 3D-representation of the overlay that there is good overlap of major structural features in the two molecules, as expected. The benzyl esters, furan rings, methyl esters and central ring structures of the molecules all appear to be within close proximity. This is emphasised in the

2D-representation where each of the electrostatic features of MPB are matched with features in herkinorin, except for the hydrogen bond acceptor group in the furan ring. This mismatch, however, seems to just reflect the orientation of the furan rings and would likely not be present if the ROCS algorithm allowed for structural flexibility. The shape overlap of the molecules is also quite similar. A structural mismatch depicted in each representation are the methyl ester groups of each structure, which appear to be in a different orientation. Additionally, the valerolactone ring of herkinorin, which does not have an analogous feature in MPB, extends beyond the shape outline of MPB in the 2D-representation. Based on this analysis there appears to be ample data to suggest that herkinorin is both structurally similar to MPB, based on both shape and electrostatic features. Thus, without further disqualifying information, it may be reasonable to hypothesise that they have similar biological interactions.

Very recently, a paper was published proposing, for the first time, a binding mode of herkinorin in the μ-opioid receptor [313]. This proposed binding mode was generated through the use of structure-based *in silico* techniques, namely the use of docking and molecular dynamics with the crystal structure 5C1M (used in the present study) and as such requires validation through biological studies. Nevertheless, the publication of this study offers the opportunity to assess the present work with MPB in a retrospective manner. The key claims of the study include the proposition that herkinorin binds to the μ-receptor in a novel binding mode by interacting with an allosteric sodium ion binding site. The novel binding mode of herkinorin is suggested to involve key interactions with a tyrosine residue, Tyr 326. A depiction of the proposed model is included in Figure 4.12.

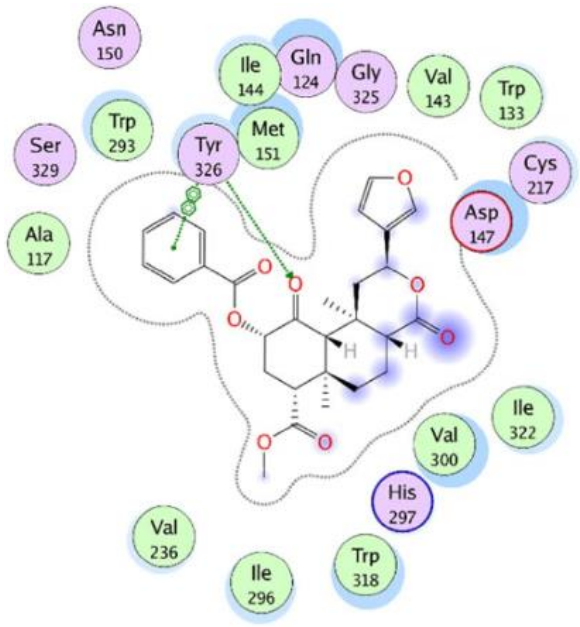

Figure 4.12: Proposed binding mode of herkinorin in the μ-opioid receptor. *Residues are colour coded as non-polar (green), polar (purple), acidic (purple with red outline) and basic (purple with blue outline). Key interactions are depicted with green arrows. Blue shading around atoms indicates exposure to solvent. (Reprinted with permission from J Comput Aided Mol Des, 31 Mar 2017, Online. Copyright 2017 Springer).*

The interaction between herkinorin and the Tyr 326 residue appears two-fold, involving π-π stacking interactions with the benzyl ring of herkinorin and a hydrogen bond interaction with the carbonyl of herkinorin. While the benzyl ring of herkinorin has been demonstrated to be approximately analogous with that of MPB, no such carbonyl group is present in MPB and as such, part of this key interaction would not be formed between MPB and Tyr 326. It was previously described in Section 4.2.1.2, that removal of the carbonyl group in salvinorin-type structures was not deleterious to κ-opioid binding. An interpretation in this present study however could be that the position of the carbonyl in herkinorin is important for binding with the Tyr 326 residue of the μ-receptor, and its absence diminishes activity. This observation may not have been made in previous studies of the κ-receptor as the aromatic ester of herkinorin is understood to be the key determinant of μ-receptor selectivity. The Tyr 326 residue of the μ-receptor is analogous to the Tyr 320 residue of the κ-receptor, however it has been suggested that a key difference in orientation exists between the residues [313]. This difference in tyrosine residue orientation may account for the

difference in receptor selectivity between herkinorin and salvinorin A as the Tyr 326 residue of the μ-receptor may better facilitate binding of an aromatic ring.

The region surrounding the Tyr 326 residue has been previously highlighted as a region associated with allosteric binding of sodium ions, and has been proposed as a key site in the recruitment of β-arrestin, as mentioned previously (see Section 4.2.1.2). The proposed binding of herkinorin to this site may therefore explain the previously mentioned ability for herkinorin to prevent β-arrestin recruitment, either through direct inhibition of sodium ion binding to the allosteric site, or by indirect inhibition via malformation of the allosteric site. While this proposed binding mode of herkinorin is very recent and has not been subjected to crystallographic or site-directed mutagenesis studies to scrutinise its claims, its ability to rationalise the previously made claims that herkinorin inhibits β-arrestin recruitment offers some evidence of its validity.

It has been previously mentioned (see Section 4.2.1.3) that traditional opioid modulators bind to opioid receptors through a conserved ionic interaction with an aspartic acid residue (Asp 147 in the 5C1M structure). It is apparent in the proposed binding mode of herkinorin that Asp 147, as an anionic residue, is not able to form a traditional ionic interaction with herkinorin. Instead, Asp 147 may be involved in weaker ion-dipole interactions with the furan or valerolactone rings of herkinorin. In the present study, it was decided to not use previously established binding modes of μ-receptor agonists as a reference for MPB binding as it was thought that the binding mode of diterpenoid opioids were unlikely to conform to the same model. The findings of this recent publication would seem to be in agreement with this assessment as all established models of μ-receptor binding involve ionic interactions with an aspartic acid residue.

4.3. Conclusions and future directions

In this study, chemical similarities between PAB and a set of unique opioid structures from the clerodane diterpenoid family were explored based on the principle that biological function often follows shape and chemical similarity. Chemical similarities were explored using 3D-based *in silico* methods including ligand-based ROCS analysis and structure-based docking. The results of these approaches directed the study to conclude that significant evidence for structural similarity existed between PAB and herkinorin, a μ-selective opioid agonist. Further assessment of the SAR of herkinorin and similar analogues suggested that a methyl ester transformation of PAB (MPB) would result in even greater chemical similarity. Thus, this ester was synthesised and screened *in vitro* against the μ-opioid receptor, but no significant binding was observed up to a concentration of 10 μM. Post-screening analysis was carried out and it was determined that the initial crystal structure (PDB ID: 4DKL) used to perform docking analysis was unsuited to the task, as this was an antagonist bound structure. Additionally, the publication of a recent study proposing a binding mode of herkinorin in the μ-opioid receptor offered suggestion that the lack of a carbonyl feature in MPB may have been deleterious to μ-receptor binding.

Scrutiny of the *in silico* and *in vitro* methods in this experiment raised several questions, but did little to alter the conclusion that MPB was likely not a modulator of the μ-opioid receptor. Further points of investigation that may be pursued to reach a more detailed conclusion would firstly include an absolute stereochemical assignment of PAB and MPB. To this end the method of Inokuma et al. [312] may be the best approach in reaching an absolute assignment as numerous natural products including flavonoids have been successfully crystallised and assigned [314], but this approach has not yet been applied to diterpenoids and as such may require a significant investment of time to finesse the approach into a workable method. Secondly, a medicinal chemistry approach could be undertaken to construct a series of compounds, bridging the "gap" between MPB and herkinorin, to determine the chemical differences between the two molecules that define the activity cliff between the two molecules.

Chapter Five: Thesis overview

5.1. Project description

Development of therapeutic products is a vast, multidisciplinary field far beyond the scope of a single thesis to cover in exhaustive detail. The purpose of the present study was to contribute to an ongoing project and lay groundwork for possible future development of therapeutic products derived from extracts of *D. polyandra.* Knowledge of the anti-inflammatory activity of *D. polyandra* is credited primarily to the Northern Kaanju traditional owners who, for generations, have used the stem and leaves of this plant to reduce pain and swelling associated with the removal of a rotten tooth [11]. To further understand this traditional usage, a project was launched by Chuulangun Aboriginal Corporation with the University of South Australia to study the general anti-inflammatory properties and chemistry of *D. polyandra.* Anti-inflammatory activity was observed *in vivo* in mice for acute and chronic models of inflammation [12, 14]. The present study aimed to continue investigations into the activity of *D. polyandra* through the study of the active constituents PAA and PAB. The three areas of principle interest in this study were the human enzymatic metabolism of PAA, the anti-inflammatory mechanism of action of PAA and the investigation of a possible analgesic mechanism of action of PAB.

5.2. Findings of the metabolism study of PAA and PAAH

As described in Chapter 2, the human enzymatic metabolism of PAA was assessed *in vitro* to predict the nature and extent of the hepatic biotransformation of PAA. It was determined that an enzyme dependent mechanism, likely involving hCES2 enzymes in HLM, resulted in extensive hydrolysis of PAA to its de-esterified form, PAAH. An implication of this finding is that rapid hydrolysis of a drug is typically associated with short drug action. In the case of PAA, its use has been demonstrated in mice to be active through twice-daily topical applications [14]. This seemed to imply a disparity between the rate of hydrolysis and duration of action of PAA. This may suggest that the anti-inflammatory properties of PAA are mediated by the actions of PAAH. This would categorise PAA as a pro-drug, although specific testing would need to be conducted to formally characterise it as such. Previous screening of PAAH in an *in vivo* mouse model demonstrated that it was approximately half as efficacious in alleviating symptoms of inflammation compared to PAA [12]. It is unclear where this difference in activity stems from, but it is possible that it is a result of the de-esterified form being less permeable across the skin membrane. This hypothesis would support the idea that PAAH is the active form of drug and the benzyl ester functional group of PAA serves primarily as a delivery system for PAAH.

In the form of a de-esterified alcohol, PAAH underwent further metabolic breakdown. Analysis of this further biotransformation of PAAH was assessed by examining the metabolism by CYP and UGT enzymes in human liver microsomes, and SULT enzymes in human liver cytosol. It was determined that while CYP enzymes had a minor metabolic role, and SULT enzymes displayed no observable metabolic activity, UGT enzymes had a significant role in metabolising PAAH.

Based on results of the enzyme dependent metabolism of PAAH by CYP and UGT enzymes, kinetic parameters were calculated and it was determined that PAAH had a microsomal half-life of 107 ± 2.12 minutes and a microsomal intrinsic clearance of 6.44 ± 0.13 μL/min.mg. The process of *in vitro/in vivo* extrapolation was then used to scale the determined figures from microsomal clearance to whole liver clearance, which was calculated to be 1.25 L/hr, which is considered to be a slow clearance rate. This finding may have implications in dosing for potential future therapeutic uses as slow metabolic clearance

is often associated with a slow excretion, and hence, prolonged exposure to the drug. For this reason, PAA, or PAA containing plant extracts of *D. polyandra,* may be required to be administered with low doses, or at long intervals, to minimise risk of overdosing, and potential adverse drug reactions.

Enzyme metabolism by CYP and UGT enzymes was further investigated with the goal of determining the specific enzymes involved in the metabolism of PAAH. Using two complementary approaches, namely the use of selective enzyme inhibitors in HLM and recombinant enzymes of major CYP and UGT enzymes, it was determined that the key metabolising enzymes were UGT 1A1 and 2B7 and CYP 2C9 and 3A4. Structural analysis of metabolites was conducted by a combined *in silico* and *in vitro* approach. *In silico* computational models were used to predict metabolism and UPLC/MS to detect and identify metabolites produced *in vitro*. Computational modelling predicted the identity of three metabolites with indications that an acyl glucuronide would be the major species. This finding was in good agreement with UPLC/MS experiments which detected three metabolites, the major metabolite being an acyl glucuronide, and two minor *O*-glucuronides.

The contribution of UGT 1A1 and 2B7 to the regioselective formation of metabolites was also assessed by UPLC/MS and it was determined that the role of each enzyme was equivalent. This finding suggests that *in vivo* inhibition of either enzyme is unlikely to significantly affect the metabolic transformation of PAAH to its glucuronide metabolites, although as UGT 2B7 is more abundant than 1A1, inhibition of 2B7 may result in a lower rate of clearance. Given the already slow clearance of PAAH, co-administration of drugs associated with UGT 2B7 inhibition, such as the antifungal medication fluconazole [315], may be contraindicated, although this would have to be studied further to determine if there is any clinical consequence to co-administration. While the *O*-glucuronides were not able to be successfully distinguished from each other, it was observed that one *O*-glucuronide metabolite was resistant to hydrolysis by β-glucuronidase. This may form part of a strategy in a future experiment to distinguish the two metabolites by selectively synthesising each glucuronide metabolite and observing their metabolism by β-glucuronidase. Alternatively, if sufficient quantity of the metabolites could be generated and purified it may be possible to determine the identity of the metabolites via 2D-NMR characterisation.

Metabolites from CYP enzymes were also analysed computationally and it was predicted that the major metabolite of PAAH would be a furan metabolite, although no CYP metabolites were able to be characterised *in vitro*. Possible reasons for a failure to detect metabolites may be due to the detection limits of the chromatographic technique used, or to protein binding of reactive metabolites. Furan metabolites are commonly recognised "red flags" in many metabolism studies as furan metabolites are often, but not always, associated with hepatotoxicity [316]. The precise mechanism for this hepatotoxicity is not uniform in all examples, but it is primarily thought to be associated with epoxide or enedione metabolites which bind to cellular proteins or DNA to trigger toxic effects [181]. Of particular note is teucrin A (shown in Figure 5.1), a furan-containing clerodane diterpenoid isolated from *Teucrium chamaedrys*, which was found to be associated with hepatotoxicity caused by CYP3A-mediated furan metabolism, which was a major metabolic clearance pathway [181, 317]. Conversely, there are several examples of widely used medications containing furan rings including prazosin and furosemide (shown in Figure 5.1), which are both used in the treatment of high blood pressure. It is worth noting that in both of these medicines furan metabolites are minor metabolic constituents and a majority of drug is cleared by alternate metabolic mechanisms [318, 319]. Given that CYP clearance of PAAH is a minor pathway of total PAAH clearance, it may therefore follow that PAAH poses a low-level of risk akin to prazosin or furosemide, although this would require further study to confirm.

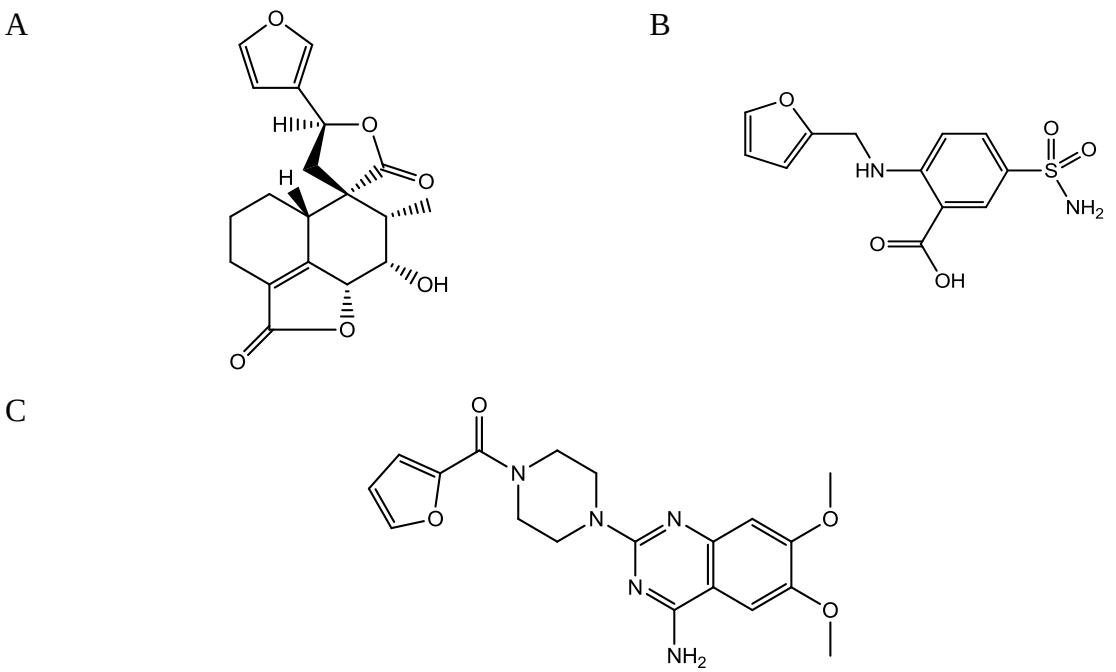

Figure 5.1: Structures of furan containing compounds. *(A) Teucrin A. (B) Furosemide. (C) Prazosin.*

Beyond the experiments performed in this study, numerous *in vitro* opportunities exist to extend this research. Currently as part of the broader project, PAA is being examined for its possible use in therapeutic products for skin inflammation and is being tested in a model of chemotherapy-induced gastrointestinal mucositis. As such, the use of skin or intestinal microsomes in metabolism studies, may provide insights into these therapeutic uses of PAA. Extending metabolic studies to microsomes of these other organs would also give a greater appreciation for full human metabolism and may highlight the importance of alternative enzyme systems independent of the liver. Beyond *in vitro* studies, the goal of most metabolism studies involves eventual translation to *in vivo* studies. This can be partially achieved through *in vitro-in vivo* extrapolation, such as in this study, but assessment of metabolism through clinical trials provides higher quality data for metabolism and kinetics. Clinical trials, as primary *in vivo* studies, can also be used to determine the significance of metabolism in drug excretion. While it was predicted that PAA would undergo relatively slow clearance via metabolic pathways, it is possible that total drug excretion may be faster than anticipated due to non-metabolic excretion pathways such as renal or biliary clearance.

5.3. Findings of the study of inflammatory pathways of PAA action

Chapter 3 related to the study of the anti-inflammatory activity of PAA, and specifically the mechanism of action that underpins this activity. This study also sought to examine the usage of *in silico* methods to enrich the *in vitro* process of determining enzyme and receptor targets of a drug by predicting activity based primarily on ligand-based similarity and structure-based docking. Previous experimental data had demonstrated that PAA was able to reduce the production of pro-inflammatory cytokines including IL-1β, IL-6 and TNFα in stimulated cells. As such, the approach in this chapter focused on enzymes and receptors associated with modulating the levels of these cytokines. The approach involved forming a hypothesis that PAA would bind to a particular receptor, analysing the hypothesis by *in silico* means and then testing the hypothesis with *in vitro* experiments.

The first target assessed by this process was caspase-1, owing to its role in the processing of IL-1β from its inactive precursor. Analysis by structure-based methods suggested that key binding features of caspase-1 inhibitors were replicated in docking simulations, despite low structural similarity established by ligand-based methods. Assessment by *in vitro* testing revealed that there was no significant difference between levels of IL-1β and pro-IL-1β in stimulated cells treated with PAA when compared to untreated controls. This suggested that caspase-1 function was not inhibited by PAA.

A phorbol ester, TPA, was used to stimulate inflammatory cytokine release in cell-based assays and has also been used to stimulate skin inflammation in mouse studies with PAA. TPA is known to initiate inflammation via the PKC pathway, thus the PKC family was also investigated. The ROCS approach was applied to PKC inhibitors and it was concluded that very little structural similarity could be observed with PAA, both in respect to shape and electrostatic features. Additionally, based on a pharmacophore map of PKC inhibitors produced in a previous study [232], it was suggested that the presence of an anionic group in PAA may significantly reduce binding affinity with PKC receptors. It was therefore predicted that no activity would be observed *in vitro*. Upon screening of a battery of twelve PKC subtypes, no significant binding activity was observed, and it was therefore concluded that PAA is unlikely to inhibit the pro-inflammatory actions of PKC.

The next target considered was NF-κB due to its ability to promote synthesis of pro-inflammatory cytokines including TNFα and IL-1β. Analysis by the ROCS approach indicated very little electrostatic similarity to NF-κB inhibitors, although shape similarity was significantly higher. Due to there being multiple mechanisms of NF-κB activation, it was decided that docking was not an appropriate approach to pursue for the receptor. Due to the high degree of shape similarity in certain NF-κB inhibitors, *in vitro* screening was pursued. Screening of NF-κB was performed indirectly by testing nitrite concentrations in cells, which revealed that PAA did not inhibit the production of nitric oxide *in vitro*. As NF-κB modulates nitric oxide production through production of iNOS, this finding indicated that PAA did not inhibit the function of NF-κB.

It was also explored as to whether a receptor upstream of NF-κB may exert some effect on NF-κB. The glucocorticoid receptor was considered for this reason as a possible target of PAAH. By applying the ROCS method to a series of steroidal and non-steroidal glucocorticoid agonists it was determined that PAAH bore moderate shape similarity, but weak electrostatic similarity, to a particular class of non-steroidal compounds. Furthermore, it was observed that PAAH was able to satisfy three out of four spheres of a pharmacophore hypothesis designed to describe glucocorticoid agonists, which suggested that PAAH may be a weak agonist of the glucocorticoid receptor. Further *in silico* analysis by docking provided support to the hypothesis that PAAH may bind to the glucocorticoid receptor by demonstrating interactions between PAAH and the glucocorticoid receptor similar to those found in known agonists. Additionally, structural mismatches between PAAH and glucocorticoid agonists identified from previous ROCS analysis were investigated via docking and it was determined that these mismatches were unlikely to result in a considerable electrostatic clash with residues in the glucocorticoid receptor. Screening by *in vitro* receptor binding was performed and revealed no significant activity up to 10 μM, however there may have been weak binding activity at the highest concentrations of PAA. If further screening is performed at higher concentrations it may reveal weak receptor binding activity with the glucocorticoid receptor. This may validate the *in silico* based hypothesis that PAAH is a weak agonist of the glucocorticoid receptor, however at these high concentrations it is unlikely that this binding activity would translate to significant anti-inflammatory activity *in vivo*.

Based on the study of four receptor targets in the inflammatory cascade, no target was positively identified as being responsible for the anti-inflammatory activities of PAA, therefore there are opportunities for further study in this area. Many more receptors exist in the inflammatory cascade that may be targets of PAA, but a scattered approach may not be the best advisable path forward. Progress may be improved by the acquisition of additional *in vitro* data, such as potential modulation of anti-inflammatory cytokines like IL-4 and IL-10. This additional data could reveal further insights and be used to identify targets that may not have otherwise been considered. While this study did not lead to the isolation of an anti-inflammatory pathway for PAA it did provide useful information by demonstrating several common pathways that do not contribute to its activity. Thus, the present study, along with previous investigations of COX-1 and COX-2 [15], contribute to the development of PAA by suggesting that it may operate by a novel mechanism of action.

In reflection of the approach utilised to combine *in silico* and *in vitro* techniques to the study of drug targets, it is apparent that the approach is not without merit. The low computational expense of ROCS analysis allows for numerous targets to be screened with a minimum investment of time and money [138]. Use of docking in prospective projects appears more controversial based on the present study since it is difficult to discern when the technology is successful, and as a result its use can become misleading [293]. There is however, good evidence that reliability of prospective docking is improved when close structural similarity with a co-crystallised ligand is established, due to receptor site/ligand complementarity [222]. For this reason, it may be recommended to reserve use of docking either for scenarios where good structural similarity can be established, through ROCS or otherwise, or for retrospective analyses, when a receptor target is already known and the objective is to rationalise its binding.

5.4. Findings of the study of MPB and the μ-opioid receptor

While studies in previous chapters were led by traditional knowledge and subsequent *in vitro* data, the study of a pain mechanism in Chapter 4 was based on an *in silico* derived hypothesis. This study followed on from a previous ROCS-based honours investigation conducted on *D. polyandra* diterpenoids which established structural similarity between PAB and a structurally distinct series of opioid compounds, based around salvinorin A. In this study, a hypothesis was formed that PAB may exert some analgesia through interactions with opioid receptors. This hypothesis was not supported by *in vitro* receptor binding data however, and it was concluded that PAB did not bind with opioid receptors.

The present study continued this investigation through analysis of structure-activity relationship (SAR) studies of salvinorin A analogues. Of particular interest was herkinorin, a benzyl ester analogue of salvinorin A with potent and selective μ-opioid receptor agonism. This analysis suggested that while PAB was not a suitable ligand of opioid receptors, a closely related methyl ester analogue (MPB) might be a suitable ligand of the μ-opioid receptor. Use of opioid receptor docking using a newly crystallised μ-opioid receptor structure [91], provided some support of this hypothesis. It was proposed that MPB and herkinorin were able to adopt similar binding modes in the μ-receptor binding site. These findings formed an important hypothesis to investigate in the development of *D. polyandra* compounds from a regulatory perspective as opioid ligands, especially μ-opioid agonists, are strictly regulated by many therapeutic governing bodies [320]. There are, therefore, significant implications in introducing a compound that can be easily modified into an opioid agonist and as such, the hypothesis should be closely investigated.

Following *in silico* analyses, it was decided to investigate MPB as a potential opioid agonist. Through the use of a methyl halide, PAB was successfully esterified to form MPB and this product was then characterised via MS and NMR analysis. Subsequently, MPB was submitted for receptor binding screening against the μ-opioid receptor, but no significant binding activity was observed at all concentrations of MPB. These results suggested that neither PAB, nor MPB, bound significantly to the μ-opioid receptor. Therefore, it followed that neither compound was likely to produce analgesia through this mechanism.

Further *in silico* modelling was performed as a result of these findings using a newer crystal structure of the μ-opioid receptor [307]. The primary benefit of this new structure was that the crystal was bound in an agonist form, compared to the previous antagonist bound structure used for analysis [91]. This new docking study yielded a different binding pose to prior docking results, suggesting that MPB and herkinorin were not capable of binding in the same mode in the μ-receptor. The active sites of each structure were vastly different, with the antagonist bound form being much larger. This may indicate that the initial suggestions that MPB and herkinorin could adopt a similar binding mode in the receptor were merely an artefact of the size of the active site.

A binding mode of herkinorin in the μ-opioid receptor was recently proposed [313] after the work in Chapter 4 was completed. This proposed binding mode provided an opportunity to gain insight into the structural differences between herkinorin and MPB that may result in the observed binding differences. This proposed binding mode provided the suggestion that the absence of a carbonyl in the structure of MPB, which is present in herkinorin, may contribute to some extent to the lack of binding activity of MPB with the μ-opioid receptor. Furthermore, the publication of this receptor binding mode was in agreement with a prior hypothesis that herkinorin adopted a different binding mode from traditional opioids.

While concerns were raised regarding the validity of the binding assay results of MPB (see Chapter 4.2.5), the *in vitro* screening and latter docking results both indicated that MPB was unlikely to bind to the μ-opioid receptor. Whilst MPB clearly has significant similarity to herkinorin, small changes in chemical structure can lead to so called 'activity cliffs'. Activity cliffs refer to the phenomena where a small change in chemical structure results in a large change in receptor binding activity. Evidently, between the structures of herkinorin and MPB there are structural differences that result in the abolition of μ-opioid binding activity. There is, therefore, opportunity to explore the nature of this activity cliff. It has been postulated that the absence of a carbonyl group, or possibly the valerolactone ring of herkinorin, which are both not present in MPB, may be where this activity cliff resides, however this would require further study to lead to a definitive conclusion. The best method to determine the structural differences which result in loss of μ-opioid binding activity would be a medicinal chemistry approach consisting of

modifications to the structure of herkinorin. This approach would involve synthesising and testing an array of compounds with small structural differences between herkinorin and MPB and determining which structural features result in deleterious actions towards binding activity.

The study in Chapter 4 further supports the idea that the use of prospective docking, should be scrutinised carefully [293]. In particular, the findings highlight the necessity of careful selection of a crystal structure. This study featured the use of two crystal structures, one antagonist bound and one agonist bound, and to each of these structures dissimilar outcomes were obtained. Therefore, in future uses of docking technology it is highly advisable to use a crystal structure bound in a form analogous to the compound being screened. It may be acceptable to use an inappropriately bound structure in some cases, especially when there are no, or low quality, alternatives available, however the findings of such docking analyses should be treated with much greater scrutiny.

5.5. Observations on *in silico* methods

Throughout this project, a methodological approach of *in silico* and *in vitro* integration has been used. This approach has previously been successfully implemented to examine diverse problems in drug discovery such as predicting distribution properties [123], metabolism [321] and drug targets [322]. As virtual screening is very much an information directed process, it can be argued that success of an *in silico* implementation is strongly dependent on the volume, and quality, of information available. In the present study *in silico* integration resulted in mixed results when analysed against *in vitro* derived data.

In Chapters 3.2.1 and 3.2.4, caspase-1 and the glucocorticoid receptor were both highlighted as potential targets of PAA by *in silico* modelling. In both of these examples the use of structure-based docking yielded results which seemed to support hypotheses regarding these targets. In contrast, use of the ligand-based ROCS method did not seem to support the hypotheses, in better agreement with the results from *in vitro* testing. These findings would seem to support the idea that ligand-based methods perform better in prospective analyses. Further support of this idea is presented in Chapters 3.2.2 and 3.2.3 where the use of ligand-based methods determined only mild similarity with modulators of PKC and NF-κB. These findings suggested that binding of PAA/PAAH to each target was unlikely, which was in agreement with results from *in vitro* testing. Based on the findings presented in this thesis it is reasonable to propose that the use of ligand-based methods are well suited to prospective analyses.

One example of the use of a structure-based method in this thesis was detailed in Chapter 2.2.15.1, where docking identified the furan ring of PAAH as the major site of CYP2C9-mediated metabolism. While this prediction was not able to be validated by *in vitro* testing, the prediction was in agreement with three other knowledge- and ligand-based methods. A key difference in this use of docking compared to later uses of docking i.e. in Chapters 3.2.1 and 3.2.4, is that this use docking was performed retrospectively, where the target was already validated *in vitro*. These findings may suggest that the use of docking is better suited to retrospective analyses, where it can be used to rationalise, rather than predict, target binding.

In Chapter 3.2.6 it was argued that Tanimoto Combo similarity was a reliable method of discerning docking success *a priori* in agreement with a previous study by Tuccinardi et al. [222]. In multiple cases where docking was used in this thesis (see Chapters 3.2.1.2, 3.2.4.2 and 4.2.1.3), a low degree of structural similarity was observed between the docked molecule (PAA/PAAH) and bound ligands of crystal structures used. In these cases, the interpretation of the binding modes predicted by docking supported the hypothesis that PAA, or PAAH, could bind to these targets, however these hypotheses were not supported by *in vitro* results. The previously mentioned use of docking in Chapter 2.2.15.1, showed PAAH had a higher Tanimoto Combo score with the bound ligand than in other uses of docking in the thesis. This higher degree of structural similarity resulted in a docking outcome in agreement with three other *in silico* methods of metabolism prediction. This may support the idea that docking is more successful when there is higher structural similarity with a crystal structure ligand.

Shape-based methods used in this thesis were based on the ROCS method of determining chemical similarity between molecules under the premise that structurally related compounds are more likely to have similar properties. The primary user considerations involved in the ROCS approach are those involved in constructing a chemical library that will be used for analysis. A chemical library should consist of a diverse range of molecules, ideally with a specific common property towards a target enzyme or receptor [323]. An issue that may arise in ROCS analysis when a query molecule is ranked highly amongst a chemical library is the previously described concept of activity cliffs. In the ROCS method any structural difference between two molecules results in a decrease in the Tanimoto score for those molecules, however the ROCS method may be unable to distinguish activity cliffs from insignificant structural changes. Thus, unless an activity cliff is well characterised, results from a ROCS analysis can potentially be misleading. In Chapter 4.2.1, it was discussed that the demethylation of salvinorin A diminished κ-receptor binding, however a less obvious activity cliff was proposed in Chapter 4.2.5, that the loss of a carbonyl group in herkinorin may be deleterious to μ-receptor binding. These examples highlight the need to study available literature to avoid ‘falling off’ activity cliffs, both in relation to characterised and uncharacterised activity cliffs when dealing with less developed areas of literature.

Overall, it may be argued that the successful implementation of *in silico* methods in drug development projects is highly dependent on the information available, either through in-house data collection or literature access. In classes of compounds, such as clerodane diterpenoids, which are not significantly studied pharmacologically, a lack of literature can limit the successful implementation of *in silico* technologies.

In the present study of *D. polyandra* clerodane diterpenoids, it may be argued that the limited number of previous pharmacological studies on this class of compounds hindered the success of the project. In well characterised chemical spaces, many pharmacological predictions can be made regarding the activity of an uncharacterised compound by assessing the literature of related compounds. In the chemical space of clerodane diterpenoids, a majority of available pharmacological literature is devoted to a few key compounds such as salvinorin A and teucrin A, both of which have been previously discussed as noteworthy pharmacological compounds. This available literature informed aspects of the study, for instance, κ-opioid receptor modulation of salvinorin A directed initial investigations into opioid receptors (Chapter 4), and CYP-mediated toxicity of teucrin A informed investigations into the potential furan metabolism of PAAH (Chapter 2).

The anti-inflammatory studies performed in Chapter 3 may have been the most affected by a lack of referencing literature, as while there are other known clerodane diterpenoids with anti-inflammatory activity [209, 210], their mechanisms are also unknown and there is no published data available regarding mechanisms that have been investigated. It may be the case that other clerodane diterpenoids have had mechanistic pathways investigated, possibly including pathways investigated in the present study, but the failure to discover the precise mechanism resulted in the data remaining unpublished. If this hypothetical negative data was available it may have influenced the direction of research in the present study. This observation echoes a common desire in research that more negative results should be published [324]. In this spirit, the contents of this thesis may contribute towards the development of other clerodane diterpenoids by describing a number of receptors and enzymes that do not appear to be a target of the compounds. This may aid in the experimental direction or design of future projects.

5.6. Final thoughts

In conclusion, this project sought to investigate, by the use of *in silico* and *in vitro* methods, the pharmacology of anti-inflammatory diterpenoid compounds with the aim of determining their metabolic fate and molecular targets associated with their activity. The major pathways and metabolites of PAA were determined in the first such study of an Australian medicinal plant compound. While a specific mechanistic pathway was not identified to explain the anti-inflammatory actions of PAA, several pathways were examined and ruled out. A further anti-nociceptive pathway through the μ-opioid receptor was investigated and it was determined that analgesic properties associated with the *D. polyandra* compounds was unlikely to be linked to modulation of opioid receptors. While the findings of these studies did not result in the determination of specific mechanisms of action, the data collected can be used to direct further investigations into the target-based actions of PAA. In addition to the pharmacological findings of this study, the strengths and weaknesses of ligand- and structure-based *in silico* methods were assessed by comparing the findings of the present study to previous examples in the literature.

Chapter Six: Methods and materials

6.1. Experimental materials, assays and software

6.1.1. Chemicals and suppliers

Table 6.1: List of chemical suppliers, chemicals and chemical grade.

Supplier	Chemical	Grade/purity/notes
Sigma-Aldrich (Sydney, Australia)	β-glucuronidase (type IX-A, *E. coli*)	Lyophilised, 30-70% biuret
	Methanol-d_4	≥ 99.8 atom % Deuterium
	Hecogenin acetate	≥ 90%
	Furafylline	≥ 98%
	Ticlopidine hydrochloride	≥ 99%
	Quinidine	≥ 98%
	CYP3cide	≥ 98%
	NADP	≥ 99%
	Glucose-6-Phosphate (G-6-P)	≥ 98%
	G-6-P dehydrogenase (type XV, *S. cerevisiae)*	Lyophilized, premium
	Glycerol	≥ 99%
	UDPGA trisodium salt	≥ 99%
	Lysozyme (recombinant, *H. sapiens*)	Lyophilised, ≥ 90%
	Folin-Ciocalteu reagent	Solution, 2 M
	Phenylmethane sulfonyl fluoride (PMSF)	≥ 98%
	Phosphoadenosine phosphosulfate (PAPS)	≥ 90%

Continued on following page

Table 6.1: Continued from previous page

Supplier	Chemical	Grade/purity/notes
Sigma-Aldrich (Sydney, Australia)	Isopropyl thiogalactopyranoside (IPTG)	≥ 99%
	TES free acid	≥ 99%
	Bovine serum albumin (BSA)	≥ 95%
	Aminolevulinic acid (δ-ALA)	≥ 98%
	Tetraethylsulfamide (TES)	≥ 99%
	Magnesium chloride ($MgCl_2$)	Anhydrous, ≥ 98%
	Potassium chloride (KCl)	Anhydrous, ≥ 99%
	Methanol (MeOH)	≥ 99.9%
	Methyl iodide (MeI)	≥ 99.5%
	Sodium hydroxide (NaOH)	Pellets, 98%
	Copper sulfate ($CuSO_4$)	≥ 99%
	Sodium tartrate	≥ 99%
	Dimethyl sulfoxide (DMSO)	≥ 99%
Merck (Baywater, Australia)	Thionyl chloride	≥ 99.9%
	Dimethyl formamide (DMF)	≥ 99.5%
	Acetonitrile	Analytical and MS grade
	Formic acid	≥ 98%
	Water (H_2O), Milli-Q Integral Water Purification System	Milli-Q
Chem Supply (Gillman, Australia)	Sodium carbonate (anhydrous)	Analytical grade
AG Scientific (San Diego, USA)	Alamethicin (*T. viride*)	≥ 98%
Cayman Chemical (Waterloo, Australia)	Fluconazole	≥ 98%
	Montelukast	≥ 98%

Continued on following page

Table 6.1: Continued from previous page

Supplier	Chemical	Grade/purity/notes
Thermo Fisher Scientific (Thebarton, Australia)	DH5α competent cells (*E. coli*) Terrific broth (*E. coli*) LB broth (Lennox) Spheroplast resuspension buffer (SRB) Lysogeny broth	Cells Solution Powder Solution Powder
E.R. Squibb and Sons (Princeton, USA)	Niflumic acid	≥ 95%
Ciba-Geigy (Melbourne, Australia)	Sulfaphenazole	≥ 95%
Life Technologies (Thebarton, Australia)	PolarScreen GR Competitor Assay, Green	Assay kit

PAA and PAB were isolated from *D. polyandra* by solvent extraction and chromatography according to Simpson et al. [325]. PAAH was subsequently produced from PAA by alkaline hydrolysis [325]. Identity and purity (>98%) of all diterpenoid compounds were established by ^{1}H and ^{13}C NMR using a Bruker Avance III 500 MHz spectrometer (Preston, Australia). Chemicals and equipment used for caspase-1 and NF-κB screening are described by Simpson et al. [14].

6.1.2. Outsourced assays

Protein kinase screening was performed by Life Technologies by SelectScreen Biochemical Kinase Profiling Services by the methods and materials described by Rodems et al. [326]. Glucocorticoid screening was performed by Life Technologies via a LanthaScreen time-resolved fluorescence resonance energy transfer (TR-FRET) described

in Section 6.3.3. Opioid receptor screening was performed by Ricerca Biosciences using a competitive binding assay by the method described in Section 6.4.3.

6.1.3. Software

In silico investigations were performed using software from Advanced Chemistry Development Inc: PhysChem History v12.01 and ADME Suite v5.0; and from OpenEye Scientific Software: Omega v2.5.1.4, ROCS v3.2.0.4, OEDocking v3.0.1 (Hybrid and FRED) and VIDA 4.2.1. Use of specific software is described further in Section 6.5.

6.2. Human enzyme metabolism of PAA and PAAH

6.2.1. Collection of human liver microsomes

Portions of five human livers (H7, H10, H12, H13 and H40) were obtained from the human liver bank of the Department of Clinical Pharmacology, Flinders University. Relevant information of the liver donors are presented in Table 6.2.

Table 6.2: Relevant data of human livers used in experiments

Liver	Age	Gender	Smoking history	Alcohol history	Drug treatment
H7	44	Female	Non-smoker	Social	Dexamethasone
H10	67	Female	Non-smoker	Social	Dopamine, morphine, frusemide, midazolam
H12	66	Male	Non-smoker	Moderate	Insulin
H13	61	Female	Non-smoker	Social	Metoprolol, methylclothiazide, bethanechol
H40	54	Female	Non-smoker	Unknown	Dopamine, dexamethasone

Ethics approval for use of human liver microsomes was obtained from the Southern Adelaide Clinical Research Ethics Committee. Human liver was immersed in ice cold phosphate KCl buffer solution (10 mM phosphate buffer, pH 7.4, 1.15% w/v KCl). The liver was finely minced with scissors and further homogenised with an IKA Ultra Turrax T25 at 20,500 rpm (Milton, Australia). The resulting liquid solutions were then transferred to ice cooled 10 mL Potter-Elvehjam homogenisers from Omni International (Newtown, Australia) with attached drill for further mincing. Care was taken to cycle use of the homogeniser to minimise heat transfer to the homogenate. The resulting homogenate was then poured into open top polycarbonate centrifuge tubes and mass balanced by addition of phosphate buffer.

The tubes were then inserted into a Beckman J2-21 M/E centrifuge with JA-20 rotor (Mount Waverley, Australia) set at 4 °C and centrifuged at 700 g for 10 minutes and then 9,500 g for a further 10 minutes. The supernatant was then extracted and transferred to ice-cooled ultra-centrifuge tubes, which were again mass balanced with phosphate buffer. The tubes were then inserted into a Beckman L8-70 M ultracentrifuge with a 50.2 Ti rotor (Mount Waverley, Australia) set at 4 °C and centrifuged at 105,000 g for 75 minutes under vacuum pressure. Centrifugation resulted in the centrifuge tubes containing a supernatant layer and deposited pellet at the bottom of the container.

The supernatant layer produced formed the cytosol fraction of the liver tissue and was extracted for further experimental use. The deposited pellet formed the microsomal fraction of the liver tissue and was resuspended in phosphate buffer solution. The pellet was then scraped off the tube surface using a round ended probe and transferred into an ice cold 10 mL Potter-Elvehjam homogeniser.

The pellet suspension was homogenised by hand then poured back into ultracentrifuge tubes, mass equilibrated by addition of phosphate buffer then returned to the ultracentrifuge unit and centrifuged again at 105,000 g for 60 minutes under vacuum pressure. This resulted in a supernatant layer and deposited pellet.

The supernatant layer was discarded, and the pellet was scraped off the tube again and resuspended in phosphate glycerol storage buffer (0.1 M phosphate buffer, pH 7.4, 20% w/v glycerol). The suspension was then transferred to an ice-cold 10 mL Potter-Elvehjam homogeniser and homogenised by hand. The resulting homogenate was then aliquoted into glass vials, and cooled on dry ice to snap freeze before storing at -80 °C.

Protein concentration of homogenates was determined by the Lowry method described further in Section 6.2.3. After quantification, equimolar portions from each liver homogenate were retained and mixed to produce a pooled microsome homogenate of all five livers. Protein concentration was determined on the pool of microsomes by the Lowry method before being aliquoted into glass vials and stored at -80 °C.

6.2.2. *E. coli* P450 expression

A transformation stock of DH5α cells (40 µL) was transferred to a lysogeny broth (LB) agar plate and incubated at 37 °C overnight to allow bacterial growth. After incubation, a single colony was isolated and used to inoculate 5 mL of LB broth, which was then sub-cultured at 37 °C with shaking (200 rpm) overnight. The sub-culture was then diluted 1:100 with pre-warmed terrific broth (TB) solution and incubated at 37 °C with shaking (160 rpm) for approximately 4 hours in a New Brunswick INNOVA 4300 incubator shaker (Chatswood, Australia). The solution was then cooled to 30 °C and supplemented with 1 mM isopropyl β-D-1-thiogalactopyranoside (IPTG) and 0.5 mM 5-aminolevulinic acid (δ-ALA) and incubated at 30 °C with shaking (160 rpm) for 40 hours.

Cultures were chilled on ice for 10 minutes then centrifuged at 5,000 g using a JA-20 rotor for 10 minutes at 4 °C. The supernatant was then discarded and the deposited pellet was weighed and resuspended in 15 mL/g TES buffer. Lysozyme (100 µL/g) was added to the cellular mixture, then diluted 1:1 with pre-chilled irrigation water (4 °C) and incubated on ice with gentle shaking. The solution was then centrifuged at 10,000 g using a JA-20 rotor for 10 minutes at 4 °C, the supernatant was discarded and the pellet was resuspended in 5 mL spheroplast resuspension buffer (SRB).

The resuspended pellet was then supplemented with 50 µL phenylmethanesulfonyl fluoride (PMSF) and 200 µL of protease inhibitors before sonication on a Sonics Vibra-Cell sonicator (Chatswood, Australia). Sonication was performed over ice at a 40% duty cycle in 8 second bursts, with 60 seconds between pulses allowing for cooling and repeated 10 times. The sonicated solution was then centrifuged at 10,000 g on a JA-20 rotor for 20 minutes at 4 °C, upon which the supernatant was collected and further ultra-centrifuged at 180,000 g on a 60Ti rotor for 105 minutes at 4 °C. The supernatant was then discarded and 500 µL of 1:1 TES/water was added and a brush was used to gently resuspend the pellet and pipetted up and down to establish homogeneity. Protein content was quantified using the Lowry protein concentration assay and samples were then frozen at -80 °C for storage.

6.2.3. Protein content quantification

Protein content of human liver microsome fractions and pools were determined by the Lowry method [327]. Lowry reagent was prepared by combining 100 parts Lowry A (0.4% sodium hydroxide and 3% sodium carbonate in water) with 1 part Lowry B (4% sodium tartrate in water) and 1 part Lowry C (2% copper sulphate in water) and mixing thoroughly by vortex. Folin's reagent was prepared by combining 1 part Folin-Ciocalteu's Phenol reagent with 1 part water and mixing thoroughly by vortex. Pooled HLM samples were prepared by making a 1-in-10 dilution of HLM to water and mixed thoroughly by vortex.

A 5-point standard curve was prepared using bovine serum albumin (BSA) as a standard protein. Table 6.3 describes the contents of each tube and each standard measurement was prepared in duplicate:

Table 6.3: Contents of standard tubes for Lowry protein assay.

Standard	Protein amount (µg)	Volume of BSA (µL)	Volume of H_2O (µL)
Blank	0	0	500
1	10	10	490
2	25	25	475
3	50	50	450
4	75	75	425

Assay samples were prepared in quadruplicate from a single pooled HLM sample by adding 25 µL of diluted HLM to 475 µL of water and mixing thoroughly by vortex. Lowry reagent, 2 mL, was added to each sample, as well as each calibration standard, mixed by vortex and allowed to stand for 10 minutes. Following addition of Lowry reagent, 250 µL of Folin's reagent was also added to each of the samples and calibration standards, thoroughly mixed by vortex and allowed to stand for 15 minutes. After all samples and standards were prepared, the absorbance of each was measured using a Varian Cary 300 Conc UV-Visible spectrophotometer (Mulgrave, Australia), scanning at 660 nm. The absorbance reading for

each of the standards was used to generate a slope, which was then used with the absorbance readings of the tested sample by Equation 6.1 to calculate the protein concentration of the sample [327]:

Equation 6.1: Protein concentration

$$Protein\ concentration = dilution\ factor\ \times \left(\frac{absorbance}{slope}\right) \times \left(\frac{1}{sample\ volume}\right)$$

6.2.4. Sample analysis by HPLC

HPLC conditions for different experiment analyses had a set of common parameters that were unchanged for all assays. A summary of unchanged parameters is included in Table 6.4.

Table 6.4: Universal HPLC conditions for sample analysis

Parameter	Details
HPLC instrument	Agilent Technologies 1100 series Agilent Technologies 1200 series
Column	Phenomenex Synergi 150 x 3 mm
Silica	4 μm HydroRP
Detection wavelength	225 nm
Column temperature	25 °C
Flow rate	1.0 mL/min

All instrumental variables were constant throughout HPLC analyses except for the analytical instrument, of which two were used throughout the study based on availability of the instruments. As the range of compounds metabolised from the primary substrate had a varying degree of polarity, a single experimental assay was not suitable for analyses of all compounds. Accordingly, several parameters were subject to variance to adjust the assay for detection of a different range of polarities. These parameters are summarised in Table 6.5.

Table 6.5: Specific HPLC conditions for sample analysis

Parameter	Experiment	Details
HPLC method	Esterase	Gradient
	UGT	Isocratic
	CYP	Isocratic
Mobile phase	Esterase	35% ACN (gradient to 55%), H_2O, 0.1% formic acid
	UGT	30% ACN, H_2O, 0.1% formic acid
	CYP	30% ACN, H_2O, 0.1% formic acid

6.2.5. Methodology for experimental incubation

6.2.5.1. Protein incubation procedure

A master-mix solution, consisting of buffer and protein solutions diluted to volume with water, was prepared by vortex mixing and was placed on ice to maintain activity of the protein enzymes. The contents of the test tubes are summarised in Table 6.6. If the experimental procedure called for a specific activation method for an enzyme family, relevant enzyme activation factors were also added to the master-mix, stirred well by vortex and allowed to stand on ice for 30-minutes prior to incubation. The substrate of investigation was then added to the master-mix solution, thoroughly stirred by vortex and then distributed to a number of ice-chilled test tubes. Incubations were performed in a volume of 200 μL unless otherwise specified.

Table 6.6: Contents of incubation experiment test tubes

Component	Variables	Concentration	Justification
Test compound	PAA PAAH	10 μM 2 μM	PAA was used for ester hydrolysis experiments. PAAH was used in other metabolism experiments
Buffer	KH_2PO_4	100 μM	Buffer used to maintain physiological conditions (pH 7.4)
Protein	HLM HLC Recombinants	1 mg/mL 1 mg/mL 1 mg/mL	Protein sources differ based on the experiment being performed
MilliQ H_2O	-	-	MilliQ water was added to make up volume in incubations
$MgCl_2$	-	40 mM	$MgCl_2$ was used in UGT experiments
Alamethicin	-	10 μg/mL	Alamethicin was used to remove the delay in onset of activity in UGT experiments
Enzyme co-factor	UDPGA NADPH PAPS	50 mM - 50 mM	Co-factors were used to initiate various metabolic pathways, UDPGA for UGT, NADPH for CYP and PAPS for SULT

The test tubes were then transferred to a tube rack and placed in the water bath instrument for a 5-minute pre-incubation to equilibrate to the new temperature conditions. Upon completion of the 5-minute pre-incubation, the incubation period was commenced and enzyme specific co-factors were added to the sample tubes, if called for by the experimental design. During the incubation period, tubes were removed in triplicate or quadruplicate, as specified, at prescribed time points over the course of the total period. Upon removal from

the water bath the enzyme reactions were terminated via the addition of 1:1 v/v 4% MeOH and AcOH, mixed well by vortex and then placed on ice to cool.

When the final tube had been transferred from the incubation instrument to ice and allowed to cool for 10 minutes, the tubes were then transferred to a Heraeus Sepatech Megafuge 1.0R centrifuge to separate the protein content from the substrate content of the tubes. After centrifugation (10 minutes, 4°C, 5,000 g), the supernatant fluid layer of each tube, containing the substrate and any resultant products that may have formed from incubation, were then aliquoted to a glass insert and placed in a suitable vial where they could then undergo HPLC analysis.

6.2.5.2. General incubation parameters

As the incubation procedure was consistent for all experiments, numerous experimental parameters were consistently used. The common parameters for all incubation methods performed are presented in Table 6.7.

Table 6.7: General parameters for experimental incubation of samples

Parameter	Value	Justification
Vortex instrument	Thermodyne Maxi Mix II (Type 37600 mixer)	Provides homogenisation in the preparation of samples
Incubation instrument	Ratek Instruments (Shaking Water Bath)	Provides temperature control and consistent mixing of samples
Centrifuge instrument	Heraeus Sepatech (Megafuge 1.0R)	Provides a means of separating proteins from substrates

6.2.5.3. Specific incubation parameters

As different experiments were performed to generate specific results, several parameters were the subject of variation to reflect the subject of investigation. Table 6.8 lists the parameters of variance and the specific values for different experiments:

Table 6.8: Specific parameters for experimental incubation of samples

Parameter	Experiment	Value	Justification
Incubation period	Esterase	120 minutes	Incubation period of 2 hours was increased to 2.5 hours for UGT and CYP experiments
	UGT	150 minutes	
	CYP	150 minutes	
Protein preparation	Esterase	None	Different enzyme families may require specific preparation methods for activation
	UGT	Alamethicin + $MgCl_2$	
	CYP	$MgCl_2$	
Enzyme co-factor	Esterase	H_2O	Different enzyme families require different co-factors to perform metabolic activities
	UGT	UDPGA (50 mM)	
	CYP	NADPH	

6.2.5.4. Preparation of NADPH generating system

The NADPH generating system used in all experiments was prepared fresh from its constituent materials before each experiment was carried out. The measurements given for each constituent of the NADPH generating system were multiplied by an appropriate factor depending on the number of experiments being carried out at a given time. The contents of each unit of NADPH generating system are recorded in Table 6.9.

Table 6.9: Contents of NADPH generating system per experiment

Constituent	Amount	Final concentration
MilliQ H_2O	46.5 µL	-
$MgCl_2$	1 µL	5 mM
G-6-P dehydrogenase	2.5 µL	2 IU
NADP	0.152 mg	1 mM
G-6-P	0.6 mg	10 mM
Total volume	50 mL	-

6.2.6. Specific enzyme studies

Screening of specific enzymes in the UGT and CYP families was performed in part by the use of specific enzyme inhibitors. A list of inhibitors used is provided in Table 6.10.

Table 6.10: List of enzyme inhibitors used in experiments.

Inhibited enzyme	Inhibitor	Concentration	Mechanism Based?	Solvent	Citation
UGT1A1	Niflumic acid	2.5 μM	Yes	DMSO	[174]
UGT1A4	Hecogenin	10 μM	Yes	Acetone + H_2O*	[328]
UGT1A9	Niflumic acid	100 μM	Yes	DMSO	[174]
UGT2B7	Fluconazole	2.5 mM	No	DMSO	[175]
CYP1A2	Furafylline	10 μM	Yes	MeOH	[329]
CYP2B6	Ticlopidine	3 μM	Yes	H_2O	[330]
CYP2C8	Montelukast	0.2 μM	Yes	MeOH	[331]
CYP2C9	Sulfaphenazole	2.5 μM	Yes	MeOH	[332]
CYP2C19	Ticlopidine	3 μM	No	H_2O	[330]
CYP2D6	Quinidine	1 μM	Yes	H_2O	[333]
CYP3A4	CYP3cide	1.5 μM	Yes	ACN + H_2O*	[168]

*Solvent systems for hecogenin and CYP3cide consist of 50:50 (v/v) solutions.

The incubation method for the inclusion of specific inhibitors followed the general incubation procedure but involved an additional step in the preparation of the master mix. For the given enzyme of interest, an appropriate inhibitor was added in the preparation of the master mix. For inhibitors with a mechanism based inhibition pathway, the master mix was given a 30-minute pre-incubation on ice to allow the inhibitor to appropriately bind to the enzyme and exert its inhibitory action. For inhibitors with a non-mechanism based inhibition pathway, no pre-incubation period was necessary and instead after addition of the inhibitor the master mix was vortexed, and the general method was followed as per Section 6.2.5.1.

6.2.7. Recombinant enzyme studies

Recombinant enzymes of most major drug metabolising enzymes were obtained from various sources for experimental use. In total, 7 CYP enzymes and 10 UGT enzymes were screened for activity. Recombinant enzyme lysates of CYP 1A2, 2B6, 2C8, 2C9, 3A4 and UGT 1A1, 1A3, 1A4, 1A6 and 1A9 were prepared by cDNA transfection of human embryonic kidney cells (HEK293) as described by Uchaipichat et al. [334]. Additional recombinant lysates of CYP 2C19 and 2D6 were acquired from the University of Queensland School of Chemistry and Molecular Biosciences (Brisbane, Australia) and were prepared from expression plasmid transformed *E. coli* as described by Parikh et al. [335]. Supersome lysates of UGT 2B4, 2B7, 2B8, 2B15 and 2B17 were commercially obtained from Corning Gentest (New York, USA).

The incubation method for recombinant enzymes broadly followed the general method described in Section 6.2.5.1 but involved some key changes. A protein solution of recombinant enzymes was used in place of human liver microsomes or cytosol as in other incubation experiments. As the recombinant enzymes were used in these experiments to establish activity rather than time dependent kinetics, measurements from only two time points (0 and 150 minutes) were taken.

6.2.8. Statistical analysis/data management

Data were collected and stored in spreadsheets using Microsoft Excel 15.0.4841.1000. Simple analysis of data including mean, standard deviation and slope determination were performed in Excel as well as the generation of graphs presented in the chapters. Further statistical analyses, including Mann-Whitney U test, ANOVA test and Dunnett's post hoc test were performed using IBM SPSS Statistics 22.0.0.0 [336].

6.2.9. Metabolite characterisation by hydrolysis

6.2.9.1. Hydrolysis by β-glucuronidase

Samples of PAAH were glucuronidated by the method described in Section 6.2.5 in the presence of UDPGA and alamethicin for 120 minutes, with the exception that reactions were not terminated by introduction of solvent (4% MeOH in AcOH), so as to not denature protein. After incubation, control tubes were terminated with solvent and to sample tubes 2000 IU of β-glucuronidase (type IX-A, *E. coli*) was introduced and allowed to incubate for a further 120 minute period. After this period samples were analysed by HPLC and UPLC/MS by the methods described in Sections 6.2.4 and 6.2.10, respectively.

6.2.9.2. Hydrolysis by weak base

Samples of PAAH were glucuronidated by the method described in Section 6.2.5 in the presence of UDPGA and alamethicin for 120 minutes, with the exception that reactions were not terminated by introduction of solvent (4% MeOH in AcOH), so as to not overly disrupt the pH of the solution. After incubation, control tubes were terminated with solvent and to sample tubes NaOH was introduced to a final concentration of 0.1 M and allowed to incubate for a further 120 minute period. After this period samples were analysed by HPLC and UPLC/MS by the methods described in Sections 6.2.4 and 6.2.10, respectively.

6.2.10. Sample analysis by UPLC/MS

UPLC/MS was used as a high powered method for glucuronide metabolite detection. Glucuronidated samples for UPLC/MS analysis were produced by HLM incubation of PAAH as previously described in Section 6.2.4. A component list for the UPLC/MS is included in Table 6.11 with specific variables pertaining to the UPLC and MS components of the system included in Table 6.12.

Table 6.11: Component list of UPLC/MS system

Parameter	Details
ULPC system	Waters Ultra Performance LC system
Solvent manager	Acquity binary solvent manager
Column housing	Acquity temperature controlled oven
Column	Acquity UPLC column (100 x 2.1 mm, 1.9 μm, HSS T3)
UV/Vis detector	Acquity TUV detector
Mass spectrometer	Waters Q-Tof Premier mass spectrometer

Table 6.12: Settings list for UPLC/MS analysis of samples

Component	Variables	Setting
UPLC	Detection wavelength	225 nm
	Column temperature	25 °C
	Flow rate	1.0 mL/min
MS	Capillary voltage	2.2 kV
	Sampling cone voltage	45 V
	Desolvation temperature	400 °C
	Desolvation gas flow	400 L/Hr
	Collision energy	10 V

6.3. Anti-inflammatory investigation of PAA and PAAH

6.3.1. Caspase-1 and NF-κB assays

To determine if PAA had inhibitory effects on caspase-1, effects on pro-IL-1β and IL-1β were examined. To examine the effect of PAA on intracellular levels of pro-IL-1β and IL-1β, an *in vitro* cell-based assay was carried out by Dr Brad Simpson (Research fellow, University of South Australia) using a human monocytic cell line (THP-1 cells). The assay consisted of preincubation of THP-1 cells in a 96-well microtitre plate (1×10^5 cells/50 μL/well) with 50 μL/well of PAA or Bay-11-7082 (in RPMI-1640 medium at varying concentrations) for a period of 1 hour. Inflammation was then instigated by stimulation with 100 μL/well of TPA (40 ng/mL) and the plate was incubated at 37 °C for 24 hours in an atmosphere of 5% CO_2 in air. After incubation, the supernatant was separated and cells were then washed twice with 200 μL of ice chilled phosphate buffered saline (PBS). Cells were then lysed with ice chilled RIPA buffer containing protease inhibitor cocktail and incubated on ice for 5 minutes. Lysate samples were then centrifuged for 10 minutes at 13,800 g at a temperature of 4°C and analysed using an ELISA kit (eBioscience platinum ELISA kit, BMS6002). Statistical significance of results was determined by one-way ANOVA followed by Dunnett's post hoc test with $*p < 0.05$ considered significant [14].

To determine if PAA had inhibitory effects on NF-κB, effects on nitric oxide production were examined via the screening of nitrite. Nitrite production can be used as a determinant of NF-κB function as NF-κB modulates the production of iNOS, and hence nitric oxide production. To determine the effect of PAA on nitrite production, an *in vitro* cell-based assay was carried out by Dr Brad Simpson using RAW 264.7 cells. The assay consisted of preincubating RAW 264.7 cells in a 96-well microtitre plate (1×10^5 cells/50 μL/well) with 50 μL/well PAA or Bay-11-7082 (positive control, in Dulbecco's Modified Eagle's Medium, DMEM) for a period of 1 hour. Inflammation was then stimulated via addition of 100 μL/well LPS (1 μg/mL) and the plate was incubated for 24 hours at 37 °C in an atmosphere of 5% CO_2 in air. Nitrite was detected by the Griess assay which involved removing the supernatant from incubated cells and adding 50 μL/well of 1% (w/v) sulfanilic acid (in 5% HCl) followed by 50 μL/well of 0.1% (w/v) N-napthylethylenediamine dihydrochloride (in 5% HCl). Samples were incubated for 10 minutes at 37°C and then

absorbance was measured using a plate reader (at 540 nm). Statistical significance of results was determined by one-way ANOVA followed by Dunnett's post hoc test with *$p < 0.05$ considered significant [14].

6.3.2. Protein kinase testing

In vitro testing of protein kinase inhibition was performed by a Life Technologies SelectScreen Biochemical Kinase Profiling Services assay. Screening of protein kinases was performed on PKCα (alpha), PKCβI (beta I), PKCβII (beta II), PKCδ (delta), PKCϵ (epsilon), PKCγ (gamma), PKCη (eta), PKCι (iota), PKν (nu), PKCθ (theta), PKCζ (zeta), PKCμ (mu) by phosphorylation inhibition of a given kinase receptor by PAA against staurosporine as a pan kinase inhibitor. In brief, the assay protocol involved combining a kinase receptor with a test inhibitor (PAA, 10 μM) in appropriate buffer and an ATP solution as co-factor to the kinase, followed by 60 minute incubation at room temperature, development by a reagent solution, further 60 minute incubation at room temperature and quantification on a fluorescence plate reader. Assay reliability was determined by Z' factor with $Z' < 0.50$ considered reliable.

6.3.3. Glucocorticoid receptor testing

In vitro testing for glucocorticoid receptor agonist activity was initially performed in-house using a purchased Life Technologies PolarScreen GR Competitor Assay, Green. Screening of GR was performed by binding inhibition of GR to a fluormone tracer (Fluormone GS1) by PAA against betamethasone as a typical GR binding ligand. In brief, the assay protocol involved combining GR protein with a stabilising agent and screening compound (PAA or PAAH) in an appropriate buffer, followed by 120 minute incubation at room temperature in the dark and subsequent quantification on a fluorescence polarisation plate reader (Victor X5 2030) courtesy of Professor Grant Booker and Dr Steven Polyak of the School of Biological Sciences (University of Adelaide). The plate reader was determined to lack sensitivity for the assay and without a suitable alternative plate reader, the assay was therefore outsourced.

Glucocorticoid receptor testing was subsequently performed by Life Technologies utilising a LanthaScreen time-resolved fluorescence resonance energy transfer (TR-FRET) assay. The LanthaScreen assay follows a similar principle of competitive binding to the PolarScreen assay, but uses a terbium-labelled anti-GST antibody to bind to the receptor and initiate fluorescence in complement with the tracer ligand. The preparation briefly described for the PolarScreen also applies to the LanthaScreen assay with the adjustment of the incorporation of a Tb-anti-GST antibody to the receptor solution. Both PAA and PAAH were submitted for screening at a concentration range starting from 10 μM and diluted in stepwise dilutions to a concentration of 0.51 nM as shown in Table 6.13.

Table 6.13: Stepwise dilution scheme of PAA and PAAH for glucocorticoid testing.

Dilution number	1	2	3	4	5	6	7	8	9	10
Concentration (nM)	10,000	3,333	1,111	370.4	123.5	41.15	13.72	4.572	1.524	0.508

6.4. Opioid investigation of PAB and its methyl ester derivative MPB

6.4.1. Synthesis of MPB by thionyl chloride reflux

To a pear-shaped flask, 4.73 mg polyandric acid B (PAB) was dissolved in 10 mL methanol observing anhydrous technique. To the flask 150 μL thionyl chloride was then transferred and sealed under N_2 gas. Light exposure was minimised by wrapping the reaction vessel in aluminium foil. The solution was refluxed for a period of 24 hours on an Asynt ADS-HP-S-NT hotplate stirrer (500 rpm, 90 °C). The endpoint of the reaction was determined using TLC by comparing the retention factor of the starting material to the reaction product and reaction was ceased when no more starting material was visible by TLC. The product was then analysed for approximate mass (*m/z* 329.20) by an ABSCIEX TripleTOF 5600 LC/MS/MS system.

6.4.2. Synthesis of MPB by methyl iodide reflux

To a solution of PAB (2.49 mg, 5.708 mM) in dimethyl formamide (DMF, 5 mL) was added methyl iodide (MeI, 1 μL, 16.06 mM). The reaction mixture was stirred at room temperature for 24 hours under N_2 gas. Light exposure was minimised by wrapping the reaction vessel in aluminium foil. The solution was refluxed for a period of 24 hours on an Asynt ADS-HP-S-NT hotplate stirrer (500 rpm, 25 °C). The endpoint of the reaction was determined using TLC by comparing the retention factor of the starting material to the reaction product and the reaction was ceased when no more starting material was visible by TLC. The reaction was then quenched by addition of water and sodium carbonate. The product was then analysed for approximate mass (*m/z* 473.55) by an ABSCIEX TripleTOF 5600 LC/MS/MS system. Product was then purified by organic extraction with petroleum ether and water and organic solvent was removed by rotary evaporator to yield a colourless, amorphous solid (2.52 mg, 98.2% yield). Purified product was then analysed with an Avance III 500 MHz NMR by ^{1}H NMR, ^{13}C NMR, HSQC and HMBC experiments.

6.4.3. MPB screening against μ-opioid receptor

Dry methyl polyandrate B (MPB 3.19 mg) was submitted for screening in a μ-opioid assay. Screening was performed by Ricerca Biosciences using cell based assays. The opioid assay was performed using Chinese Hamster Ovary (CHO-K1) cells expressing the μ-opioid receptor (MOR1) and tested against [^{3}H] DAMGO, a μ-opioid specific peptide agonist, as a positive control. Special requests were made to limit water and light exposure to prevent potential breakdown of the compound from hydrolysis and photolysis. In brief, the assay protocol consisted of incubating the test compound (MPB) for a period of 2 hours at three concentrations (0.1, 1 and 10 μM) with homogenised CHO-K1 cells (homogenised in duplicate). Assays took place in 50 mM Tris-HCl (pH 7.4) with a protease inhibitor cocktail consisting of bacitracin (100 μg/mL), bestatin (10 μg/mL), leupeptin (4 μg/mL) and chymostatin (2 μg/mL).

6.5. *In silico* methods

6.5.1. 3D-structure generation

3D-structures of molecules were generated by Omega 2.5.1.4 (OpenEye Scientific Software [132]). To accomplish this 1D-structures of molecules (stored as SMILES strings) were submitted to the Omega module using the default settings as listed in Table 6.14.

Table 6.14: Default variables used in Omega for conformer generation.

Flag	Default value	Explanation
strictstereo	True	Restricts conformer generation to the specified stereochemistry of a given SMILES string
maxconfs	200	Maximum number of conformers of each structure to be generated
buildff	mmff94s_NoEstat	Specifies the force field used to construct a conformational library
ewindow	10.0	Specifies the energy window in kcal/mol allowable for conformer generation
rms	0.5	Specifies the minimum Root Mean Square (RMS) Cartesian distance between any two conformers

6.5.2. Webserver screening

Analysis of compounds using webservers was performed by the standard methods of the webservers. Compounds to be analysed were input either by the use of SMILES strings, retaining stereochemical information (if supported by the webserver), or by structural generation using a server based applet. A list of webservers used in the study are included in Table 6.15.

Table 6.15: List of webservers used for molecular modelling purposes.

Webserver	Purpose	Features	Citation
ZINC	Structure similarity searching	>35 million compounds Vendor links to compounds	[276]
SEA	Structure similarity searching	Linked to ChEMBL, MDL DDR, WOMBAT, KEGG ENZYME sets and Starlite	[278]
MetaPred	Site of metabolism prediction	CYP and UGT prediction Specific CYP enzyme prediction	[187]
XenoSite	Site of metabolism prediction	CYP and UGT prediction Specific CYP enzyme and total HLM prediction Epoxidation prediction	[186, 337, 338]
Target Hunter	Structure similarity searching	Linked to ChEMBL ~2 million compounds ~14 million bioactivity entries	[339]

6.5.3. FILTER screening

Screening by FILTER 2.5.1.4 was performed using a set of rules defined by Mr Steven Nguyen [173] to screen three UGT isoforms as potential metabolising enzymes of PAAH. The filtration parameters are listed below along with brief descriptions of the rules. The rules were defined with respect to isoform selectivity by retrospective analysis of a training set of UGT substrates and then screened against a test set of UGT substrates to assess performance of the rules.

UGT1A1

```
MIN_HBOND_DONORS 1
MAX_HBOND_DONORS 6

MIN_XLOGP -0.8
MAX_XLOGP 3.7

SELECT 1A1 1 5 [$(c[OH]]),$(NcnC),$([CX3](=O)[OX2H1,OX1H0-])]
```

The rules for UGT1A1 filtration encompass three areas: number of hydrogen bond donors, logP values and definition of specific structural features by SMARTS strings.

UGT1A4

```
MIN_MOLWT 90
MAX_MOLWT 465

SELECT 1A4 1 5 [$([NX3;H0]),$([NX3;H1]),$([NX3;H2]),([NX4;H1+]),
$([OH]C1CCCCC1),$([OH]C1CCCC1),$([OH]C)]

NEWRULE Hydroxyl 1 [OH]
NEWRULE flavone 0 c1:c:o:c:c:c1
RULE 0 carboxylic acid
RULE 1 phenol
RULE 0 cyclopropyl
NEWRULE Opioid 0 C1CC(O)C=CC1
```

The rules for UGT1A4 filtration encompass three areas: molecular weight, definition of specific structural features by SMARTS strings and binary designation of structural features inbuilt to FILTER.

UGT2B7

```
MIN_MOLWT 155
MAX_MOLWT 500

MIN_CHIRAL_CENTERS 0
MAX_CHIRAL_CENTERS 10

SELECT 2B7 1 3 [$([CX3](=O)[OX2H1,OX1H0-
]),$([OH]C1~C~C~C~C~C1),$(c[OH]),$([OH]C1OCCC1),$(C=CC[OH]),$(Clc1ccc([NH])cc1),$(C1OC(C[
OH])CC1)]

RULE 1 phenol
NEWRULE flavone 0 c1:c:o:c:c:c1
```

The rules for UGT1A4 filtration encompass four areas: molecular weight, number of chiral centres, definition of specific structural features by SMARTS strings and binary designation of structural features inbuilt to FILTER.

6.5.4. Docking methods

Docking was used to explore potential enzyme-ligand interactions. To accomplish this crystal structures of enzymes and receptors were obtained from the RCSB Protein Data Bank and processed using Make Receptor 3.0.1, 3D structures of molecules were defined by Omega 2.5.1.4 and docking was performed with OEDocking 3.0.1 using the FRED module. Customisation of software properties was minimised by using default settings of software where possible as displayed in Table 6.16 and Table 6.17. The only user manipulation in the docking process was in the designation of the receptor site by Make Receptor 3.0.1, where an active site was user defined as the area around a bound ligand in the crystallised enzyme. Results were ranked by the default Chemgauss4 scoring system.

Table 6.16: List of generic variables for Make Receptor active site generation

Variable	Value	Description
Input file type	.pdb	Standard file format for protein structures
Box size	Default	Automatically defined around ligand, or area defined by molecular cavity
Site size	Balanced	Can be extended towards either solvent or protein
Constraints	Default	Not used unless defined in chapters

Table 6.17: List of generic variables for OEDocking screening

Variable	Value	Description
Input file type	.mol2 or .sdf (queries) .oeb (protein)	Either type of query file .oeb
Docking module	FRED or Hybrid	Different modules are used depending on structural similarity between the molecule being docked and a co-crystallised ligand. Hybrid = TanimotoCombo >1.000 FRED = TanimotoCombo <1.000

6.5.5. Overlay analysis

Overlay analysis was used to investigate structural similarities between molecules. To accomplish this, 3D structures of molecules were defined by Omega 2.5.1.4 and overlay analysis was performed with vROCS 3.2.0.4. Customisation of software properties was negated by using default settings of the software. Results were ranked by the default TanimotoCombo scoring system and component scores of ShapeTanimoto and ColorTanimoto were retained for analysis. A list of generic values used for vROCS analysis is included in Table 6.18. Any altered variables are described in their respective chapters.

Table 6.18: List of generic variables for vROCS analysis.

Variable	Value	Description
Input file type	.mol2 or .sdf	File type does not matter greatly for these experiments
Query used	Lowest energy	Multiple conformers of a query (or multiple queries) can be used for ROCS screening, a single "lowest" energy conformer was used.
Color force field	Implicit Mills Dean	Measure of chemical similarity between query and data base molecule
Rank by	TanimotoCombo	Scoring function as aggregate of both shape and color scores
Random starts	50	Number of times molecules are overlaid to ensure overlay is of the highest quality possible

References

1. Bendikov, M.Y., J.O. Miners, B.S. Simpson, D.J. Elliot, S.J. Semple, D.J. Claudie, R.A. McKinnon, E.M.J. Gillam, and M.J. Sykes, *In vitro metabolism of the anti-inflammatory clerodane diterpenoid polyandric acid A and its hydrolysis product by human liver microsomes and recombinant cytochrome P450 and UDP-glucuronosyltransferase enzymes.* Xenobiotica, 2017. **47**(6): p. 461-469.
2. Bendikov, M., *In silico directed investigation of novel diterpenoid compounds isolated from Dodonaea polyandra*, in *Sansom Institute for Health Research*. 2011, University of South Australia: Adelaide.
3. Brownstein, M.J., *A brief history of opiates, opioid peptides, and opioid receptors.* Proc Natl Acad Sci USA, 1993. **90**(12): p. 5391-5393.
4. Krikorian, A.D., *Were the opium poppy and opium known in the ancient near east?* J Hist Biol, 1975. **8**(1): p. 95-114.
5. van Middendorp, J.J., G.M. Sanchez, and A.L. Burridge, *The Edwin Smith papyrus: a clinical reappraisal of the oldest known document on spinal injuries.* Eur Spine J, 2010. **19**(11): p. 1815-1823.
6. Newman, D.J. and G.M. Cragg, *Natural products as sources of new drugs over the 30 years from 1981 to 2010.* J Nat Prod, 2012. **75**(3): p. 311-335.
7. Newman, D.J. and G.M. Cragg, *Natural products as sources of new drugs from 1981 to 2014.* J Nat Prod, 2016. **79**(3): p. 629-661.
8. Harvey, A.L., *Natural products in drug discovery.* Drug Discov Today, 2008. **13**(19–20): p. 894-901.
9. Koehn, F.E. and G.T. Carter, *The evolving role of natural products in drug discovery.* Nat Rev Drug Discov, 2005. **4**(3): p. 206-220.
10. Barr, A., C.J. Smith, G. Wightman, T. Knight, L. Mills, M. Andrews, and V. Alexander, *Traditional Aboriginal medicines in the Northern Territory of Australia / by Aboriginal communities of the Northern Territory*, in *Conservation Commission of the Northern Territory*. 1993: Darwin.
11. Simpson, B.S., D.J. Claudie, N.M. Smith, J. Wang, R.A. McKinnon, and S.J. Semple, *Evaluation of the anti-inflammatory properties of Dodonaea polyandra, a Kaanju traditional medicine.* J Ethnopharmacol, 2010. **132**(1): p. 340-343.

12. Simpson, B.S., D.J. Claudie, J.P. Gerber, S.M. Pyke, J. Wang, R.A. McKinnon, and S.J. Semple, *In vivo activity of benzoyl ester clerodane diterpenoid derivatives from Dodonaea polyandra.* J Nat Prod, 2011. **74**(4): p. 650-657.
13. Tokoroyama, T., *Synthesis of clerodane diterpenoids and related compounds - stereoselective construction of the decalin skeleton with multiple contiguous stereogenic centers.* Synthesis, 2000. **5**: p. 611-633.
14. Simpson, B.S., X. Luo, M. Costabile, G.E. Caughey, J. Wang, D.J. Claudie, R.A. McKinnon, and S.J. Semple, *Polyandric acid A, a clerodane diterpenoid from the Australian medicinal plant Dodonaea polyandra, attenuates pro-inflammatory cytokine secretion in vitro and in vivo.* J Nat Prod, 2014. **77**(1): p. 85-91.
15. Simpson, B.S., *Chemical and pharmacological investigation of Dodonaea polyandra*, in *Sansom Institute for Health Research*. 2011, University of South Australia: Adelaide.
16. Ciaccia, L., *Fundamentals of inflammation.* Yale J Biol Med, 2011. **84**(1): p. 64-65.
17. Kuehl, F. and R. Egan, *Prostaglandins, arachidonic acid, and inflammation.* Science, 1980. **210**(4473): p. 978-984.
18. Ricciotti, E. and G.A. FitzGerald, *Prostaglandins and inflammation.* Arterioscl Throm Vas, 2011. **31**(5): p. 986-1000.
19. Medzhitov, R., *Origin and physiological roles of inflammation.* Nature, 2008. **454**(7203): p. 428-435.
20. Stables, M.J. and D.W. Gilroy, *Old and new generation lipid mediators in acute inflammation and resolution.* Prog Lipid Res, 2011. **50**(1): p. 35-51.
21. Hawkey, C.J., *COX-2 inhibitors.* Lancet, 1999. **353**(9149): p. 307-314.
22. Hawkey, C.J., *COX-1 and COX-2 inhibitors.* Best Pract Res Clin Gastroenterol, 2001. **15**(5): p. 801-820.
23. Murakami, M. and T. Hirano, *The molecular mechanisms of chronic inflammation development.* Front Immunol, 2012. **3**: p. 323.
24. Dantzer, R., J.C. O'Connor, G.G. Freund, R.W. Johnson, and K.W. Kelley, *From inflammation to sickness and depression: when the immune system subjugates the brain.* Nat Rev Neurosci, 2008. **9**(1): p. 46-56.
25. Bultink, I.E.M., M. Vis, I.E. van der Horst-Bruinsma, and W.F. Lems, *Inflammatory rheumatic disorders and bone.* Curr Rheumatol Rep, 2012. **14**(3): p. 224-230.

26. Choy , E.H.S. and G.S. Panayi *Cytokine pathways and joint inflammation in rheumatoid arthritis.* N Engl J Med, 2001. **344**(12): p. 907-916.
27. Barnes, P.J., *How corticosteroids control inflammation: Quintiles Prize Lecture 2005.* Brit J Pharmacol, 2006. **148**(3): p. 245-254.
28. Cavaillon, J.M. and M. Adib-Conquy, *The pro-inflammatory cytokine cascade*, in *Immune response in the critically ill*, J.C. Marshall and J. Cohen, Editors. 2002, Springer Berlin Heidelberg: Berlin, Heidelberg. p. 37-66.
29. Dunster, J.L., *The macrophage and its role in inflammation and tissue repair: mathematical and systems biology approaches.* Rev Syst Biol Med, 2016. **8**(1): p. 87-99.
30. Khanapure, S.P., D.S. Garvey, D.R. Janero, and L.G. Letts, *Eicosanoids in inflammation: biosynthesis, pharmacology, and therapeutic frontiers.* Curr Top Med Chem, 2007. **7**(3): p. 311-340.
31. Park, J.Y., M.H. Pillinger, and S.B. Abramson, *Prostaglandin E2 synthesis and secretion: The role of PGE2 synthases.* Cl Immunol, 2006. **119**(3): p. 229-240.
32. Michelassi, F., L. Landa, R.D. Hill, E. Lowenstein, W.D. Watkins, A.J. Petkau, and W.M. Zapol, *Leukotriene D4: A potent coronary artery vasoconstrictor associated with impaired ventricular contraction.* Science, 1982. **217**(4562): p. 841-843.
33. Kawahara, K., H. Hohjoh, T. Inazumi, S. Tsuchiya, and Y. Sugimoto, *Prostaglandin E2-induced inflammation: Relevance of prostaglandin E receptors.* BBA-Mol Cell Biol L, 2015. **1851**(4): p. 414-421.
34. Asboth, G., S. Phaneuf, G.N. Europe-Finner, M. Toth, and A.L. Bernal, *Prostaglandin E2 activates phospholipase C and elevates intracellular calcium in cultured myometrial cells: involvement of EP1 and EP3 receptor subtypes.* Endocrinology, 1996. **137**(6): p. 2572-2579.
35. Choung, J., L. Taylor, K. Thomas, X. Zhou, H. Kagan, X. Yang, and P. Polgar, *Role of EP2 receptors and cAMP in prostaglandin E2 regulated expression of type I collagen alpha1, lysyl oxidase, and cyclooxygenase-1 genes in human embryo lung fibroblasts.* J Cell Biochem, 1998. **71**(2): p. 254-263.
36. Dey, I., M. Lejeune, and K. Chadee, *Prostaglandin E2 receptor distribution and function in the gastrointestinal tract.* Brit J Pharmacol, 2006. **149**(6): p. 611-623.
37. Zarghi, A. and S. Arfaei, *Selective COX-2 Inhibitors: A Review of Their Structure-Activity Relationships.* Iran J Pharma Res, 2011. **10**(4): p. 655-683.

38. Cashman, J.N., *The mechanisms of action of NSAIDs in analgesia.* Drugs, 1996. **52**(5): p. 13-23.
39. Wallace, J.L., *How do NSAIDs cause ulcer disease?* Best Pract Res Clin Gastroenterol, 2000. **14**(1): p. 147-59.
40. Dickman, A. and J. Ellershaw, *NSAIDs: Gastroprotection or selective COX-2 inhibitor?* Palliat Med, 2004. **18**(4): p. 275-286.
41. Murakami, M. and I. Kudo, *Prostaglandin E synthase: a novel drug target for inflammation and cancer.* Curr Pharm Des, 2006. **12**(8): p. 943-954.
42. Burke, J.E. and E.A. Dennis, *Phospholipase A2 structure/function, mechanism, and signaling.* J Lipid Res, 2009. **50**: p. 237-242.
43. Chen, Y., H. Liu, S. Xu, T. Wang, and W. Li, *Targeting microsomal prostaglandin E2 synthase-1 (mPGES-1): The development of inhibitors as an alternative to non-steroidal anti-inflammatory drugs (NSAIDs).* MedChemComm, 2015. **6**(12): p. 2081-2123.
44. Mukherjee, A.K., R. Doley, and D. Saikia, *Isolation of a snake venom phospholipase A2 (PLA2) inhibitor (AIPLAI) from leaves of Azadirachta indica (Neem): Mechanism of PLA2 inhibition by AIPLAI in vitro condition.* Toxicon, 2008. **51**(8): p. 1548-1553.
45. Meyer, M.C., P. Rastogi, C.S. Beckett, and J. McHowat, *Phospholipase A2 inhibitors as potential anti-inflammatory agents.* Curr Pharm Des, 2005. **11**(10): p. 1301-1312.
46. Carlson, N.G., W.A. Wieggel, J. Chen, A. Bacchi, S.W. Rogers, and L.C. Gahring, *Inflammatory cytokines IL-1α, IL-1β, IL-6, and TNFα impart neuroprotection to an excitotoxin through distinct pathways.* J Immunol, 1999. **163**(7): p. 3963-3968.
47. Turner, M.D., B. Nedjai, T. Hurst, and D.J. Pennington, *Cytokines and chemokines: At the crossroads of cell signalling and inflammatory disease.* BBA-Mol Cell Res, 2014. **1843**(11): p. 2563-2582.
48. Sollberger, G., G.E. Strittmatter, M. Garstkiewicz, J. Sand, and H.D. Beer, *Caspase-1: The inflammasome and beyond.* Innate Immun, 2014. **20**(2): p. 115-125.
49. Miao, E.A., J.V. Rajan, and A. Aderem, *Caspase-1-induced pyroptotic cell death.* Immunol Rev, 2011. **243**(1): p. 206-214.
50. Tsuzaki, M., G. Guyton, W. Garrett, J.M. Archambault, W. Herzog, L. Almekinders, D. Bynum, X. Yang, and A.J. Banes, *IL-1 beta induces COX2, MMP-1, -3 and -13, ADAMTS-4, IL-1β and IL-6 in human tendon cells.* J Orthop Res, 2003. **21**(2): p. 256-264.

51. Lim, J.W., H. Kim, and K.H. Kim, *Nuclear factor-κB regulates cyclooxygenase-2 expression and cell proliferation in human gastric cancer cells.* Lab Invest, 2001. **81**(3): p. 349-360.
52. Gupta, S.C., C. Sundaram, S. Reuter, and B.B. Aggarwal, *Inhibiting NF-κB activation by small molecules as a therapeutic strategy.* Biochim Biophys Acta, 2010. **1799**(10-12): p. 775-787.
53. Popa, C., M.G. Netea, P.L. van Riel, J.W. van der Meer, and A.F. Stalenhoef, *The role of TNFα in chronic inflammatory conditions, intermediary metabolism, and cardiovascular risk.* J Lipid Res, 2007. **48**(4): p. 751-62.
54. Masli, S. and B. Turpie, *Anti-inflammatory effects of tumour necrosis factor TNFα are mediated via TNF-R2 (p75) in tolerogenic transforming growth factor-beta-treated antigen-presenting cells.* Immunology, 2009. **127**(1): p. 62-72.
55. Kim, H., R. Zamel, X.H. Bai, and M. Liu, *PKC activation induces inflammatory response and cell death in human bronchial epithelial cells.* PLoS ONE, 2013. **8**(5): p. e64182.
56. Passos, G.F., R. Medeiros, R. Marcon, A.F.Z. Nascimento, J.B. Calixto, and L.F. Pianowski, *The role of PKC/ERK1/2 signaling in the anti-inflammatory effect of tetracyclic triterpene euphol on TPA-induced skin inflammation in mice.* Eur J Pharmacol, 2013. **698**(1–3): p. 413-420.
57. Chen, C., C. Chou, Y. Sun, and W. Huang, *Tumor necrosis factor alpha-induced activation of downstream NF-κB site of the promoter mediates epithelial ICAM-1 expression and monocyte adhesion. Involvement of PKCα, tyrosine kinase, and IKK2, but not MAPKs, pathway.* Cell Signal, 2001. **13**(8): p. 543-553.
58. Gabay, C., *Interleukin-6 and chronic inflammation.* Arthritis Res Ther, 2006. **8**(2): p. 3.
59. Scheller, J., A. Chalaris, D. Schmidt-Arras, and S. Rose-John, *The pro- and anti-inflammatory properties of the cytokine interleukin-6.* BBA-Mol Cell Res, 2011. **1813**(5): p. 878-888.
60. Hodge, D.R., E.M. Hurt, and W.L. Farrar, *The role of IL-6 and STAT3 in inflammation and cancer.* Eur J Cancer, 2005. **41**(16): p. 2502-2512.
61. Kaplan, M.H., *STAT signaling in inflammation.* JAK-STAT, 2013. **2**(1): p. e24198.
62. Korn, T., E. Bettelli, M. Oukka, and V.K. Kuchroo, *IL-17 and Th17 Cells.* Annu Rev Immunol, 2009. **27**: p. 485-517.

63. Wang, Y., A.H.H. van Boxel-Dezaire, H. Cheon, J. Yang, and G.R. Stark, *STAT3 activation in response to IL-6 is prolonged by the binding of IL-6 receptor to EGF receptor.* Proc Nat Acad Sci USA, 2013. **110**(42): p. 16975-16980.
64. Arias-Salvatierra, D., E.K. Silbergeld, L.C. Acosta-Saavedra, and E.S. Calderon-Aranda, *Role of nitric oxide produced by iNOS through NF-κB pathway in migration of cerebellar granule neurons induced by lipopolysaccharide.* Cell Signal, 2011. **23**(2): p. 425-435.
65. Sharma, J.N., A. Al-Omran, and S.S. Parvathy, *Role of nitric oxide in inflammatory diseases.* Inflammopharmacology, 2007. **15**(6): p. 252-259.
66. Coleman, J.W., *Nitric oxide in immunity and inflammation.* Int Immunopharmacol, 2001. **1**(8): p. 1397-1406.
67. Schindler, H. and C. Bogdan, *NO as a signaling molecule: Effects on kinases.* Int Immunopharmacol, 2001. **1**(8): p. 1443-1455.
68. Salvemini, D., T.P. Misko, J.L. Masferrer, K. Seibert, M.G. Currie, and P. Needleman, *Nitric oxide activates cyclooxygenase enzymes.* Proc Nat Acad Sci USA, 1993. **90**(15): p. 7240-7244.
69. Kadmiel, M. and J.A. Cidlowski, *Glucocorticoid receptor signaling in health and disease.* Trends Pharmacol Sci, 2013. **34**(9): p. 518-530.
70. Barnes, P.J., *Anti-inflammatory actions of glucocorticoids: Molecular mechanisms.* Clin Sci, 1998. **94**(6): p. 557-572.
71. Ishida-Takahashi, R., S. Uotani, T. Abe, M. Degawa-Yamauchi, T. Fukushima, N. Fujita, H. Sakamaki, H. Yamasaki, Y. Yamaguchi, and K. Eguchi, *Rapid inhibition of leptin signaling by glucocorticoids in vitro and in vivo.* J Biol Chem, 2004. **279**(19): p. 19658-19664.
72. Basbaum, A.I., D.M. Bautista, G. Scherrer, and D. Julius, *Cellular and molecular mechanisms of pain.* Cell, 2009. **139**(2): p. 267-284.
73. Zamponi, G.W., R.J. Lewis, S.M. Todorovic, S.P. Arneric, and T.P. Snutch, *Role of voltage-gated calcium channels in ascending pain pathways.* Brain Res Rev, 2009. **60**(1): p. 84-89.
74. Liou, J.T., F.C. Liu, S.T. Hsin, C.Y. Yang, and P.W. Lui, *Inhibition of the cyclic adenosine monophosphate pathway attenuates neuropathic pain and reduces phosphorylation of cyclic adenosine monophosphate response element-binding in the*

spinal cord after partial sciatic nerve ligation in rats. Anesth Analg, 2007. **105**(6): p. 1830-1837.

75. Leenders, A.G.M. and Z.H. Sheng, *Modulation of neurotransmitter release by the second messenger-activated protein kinases: Implications for presynaptic plasticity.* Pharmacol Therapeut, 2005. **105**(1): p. 69-84.
76. Ong, C.K.S., P. Lirk, C.H. Tan, and R.A. Seymour, *An evidence-based update on nonsteroidal anti-inflammatory drugs.* J Clin Med Res, 2007. **5**(1): p. 19-34.
77. Botting, R.M., *Mechanism of action of acetaminophen: Is there a cyclooxygenase 3?* Clin Infect Dis, 2000. **31**(5): p. 202-210.
78. Hinz, B., O. Cheremina, and K. Brune, *Acetaminophen (paracetamol) is a selective cyclooxygenase-2 inhibitor in man.* FASEB J, 2008. **22**(2): p. 383-390.
79. Costa, B., D. Siniscalco, A.E. Trovato, F. Comelli, M.L. Sotgiu, M. Colleoni, S. Maione, F. Rossi, and G. Giagnoni, *AM404, an inhibitor of anandamide uptake, prevents pain behaviour and modulates cytokine and apoptotic pathways in a rat model of neuropathic pain.* Brit J Pharmacol, 2006. **148**(7): p. 1022-1032.
80. Högestätt, E.D., B.A.G. Jönsson, A. Ermund, D.A. Andersson, H. Björk, J.P. Alexander, B.F. Cravatt, A.I. Basbaum, and P.M. Zygmunt, *Conversion of acetaminophen to the bioactive N-acylphenolamine AM404 via fatty acid amide hydrolase-dependent arachidonic acid conjugation in the nervous system.* J Biol Chem, 2005. **280**(36): p. 31405-31412.
81. Brownstein, M.J., *A brief history of opiates, opioid peptides, and opioid receptors.* Proc Nat Acad Sci USA, 1993. **90**(12): p. 5391-5393.
82. Dennis, B.B., M. Bawor, J. Paul, C. Plater, G. Pare, A. Worster, M. Varenbut, J. Daiter, D.C. Marsh, D. Desai, L. Thabane, and Z. Samaan, *Pain and opioid addiction: A systematic review and evaluation of pain measurement in patients with opioid dependence on methadone maintenance treatment.* Curr Drug Abuse Rev, 2016. **9**(1): p. 49-60.
83. Peng, J., S. Sarkar, and S.L. Chang, *Opioid receptor expression in human brain and peripheral tissues using absolute quantitative real-time RT-PCR.* Drug Alcohol Depen, 2012. **124**(3): p. 223-228.
84. Lambert, D.G., *The nociceptin/orphanin FQ receptor: a target with broad therapeutic potential.* Nat Rev Drug Discov, 2008. **7**(8): p. 694-710.

85. Al-Hasani, R. and M.R. Bruchas, *Molecular mechanisms of opioid receptor-dependent signaling and behavior.* Anesthesiology, 2011. **115**(6): p. 1363-1381.
86. Saitoh, A. and M. Yamada, *Antidepressant-like effects of δ-opioid receptor agonists in animal models.* Curr Neuropharmacol, 2012. **10**(3): p. 231-238.
87. Chavkin, C., *The therapeutic potential of κ-opioids for treatment of pain and addiction.* Neuropsychopharmacology, 2011. **36**(1): p. 369-370.
88. Pogozheva, I.D., M.J. Przydzial, and H.I. Mosberg, *Homology modeling of opioid receptor-ligand complexes using experimental constraints.* AAPS J, 2005. **7**(2): p. 434-448.
89. Mansour, A., L.P. Taylor, J.L. Fine, R.C. Thompson, M.T. Hoversten, H.I. Mosberg, S.J. Watson, and H. Akil, *Key residues defining the μ-opioid receptor binding pocket: A site-directed mutagenesis study.* J Neurochem, 1997. **68**(1): p. 344-353.
90. Pogozheva, I.D., A.L. Lomize, and H.I. Mosberg, *Opioid receptor three-dimensional structures from distance geometry calculations with hydrogen bonding constraints.* Biophys J, 1998. **75**(2): p. 612-634.
91. Manglik, A., A.C. Kruse, T.S. Kobilka, F.S. Thian, J.M. Mathiesen, R.K. Sunahara, L. Pardo, W.I. Weis, B.K. Kobilka, and S. Granier, *Crystal structure of the μ-opioid receptor bound to a morphinan antagonist.* Nature, 2012. **485**(7398): p. 321-326.
92. Wu, H., D. Wacker, M. Mileni, V. Katritch, G.W. Han, E. Vardy, W. Liu, A.A. Thompson, X.-P. Huang, F.I. Carroll, S.W. Mascarella, R.B. Westkaemper, P.D. Mosier, B.L. Roth, V. Cherezov, and R.C. Stevens, *Structure of the human [kgr]-opioid receptor in complex with JDTic.* Nature, 2012. **485**(7398): p. 327-332.
93. Granier, S., A. Manglik, A.C. Kruse, T.S. Kobilka, F.S. Thian, W.I. Weis, and B.K. Kobilka, *Structure of the δ-opioid receptor bound to naltrindole.* Nature, 2012. **485**(7398): p. 400-404.
94. Thompson, A.A., W. Liu, E. Chun, V. Katritch, H. Wu, E. Vardy, X.P. Huang, C. Trapella, R. Guerrini, G. Calo, B.L. Roth, V. Cherezov, and R.C. Stevens, *Structure of the nociceptin/orphanin FQ receptor in complex with a peptide mimetic.* Nature, 2012. **485**(7398): p. 395-399.
95. Cox, B.M., *Recent developments in the study of opioid receptors.* Mol Pharmacol, 2013. **83**(4): p. 723-728.
96. Pasternak, G.W. and Y.X. Pan, *Mu opioids and their receptors: Evolution of a concept.* Pharmacol Rev, 2013. **65**(4): p. 1257-1317.

97. Johnson, M.W., K.A. MacLean, C.J. Reissig, T.E. Prisinzano, and R.R. Griffiths, *Human psychopharmacology and dose-effects of salvinorin A, a κ-opioid agonist hallucinogen present in the plant Salvia divinorum.* Drug Alcohol Depen, 2011. **115**(1-2): p. 150-155.

98. McCurdy, C.R., K.J. Sufka, G.H. Smith, J.E. Warnick, and M.J. Nieto, *Antinociceptive profile of salvinorin A, a structurally unique κ-opioid receptor agonist.* Pharmacol Biochem Behav, 2006. **83**(1): p. 109-113.

99. Roth, B.L., K. Baner, R. Westkaemper, D. Siebert, K.C. Rice, S. Steinberg, P. Ernsberger, and R.B. Rothman, *Salvinorin A: A potent naturally occurring nonnitrogenous κ opioid selective agonist.* Proc Nat Acad Sci USA, 2002. **99**(18): p. 11934-11939.

100. Omiecinski, C.J., J.P. Vanden Heuvel, G.H. Perdew, and J.M. Peters, *Xenobiotic metabolism, disposition, and regulation by receptors: From biochemical phenomenon to predictors of major toxicities.* Toxicol Sci, 2011. **120**(1): p. 49-75.

101. Nebert, D.W. and D.W. Russell, *Clinical importance of the cytochromes P450.* Lancet, 2002. **360**(9340): p. 1155-1162.

102. Zanger, U.M. and M. Schwab, *Cytochrome P450 enzymes in drug metabolism: Regulation of gene expression, enzyme activities, and impact of genetic variation.* Pharmacol Ther, 2013. **138**(1): p. 103-141.

103. Rowland, A., J.O. Miners, and P.I. Mackenzie, *The UDP-glucuronosyltransferases: Their role in drug metabolism and detoxification.* Int J Biochem Cell Biol, 2013. **45**(6): p. 1121-1132.

104. Meech, R., J.O. Miners, B.C. Lewis, and P.I. Mackenzie, *The glycosidation of xenobiotics and endogenous compounds: versatility and redundancy in the UDP glycosyltransferase superfamily.* Pharmacol Ther, 2012. **134**(2): p. 200-218.

105. Sanghani, S.P., P.C. Sanghani, M.A. Schiel, and W.F. Bosron, *Human carboxylesterases: An update on CES1, CES2 and CES3.* Protein Pept Lett, 2009. **16**(10): p. 1207-1214.

106. Laizure, S.C., V. Herring, Z. Hu, K. Witbrodt, and R.B. Parker, *The role of human carboxylesterases in drug metabolism: have we overlooked their importance?* Pharmacotherapy, 2013. **33**(2): p. 210-222.

107. Hosokawa, M., *Structure and catalytic properties of carboxylesterase isozymes involved in metabolic activation of prodrugs.* Molecules, 2008. **13**(2): p. 412-431.

108. Ramesh, M., P. Ahlawat, and N.R. Srinivas, *Irinotecan and its active metabolite, SN-38: review of bioanalytical methods and recent update from clinical pharmacology perspectives.* Biomedical Chromatography, 2010. **24**(1): p. 104-123.
109. Gamage, N., A. Barnett, N. Hempel, R.G. Duggleby, K.F. Windmill, J.L. Martin, and M.E. McManus, *Human Sulfotransferases and Their Role in Chemical Metabolism.* Toxicol Sci, 2006. **90**(1): p. 5-22.
110. Salinas, A.E. and M.G. Wong, *Glutathione S-transferases--a review.* Curr Med Chem, 1999. **6**(4): p. 279-309.
111. Youdim, M.B.H., D. Edmondson, and K.F. Tipton, *The therapeutic potential of monoamine oxidase inhibitors.* Nat Rev Neurosci, 2006. **7**(4): p. 295-309.
112. Williams, J.A., R. Hyland, B.C. Jones, D.A. Smith, S. Hurst, T.C. Goosen, V. Peterkin, J.R. Koup, and S.E. Ball, *Drug-drug interactions for UDP-Glucuronosyltransferase substrates: A pharmacokinetic explanation for typically observed low exposure ratios.* Drug Metab Dispos, 2004. **32**(11): p. 1201-1208.
113. Cerny, M.A., *Prevalence of non-cytochrome P450-mediated metabolism in FDA-approved oral and intravenous drugs: 2006-2015.* Drug Metab Dispos, 2016. **44**(8): p. 1246-1252.
114. Kola, I. and J. Landis, *Can the pharmaceutical industry reduce attrition rates?* Nat Rev Drug Discov, 2004. **3**(8): p. 711-716.
115. Hughes, J.P., S. Rees, S.B. Kalindjian, and K.L. Philpott, *Principles of early drug discovery.* Br J Clin Pharmacol, 2011. **162**(6): p. 1239-1249.
116. Cook, D., D. Brown, R. Alexander, R. March, P. Morgan, G. Satterthwaite, and M.N. Pangalos, *Lessons learned from the fate of AstraZeneca's drug pipeline: A five-dimensional framework.* Nat Rev Drug Discov, 2014. **13**(6): p. 419-431.
117. Ji, H.F., X.J. Li, and H.Y. Zhang, *Natural products and drug discovery. Can thousands of years of ancient medical knowledge lead us to new and powerful drug combinations in the fight against cancer and dementia?* EMBO Reports, 2009. **10**(3): p. 194-200.
118. Barter, Z.E., M.K. Bayliss, P.H. Beaune, A.R. Boobis, D.J. Carlile, R.J. Edwards, J.B. Houston, B.G. Lake, J.C. Lipscomb, O.R. Pelkonen, G.T. Tucker, and A. Rostami-Hodjegan, *Scaling factors for the extrapolation of in vivo metabolic drug clearance from in vitro data: reaching a consensus on values of human microsomal*

protein and hepatocellularity per gram of liver. Curr Drug Metab, 2007. **8**(1): p. 33-45.

119. Gill, K.L., J.B. Houston, and A. Galetin, *Characterization of in vitro glucuronidation clearance of a range of drugs in human kidney microsomes: Comparison with liver and intestinal glucuronidation and impact of albumin.* Drug Metab Dispos, 2012. **40**(4): p. 825-835.
120. DiMasi, J.A., H.G. Grabowski, and R.W. Hansen, *The cost of drug development.* New Engl J Med, 2015. **372**(20): p. 1972-1972.
121. Danchin, A., C. Medigue, O. Gascuel, H. Soldano, and A. Henaut, *From data banks to data bases.* Res Microbiol, 1991. **142**(7-8): p. 913-916.
122. Wadood, A., N. Ahmed, L. Shah, A. Ahmad, H. Hassan, and S. Shams, *In-silico drug design: An approach which revolutionarised the drug discovery process.* OA Drug Des Deliv, 2013. **1**(1).
123. Zhang, Y.Y., H. Liu, S.G. Summerfield, C.N. Luscombe, and J. Sahi, *Integrating in Silico and in Vitro Approaches To Predict Drug Accessibility to the Central Nervous System.* Mol Pharm, 2016. **13**(5): p. 1540-50.
124. Shoichet, B.K., *Virtual screening of chemical libraries.* Nature, 2004. **432**(7019): p. 862-865.
125. Anderson, A.C., *The process of structure-based drug design.* Chem Biol, 2003. **10**(9): p. 787-797.
126. Wlodawer, A., W. Minor, Z. Dauter, and M. Jaskolski, *Protein crystallography for aspiring crystallographers or how to avoid pitfalls and traps in macromolecular structure determination.* FEBS J, 2013. **280**(22): p. 5705-36.
127. Pasternak, G.W. and Y.-X. Pan, *Mu Opioids and Their Receptors: Evolution of a Concept.* Pharmacol Rev, 2013. **65**(4): p. 1257-1317.
128. Radominska-Pandya, A., S.M. Bratton, M.R. Redinbo, and M.J. Miley, *The crystal structure of human UDP-glucuronosyltransferase 2B7 C-terminal end is the first mammalian UGT target to be revealed: The significance for human UGTs from both the 1A and 2B families.* Drug Metab Rev, 2010. **42**(1): p. 133-144.
129. Berman, H.M., J. Westbrook, Z. Feng, G. Gilliland, T.N. Bhat, H. Weissig, I.N. Shindyalov, and P.E. Bourne, *The protein data bank.* Nucleic Acids Res, 2000. **28**(1): p. 235-242.

130. Vyas, V.K., R.D. Ukawala, M. Ghate, and C. Chintha, *Homology Modeling a Fast Tool for Drug Discovery: Current Perspectives.* Indian J Pharm Sci, 2012. **74**(1): p. 1-17.
131. Meng, X.Y., H.X. Zhang, M. Mezei, and M. Cui, *Molecular docking: A powerful approach for structure-based drug discovery.* Curr Comput-Aid Drug, 2011. **7**(2): p. 146-157.
132. OpenEye, *Omega 2.5.1.4*. 2013, OpenEye Scientific Software, Inc.: Santa Fe, NM.
133. OpenEye, *OEDocking 3.0.1*. 2012, OpenEye Scientific Software, Inc.: Santa Fe, NM.
134. Schulz-Gasch, T. and M. Stahl, *Binding site characteristics in structure-based virtual screening: evaluation of current docking tools.* J Mol Model, 2003. **9**(1): p. 47-57.
135. Karplus, M. and J.A. McCammon, *Molecular dynamics simulations of biomolecules.* Nat Struct Mol Biol, 2002. **9**(9): p. 646-652.
136. Qing, X.Y., X.Y. Lee, J. De Raeymaeker, J.R.H. Tame, K.Y.J. Zhang, M. De Maeyer, and A.R.D. Voet, *Pharmacophore modeling: advances, limitations, and current utility in drug discovery.* J Rec Lig Chan Res, 2014. **7**(1): p. 81-92.
137. Onnis, V., G.K. Kinsella, G. Carta, W.N. Jagoe, T. Price, D.C. Williams, D. Fayne, and D.G. Lloyd, *Virtual screening for the identification of novel nonsteroidal glucocorticoid modulators.* J Med Chem, 2010. **53**(8): p. 3065-3074.
138. OpenEye, *ROCS 3.2.0.4*. 2013, OpenEye Scientific Software, Inc.: Santa Fe, NM.
139. Bajusz, D., A. Rácz, and K. Héberger, *Why is Tanimoto index an appropriate choice for fingerprint-based similarity calculations?* J Cheminform, 2015. **7**: p. 20.
140. Rush, T.S., J.A. Grant, L. Mosyak, and A. Nicholls, *A shape-based 3-D scaffold hopping method and its application to a bacterial protein−protein interaction.* J Med Chem, 2005. **48**(5): p. 1489-1495.
141. Langdon, S.R., I.M. Westwood, R.L.M. van Montfort, N. Brown, and J. Blagg, *Scaffold-focused virtual screening: Prospective application to the discovery of TTK inhibitors.* J Chem Inf Model, 2013. **53**(5): p. 1100-1112.
142. Long, A., *Drug metabolism in silico – the knowledge-based expert system approach. Historical perspectives and current strategies.* Drug Discov Today, 2013. **10**(1): p. 147-153.

143. Sliwoski, G., S. Kothiwale, J. Meiler, and E.W. Lowe, *Computational methods in drug discovery.* Pharmacol Rev, 2014. **66**(1): p. 334-395.
144. Ghose, A.K., T. Herbertz, J.M. Salvino, and J.P. Mallamo, *Knowledge-based chemoinformatic approaches to drug discovery.* Drug Discov Today, 2006. **11**(23–24): p. 1107-1114.
145. Jónsdóttir, S.O., F.S. Jørgensen, and S. Brunak, *Prediction methods and databases within chemoinformatics: emphasis on drugs and drug candidates.* Bioinformatics, 2005. **21**(10): p. 2145-2160.
146. Lipinski, C.A., F. Lombardo, B.W. Dominy, and P.J. Feeney, *Experimental and computational approaches to estimate solubility and permeability in drug discovery and development settings.* Adv Drug Deliver Rev, 1997. **23**(1): p. 3-25.
147. Leeson, P., *Drug discovery: Chemical beauty contest.* Nature, 2012. **481**(7382): p. 455-456.
148. FDA, *Guidance for Industry: Safety Testing of Drug metabolites*, C.f.D.E.a. Research, Editor. 2008, Food and Drug Administration: Rockville, MD.
149. EMA, *Guideline on the investigation of drug interactions*, C.f.H.M. Products, Editor. 2012, European Medicines Agency: London, UK.
150. Masimirembwa, C.M., U. Bredberg, and T.B. Andersson, *Metabolic stability for drug discovery and development: pharmacokinetic and biochemical challenges.* Clin Pharmacokinet, 2003. **42**(6): p. 515-528.
151. Harper, T.W. and P.J. Brassil, *Reaction phenotyping: Current industry efforts to identify enzymes responsible for metabolizing drug candidates.* AAPS PharmSciTech, 2008. **10**(1): p. 200-207.
152. Miners, J.O., M.E. Veronese, and D.J. Birkett, *Chapter 31. In Vitro Approaches for the Prediction of Human Drug Metabolism*, in *Annu Rep Med Chem*. 1994, Academic Press. p. 307-316.
153. Miners, J.O., P.I. Mackenzie, and K.M. Knights, *The prediction of drug-glucuronidation parameters in humans: UDP-glucuronosyltransferase enzyme-selective substrate and inhibitor probes for reaction phenotyping and in vitro–in vivo extrapolation of drug clearance and drug-drug interaction potential.* Drug Metab Rev, 2010. **42**(1): p. 196-208.
154. Hosokawa, M., *Structure and Catalytic Properties of Carboxylesterase Isozymes Involved in Metabolic Activation of Prodrugs.* Molecules, 2008. **13**(2): p. 412.

155. Schmidt, M.S., T.E. Prisinzano, K. Tidgewell, W. Harding, E.R. Butelman, M.J. Kreek, and D.J. Murry, *Determination of Salvinorin A in body fluids by high performance liquid chromatography-atmospheric pressure chemical ionization.* J Chromatogr B Analyt Technol Biomed Life Sci, 2005. **818**(2): p. 221-225.
156. Hatfield, M.J. and P.M. Potter, *Carboxylesterase inhibitors.* Expert Opin Ther Pat, 2011. **21**(8): p. 1159-1171.
157. Umehara, K., M. Zollinger, E. Kigondu, M. Witschi, C. Juif, F. Huth, H. Schiller, K. Chibale, and G. Camenisch, *Esterase phenotyping in human liver in vitro: specificity of carboxylesterase inhibitors.* Xenobiotica, 2016. **46**(10): p. 862-7.
158. Venkatakrishnan, K., L.L. von Moltke, and D.J. Greenblatt, *Human cytochromes P450 mediating phenacetin O-deethylation in vitro: validation of the high affinity component as an index of CYP1A2 activity.* J Pharm Sci, 1998. **87**(12): p. 1502-7.
159. Fisher, M.B., K. Campanale, B.L. Ackermann, M. VandenBranden, and S.A. Wrighton, *In vitro glucuronidation using human liver microsomes and the pore-forming peptide alamethicin.* Drug Metab Dispos, 2000. **28**(5): p. 560-566.
160. James, M.O. and S. Ambadapadi, *Interactions of cytosolic sulfotransferases with xenobiotics.* Drug Metab Rev, 2013. **45**(4): p. 401-414.
161. Reith, D., N.J. Medlicott, R. Kumara De Silva, L. Yang, J. Hickling, and M. Zacharias, *Simultaneous modelling of the Michaelis-Menten kinetics of paracetamol sulphonation and glucuronidation.* Clin Exp Pharmacol Physiol, 2009. **36**(1): p. 35-42.
162. Rowland, M., L.Z. Benet, and G.G. Graham, *Clearance concepts in pharmacokinetics.* J Pharmacokinet Biop, 1973. **1**(2): p. 123-136.
163. Wilkinson, G.R. and D.G. Shand, *Commentary: a physiological approach to hepatic drug clearance.* Clin Pharmacol Ther, 1975. **18**(4): p. 377-90.
164. Jamei, M., S. Marciniak, D. Edwards, K. Wragg, K. Feng, A. Barnett, and A. Rostami-Hodjegan, *The Simcyp Population Based Simulator: Architecture, Implementation, and Quality Assurance.* In Silico Pharmacol, 2013. **1**(1): p. 1-14.
165. ACD, *PhysChem History, v12.0*. 2010, Advanced Chemical Development, Inc.: Toronto, ON, Canada.
166. Parker, R.B., Z.Y. Hu, B. Meibohm, and S.C. Laizure, *Effects of alcohol on human carboxylesterase drug metabolism.* Clin Pharmacokinet, 2015. **54**(6): p. 627-638.

167. Miners, J.O., M.E. Veronese, and D.J. Birkett, *[15] Use of tolbutamide as a substrate probe for human hepatic cytochrome P450 2C9*, in *Methods Enzymol*. 1996, Academic Press. p. 139-145.

168. Walsky, R.L., R.S. Obach, R. Hyland, P. Kang, S. Zhou, M. West, K.F. Geoghegan, C.J. Helal, G.S. Walker, T.C. Goosen, and M.A. Zientek, *Selective Mechanism-Based Inactivation of CYP3A4 by CYP3cide (PF-04981517) and Its Utility as an In Vitro Tool for Delineating the Relative Roles of CYP3A4 versus CYP3A5 in the Metabolism of Drugs.* Drug Metab Dispos, 2012. **40**(9): p. 1686-1697.

169. Elliot, D.J., B.C. Lewis, E.M.J. Gillam, D.J. Birkett, A.S. Gross, and J.O. Miners, *Identification of the human cytochromes P450 catalysing the rate-limiting pathways of gliclazide elimination.* Br J Clin Pharmacol, 2007. **64**(4): p. 450-457.

170. Williams, J.A., R. Hyland, B.C. Jones, D.A. Smith, S. Hurst, T.C. Goosen, V. Peterkin, J.R. Koup, and S.E. Ball, *Drug-drug interactions for UDP-glucuronosyltransferase substrates: a pharmacokinetic explanation for typically observed low exposure (AUCi/AUC) ratios.* Drug Metab Dispos, 2004. **32**(11): p. 1201-8.

171. Miners, J.O. and D.J. Birkett, *Cytochrome P4502C9: an enzyme of major importance in human drug metabolism.* Br J Clin Pharmacol, 1998. **45**(6): p. 525-538.

172. Ince, I., C.A. Knibbe, M. Danhof, and S.N. de Wildt, *Developmental changes in the expression and function of cytochrome P450 3A isoforms: evidence from in vitro and in vivo investigations.* Clin Pharmacokinet, 2013. **52**(5): p. 333-45.

173. Nguyen, S., *An in silico approach to investigate glucuronidation: Application to HIV drug discovery and development*, in *School of Pharmacy and Medical Sciences*. 2010, The University of South Australia: Adelaide, South Australia. p. 80.

174. Miners, J.O., K. Bowalgaha, D.J. Elliot, P. Baranczewski, and K.M. Knights, *Characterization of Niflumic Acid as a Selective Inhibitor of Human Liver Microsomal UDP-Glucuronosyltransferase 1A9: Application to the Reaction Phenotyping of Acetaminophen Glucuronidation.* Drug Metabolism and Disposition, 2011. **39**(4): p. 644-652.

175. Uchaipichat, V., L.K. Winner, P.I. Mackenzie, D.J. Elliot, J.A. Williams, and J.O. Miners, *Quantitative prediction of in vivo inhibitory interactions involving glucuronidated drugs from in vitro data: the effect of fluconazole on zidovudine glucuronidation.* Br J Clin Pharmacol, 2006. **61**(4): p. 427-439.

176. Bowalgaha, K., D.J. Elliot, P.I. Mackenzie, K.M. Knights, S. Swedmark, and J.O. Miners, *S-Naproxen and desmethylnaproxen glucuronidation by human liver microsomes and recombinant human UDP-glucuronosyltransferases (UGT): Role of UGT2B7 in the elimination of naproxen.* Br J Clin Pharmacol, 2005. **60**(4): p. 423-33.

177. Uchaipichat, V., P. Raungrut, N. Chau, B. Janchawee, A.M. Evans, and J.O. Miners, *Effects of ketamine on human UDP-glucuronosyltransferases in vitro predict potential drug-drug interactions arising from ketamine inhibition of codeine and morphine glucuronidation.* Drug Metab Dispos, 2011. **39**(8): p. 1324-8.

178. Miners, J.O., K. Bowalgaha, D.J. Elliot, P. Baranczewski, and K.M. Knights, *Characterization of niflumic acid as a selective inhibitor of human liver microsomal UDP-glucuronosyltransferase 1A9: Application to the reaction phenotyping of acetaminophen glucuronidation.* Drug Metab Dispos, 2011. **39**(4): p. 644-652.

179. Dong, D., T. Zhang, D. Lu, J. Liu, and B. Wu, *In vitro characterization of belinostat glucuronidation: demonstration of both UGT1A1 and UGT2B7 as the main contributing isozymes.* Xenobiotica, 2016. **47**(4): p. 277-283.

180. Baer, B.R., A.E. Rettie, and K.R. Henne, *Bioactivation of 4-Ipomeanol by CYP4B1: Adduct Characterization and Evidence for an Enedial Intermediate.* Chem Res Toxicol, 2005. **18**(5): p. 855-864.

181. Peterson, L.A., *Reactive metabolites in the biotransformation of molecules containing a furan ring.* Chem Res Toxicol, 2012. **26**(1): p. 6-25.

182. Rowland, A., K.M. Knights, P.I. Mackenzie, and J.O. Miners, *The "albumin effect" and drug glucuronidation: bovine serum albumin and fatty acid-free human serum albumin enhance the glucuronidation of UDP-glucuronosyltransferase (UGT) 1A9 substrates but not UGT1A1 and UGT1A6 activities.* Drug Metab Dispos, 2008. **36**(6): p. 1056-62.

183. Rowland, A., P. Gaganis, D.J. Elliot, P.I. Mackenzie, K.M. Knights, and J.O. Miners, *Binding of Inhibitory Fatty Acids Is Responsible for the Enhancement of UDP-Glucuronosyltransferase 2B7 Activity by Albumin: Implications for in Vitro-in Vivo Extrapolation.* J Pharmacol Exp Ther, 2007. **321**(1): p. 137-147.

184. Ogu, C.C. and J.L. Maxa, *Drug interactions due to cytochrome P450.* Proceedings (Baylor University. Medical Center), 2000. **13**(4): p. 421-423.

185. Kiang, T.K.L., M.H.H. Ensom, and T.K.H. Chang, *UDP-glucuronosyltransferases and clinical drug-drug interactions.* Pharmacol Ther, 2005. **106**(1): p. 97-132.

186. Dang, N.L., T.B. Hughes, V. Krishnamurthy, and S.J. Swamidass, *A Simple Model Predicts UGT-Mediated Metabolism.* Bioinformatics, 2016. **32**(20): p. 3183-3189.

187. Mishra, N.K., S. Agarwal, and G.P.S. Raghava, *Prediction of cytochrome P450 isoform responsible for metabolizing a drug molecule.* BMC Pharmacology, 2010. **10**(1): p. 1-9.

188. Peng, J., J. Lu, Q. Shen, M. Zheng, X. Luo, W. Zhu, H. Jiang, and K. Chen, *In silico site of metabolism prediction for human UGT-catalyzed reactions.* Bioinformatics, 2014. **30**(3): p. 398-405.

189. Romberg, R.W. and L. Lee, *Comparison of the hydrolysis rates of morphine-3-glucuronide and morphine-6-glucuronide with acid and beta-glucuronidase.* J Anal Toxicol, 1995. **19**(3): p. 157-162.

190. Shipkova, M., V.W. Armstrong, M. Oellerich, and E. Wieland, *Acyl glucuronide drug metabolites: toxicological and analytical implications.* Ther Drug Monit, 2003. **25**(1): p. 1-16.

191. Chen, Y.K., S.Q. Chen, X. Li, and S. Zeng, *Quantitative regioselectivity of glucuronidation of quercetin by recombinant UDP-glucuronosyltransferases 1A9 and 1A3 using enzymatic kinetic parameters.* Xenobiotica, 2005. **35**(10-11): p. 943-954.

192. Tachibana, M., M. Tanaka, Y. Masubuchi, and T. Horie, *Acyl glucuronidation of fluoroquinone antibiotics by the UDP-glucuronosyltransferase 1A subfamily in human liver microsomes.* Drug Metab Dispos, 2005. **33**(6): p. 803-811.

193. Shipkova, M., E. Schütz, V.W. Armstrong, P.D. Niedmann, M. Oellerich, and E. Wieland, *Determination of the acyl glucuronide metabolite of mycophenolic acid in human plasma by HPLC and emit.* Clin Chem, 2000. **46**(3): p. 365-372.

194. Sykes, M.J., R.A. McKinnon, and J.O. Miners, *Prediction of metabolism by cytochrome P450 2C9: Alignment and docking studies of a validated database of substrates.* J Med Chem, 2008. **51**(4): p. 780-791.

195. Wester, M.R., J.K. Yano, G.A. Schoch, C. Yang, K.J. Griffin, C.D. Stout, and E.F. Johnson, *The Structure of Human Cytochrome P450 2C9 Complexed with Flurbiprofen at 2.0-Å Resolution.* J Biol Chem, 2004. **279**(34): p. 35630-35637.

196. Ridderstrom, M., C. Masimirembwa, S. Trump-Kallmeyer, M. Ahlefelt, C. Otter, and T.B. Andersson, *Arginines 97 and 108 in CYP2C9 are important determinants of the catalytic function.* Biochem Biophys Res Commun, 2000. **270**(3): p. 983-7.

197. Williams, P.A., J. Cosme, A. Ward, H.C. Angove, D. Matak Vinkovic, and H. Jhoti, *Crystal structure of human cytochrome P450 2C9 with bound warfarin.* Nature, 2003. **424**(6947): p. 464-468.

198. Chen, L.J., E.F. DeRose, and L.T. Burka, *Metabolism of furans in vitro: ipomeanine and 4-ipomeanol.* Chem Res Toxicol, 2006. **19**(10): p. 1320-9.

199. Kent, U.M., H.L. Lin, K.R. Noon, D.L. Harris, and P.F. Hollenberg, *Metabolism of bergamottin by cytochromes P450 2B6 and 3A5.* J Pharmacol Exp Ther, 2006. **318**(3): p. 992-1005.

200. Meunier, B., S.P. de Visser, and S. Shaik, *Mechanism of oxidation reactions catalyzed by cytochrome p450 enzymes.* Chem Rev, 2004. **104**(9): p. 3947-80.

201. Matlock, M.K., T.B. Hughes, and S.J. Swamidass, *XenoSite server: a web-available site of metabolism prediction tool.* Bioinformatics, 2015. **31**(7): p. 1136-7.

202. Mishra, N.K., S. Agarwal, and G.P. Raghava, *Prediction of cytochrome P450 isoform responsible for metabolizing a drug molecule.* BMC Pharmacol, 2010. **10**: p. 8.

203. Gillette, J.R., *Factors affecting drug metabolism.* Ann New York Acad Sci, 1971. **179**(1): p. 43-66.

204. Rudmann, D.G., *On-target and off-target-based toxicologic effects.* Toxicol Path, 2012. **41**(2): p. 310-314.

205. Hutter, M.C., *In silico prediction of drug properties.* Curr Med Chem, 2009. **16**(2): p. 189-202.

206. Ekins, S., J. Mestres, and B. Testa, *In silico pharmacology for drug discovery: methods for virtual ligand screening and profiling.* Brit J Pharmacol, 2007. **152**(1): p. 9-20.

207. Kitchen, D.B., H. Decornez, J.R. Furr, and J. Bajorath, *Docking and scoring in virtual screening for drug discovery: Methods and applications.* Nat Rev Drug Discov, 2004. **3**(11): p. 935-949.

208. Kuhn, M., M. Campillos, P. González, L.J. Jensen, and P. Bork, *Large-scale prediction of drug–target relationships.* FEBS Lett, 2008. **582**(8): p. 1283-1290.

209. Salinas-Sanchez, D.O., M. Herrera-Ruiz, S. Perez, E. Jimenez-Ferrer, and A. Zamilpa, *Anti-inflammatory activity of hautriwaic acid isolated from Dodonaea viscosa leaves.* Molecules, 2012. **17**(4): p. 4292-4299.

210. Vargas, F.d.S., P.D.O.d. Almeida, E.S. Aranha, A.P.d.A. Boleti, P. Newton, M.C.d. Vasconcellos, V.F. Junior, and E.S. Lima, *Biological activities and cytotoxicity of diterpenes from Copaifera spp. Oleoresins.* Molecules, 2015. **20**(4): p. 6194-210.

211. Salinas-Sánchez, D.O., A. Zamilpa, S. Pérez, M. Herrera-Ruiz, J. Tortoriello, M. González-Cortazar, and E. Jiménez-Ferrer, *Effect of hautriwaic acid isolated from Dodonaea viscosa in a model of kaolin/carrageenan-induced monoarthritis.* Planta Medica, 2015. **81**(14): p. 1240-1247.

212. Veiga Junior, V.F., E.C. Rosas, M.V. Carvalho, M.G. Henriques, and A.C. Pinto, *Chemical composition and anti-inflammatory activity of copaiba oils from Copaifera cearensis Huber ex Ducke, Copaifera reticulata Ducke and Copaifera multijuga Hayne--a comparative study.* J Ethnopharmacol, 2007. **112**(2): p. 248-54.

213. Okamoto, Y., H. Anan, E. Nakai, K. Morihira, Y. Yonetoku, H. Kurihara, H. Sakashita, Y. Terai, M. Takeuchi, T. Shibanuma, and Y. Isomura, *Peptide based interleukin-1 beta converting enzyme (ICE) inhibitors: synthesis, structure activity relationships and crystallographic study of the ICE-inhibitor complex.* Chem Pharm Bull (Tokyo), 1999. **47**(1): p. 11-21.

214. Rano, T.A., T. Timkey, E.P. Peterson, J. Rotonda, D.W. Nicholson, J.W. Becker, K.T. Chapman, and N.A. Thornberry, *A combinatorial approach for determining protease specificities: application to interleukin-1beta converting enzyme (ICE).* Chem Biol, 1997. **4**(2): p. 149-55.

215. Wilson, K.P., J.A. Black, J.A. Thomson, E.E. Kim, J.P. Griffith, M.A. Navia, M.A. Murcko, S.P. Chambers, R.A. Aldape, S.A. Raybuck, and et al., *Structure and mechanism of interleukin-1 beta converting enzyme.* Nature, 1994. **370**(6487): p. 270-5.

216. O'Brien, T., B.T. Fahr, M.M. Sopko, J.W. Lam, N.D. Waal, B.C. Raimundo, H.E. Purkey, P. Pham, and M.J. Romanowski, *Structural analysis of caspase-1 inhibitors derived from Tethering.* Acta Crystallogr Sect F Struct Biol Cryst Commun, 2005. **61**(Pt 5): p. 451-8.

217. Romanowski, M.J., J.M. Scheer, T. O'Brien, and R.S. McDowell, *Crystal structures of a ligand-free and malonate-bound human caspase-1: implications for the mechanism of substrate binding.* Structure, 2004. **12**(8): p. 1361-71.
218. Scheer, J.M., M.J. Romanowski, and J.A. Wells, *A common allosteric site and mechanism in caspases.* Proc Natl Acad Sci U S A, 2006. **103**(20): p. 7595-600.
219. Datta, D., J.M. Scheer, M.J. Romanowski, and J.A. Wells, *An allosteric circuit in caspase-1.* J Mol Biol, 2008. **381**(5): p. 1157-67.
220. Rosen-Wolff, A., M. Romanowski, S. Flecks, N. Quoos, H. Nguyen, L. Ritter, J. Gramatte, C. Petzold, M. Gahr, and J. Roesler, *Mutated, structurally altered caspase-1 with decreased enzymatic and increased RIP2-meditated inflammatory activity leads to a new type of periodic fever (ICE fever).* Clin Exp Rheumatol, 2008. **26**(2): p. 175-175.
221. Galatsis, P., B. Caprathe, J. Gilmore, A. Thomas, K. Linn, S. Sheehan, W. Harter, C. Kostlan, E. Lunney, C. Stankovic, J. Rubin, K. Brady, H. Allen, and R. Talanian, *Succinic acid amides as P2–P3 replacements for inhibitors of interleukin-1β converting enzyme (ICE or caspase 1).* Bioorg Med Chem Lett, 2010. **20**(17): p. 5184-5190.
222. Tuccinardi, T., M. Botta, A. Giordano, and A. Martinelli, *Protein kinases: Docking and homology modeling reliability.* J Chem Inf Model, 2010. **50**(8): p. 1432-1441.
223. Kirchmair, J., S. Distinto, P. Markt, D. Schuster, G.M. Spitzer, K.R. Liedl, and G. Wolber, *How to optimize shape-based virtual screening: Choosing the right query and including chemical information.* J Chem Inf Model, 2009. **49**(3): p. 678-692.
224. Sollberger, G., G.E. Strittmatter, M. Garstkiewicz, J. Sand, and H.-D. Beer, *Caspase-1: The inflammasome and beyond.* Innate Immunity, 2014. **20**(2): p. 115-125.
225. Randle, J.C., M.W. Harding, G. Ku, M. Schonharting, and R. Kurrle, *ICE/Caspase-1 inhibitors as novel anti-inflammatory drugs.* Expert Opin Investig Drugs, 2001. **10**(7): p. 1207-9.
226. Loher, F., C. Bauer, N. Landauer, K. Schmall, B. Siegmund, H.A. Lehr, M. Dauer, M. Schoenharting, S. Endres, and A. Eigler, *The interleukin-1 β-converting enzyme inhibitor pralnacasan reduces dextran sulfate sodium-induced murine colitis and T helper 1 T-cell activation.* J Pharmacol Exp Ther, 2004. **308**(2): p. 583-90.
227. Vertex and Aventis, *Aventis and Vertex Pharmaceuticals Voluntarily Discontinue Phase IIb Clinical Trials of Pralnacasan in Rheumatoid Arthritis*. 2003.

228. Fischer, U. and K. Schulze-Osthoff, *Apoptosis-based therapies and drug targets.* Cell Death Differ, 2005. **12**(S1): p. 942-961.

229. Fabbro, D., S.W. Cowan-Jacob, and H. Moebitz, *Ten things you should know about protein kinases: IUPHAR Review 14.* Br J Pharmacol, 2015. **172**(11): p. 2675-2700.

230. Kuchera, S., H. Barth, P. Jacobson, A. Metz, C. Schaechtele, and D. Schrier, *Anti-inflammatory properties of the Protein Kinase C inhibitor, 3-[1-[3-(dimethylamino)propyl]-1H-indol-3-yl]-4-(1H-indol-3-yl)-1H- pyrrole-2,5-dione monohydrochloride (GF109203X) in the PMA-mouse ear edema model.* Agents Actions, 1993. **39** p. 169-73.

231. Bioscience, T., *Protein Kinase C,* in *Protein Kinase C inhibitors*, T. Bioscience, Editor. 2017, Tocris Bioscience: Bristol, UK. p. 1.

232. McGregor, M.J., *A pharmacophore map of small molecule protein kinase inhibitors.* J Chem Inf Model, 2007. **47**(6): p. 2374-2382.

233. Zheng, J., E.A. Trafny, D.R. Knighton, N.H. Xuong, S.S. Taylor, L.F. Ten Eyck, and J.M. Sowadski, *2.2 A refined crystal structure of the catalytic subunit of cAMP-dependent protein kinase complexed with MnATP and a peptide inhibitor.* Acta Crystallogr D Biol Crystallogr, 1993. **49**(3): p. 362-5.

234. Xu, Z.B., D. Chaudhary, S. Olland, S. Wolfrom, R. Czerwinski, K. Malakian, L. Lin, M.L. Stahl, D. Joseph-McCarthy, C. Benander, L. Fitz, R. Greco, W.S. Somers, and L. Mosyak, *Catalytic domain crystal structure of protein kinase C-theta (PKCtheta).* J Biol Chem, 2004. **279**(48): p. 50401-9.

235. Leonard, T.A., B. Różycki, L.F. Saidi, G. Hummer, and J.H. Hurley, *Crystal structure and allosteric activation of Protein Kinase C βII.* Cell, 2011. **144**(1): p. 55-66.

236. Pappa, H., J. Murray-Rust, L.V. Dekker, P.J. Parker, and N.Q. McDonald, *Crystal structure of the C2 domain from protein kinase C-δ.* Structure, 1998. **6**(7): p. 885-894.

237. Karin, M., *Inflammation-activated protein kinases as targets for drug development.* Proc Am Thorac Soc, 2005. **2**(4): p. 386-395.

238. Ways, D.K., W. Qin, T.O. Garris, J. Chen, E. Hao, D.R. Cooper, S.J. Usala, P.J. Parker, and P.P. Cook, *Effects of chronic phorbol ester treatment on protein kinase C activity, content, and gene expression in the human monoblastoid U937 cell.* Cell Growth Differ, 1994. **5**(2): p. 161-9.

239. Bruder, J.M., W.D. Krebs, T.M. Nett, and M.E. Wierman, *Phorbol ester activation of the protein kinase C pathway inhibits gonadotropin-releasing hormone gene expression.* Endocrinology, 1992. **131**(6): p. 2552-8.

240. Lawrence, T., *The nuclear factor NF-κB pathway in inflammation.* Cold Spring Harb Perspect Biol, 2009. **1**(6): p. a001651.

241. Bioscience, T., *NF-KB and IKB Inhibitors*, in *NF-KB and IKB inhibitors*, T. Bioscience, Editor. 2017, Tocris Bioscience: Bristol, UK. p. 1.

242. Baldi, P. and R. Nasr, *When is chemical similarity significant? The statistical distribution of chemical similarity scores and its extreme values.* J Chem Inf Model, 2010. **50**(7): p. 1205-1222.

243. Mishra, K., A.P. Dash, and N. Dey, *Andrographolide: A novel antimalarial diterpene lactone compound from Andrographis paniculata and its interaction with curcumin and artesunate.* J Trop Med, 2011. **2011**: p. 6.

244. Ghosh, G., G. van Duyne, S. Ghosh, and P.B. Sigler, *Structure of NF-κB p50 homodimer bound to a κB site.* Nature, 1995. **373**(6512): p. 303-310.

245. Moorthy, A.K., D.B. Huang, V.Y. Wang, D. Vu, and G. Ghosh, *X-ray structure of a NF-κB p50/RelB/DNA complex reveals assembly of multiple dimers on tandem κB sites.* J Mol Biol, 2007. **373**(3): p. 723-734.

246. Ashkenazi, S., A. Plotnikov, A. Bahat, E. Ben-Zeev, S. Warszawski, and R. Dikstein, *A novel allosteric mechanism of NF-κB dimerization and DNA binding targeted by an anti-inflammatory drug.* Mol Cell Biol, 2016. **36**(8): p. 1237-1247.

247. Xie, Q.W., Y. Kashiwabara, and C. Nathan, *Role of transcription factor NF-kappa B/Rel in induction of nitric oxide synthase.* J Biol Chem, 1994. **269**(7): p. 4705-8.

248. Zheng, Y., B. Yu, K. Ji, Z. Pan, V. Chittavong, and B. Wang, *Esterase-Sensitive Prodrugs with Tunable Release Rates and Direct Generation of Hydrogen Sulfide.* Angew Chem Int Ed Engl, 2016. **55**(14): p. 4514-8.

249. Lee, J., M.H. Rhee, E. Kim, and J.Y. Cho, *BAY-11-7082 is a broad-spectrum inhibitor with anti-inflammatory activity against multiple targets.* Mediators Inflamm, 2012. **2012**: p. 11.

250. Yamamoto, Y. and R.B. Gaynor, *Therapeutic potential of inhibition of the NF-κB pathway in the treatment of inflammation and cancer.* J Clin Invest, 2001. **107**(2): p. 135-142.

251. Ben-Neriah, Y. and M. Karin, *Inflammation meets cancer, with NF-κB as the matchmaker.* Nat Immunol, 2011. **12**(8): p. 715-723.

252. Xia, Y.F., B.Q. Ye, Y.D. Li, J.G. Wang, X.J. He, X. Lin, X. Yao, D. Ma, A. Slungaard, R.P. Hebbel, N.S. Key, and J.G. Geng, *Andrographolide attenuates inflammation by inhibition of NF-kappa B activation through covalent modification of reduced cysteine 62 of p50.* J Immunol, 2004. **173**(6): p. 4207-17.

253. Johnson, T.A., J. Sohn, Y.M. Vaske, K.N. White, T.L. Cohen, H.C. Vervoort, K. Tenney, F.A. Valeriote, L.F. Bjeldanes, and P. Crews, *Myxobacteria versus sponge-derived alkaloids: the bengamide family identified as potent immune modulating agents by scrutiny of LC-MS/ELSD libraries.* Bioorg Med Chem, 2012. **20**(14): p. 4348-4355.

254. Lee, J.H., H.S. Jung, P.M. Giang, X. Jin, S. Lee, P.T. Son, D. Lee, Y.S. Hong, K. Lee, and J.J. Lee, *Blockade of nuclear factor-κB signaling pathway and anti-inflammatory activity of cardamomin, a chalcone analog from Alpinia conchigera.* J Pharmacol Exp Ther, 2006. **316**(1): p. 271-278.

255. Royuela, M., G. Rodriguez-Berriguete, B. Fraile, and R. Paniagua, *TNFα/IL-1/NF-κB transduction pathway in human cancer prostate.* Histol Histopathol, 2008. **23**(10): p. 1279-1290.

256. Sun, Z. and R. Andersson, *NF-κB activation and inhibition: A review.* Shock, 2002. **18**(2): p. 99-106.

257. Miller, S.C., R. Huang, S. Sakamuru, S.J. Shukla, M.S. Attene-Ramos, P. Shinn, D. Van Leer, W. Leister, C.P. Austin, and M. Xia, *Identification of known drugs that act as inhibitors of NF-κB signaling and their mechanism of action.* Biochem Pharmacol, 2010. **79**(9): p. 1272-1280.

258. Lu, W.J., K.H. Lin, M.J. Hsu, D.S. Chou, G. Hsiao, and J.R. Sheu, *Suppression of NF-κB signaling by andrographolide with a novel mechanism in human platelets: regulatory roles of the p38 MAPK-hydroxyl radical-ERK2 cascade.* Biochem Pharmacol, 2012. **84**(7): p. 914-924.

259. Weber, C.K., S. Liptay, T. Wirth, G. Adler, and R.M. Schmid, *Suppression of NF-kappaB activity by sulfasalazine is mediated by direct inhibition of IkappaB kinases alpha and beta.* Gastroenterology, 2000. **119**(5): p. 1209-18.

260. Rajagopal, S., R.A. Kumar, D.S. Deevi, C. Satyanarayana, and R. Rajagopalan, *Andrographolide, a potential cancer therapeutic agent isolated from Andrographis paniculata.* J Exp Ther Oncol, 2003. **3**(3): p. 147-158.

261. Fouad, D., E. Siendones, G. Costan, and J. Muntane, *Role of NF-κB activation and nitric oxide expression during PGE protection against d-galactosamine-induced cell death in cultured rat hepatocytes.* Liver Int, 2004. **24**(3): p. 227-236.

262. Strickson, S., D.G. Campbell, C.H. Emmerich, A. Knebel, L. Plater, M.S. Ritorto, N. Shpiro, and P. Cohen, *The anti-inflammatory drug BAY-11-7082 suppresses the MyD88-dependent signalling network by targeting the ubiquitin system.* Biochem J, 2013. **451**(3): p. 427-437.

263. Smoak, K.A. and J.A. Cidlowski, *Mechanisms of glucocorticoid receptor signaling during inflammation.* Mech Ageing Dev, 2004. **125**(10–11): p. 697-706.

264. Carugo, O. and S. Pongor, *A normalized root-mean-spuare distance for comparing protein three-dimensional structures.* Protein Sci, 2001. **10**(7): p. 1470-1473.

265. Edman, K., R. Ahlgren, M. Bengtsson, H. Bladh, S. Bäckström, J. Dahmén, K. Henriksson, P. Hillertz, V. Hulikal, A. Jerre, L. Kinchin, C. Kåse, M. Lepistö, I. Mile, S. Nilsson, A. Smailagic, J. Taylor, A. Tjörnebo, L. Wissler, and T. Hansson, *The discovery of potent and selective non-steroidal glucocorticoid receptor modulators, suitable for inhalation.* Bioorg Med Chem Lett, 2014. **24**(11): p. 2571-2577.

266. He, Y., W. Yi, K. Suino-Powell, X.E. Zhou, W.D. Tolbert, X. Tang, J. Yang, H. Yang, J. Shi, L. Hou, H. Jiang, K. Melcher, and H.E. Xu, *Structures and mechanism for the design of highly potent glucocorticoids.* Cell Res, 2014. **24**(6): p. 713-726.

267. Carson, M.W., J.G. Luz, C. Suen, C. Montrose, R. Zink, X. Ruan, C. Cheng, H. Cole, M.D. Adrian, D.T. Kohlman, T. Mabry, N. Snyder, B. Condon, M. Maletic, D. Clawson, A. Pustilnik, and M.J. Coghlan, *Glucocorticoid receptor modulators informed by crystallography lead to a new rationale for receptor selectivity, function, and implications for structure-based design.* J Med Chem, 2014. **57**(3): p. 849-860.

268. Biggadike, K., R.K. Bledsoe, D.M. Coe, T.W. Cooper, D. House, M.A. Iannone, S.J. Macdonald, K.P. Madauss, I.M. McLay, T.J. Shipley, S.J. Taylor, T.B. Tran, I.J. Uings, V. Weller, and S.P. Williams, *Design and x-ray crystal structures of high-potency nonsteroidal glucocorticoid agonists exploiting a novel binding site on the receptor.* Proc Natl Acad Sci USA, 2009. **106**(43): p. 18114-18119.

269. Madauss, K.P., R.K. Bledsoe, I. McLay, E.L. Stewart, I.J. Uings, G. Weingarten, and S.P. Williams, *The first X-ray crystal structure of the glucocorticoid receptor bound to a non-steroidal agonist.* Bioorg Med Chem Lett, 2008. **18**(23): p. 6097-6099.

270. Biggadike, K., R.K. Bledsoe, A.M. Hassell, B.E. Kirk, I.M. McLay, L.M. Shewchuk, and E.L. Stewart, *X-ray crystal structure of the novel enhanced-affinity glucocorticoid agonist fluticasone furoate in the glucocorticoid receptor-ligand binding domain.* J Med Chem, 2008. **51**(12): p. 3349-3352.

271. Suino-Powell, K., Y. Xu, C. Zhang, Y.G. Tao, W.D. Tolbert, S.S. Simons, and H.E. Xu, *Doubling the size of the glucocorticoid receptor ligand binding pocket by deacylcortivazol.* Mol Cell Biol, 2008. **28**(6): p. 1915-1923.

272. Bledsoe, R.K., V.G. Montana, T.B. Stanley, C.J. Delves, C.J. Apolito, D.D. McKee, T.G. Consler, D.J. Parks, E.L. Stewart, T.M. Willson, M.H. Lambert, J.T. Moore, K.H. Pearce, and H.E. Xu, *Crystal structure of the glucocorticoid receptor ligand binding domain reveals a novel mode of receptor dimerization and coactivator recognition.* Cell, 2002. **110**(1): p. 93-105.

273. Kauppi, B., C. Jakob, M. Farnegardh, J. Yang, H. Ahola, M. Alarcon, K. Calles, O. Engstrom, J. Harlan, S. Muchmore, A.K. Ramqvist, S. Thorell, L. Ohman, J. Greer, J.A. Gustafsson, J. Carlstedt-Duke, and M. Carlquist, *The three-dimensional structures of antagonistic and agonistic forms of the glucocorticoid receptor ligand-binding domain: RU-486 induces a transconformation that leads to active antagonism.* J Biol Chem, 2003. **278**(25): p. 22748-22754.

274. Patel, R., J. Williams-Dautovich, and C.L. Cummins, *Minireview: New molecular mediators of glucocorticoid receptor activity in metabolic tissues.* Mol Endocrinol, 2014. **28**(7): p. 999-1011.

275. Murakami, M. and I. Kudo, *Phospholipase A2.* J Biochem, 2002. **131**(3): p. 285-292.

276. Irwin, J.J., T. Sterling, M.M. Mysinger, E.S. Bolstad, and R.G. Coleman, *ZINC: A free tool to discover chemistry for biology.* J Chem Inf Model, 2012. **52**(7): p. 1757-1768.

277. de Rosa, S., A. Crispino, A. de Giulio, C. Iodice, R. Pronzato, and N. Zabodnik, *Cacospongionolide B, a new sesterterpene from the sponge Fasciospongia cavernosa.* J Nat Prod, 1995. **58**(11): p. 1776-1780.

278. Keiser, M.J., B.L. Roth, B.N. Armbruster, P. Ernsberger, J.J. Irwin, and B.K. Shoichet, *Relating protein pharmacology by ligand chemistry.* Nat Biotech, 2007. **25**(2): p. 197-206.

279. Pastor, P.G., S. De Rosa, A. De Giulio, M. Payá, and M.J. Alcaraz, *Modulation of acute and chronic inflammatory processes by cacospongionolide B, a novel inhibitor of human synovial phospholipase A2.* Brit J Pharmacol, 1999. **126**(1): p. 301-311.

280. Lu, X., K. Huang, and Q. You, *Enoyl acyl carrier protein reductase inhibitors: A patent review (2006 - 2010).* Expert Opin Ther Pat, 2011. **21**(7): p. 1007-1022.

281. Sharma, S., T.N.C. Ramya, A. Surolia, and N. Surolia, *Triclosan as a systemic antibacterial agent in a mouse model of acute bacterial challenge.* Antimicrob Agents Chemother, 2003. **47**(12): p. 3859-3866.

282. Muhammad, A., I. Anis, Z. Ali, S. Awadelkarim, A. Khan, A. Khalid, M.R. Shah, M. Galal, I.A. Khan, and M. Iqbal Choudhary, *Methylenebissantin: A rare methylene-bridged bisflavonoid from Dodonaea viscosa which inhibits Plasmodium falciparum enoyl-ACP reductase.* Bioorg Med Chem Lett, 2012. **22**(1): p. 610-612.

283. Tanimoto, T., *An elementary mathematical theory of classification and prediction*. Internal IBM Technical Report. Vol. 8. 1957: IBM. 10.

284. Cereto-Massague, A., M.J. Ojeda, C. Valls, M. Mulero, S. Garcia-Vallve, and G. Pujadas, *Molecular fingerprint similarity search in virtual screening.* Methods, 2015. **71**: p. 58-63.

285. Nicholls, A., G.B. McGaughey, R.P. Sheridan, A.C. Good, G. Warren, M. Mathieu, S.W. Muchmore, S.P. Brown, J.A. Grant, J.A. Haigh, N. Nevins, A.N. Jain, and B. Kelley, *Molecular shape and medicinal chemistry: A perspective.* J Med Chem, 2010. **53**(10): p. 3862-3886.

286. van Drie, J.H., *Pharmacophore discovery--lessons learned.* Curr Pharm Des, 2003. **9**(20): p. 1649-64.

287. McGaughey, G.B., R.P. Sheridan, C.I. Bayly, J.C. Culberson, C. Kreatsoulas, S. Lindsley, V. Maiorov, J.F. Truchon, and W.D. Cornell, *Comparison of topological, shape, and docking methods in virtual screening.* J Chem Inf Model, 2007. **47**(4): p. 1504-1519.

288. Hawkins, P.C.D., A.G. Skillman, and A. Nicholls, *Comparison of shape-matching and docking as virtual screening tools.* J Med Chem, 2007. **50**(1): p. 74-82.

289. OpenEye. *Docking Algorithm*. 2012; Available from: **https://docs.eyesopen.com/oedocking/algorithm.html**.

290. Kruger, D.M. and A. Evers, *Comparison of structure- and ligand-based virtual screening protocols considering hit list complementarity and enrichment factors.* ChemMedChem, 2010. **5**(1): p. 148-158.

291. Noha, S.M., A.G. Atanasov, D. Schuster, P. Markt, N. Fakhrudin, E.H. Heiss, O. Schrammel, J.M. Rollinger, H. Stuppner, V.M. Dirsch, and G. Wolber, *Discovery of a novel IKK-β inhibitor by ligand-based virtual screening techniques.* bioorg Med Chem Lett, 2011. **21**(1): p. 577-583.

292. Vilar, S. and S. Costanzi, *Predicting the biological activities through QSAR analysis and docking-based scoring.* Methods Mol Biol, 2012. **914**: p. 271-84.

293. Enyedy, I.J. and W.J. Egan, *Can we use docking and scoring for hit-to-lead optimization?* J Comput Aided Mol Des, 2008. **22**(3-4): p. 161-168.

294. Urban, P., G. Truan, and D. Pompon, *Access channels to the buried active site control substrate specificity in CYP1A P450 enzymes.* Biochim Biophys Acta, 2015. **1850**(4): p. 696-707.

295. Furse, K.E., D.A. Pratt, C. Schneider, A.R. Brash, N.A. Porter, and T.P. Lybrand, *Molecular dynamics simulations of arachidonic acid-derived pentadienyl radical intermediate complexes with COX-1 and COX-2: Insights into oxygenation regio and stereoselectivity.* Biochemistry, 2006. **45**(10): p. 3206-3218.

296. Kingsley, L.J. and M.A. Lill, *Substrate tunnels in enzymes: Structure-function relationships and computational methodology.* Proteins, 2015. **83**(4): p. 599-611.

297. Huang, Q., Q. Liu, and Q. Hao, *Crystal structures of Fms1 and its complex with spermine reveal substrate specificity.* J Mol Biol, 2005. **348**(4): p. 951-959.

298. Dimova, D., K. Heikamp, D. Stumpfe, and J. Bajorath, *Do medicinal chemists learn from activity cliffs? A systematic evaluation of cliff progression in evolving compound data sets.* J Med Chem, 2013. **56**(8): p. 3339-3345.

299. Stumpfe, D., Y. Hu, D. Dimova, and J. Bajorath, *Recent progress in understanding activity cliffs and their utility in medicinal chemistry.* J Med Chem, 2014. **57**(1): p. 18-28.

300. Tidgewell, K., W.W. Harding, A. Lozama, H. Cobb, K. Shah, P. Kannan, C.M. Dersch, D. Parrish, J.R. Deschamps, R.B. Rothman, and T.E. Prisinzano, *Synthesis*

of salvinorin A analogues as opioid receptor probes. J Nat Prod, 2006. **69**(6): p. 914-918.

301. Prisinzano, T.E. and R.B. Rothman, *Salvinorin A analogs as probes in opioid pharmacology.* Chem Rev, 2008. **108**(5): p. 1732-1743.
302. Riley, A.P., C.E. Groer, D. Young, A.W. Ewald, B.M. Kivell, and T.E. Prisinzano, *Synthesis and κ-opioid receptor activity of furan-substituted salvinorin A analogues.* J Med Chem, 2014. **57**(24): p. 10464-10475.
303. Butelman, E.R., S. Rus, D.S. Simpson, A. Wolf, T.E. Prisinzano, and M.J. Kreek, *The effects of herkinorin, the first mu-selective ligand from a salvinorin A-derived scaffold, in a neuroendocrine biomarker assay in nonhuman primates.* J Pharmacol Exp Ther, 2008. **327**(1): p. 154-60.
304. Lamb, K., K. Tidgewell, D.S. Simpson, L.M. Bohn, and T.E. Prisinzano, *Antinociceptive effects of herkinorin, a MOP receptor agonist derived from salvinorin A in the formalin test in rats: New concepts in μ-opioid receptor pharmacology: From a symposium on new concepts in mu-opioid pharmacology.* Drug Alcohol Depen, 2012. **121**(3): p. 181-188.
305. Groer, C.E., K. Tidgewell, R.A. Moyer, W.W. Harding, R.B. Rothman, T.E. Prisinzano, and L.M. Bohn, *An opioid agonist that does not induce μ-opioid receptor-arrestin interactions or receptor internalization.* Mol Pharmacol, 2007. **71**(2): p. 549-557.
306. Williams, J.T., S.L. Ingram, G. Henderson, C. Chavkin, M. von Zastrow, S. Schulz, T. Koch, C.J. Evans, and M.J. Christie, *Regulation of μ-Opioid Receptors: Desensitization, Phosphorylation, Internalization, and Tolerance.* Pharmacol rev, 2013. **65**(1): p. 223-254.
307. Huang, W., A. Manglik, A.J. Venkatakrishnan, T. Laeremans, E.N. Feinberg, A.L. Sanborn, H.E. Kato, K.E. Livingston, T.S. Thorsen, R.C. Kling, S. Granier, P. Gmeiner, S.M. Husbands, J.R. Traynor, W.I. Weis, J. Steyaert, R.O. Dror, and B.K. Kobilka, *Structural insights into μ-opioid receptor activation.* Nature, 2015. **524**(7565): p. 315-321.
308. Kane, B.E., M.J. Nieto, C.R. McCurdy, and D.M. Ferguson, *A unique binding epitope for salvinorin A, a non-nitrogenous κ-opioid receptor agonist.* FEBS J, 2006. **273**(9): p. 1966-1974.

309. Simpson, B.S., *Extraction of PAA from Dodonaea polyandra*, M.Y. Bendikov, Editor. 2011: Adelaide.

310. Hevener, K.E., W. Zhao, D.M. Ball, K. Babaoglu, J. Qi, S.W. White, and R.E. Lee, *Validation of molecular docking programs for virtual screening against dihydropteroate synthase.* J Chem Inf Model, 2009. **49**(2): p. 444-460.

311. Wieder, E.D. and M.H. Fox, *Isolation and characterization of a Chinese hamster ovary cell mutant with improved staining for indo-1.* Cytometry, 1994. **17**(1): p. 33-8.

312. Inokuma, Y., S. Yoshioka, J. Ariyoshi, T. Arai, Y. Hitora, K. Takada, S. Matsunaga, K. Rissanen, and M. Fujita, *X-ray analysis on the nanogram to microgram scale using porous complexes.* Nature, 2013. **495**(7442): p. 461-466.

313. Marmolejo-Valencia, A.F. and K. Martinez-Mayorga, *Allosteric modulation model of the μ-opioid receptor by herkinorin, a potent not alkaloidal agonist.* J Comput Aided Mol Des, 2017. **31**(5): p. 467-482.

314. Hoshino, M., A. Khutia, H. Xing, Y. Inokuma, and M. Fujita, *The crystalline sponge method updated.* IUCrJ, 2016. **3**(2): p. 139-151.

315. Sahai, J., K. Gallicano, A. Pakuts, and D.W. Cameron, *Effect of fluconazole on zidovudine pharmacokinetics in patients infected with human immunodeficiency virus.* J Infect Dis, 1994. **169**(5): p. 1103-1107.

316. Stepan, A.F., D.P. Walker, J. Bauman, D.A. Price, T.A. Baillie, A.S. Kalgutkar, and M.D. Aleo, *Structural alert/reactive metabolite concept as applied in medicinal chemistry to mitigate the risk of idiosyncratic drug toxicity: A perspective based on the critical examination of trends in the top 200 drugs marketed in the United States.* Chem Res Toxicol, 2011. **24**(9): p. 1345-1410.

317. Kouzi, S.A., R.J. McMurty, and S.D. Nelson, *Hepatotoxicity of germander (Teucrium chamaedrys L.) and one of its constituent neoclerodane diterpenes teucrin A in the mouse.* Chem Res Toxicol, 1994. **7**(6): p. 850-856.

318. Erve, J.C., S.C. Vashishtha, O. Ojewoye, A. Adedoyin, R. Espina, W. Demaio, and R.E. Talaat, *Metabolism of prazosin in rat and characterization of metabolites in plasma, urine, faeces, brain and bile using liquid chromatography/mass spectrometry (LC/MS).* Xenobiotica, 2008. **38**(5): p. 540-558.

319. Yang, K.H., Y.H. Choi, U. Lee, J.H. Lee, and M.G. Lee, *Effects of cytochrome P450 inducers and inhibitors on the pharmacokinetics of intravenous furosemide in rats:*

involvement of CYP2C11, 2E1, 3A1 and 3A2 in furosemide metabolism. J Pharm Pharmacol, 2009. **61**(1): p. 47-54.

320. Manjiani, D., D.B. Paul, S. Kunnumpurath, A.D. Kaye, and N. Vadivelu, *Availability and utilization of opioids for pain management: Global issues.* The Ochsner Journal, 2014. **14**(2): p. 208-215.
321. Kirchmair, J., A.H. Goller, D. Lang, J. Kunze, B. Testa, I.D. Wilson, R.C. Glen, and G. Schneider, *Predicting drug metabolism: Experiment and/or computation?* Nat Rev Drug Discov, 2015. **14**(6): p. 387-404.
322. Yin, L., L. Zheng, L. Xu, D. Dong, X. Han, Y. Qi, Y. Zhao, Y. Xu, and J. Peng, *In-silico prediction of drug targets, biological activities, signal pathways and regulating networks of dioscin based on bioinformatics.* BMC Complem Altern M, 2015. **15**: p. 41.
323. Orry, A.J.W., R.A. Abagyan, and C.N. Cavasotto, *Structure-based development of target-specific compound libraries.* Drug Discov Today, 2006. **11**(5–6): p. 261-266.
324. Matosin, N., E. Frank, M. Engel, J.S. Lum, and K.A. Newell, *Negativity towards negative results: A discussion of the disconnect between scientific worth and scientific culture.* Dis Model Mech, 2014. **7**(2): p. 171-173.
325. Simpson, B.S., D.J. Claudie, J.P. Gerber, S.M. Pyke, J. Wang, R.A. McKinnon, and S.J. Semple, *In Vivo Activity of Benzoyl Ester Clerodane Diterpenoid Derivatives from Dodonaea polyandra.* Journal of Natural Products, 2011. **74**(4): p. 650-657.
326. Rodems, S.M., B.D. Hamman, C. Lin, J. Zhao, S. Shah, D. Heidary, L. Makings, J.H. Stack, and B.A. Pollok, *A FRET-based assay platform for ultra-high density drug screening of protein kinases and phosphatases.* Assay Drug Dev Technol, 2002. **1**(1 Pt 1): p. 9-19.
327. Lowry, O.H., N.J. Rosebrough, A.L. Farr, and R.J. Randall, *Protein measurement with the folin phenol reagent.* J Biol Chem, 1951. **193**(1): p. 265-275.
328. Uchaipichat, V., P.I. Mackenzie, D.J. Elliot, and J.O. Miners, *Selectivity of substrate (trifluroperazine) and inhibitor (amytriptiline, androsterone, canreonic acid, hecogenin, phenylbutazone, quinidine, quinine, and sulfinpyrazone) "probes" for human UDP-glucuronosyltransferases.* Drug Metab Dispos, 2006. **34**(3): p. 449-456.
329. Racha, J.K., A.E. Rettie, and K.L. Kunze, *Mechanism-based inactivation of human cytochrome P450 1A2 by furafylline: Detection of a 1:1 adduct to protein and*

evidence for the formation of a novel imidazomethide intermediate. Biochemistry, 1998. **37**(20): p. 7407-7419.

330. Ha-Duong, N.T., S. Dijols, A.C. Macherey, J.A. Goldstein, P.M. Dansette, and D. Mansuy, *Ticlopidine as a Selective Mechanism-Based Inhibitor of Human Cytochrome P450 2C19†.* Biochemistry, 2001. **40**(40): p. 12112-12122.
331. VandenBrink, B.M., R.S. Foti, D.A. Rock, L.C. Wienkers, and J.L. Wahlstrom, *Evaluation of CYP2C8 Inhibition In Vitro: Utility of Montelukast as a Selective CYP2C8 Probe Substrate.* Drug Metab Dispos, 2011. **39**(9): p. 1546-1554.
332. Mancy, A., S. Dijols, S. Poli, P. Guengerich, and D. Mansuy, *Interaction of sulfaphenazole derivatives with human liver cytochromes P450 2C: Molecular origin of the specific inhibitory effects of sulfaphenazole on CYP 2C9 and consequences for the substrate binding site topology of CYP 2C9.* Biochemistry, 1996. **35**(50): p. 16205-16212.
333. Bramer, S.L. and A. Suri, *Inhibition of CYP2D6 by quinidine and its effects on the metabolism of cilostazol.* Clin Pharmacokinet, 1999. **37**(2): p. 41-51.
334. Uchaipichat, V., P.I. Mackenzie, X.H. Guo, D. Gardner-Stephen, A. Galetin, J.B. Houston, and J.O. Miners, *Human UDP-glucuronosyltransferases: Isoform selectivity and kinetics of 4-methylumbelliferone and 1-napthol glucuronidation, effects of organic solvents, and inhibition by diclofenac and probenecid.* Drug Metab Dispos, 2004. **32**(4): p. 413-423.
335. Parikh, A., E.M.J. Gillam, and F.P. Guengerich, *Drug metabolism by Escherichia coli expressing human cytochromes P450.* Nat Biotech, 1997. **15**(8): p. 784-788.
336. IBM, *IBM SPSS Statistics for Windows, Version 22.0*. 2013, IVM Corp.: Armonk, NY.
337. Zaretzki, J., M. Matlock, and S.J. Swamidass, *XenoSite: Accurately Predicting CYP-Mediated Sites of Metabolism with Neural Networks.* J Chem Inf Model, 2013. **53**(12): p. 3373-3383.
338. Hughes, T.B., G.P. Miller, and S.J. Swamidass, *Modeling epoxidation of drug-like molecules with a deep machine learning network.* ACS Cent Sci, 2015. **1**(4): p. 168-180.
339. Wang, L., C. Ma, P. Wipf, H. Liu, W. Su, and X.Q. Xie, *TargetHunter: an in silico target identification tool for predicting therapeutic potential of small organic molecules based on chemogenomic database.* AAPS J, 2013. **15**(2): p. 395-406.

Appendix 1: MS fragmentation of peaks corresponding to PAAH-glucuronide (523.22 Da)

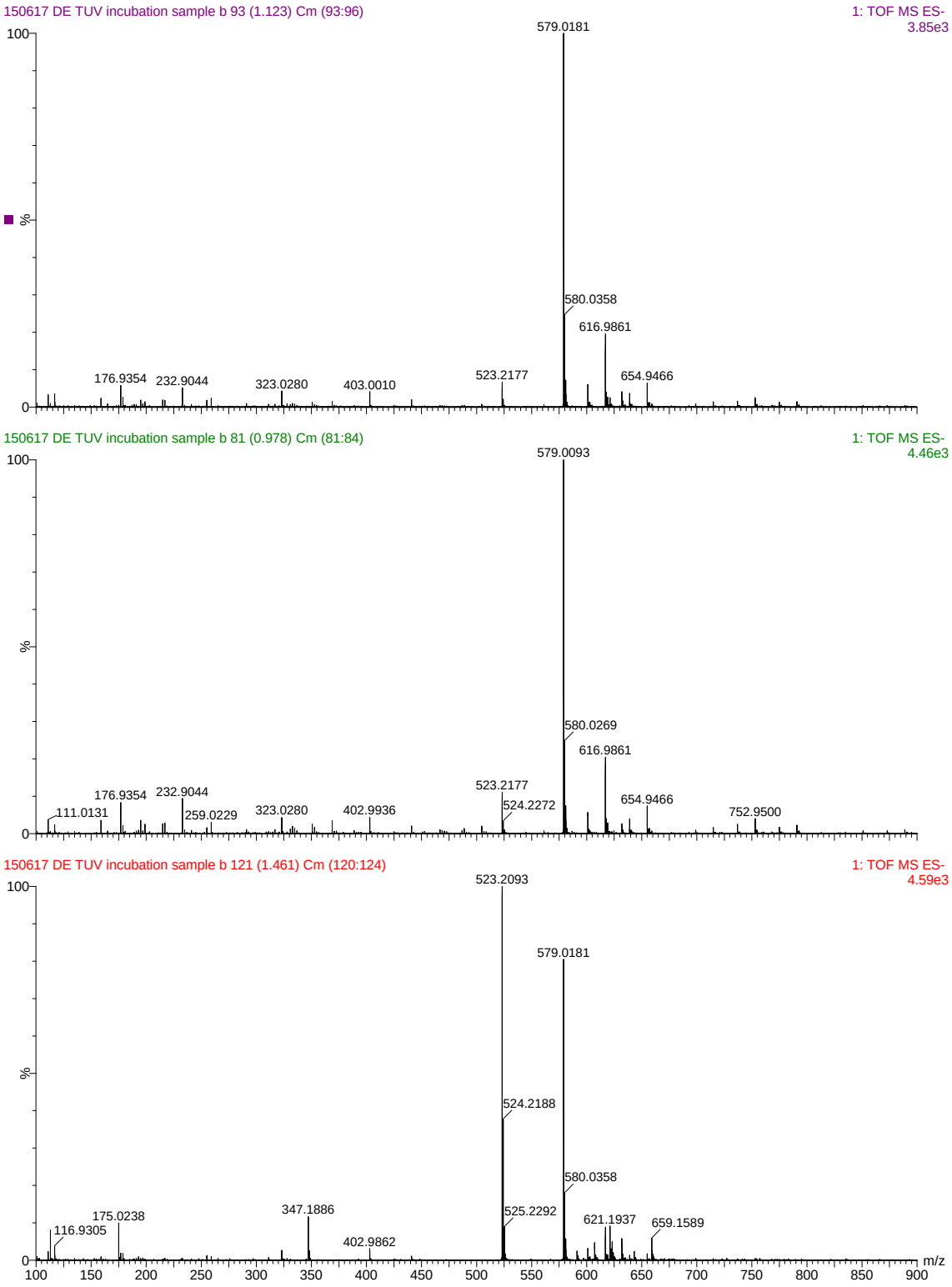

MS instrument: Waters Q-Tof Premier

Scan mode: Negative ion $[M-H]^-$

Appendix 2: 2D-structures of caspase-1 inhibitors retrieved from PDB crystal structures.

Compound name	Structure
1	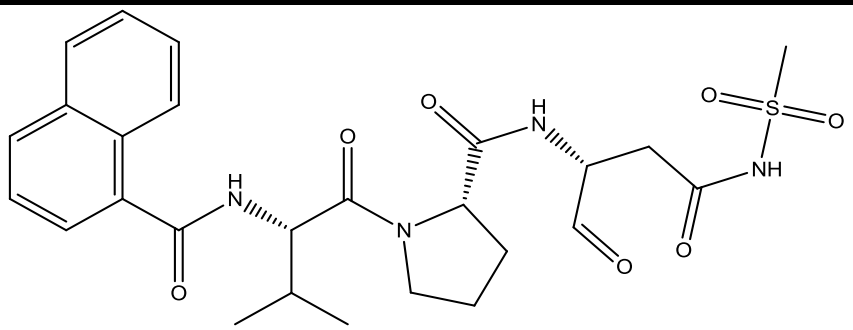
2	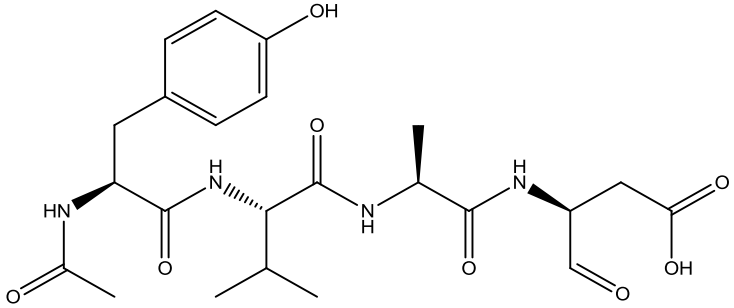
3	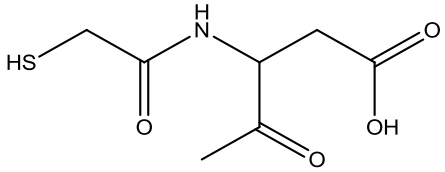
4	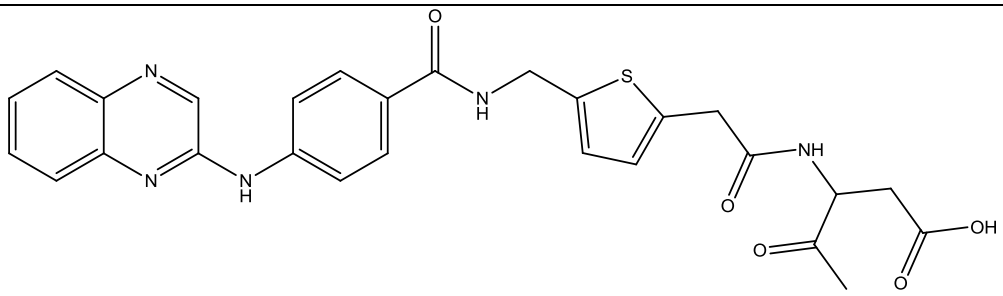
5	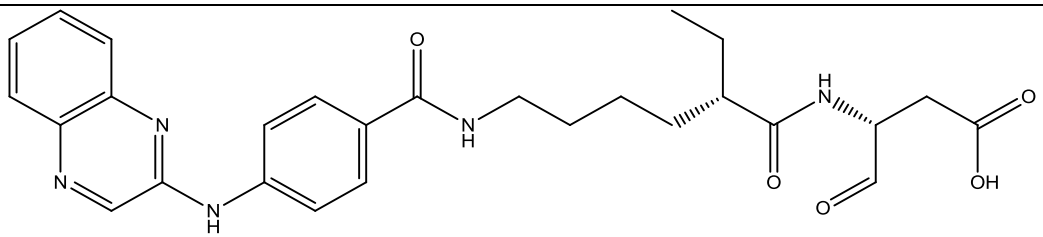

6	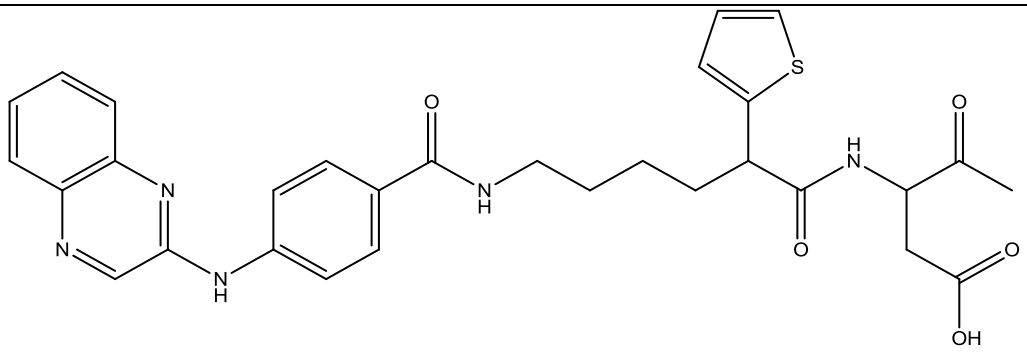
7	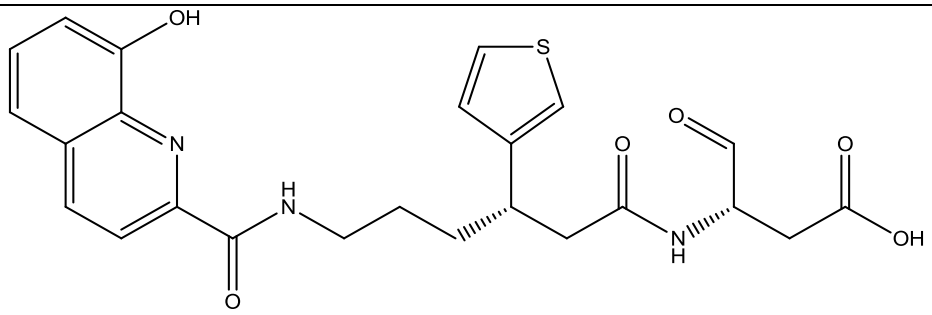
8	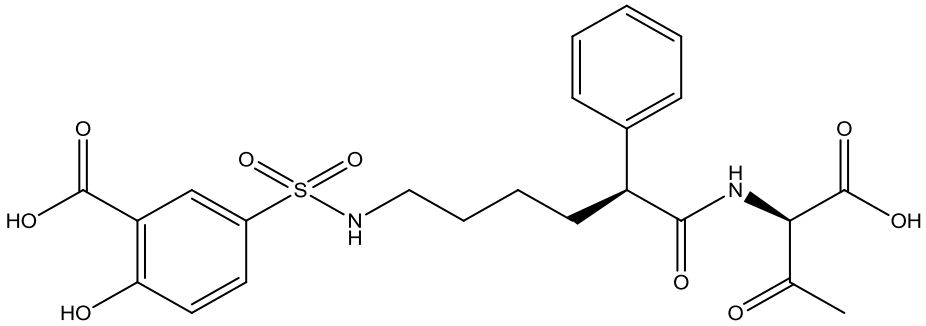
9	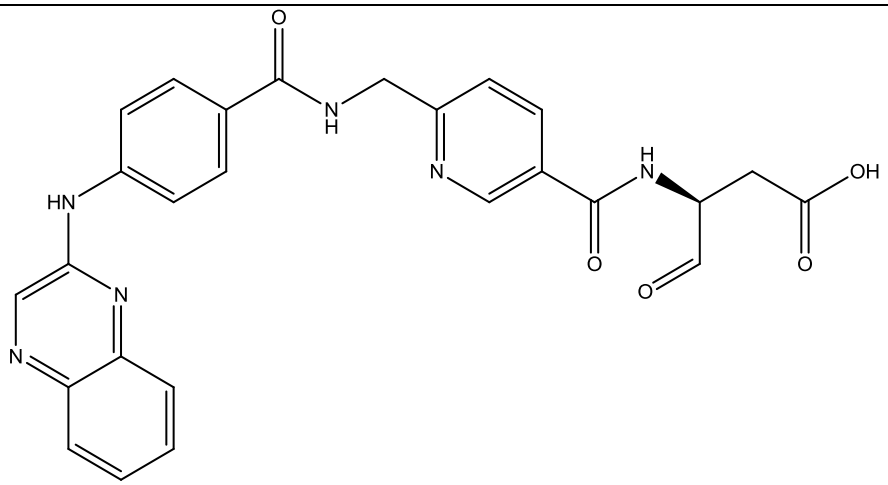

10	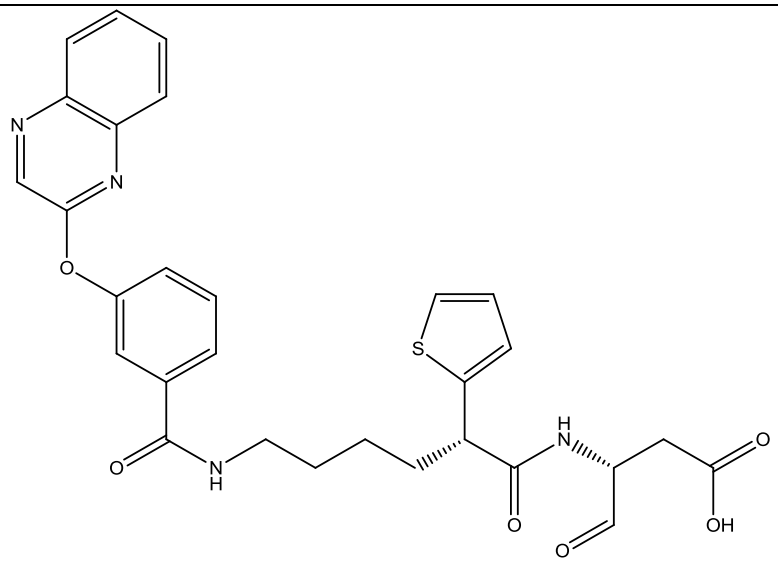
11	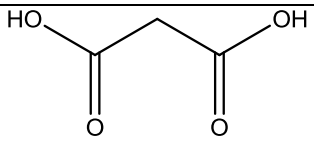
12	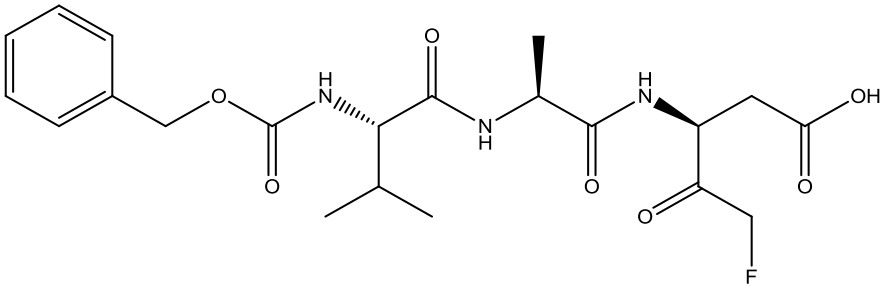
13	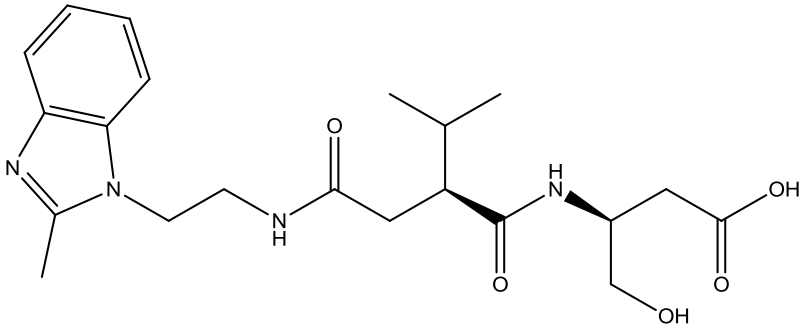

Appendix 3: 2D-structures of PKC inhibitors retrieved from literature.

Compound name	Structure
C-1	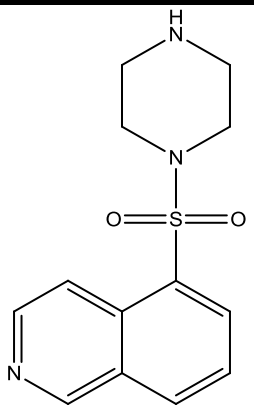
Go 6976	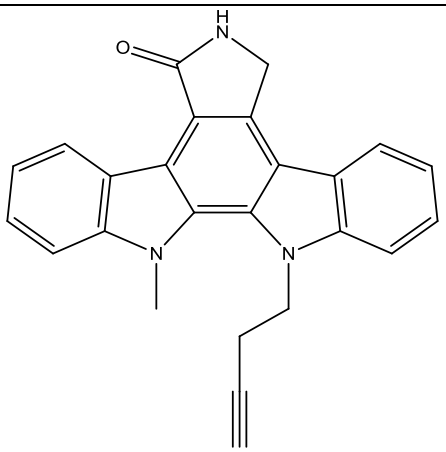
CGP 53353	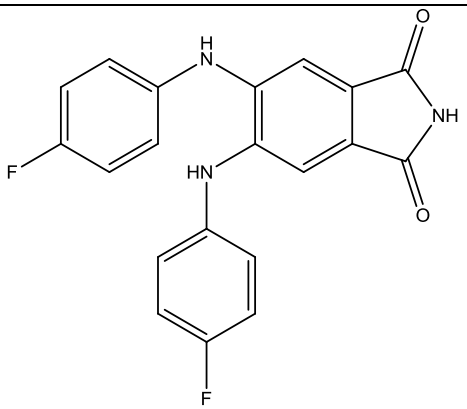
K-252c	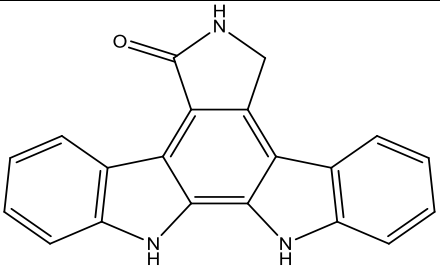

Go 6983	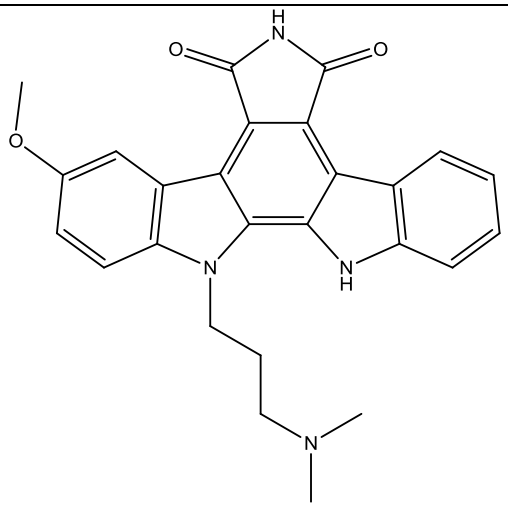
Chelerythrine	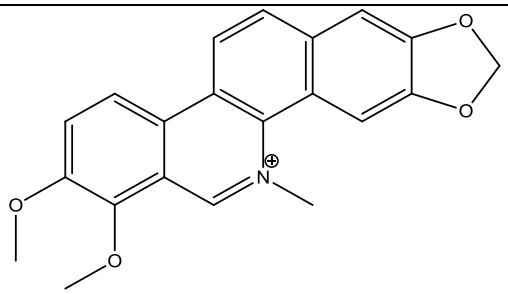
D-erythro-Sphingosine	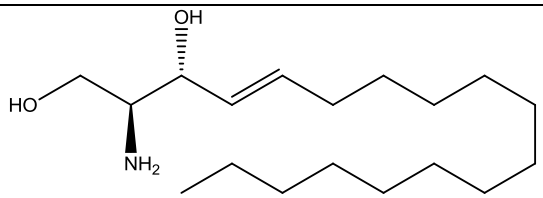
Ro 32-0432	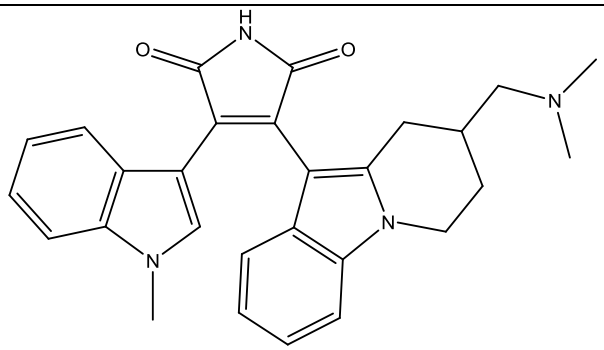
GF 109203X	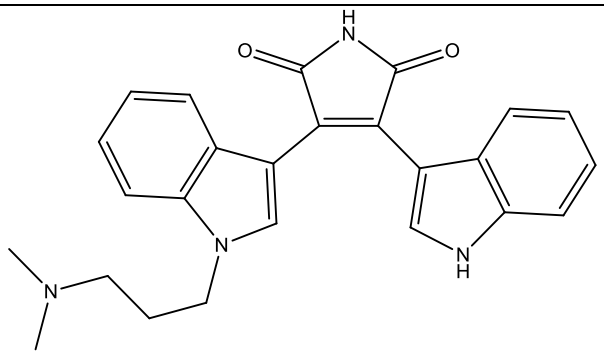

Rottlerin	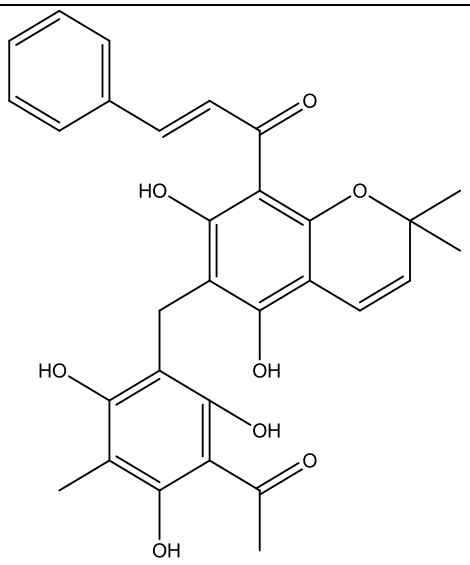
Bisindolylmaleimide II	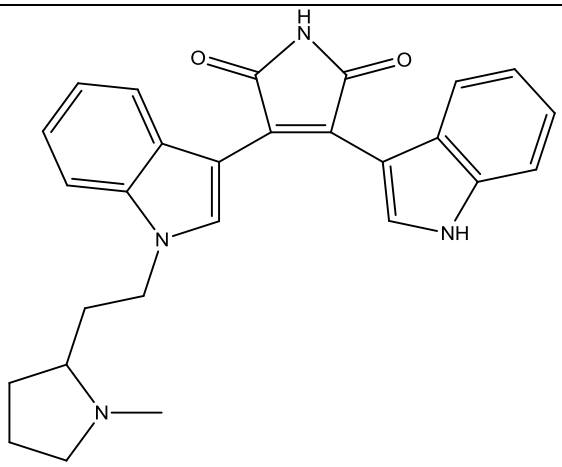
LY 333531	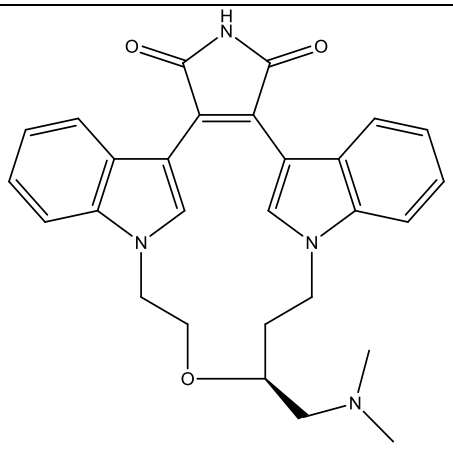

PKC 412	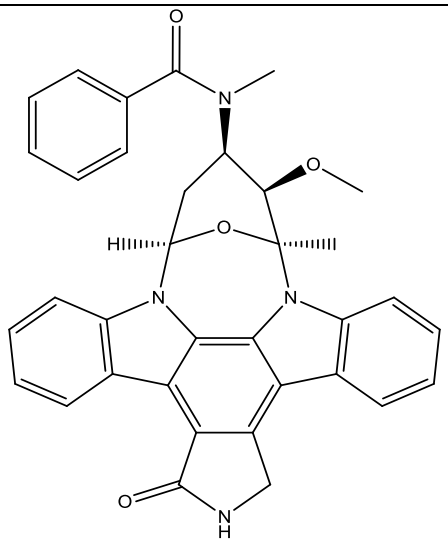
TCS 21311	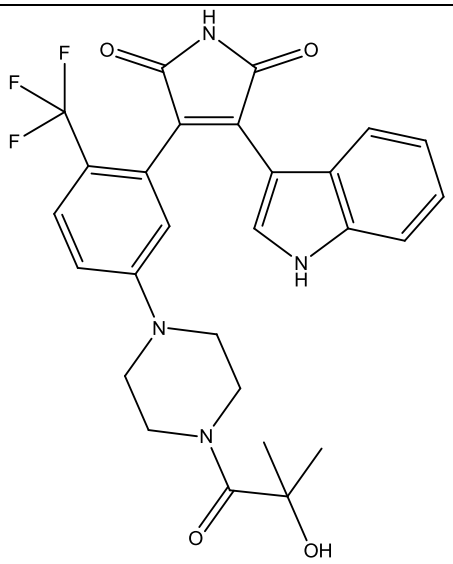
Calphostin C	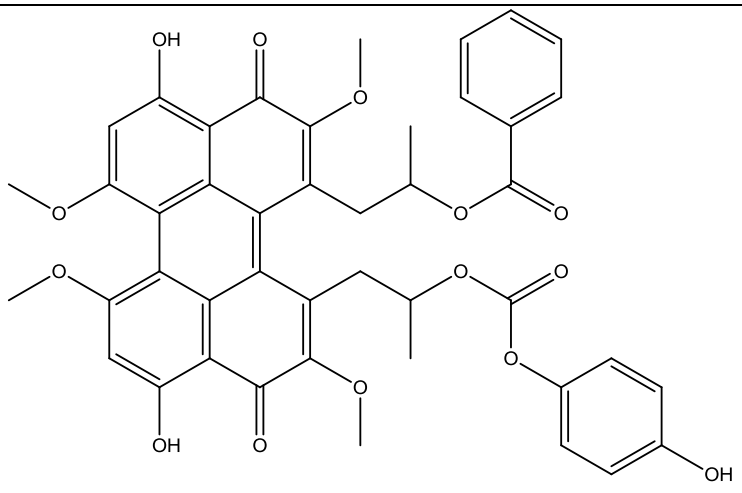

Appendix 4: 2D-structures of NF-κB inhibitors retrieved from literature.

Compound name	Structure
Andrographolide	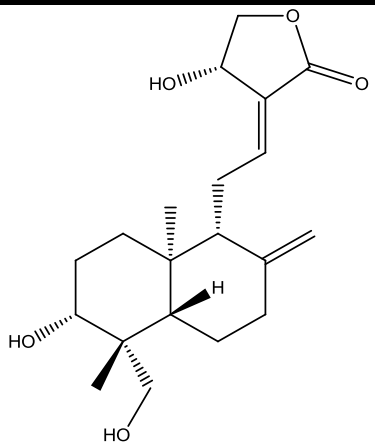
Cardamonin	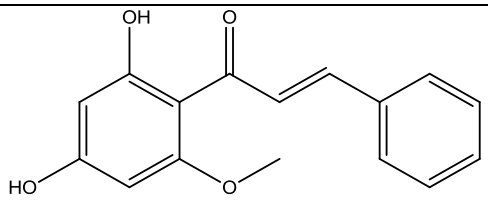
Caffeic acid phenethyl ester	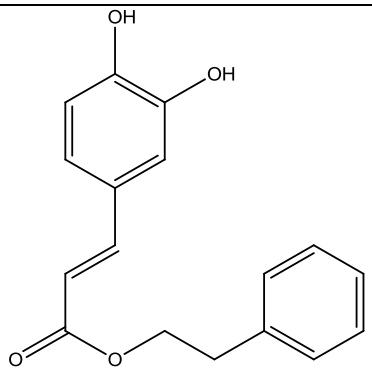
ML 120B	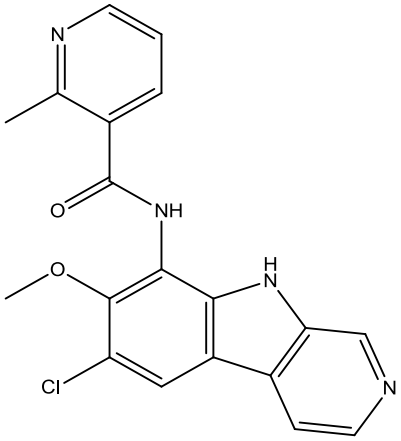

PS 1145	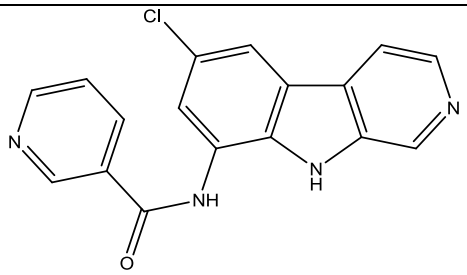
Arctigenin	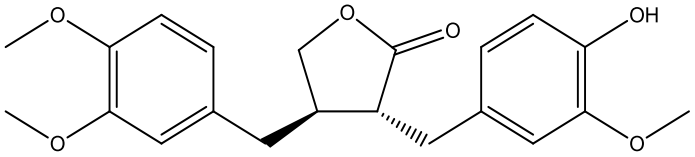
Tanshinone IIA	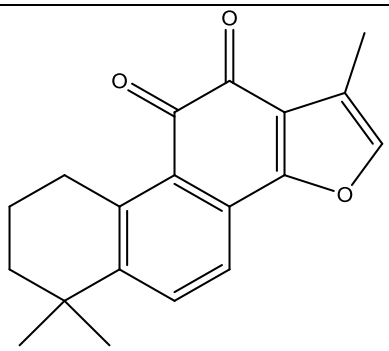
ML 130	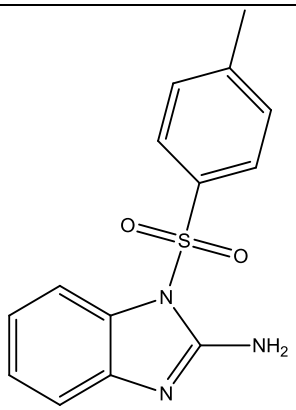
Ro 106-9920	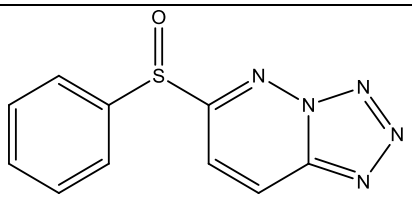
Honokiol	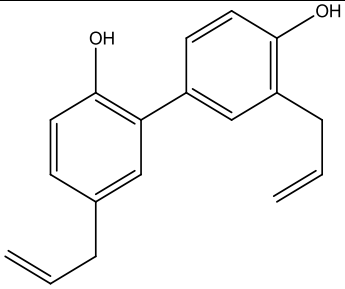

Bay 11-7085	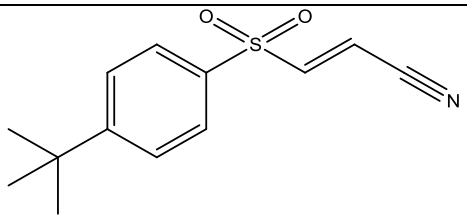
HU 211	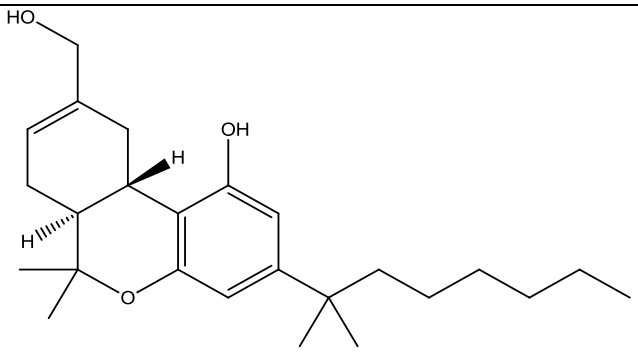
Gliotoxin	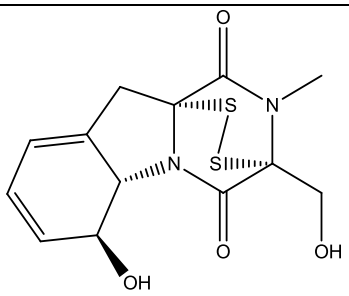
10Z-Hymenialdisine	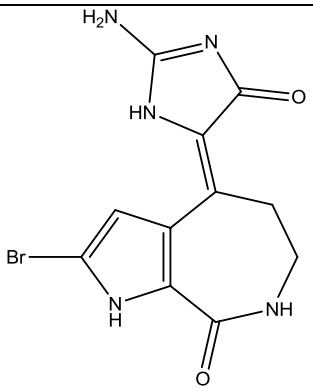
Bay 11-7821	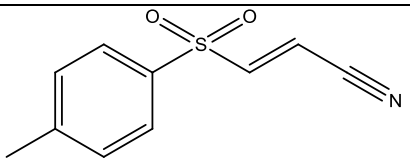
Amlexanox	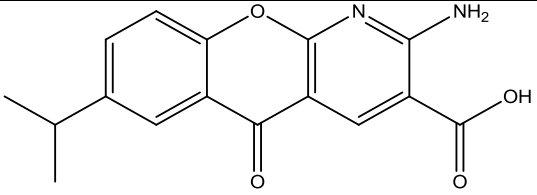

ACHP	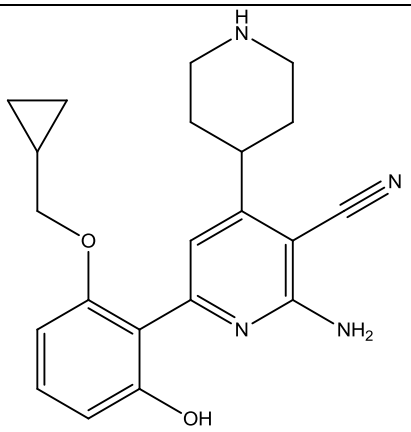
TPCA-1	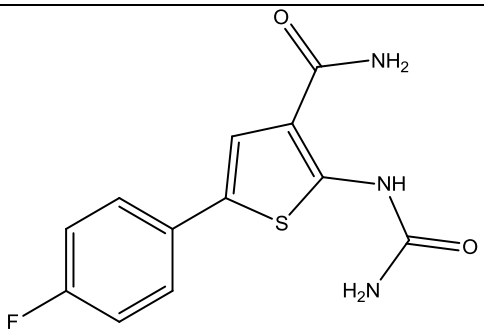
Luteolin	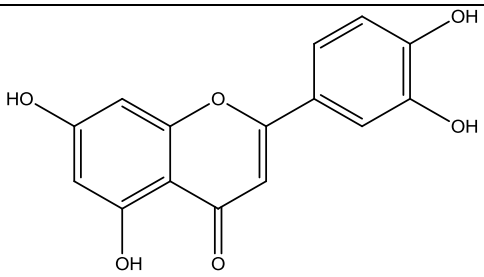
SC 514	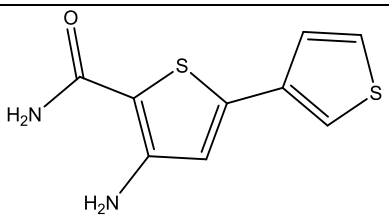
IMD 0354	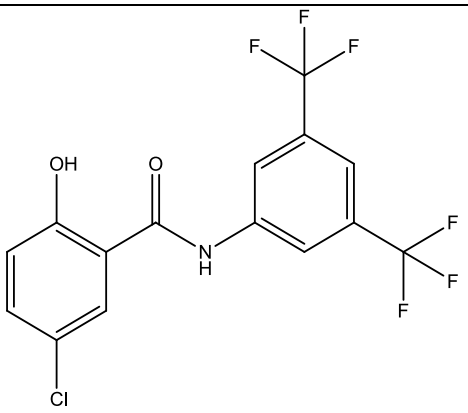

CID 2858522	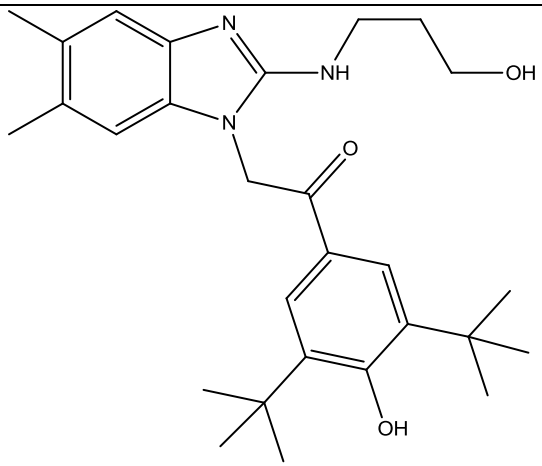
Sulfasalazine	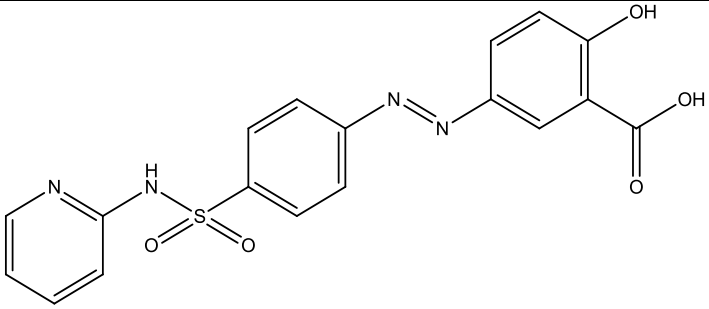
SP 100030	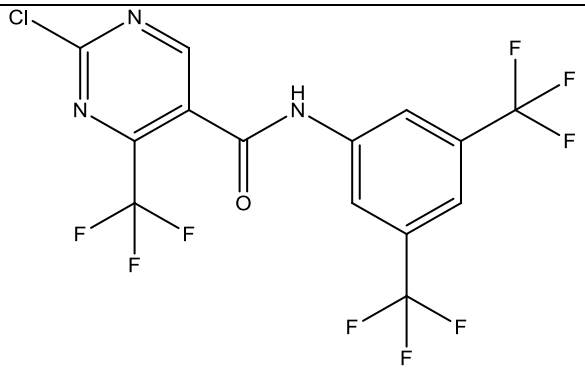
BMS 345541	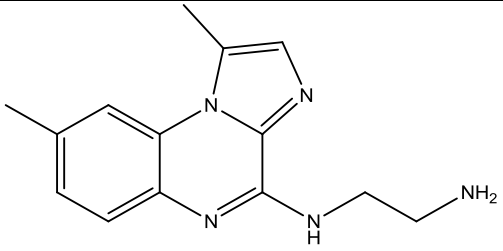

Piceatannol	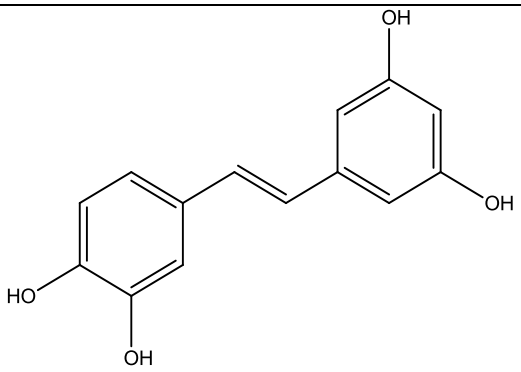
Celastrol	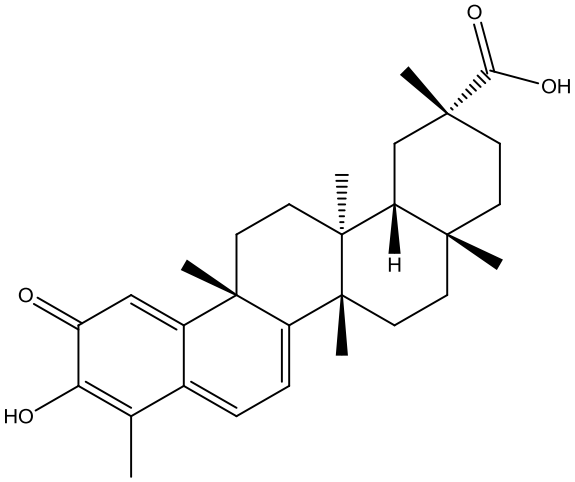
Pristimerin	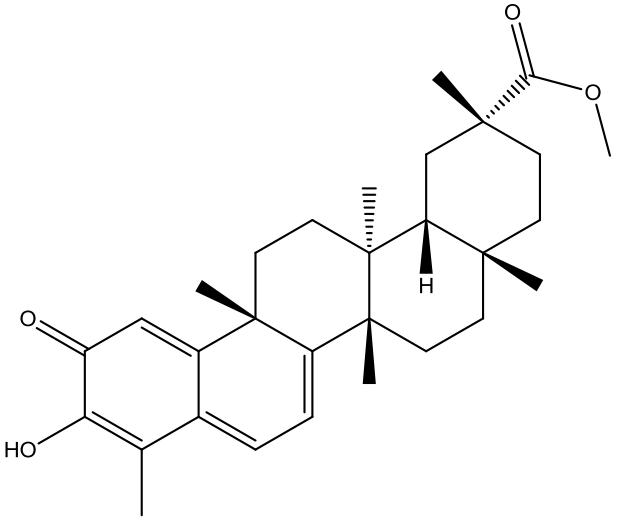

IKK 16	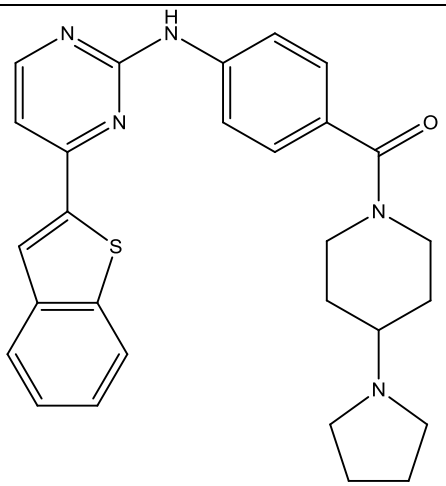
PF 184	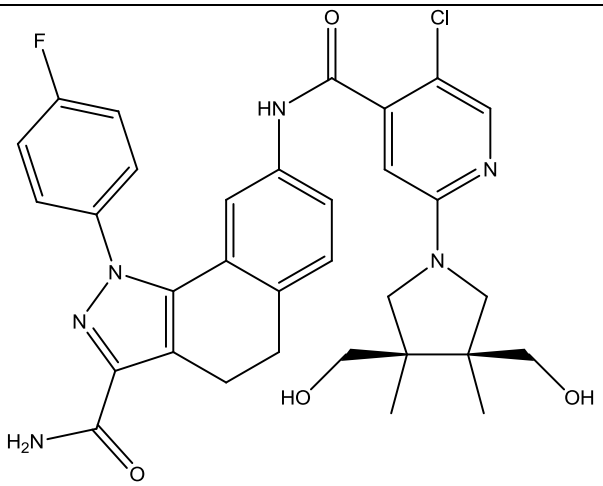
Bengamide_B	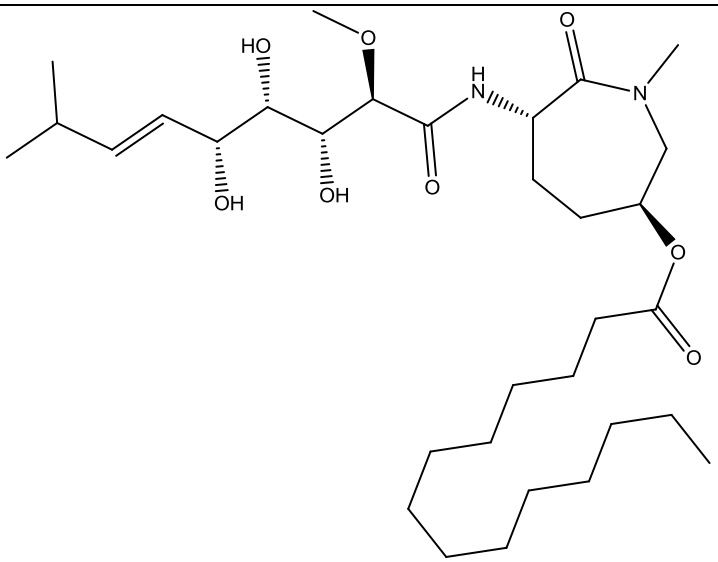

Appendix 5: 2D-structures of glucocorticoid modulators from Onnis et al. (2010).

Compound name	Structure
GR1	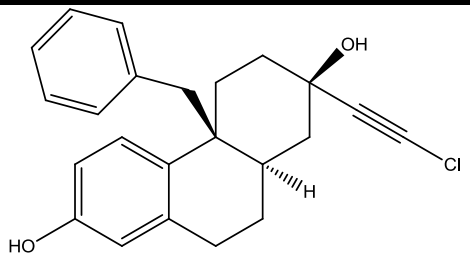
GR2	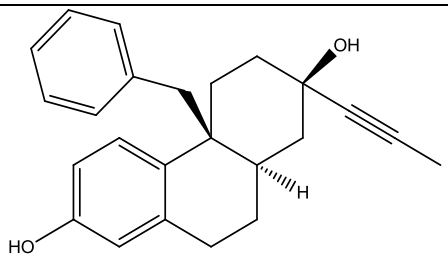
GR3	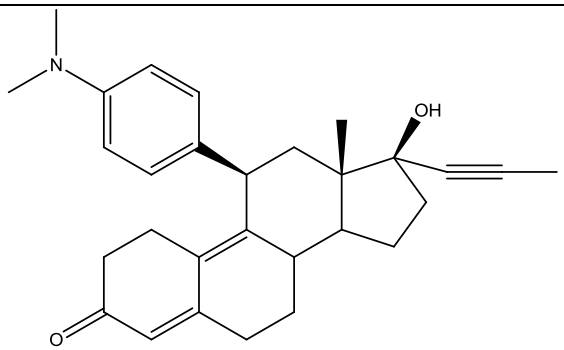
GR4	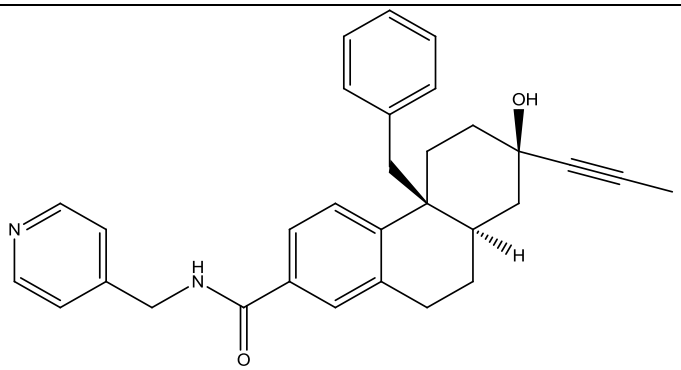
GR5	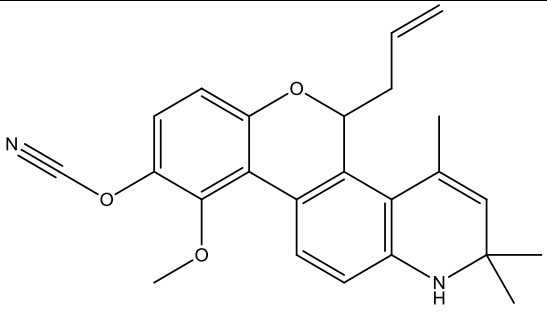

GR6	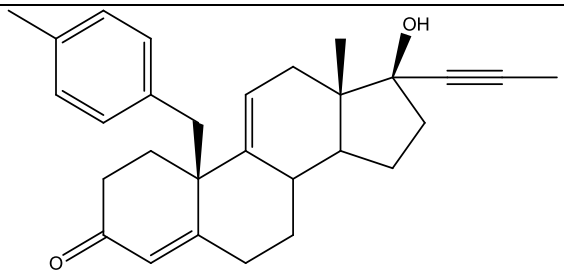
GR7	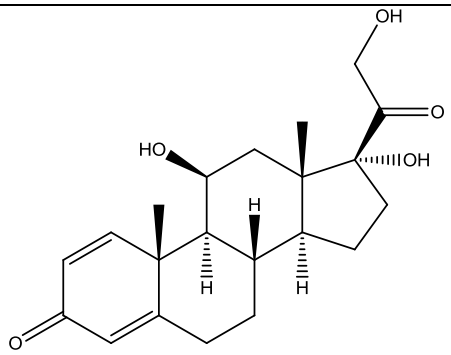
GR8	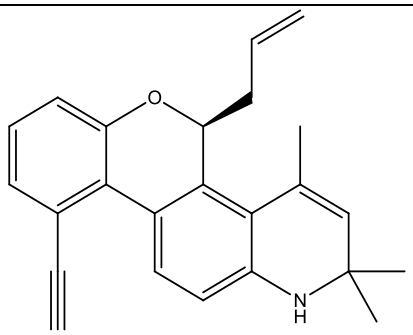
GR9	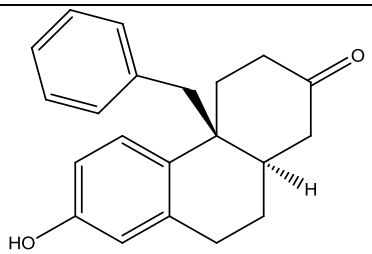
GR10	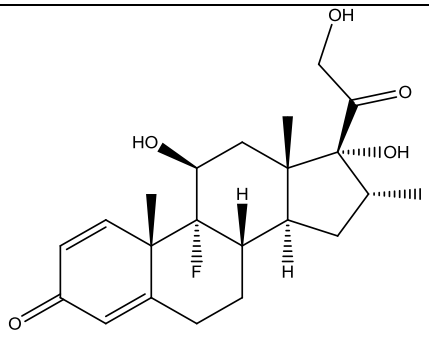

GR11	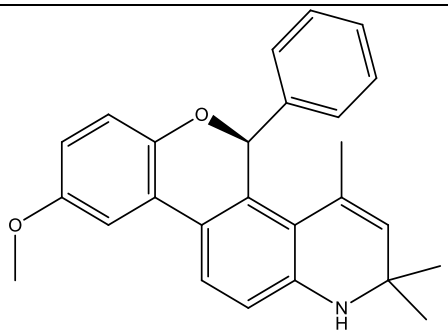
GR12	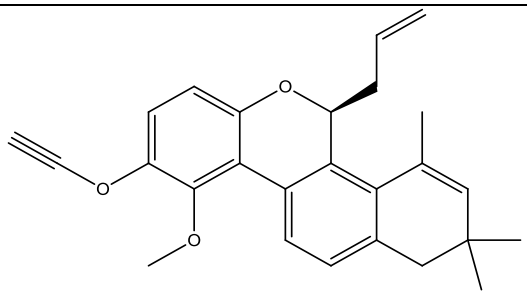
GR13	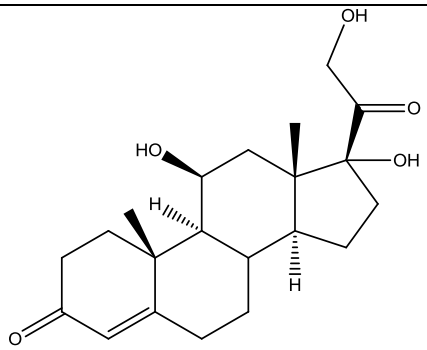
GR14	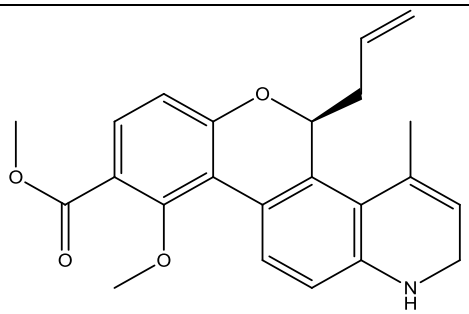
GR15	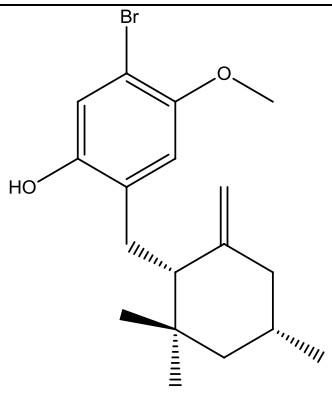

GR16	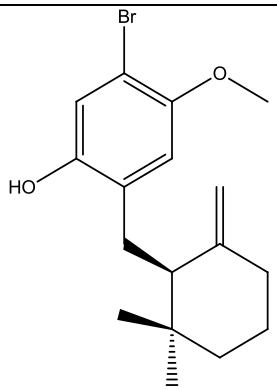
GR17	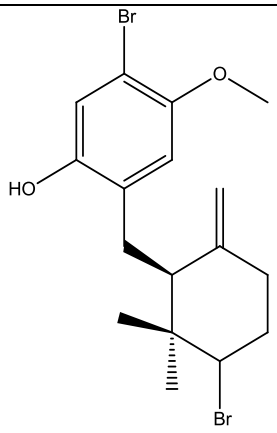
GR18	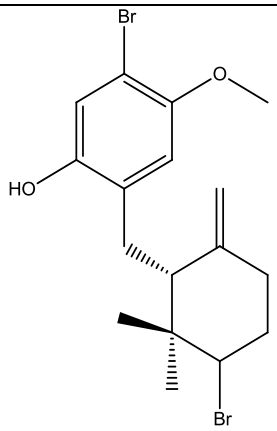
GR19	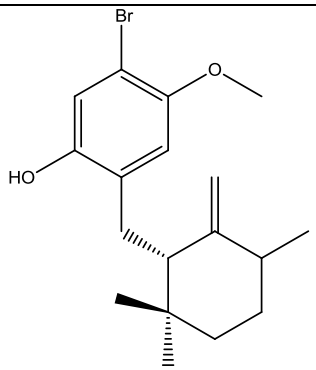

Appendix 6: 2D-structures of glucocorticoid agonists accessed from RCSB PDB.

Compound name	Structure
Dexamethasone	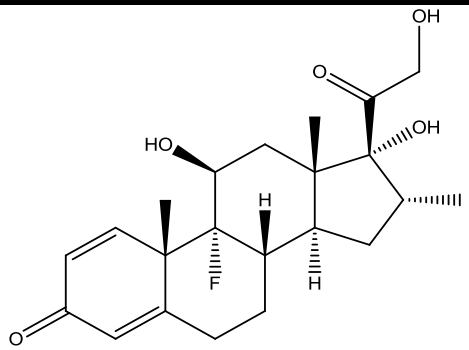
Desisobutyrylciclesonide	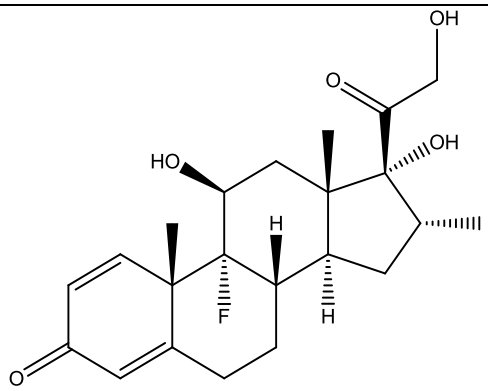
NN7	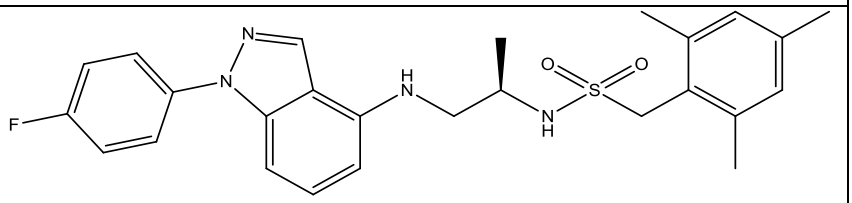
Mometasone furoate	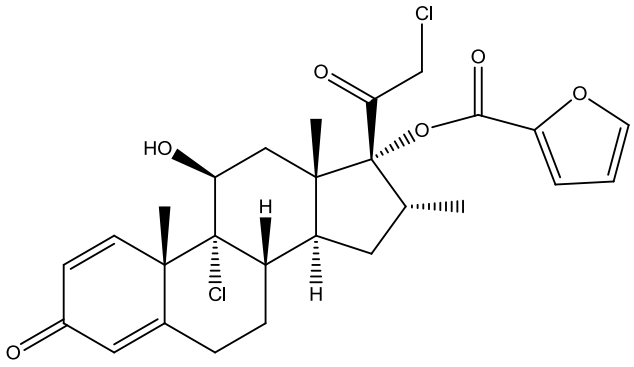

Cortisol	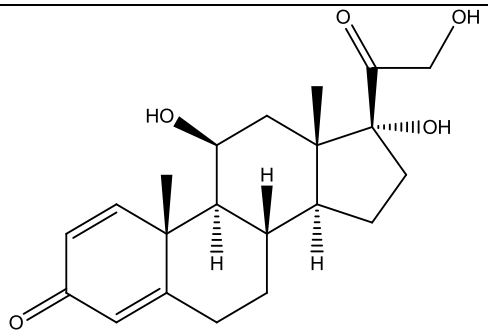
Dibenzoxapine sulfonamide	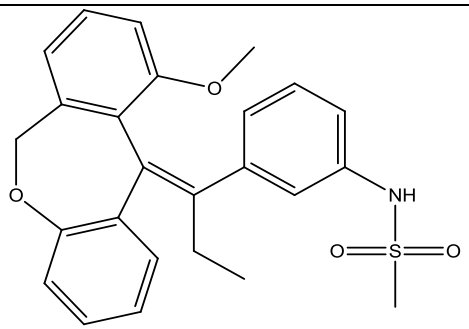
Alaninamide	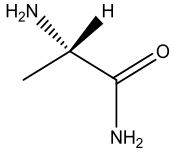
D-prolinamide	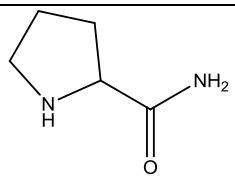
GSK866	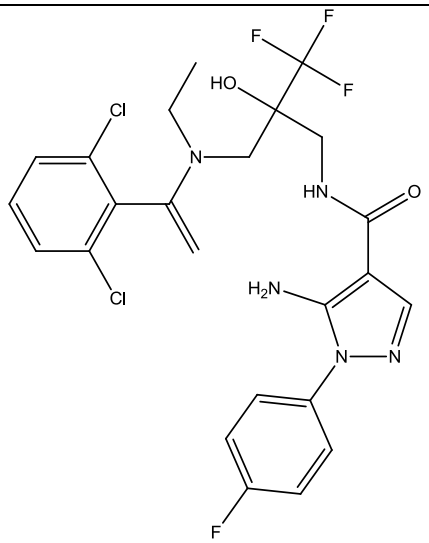

Fluticasone furoate	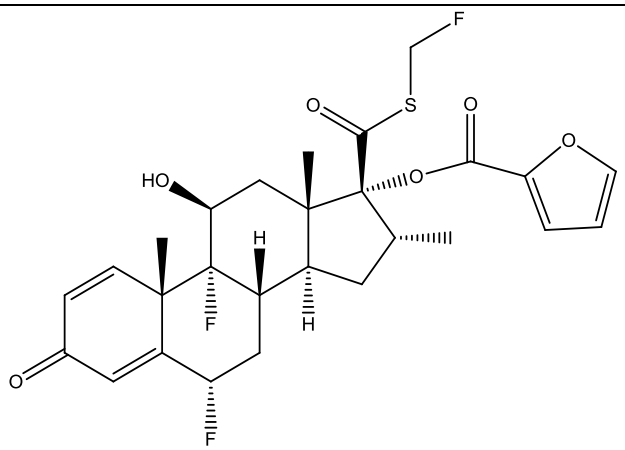
Deacylcortivazol	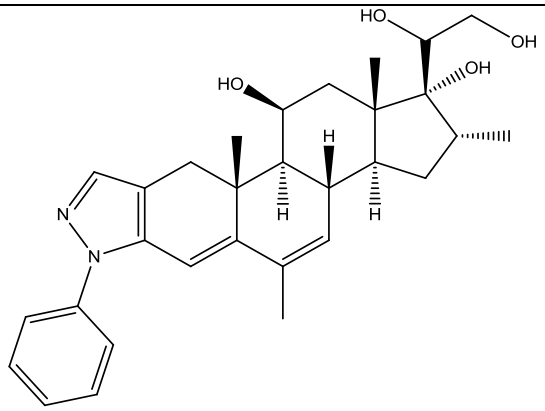

Appendix 7: Mass spectrum of thionyl chloride synthesis product

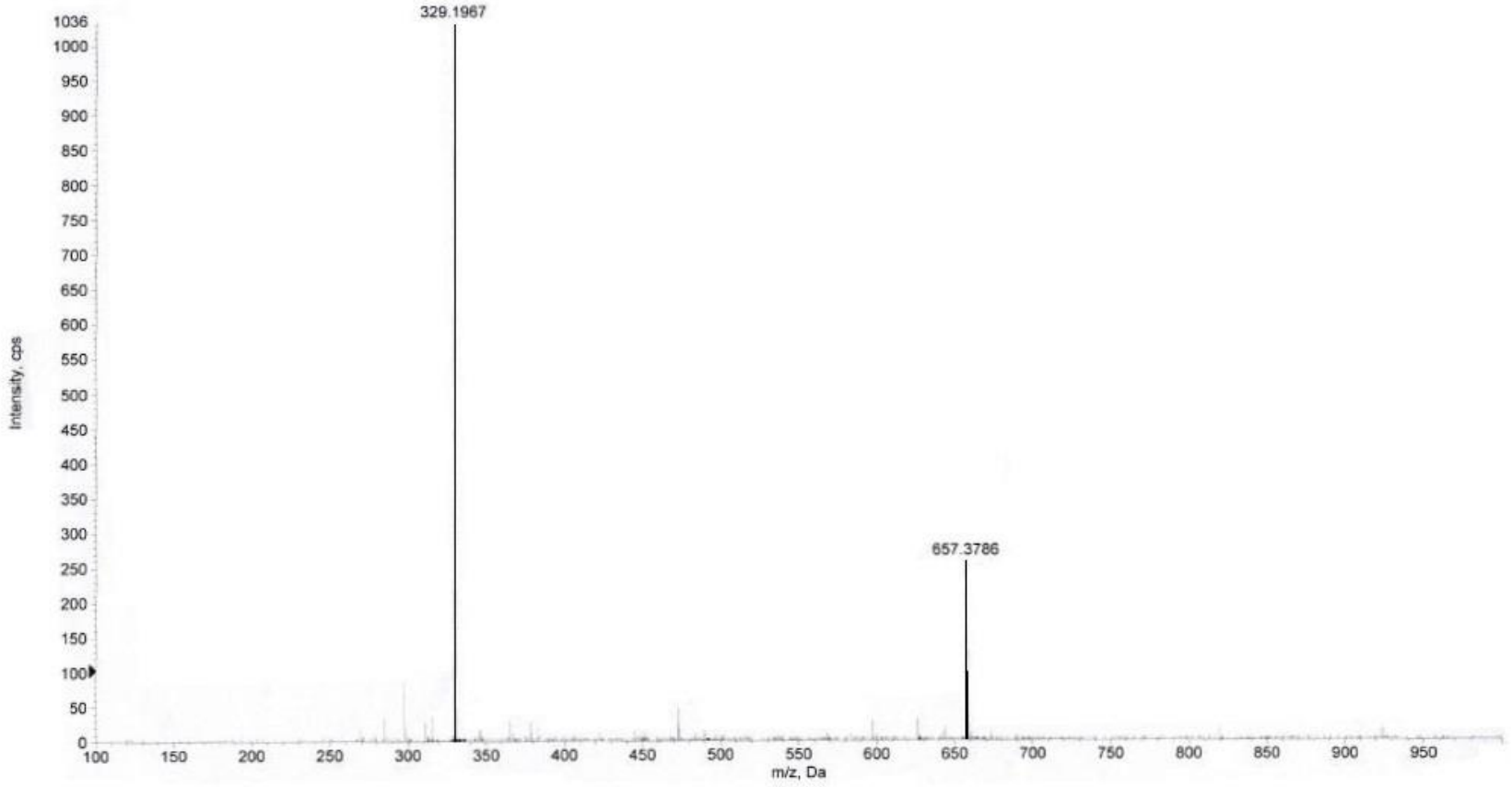

MS instrument: AB SCIEX TripleTOF 5600

Scan mode: Negative ion $[M-H]^-$

Appendix 8: Mass spectrum of methyl iodide synthesis product

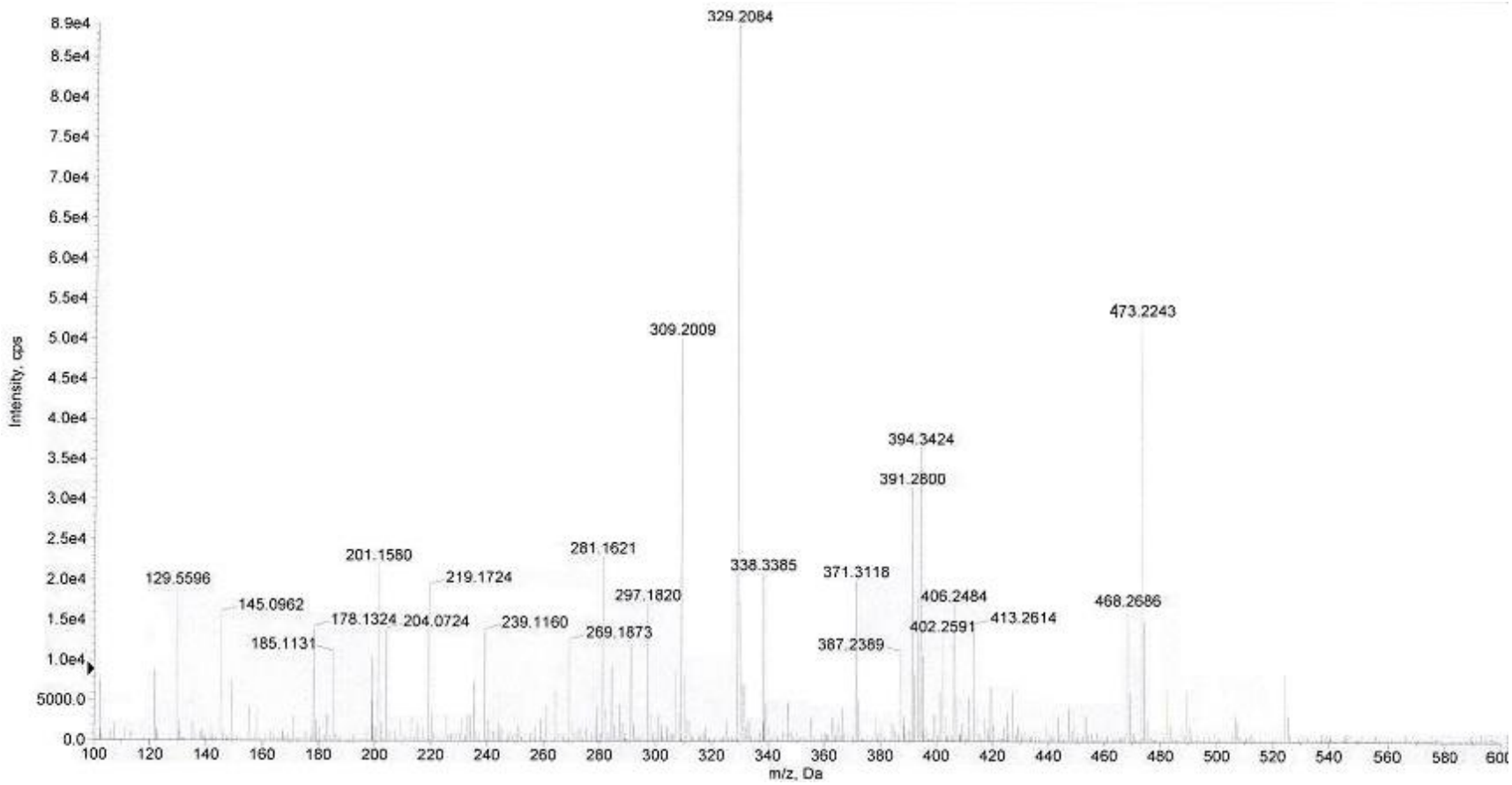

MS instrument: AB SCIEX TripleTOF 5600

Scan mode: Negative ion $[M-H]^-$



Xenobiotica
the fate of foreign compounds in biological systems

ISSN: 0049-8254 (Print) 1366-5928 (Online) Journal homepage: http://www.tandfonline.com/loi/ixen20

In vitro metabolism of the anti-inflammatory clerodane diterpenoid polyandric acid A and its hydrolysis product by human liver microsomes and recombinant cytochrome P450 and UDP-glucuronosyltransferase enzymes

Matthew Y. Bendikov, John O. Miners, Bradley S. Simpson, David J. Elliot, Susan J. Semple, David J. Claudie, Ross A. McKinnon, Elizabeth M. J. Gillam & Matthew J. Sykes

To cite this article: Matthew Y. Bendikov, John O. Miners, Bradley S. Simpson, David J. Elliot, Susan J. Semple, David J. Claudie, Ross A. McKinnon, Elizabeth M. J. Gillam & Matthew J. Sykes (2016): In vitro metabolism of the anti-inflammatory clerodane diterpenoid polyandric acid A and its hydrolysis product by human liver microsomes and recombinant cytochrome P450 and UDP-glucuronosyltransferase enzymes, Xenobiotica, DOI: 10.1080/00498254.2016.1203041

To link to this article: http://dx.doi.org/10.1080/00498254.2016.1203041

Published online: 14 Jul 2016.

Submit your article to this journal

View related articles

View Crossmark data

Full Terms & Conditions of access and use can be found at
http://www.tandfonline.com/action/journalInformation?journalCode=ixen20

Download by: [University Of South Australia Library] **Date:** 14 July 2016, At: 21:33

http://tandfonline.com/ixen
ISSN: 0049-8254 (print), 1366-5928 (electronic)

Xenobiotica

Xenobiotica, Early Online: 1–9
© 2016 Informa UK Limited, trading as Taylor & Francis Group. DOI: 10.1080/00498254.2016.1203041

Taylor & Francis
Taylor & Francis Group

RESEARCH ARTICLE

In vitro metabolism of the anti-inflammatory clerodane diterpenoid polyandric acid A and its hydrolysis product by human liver microsomes and recombinant cytochrome P450 and UDP-glucuronosyltransferase enzymes

Matthew Y. Bendikov[1,2], John O. Miners[1,3], Bradley S. Simpson[3,4], David J. Elliot[5], Susan J. Semple[4], David J. Claudie[6], Ross A. McKinnon[3], Elizabeth M. J. Gillam[7], and Matthew J. Sykes[2]

[1]Department of Clinical Pharmacology, School of Medicine, Flinders University, Adelaide, Australia, [2]Centre for Drug Discovery and Development, Sansom Institute for Health Research, University of South Australia, Adelaide, Australia, [3]Flinders Centre for Innovation in Cancer, School of Medicine, Flinders University, Adelaide, Australia, [4]Quality Use of Medicines and Pharmacy Research Centre, Sansom Institute for Health Research, University of South Australia, Adelaide, Australia, [5]Department of Clinical Pharmacology, Flinders Medical Centre, Adelaide, Australia, [6]Chuulangun Aboriginal Corporation, Cairns Mail Centre, Cairns, Australia, and [7]School of Chemistry and Molecular Biosciences, the University of Queensland, Brisbane, Australia

Downloaded by [University Of South Australia Library] at 21:33 14 July 2016

Abstract

1. The metabolism of the anti-inflammatory diterpenoid polyandric acid A (PAA), a constituent of the Australian Aboriginal medicinal plant *Dodonaea polyandra*, and its de-esterified alcohol metabolite, hydrolysed polyandric acid A (PAAH) was studied *in vitro* using human liver microsomes (HLM) and recombinant UDP-glucuronosyltransferase (UGT) and cytochrome P450 (CYP) enzymes.
2. Hydrolysis of PAA to yield PAAH occurred upon incubation with HLM. Further incubations of PAAH with HLM in the presence of UGT and CYP cofactors resulted in significant depletion, with UGT-mediated depletion as the major pathway.
3. Reaction phenotyping utilising selective enzyme inhibitors and recombinant human UGT and CYP enzymes revealed UGT2B7 and UGT1A1, and CYP2C9 and CYP3A4 as the major enzymes involved in the metabolism of PAAH.
4. Analysis of incubations of PAAH with UDP-glucuronic acid-supplemented HLM and recombinant enzymes by UPLC/MS/MS identified three glucuronide metabolites. The metabolites were further characterised by β-glucuronidase and mild alkaline hydrolysis. The acyl glucuronide of PAAH was shown to be the major metabolite.
5. This study demonstrates the *in vitro* metabolism of PAA and PAAH and represents the first systematic study of the metabolism of an active constituent of an Australian Aboriginal medicinal plant.

Keywords

Clerodane diterpenoid, cytochrome P450, esterases, glucuronidation, *in vitro–in vivo* extrapolation, polyandric acid A, reaction phenotyping, UDP-glucuronosyltransferase

History

Received 10 April 2016
Revised 13 June 2016
Accepted 14 June 2016
Published online 12 July 2016

Introduction

Dodonaea polyandra (Sapindaceae) is a plant species native to the Cape York Peninsula of Queensland, Australia. Aboriginal traditional owners of the Northern Kaanju (Kuuku I'yu) homelands located on the Cape York Peninsula have traditionally used the leaf and stem from this species for the treatment of pain and inflammation associated with toothache and other disorders of the oral cavity (Simpson et al., 2011). The anti-inflammatory properties of *D. polyandra* are the subject of ongoing investigations and the medicinal qualities of the plant are thought to be associated primarily with a series of clerodane diterpenoids. In particular, PAA (Figure 1) has been shown to have the most significant anti-inflammatory activity (Simpson et al., 2014).

PAA is a benzoyl ester clerodane diterpenoid that has been found to possess significant anti-inflammatory activity in acute and chronic *in vivo* mouse ear oedema models (Simpson et al., 2014). Furthermore, PAA reduces the secretion of several pro-inflammatory cytokines including interleukin-1β, interleukin-6 and tumor necrosis factor-α both *in vitro* and *in vivo*. Based on these data, there has been interest in developing PAA as a therapeutic product for use in skin, oral and gastrointestinal inflammatory disorders (Simpson et al., 2015). The structurally related diterpenoid hautriwaic acid, isolated from the widely used medicinal plant species

Address for correspondence: Dr. Matthew J. Sykes, University of South Australia, Frome Road, Adelaide 5000, Australia. Tel: +61 8 830 22598. E-mail: matt.sykes@unisa.edu.au

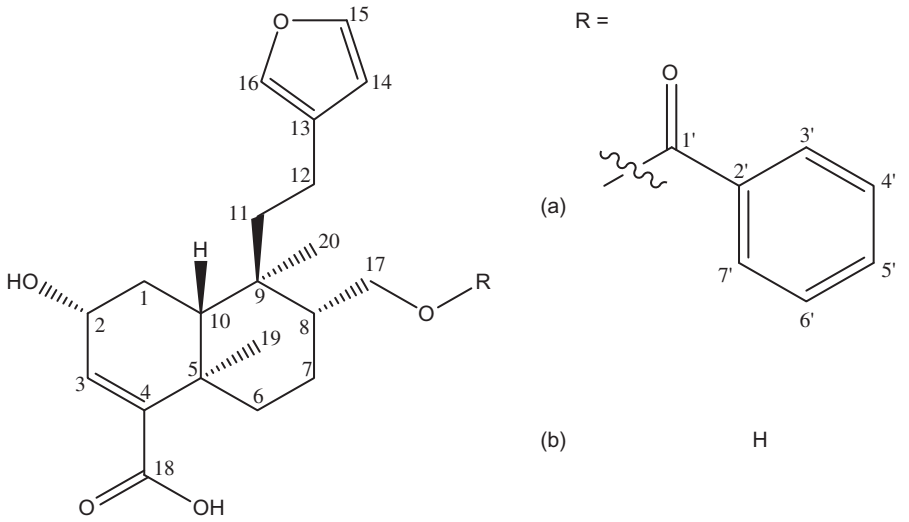

Figure 1. Structures of (a) polyandric acid A (PAA) and (b) hydrolysed polyandric acid A (PAAH).

Downloaded by [University Of South Australia Library] at 21:33 14 July 2016

Dodonaea viscosa, has also been investigated by Salinas-Sánchez et al. (2015) as an anti-inflammatory agent, specifically in an *in vivo* arthritis model.

Clerodane diterpenoids are an uncommon subclass of the terpenoid family and information regarding their metabolism is sparse, except for a few pharmacologically significant examples such as salvinorin A, isolated from *Salvia divinorum* (Teksin et al., 2009) and teucrin A, isolated from *Teucrium chaemadrys* (Druckova & Marnett, 2006). Salvinorin A is a potent hallucinogen used as a recreational drug, as well as a non-alkaloid opioid agonist (Roth et al., 2002; Sheffler & Roth, 2003). Teucrin A, a constituent of wild germander, gained prominence as an anti-inflammatory and weight control supplement but its use was later linked to severe hepatotoxicity and death via a mechanism involving metabolic activation (Druckova et al., 2007). Due to limited data related to the human metabolism of clerodane diterpenoids and the potential use of *D. polyandra* as a therapeutic intervention for inflammation, there is scope for the study of the metabolic fate of PAA in humans (Simpson et al., 2010).

It is well established that a metabolism and kinetic profile is an essential component in the development of new chemical entities (Kumar & Surapaneni, 2001). Such studies may be especially important for natural medicines, which may contain a number of active compounds and are known to be associated with numerous pharmacokinetic interactions (Meng & Liu, 2014). Major regulatory bodies, such as the US Food and Drug Administration (FDA) and the European Medicines Agency (EMA) require, at minimum, *in vitro* evaluation of metabolism for new chemical entities before they can receive approval for clinical use (EMA, 2012; FDA, 2008). Metabolic stability and reaction phenotyping methods represent powerful tools in the *in vitro* study of drug metabolism. The use of human liver microsomes (HLM) in the investigation of drug metabolic stability together with cDNA-expressed enzymes and HLM in combination with selective inhibitors of cytochromes P450 (CYP) and UDP-glucuronosyl-transferase (UGT) enzymes are now widely accepted approaches for the characterisation of key metabolic parameters of new chemical entities (Harper & Brassil, 2008; Masimirembwa et al., 2003; Miners et al., 1994, 2010).

This study was undertaken to characterise the human liver metabolism of PAA *in vitro*. The *in vitro* reaction phenotyping experiments utilising HLM, selective UGT and CYP inhibitors and recombinant human CYP and UGT enzymes were used in this study to elucidate the enzymology and kinetics of the metabolism of PAA and its de-esterified hydrolysis product PAAH. In addition to improving knowledge of human clerodane diterpenoid metabolism, this study represents the first such investigation of the human metabolism of an active constituent of an Australian Aboriginal traditional medicinal plant.

Materials and methods

Materials

β-Glucuronidase (type IX-A from *E*scherichia *coli*), deuterated methanol, hecogenin, furafylline, ticlopidine, quinidine, CYP3cide, NADP, G-6-P, G-6-P dehydrogenase, 3′-phosphoadenosine, 5′-phosphosulfate (PAPS) and UDP-glucuronic acid (UDPGA) were purchased from Sigma-Aldrich (Sydney, Australia); alamethicin (*Trichoderma viride*) from AG Scientific (San Diego, CA); and fluconazole and montelukast from Cayman Chemical (Waterloo, Australia). Niflumic acid and sulfaphenazole were gifts from E.R. Squibb and Sons (Princeton, NJ) and Ciba-Geigy (Melbourne, Australia), respectively. All solvents used for mass spectrometry (MS) were of MS grade while all other solvents and reagents were of analytical reagent grade. PAA (15,16-epoxy-8α-(benzoyloxy)methyl-2-oxocleroda-3,13(16),14-trien-18-oic acid) was isolated from *D. polyandra* by solvent extraction and chromatography according to Simpson et al. (2011). PAAH (15,16-epoxy-8-hydroxymethyl-2-oxocleroda-3,13(16),14-trien-18-oic acid) was subsequently produced from PAA by alkaline hydrolysis (Simpson et al., 2011). Identity and purity (>98%) of both compounds were established by ^{1}H and ^{13}C NMR using a Bruker Avance III 500 MHz spectrometer (Preston, Australia).

Human liver microsomes and recombinant enzymes

Approval for the use of human liver tissue for *in vitro* drug metabolism studies was obtained from the Southern Adelaide

Downloaded by [University Of South Australia Library] at 21:33 14 July 2016

Clinical Research Ethics Committee. HLM were prepared by differential centrifugation, as described by Bowalgaha et al. (2005), and cytosol (HLC) was retained. The protein content of HLM and the lysates of human embryonic kidney (HEK293) cells expressing human UGT enzymes was measured according to Lowry et al. (1951). HLM pools were prepared from five individual livers (H7, H10, H12, H13, H40) obtained from the human liver bank of the Department of Clinical Pharmacology, Flinders University (Adelaide, Australia). Recombinant CYP enzymes were expressed in *E. coli* by the following published methods; CYP1A2 by Polasek et al. (2006), CYP2C8 and CYP2C9 by Boye et al. (2004), CYP2C19 by Cuttle et al. (2000) and CYP2B6, CYP2D6 and CYP3A4 by Parikh et al. (1997), while UGT1A1, UGT1A3, UGT1A4, UGT1A6 and UGT1A9 were expressed in HEK293 cells as reported by Uchaipichat et al. (2004). Supersomes expressing UGT2B4, UGT2B7, UGT2B8 and UGT2B17 were purchased from Corning Gentest (Tewksbury, MA) given the low activity of UGT2B enzymes expressed in HEK293 cells.

Incubations of PAA and PAAH with human liver microsomes and recombinant enzymes

Incubations of PAA and PAAH with protein (HLM, 1 mg/mL; lysates of HEK293 cells expressing recombinant UGT enzymes, 1 mg/mL; or recombinant CYP enzymes, 5 pmol/mL) were performed in a total volume of 200 µL in 0.1 M potassium phosphate buffer (pH 7.4). The concentration of PAA for stability experiments was 10 µM, while the concentration of PAAH in HLM, UGT and CYP metabolism experiments was 2 µM. It was assumed that a PAA concentration of 2 µM was below the K_m values for the metabolic pathways of PAAH, thereby permitting calculation of CL_{int} from depletion data (see later). For the substrate depletion experiments utilising HLM as the enzyme source, microsomes were pre-incubated on ice for 30 min with the pore-forming agent alamethicin (50 µg/mg) prior to their addition to incubations (Boase & Miners, 2002; Fisher et al., 2000). Reactions were initiated by the addition of the appropriate cofactors: 5 mM UDPGA for glucuronidation and NADPH generating system (1 mM NADP, 10 mM G-6-P and 2 IU G-6-P dehydrogenase) for experiments investigating CYP catalysed metabolism. Incubations were performed in a shaking water bath (Ratek Instruments, Melbourne, Australia) at 37 °C for 120 or 150 min, as indicated in ''Results'' section, after which time reactions were terminated with 200 µL of 4% acetic acid in methanol. Samples were centrifuged at 5000*g* for 10 min at 4 °C and the supernatant layer was separated for analysis. Compounds (and concentrations) used as selective inhibitors of human liver microsomal CYP and UGT enzyme inhibitors are shown in Table 1. Control experiments were performed without chemical inhibitors, but with an equivalent concentration of solvent. The mechanism-based inhibitors furafylline, ticlopidine and CYP3cide were pre-incubated with HLM for 30 min prior to the addition of substrate. Experiments with recombinant enzymes were performed using the same conditions as HLM, but with recombinant protein in place of HLM.

Table 1. CYP and UGT enzyme selective inhibitors.

Enzyme	Inhibitor	Concentration	Reference
UGT1A1	Niflumic acid	100 µM	Miners et al. (2011b)
UGT1A4	Hecogenin	10 µM	Uchaipichat et al. (2006a)
UGT1A9	Niflumic acid	2.5 µM	Miners et al. (2011b)
UGT2B7	Fluconazole	2.5 mM	Uchaipichat et al. (2006b)
CYP1A2	Furafylline	10 µM	Tassaneeyakul et al. (1994)
CYP2B6	Ticlopidine	3 µM	Ha-Duong et al. (2001)
CYP2C8	Montelukast	0.2 µM	VandenBrink et al. (2011)
CYP2C9	Sulfaphenazole	2.5 µM	Miners et al. (1996)
CYP2C19	Ticlopidine	3 µM	Ha-Duong et al. (2001)
CYP2D6	Quinidine	1 µM	Bramer & Suri (1999)
CYP3A4	CYP3cide	1.5 µM	Walsky et al. (2012)

HPLC quantification of PAA and PAAH

PAA and PAAH were quantified by HPLC using an Agilent Technologies 1100 series instrument (Mulgrave, Australia) fitted with a Phenomenex Synergi HydroRP C18 column (150 mm × 3 mm, 4 µM; Phenomenex Incorporated, Lane Cove, Australia). The column temperature was maintained at 25 °C with a mobile phase flow rate of 1 mL/min. The detection wavelength was 225 nm. In experiments investigating PAA hydrolysis, PAA and PAAH were separated by gradient elution: mobile phase A consisted of 30% acetonitrile (ACN) and 70% H_2O acidified with 0.1% formic acid, while mobile phase B consisted of ACN alone. The initial mobile phase composition was 92.5% mobile phase A and 7.5% mobile phase B for 2.5 min, followed by an increase of mobile phase B to 35% over 0.5 min which was then held for 5.5 min, and then a decrease of mobile phase B to 0% over 0.5 min. Retention times of PAA and PAAH under these conditions were 3.13 and 8.24 min, respectively. PAA and PAAH concentrations in incubation samples were quantified using standard curves prepared from samples over the concentration range 1–10 µM. Isocratic elution using mobile phase A alone was employed for the analysis of PAAH in experiments investigating the depletion of this compound. The retention time of PAAH using the latter conditions was 5.24 min.

UPLC–MS analysis and hydrolysis of glucuronide metabolites

Incubation samples of PAAH with HLM and recombinant enzymes (2 mg/mL) and UDPGA were analysed using a Waters Ultra Performance Liquid Chromatography (UPLC) system fitted with an Acquity HSS T3 column (100 mm × 2.1 mm, 1.8 µm; Waters Corporation, Milford, MA). The Acquity UPLC consisted of a binary solvent manager, temperature controlled column oven and TUV detector coupled to a Micromass Q-Tof Premier Mass Spectrometer (Waters Corporation, Milford, MA). The UPLC mobile phase consisted of 32.5% ACN and 67.5% H_2O containing 0.1% formic acid. Samples were analysed in negative-ion mode. Mass spectrometry conditions were: capillary voltage 2.2 kV, sampling cone voltage 45 V, desolvation temperature 400 °C, desolvation gas flow 400 L/h and collision energy 10 V. The identity of individual metabolites was investigated by mild alkaline and β-glucuronidase (type IX-A, *E. coli*) hydrolysis. Alkaline hydrolysis was performed by incubating samples with 0.1 M NaOH for a period of 120 min at 37 °C in

a shaking water bath, followed by UPLC–MS analysis. Similarly, samples from incubations with 2000 units of β-glucuronidase (from *E. coli*) for a period of 120 min at 37 °C were analysed by UPLC–MS.

Data analysis

The fraction of PAAH unbound in incubations of HLM was estimated using the algorithm of Hallifax & Houston (2006):

$$f_{u,mic} = \frac{1}{1 + 10^{0.072 \times logD^2 + 0.067 \times logD - 1.126}} \quad (1)$$

Log *D* (0.28) was computationally determined using PhysChem History by Advanced Chemical Development, Inc. (Toronto, ON (ACD, 2010)). The calculated $f_{u,mic}$ was 0.93, consistent with the low non-specific binding expected for an organic acid (Sykes et al., 2006). Thus, correction of CL_{int} (see below) for non-specific binding to HLM was not required.

Elimination half-lives ($t_{1/2}$, min) of PAA and PAAH were calculated from substrate depletion experiments using the first-order elimination rate constant. *In vitro* intrinsic clearance (CL_{int}, μL/min/μg) was subsequently derived from the elimination half-life as:

$$CL_{int} = \frac{ln2 \times volume}{t_{1/2} \times protein\ amount} \quad (2)$$

where *volume* refers to the incubation volume (μL) and *protein amount* refers to the mass of protein present in the incubation (mg).

CL_{int} was used to estimate the *in vivo* hepatic clearance (CL_H) for various metabolic routes using the equation for the well-stirred model of hepatic drug clearance:

$$CL_H = \frac{Q_H \times f_u \times CL_{int}}{Q_H + f_u \times CL_{int}} \quad (3)$$

where Q_H is hepatic blood flow (20.7 mL/min kg or 1.45 L/min for a 70 kg person) and f_u refers to the fraction unbound in blood. The value of f_u was calculated as 0.03 using the SimCYP ADME calculator (Jamei et al., 2013) employing computationally determined values of log *P* (3.11) and pK_a (4.63), both using PhysChem History.

Statistical significance for differences between kinetic constants was determined using the Mann–Whitney *U*-test. A p value <0.05 was regarded as statistically significant. Data presented in Figures 2–5 and Table 2 are the means of triplicate or quadruplicate experiments, as indicated.

Results

Hydrolysis of PAA by HLM

PAA was hydrolysed spontaneously in the presence of HLM without the addition of any cofactor. No hydrolysis of PAA was observed in the absence of HLM. Over the 120 min incubation, PAA was depleted by 68% with a $t_{1/2}$ of 67.0 ± 7.86 min (Figure 2). The de-esterified alcohol of PAA (i.e. PAAH) was identified as the sole product by comparison of the HPLC retention time with that of the authentic standard. Approximate mass balance was established (Figure 2).

Depletion of PAAH by HLM

No depletion of PAAH by HLM was observed in the absence of UDPGA or NADPH. Similarly, there was no depletion of PAAH by HLC supplemented with PAPS. In incubations supplemented with UDPGA, 51% depletion was observed over 150 min (Figure 3). Lesser depletion was observed in incubations supplemented with NADPH; 12% over 150 min. Combination of both cofactors resulted in a total substrate depletion of 62%. Derived $t_{1/2}$, CL_{int} and CL_H values are reported in Table 2. The CL_{int} value for PAAH elimination in the presence of UDPGA was approximately four-fold higher than for incubations performed in the presence of NADPH. Conversely, the $t_{1/2}$ for incubations performed in the presence of NADPH was approximately four-fold longer than for depletion in the presence of UDPGA. The sum of the CL_{int} values for elimination in the presence of the separate cofactors (5.60 μL/min mg) was close to the CL_{int} observed in the presence of the combined cofactors (6.44 μL/min mg).

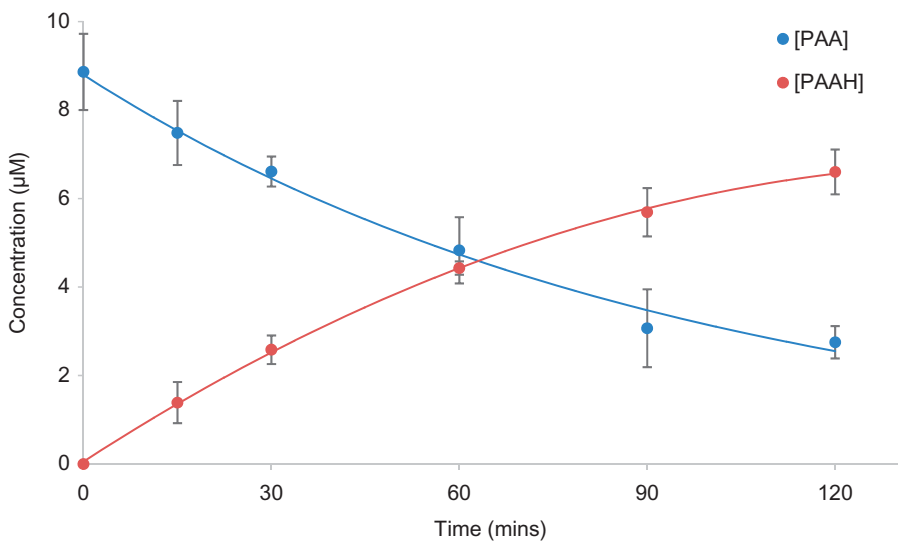

Figure 2. Hydrolysis of PAA to PAAH by HLM (1 mg/mL) at pH 7.4. Incubations were performed at 37 °C for 120 min. Results are presented as the mean ± SD ($n = 3$).

Downloaded by [University Of South Australia Library] at 21:33 14 July 2016

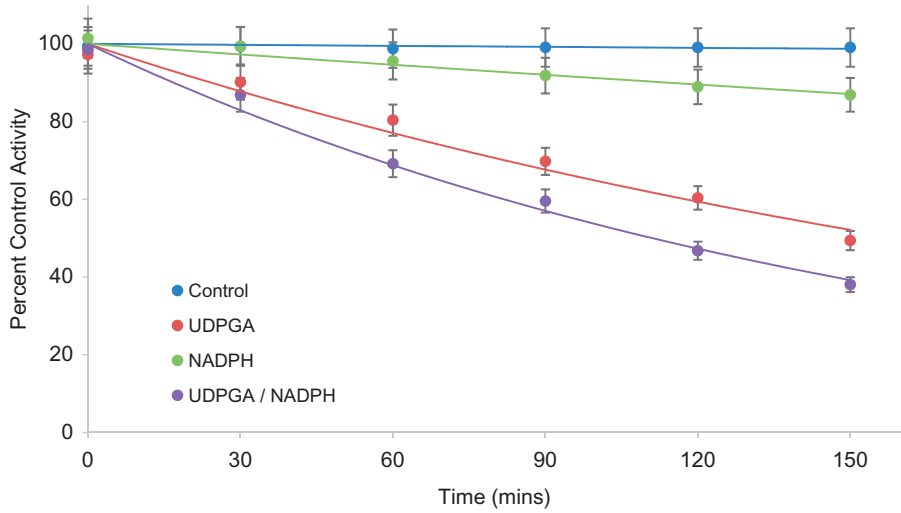

Figure 3. The depletion of PAAH (2 µM) by HLM (1 mg/mL) at pH 7.4 with enzyme cofactors (UDPGA and NADPH). Incubations were performed at 37 °C for 150 min. Results are presented as the mean ± SD ($n = 4$).

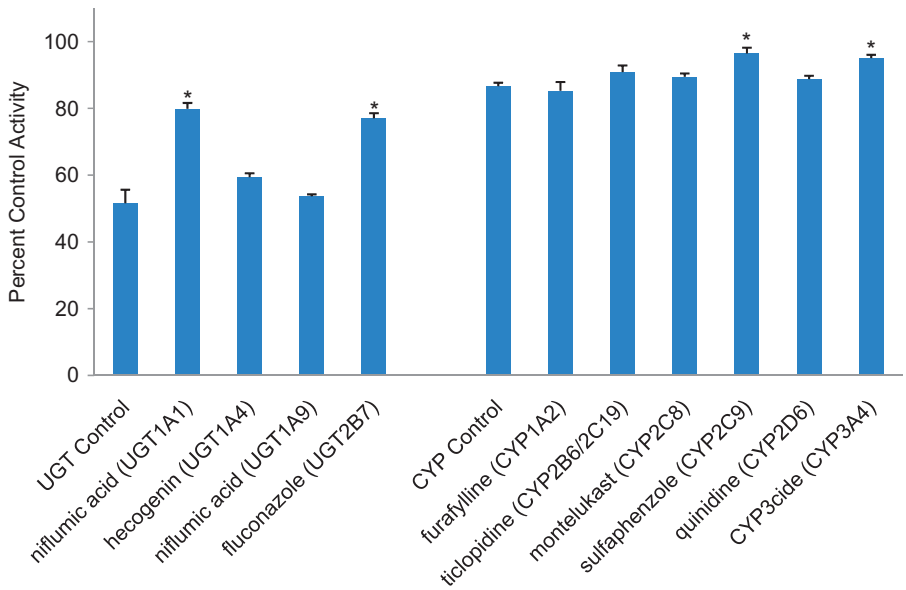

Figure 4. The effects of selective UGT and CYP enzyme inhibitors on the depletion of PAAH (2 µM) by HLM (1 mg/mL) at pH 7.4. Incubations were performed at 37 °C for 150 min. Controls for UGT and CYP consisted of HLM with cofactor and no chemical inhibitor. Results are presented as the mean ± SD ($n = 4$). *$p < 0.05$, significant difference observed between UGT1A1, UGT2B7, CYP2C9 and CYP3A4 and the respective controls.

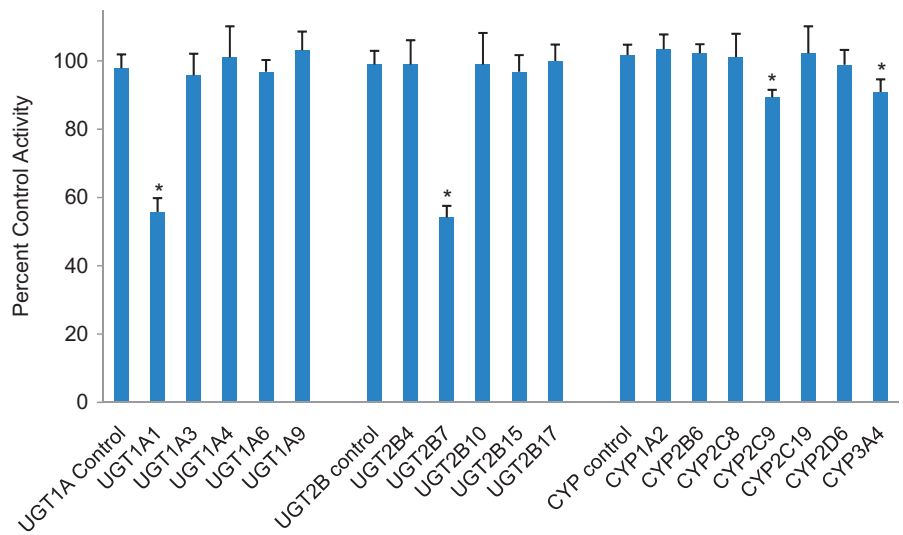

Figure 5. The depletion of PAAH (2 µM) by recombinant CYP (5 pmol/mL) and UGT (1 mg/mL of HEK293 cell lysate protein or Supersome protein) enzymes at pH 7.4. Incubations were performed at 37 °C for 150 min. Controls correspond to incubations of PAAH with un-transfected enzyme sources. Results are presented as the mean ± SD ($n = 4$). *$p < 0.05$, significant difference was observed between UGT1A1 and UGT2B7 and CYP2C9 and CYP3A4 and respective controls.

Downloaded by [University Of South Australia Library] at 21:33 14 July 2016

Downloaded by [University Of South Australia Library] at 21:33 14 July 2016

Depletion of PAAH by individual CYP and UGT enzymes

The effects of selective inhibitors of UGT 1A1, 1A4, 1A9 and 2B7 and CYP 1A2, 2B6/2C19, 2C8, 2D6 and 3A4 on the depletion of PAAH by incubations of HLM supplemented with either NADPH or UDPGA are shown in Figure 4. Depletion of PAAH by UDPGA-supplemented HLM was significantly reduced from approximately 50% to approximately 20% by pre-incubation with niflumic acid (100 μM) and fluconazole (2.5 mM). Similarly, depletion of PAAH by NADPH-supplemented HLM was significantly reduced from approximately 15% to 5% by pre-incubation with sulfaphenazole and CYP3cide. Other UGT (niflumic acid (2.5 μM) and hecogenin) and CYP (furafylline, ticlodipine, montelukast and quinidine) enzyme selective inhibitors did not significantly affect PAAH depletion. The depletion of PAAH by incubations of cofactor supplemented recombinant UGT and CYP enzymes is shown in Figure 5. Significant depletion of PAAH was observed only with UGT1A1, UGT2B7, CYP2C9 and CYP3A4. The depletion observed with each recombinant UGT enzyme (∼50%) was approximately four-fold higher than depletion with each recombinant CYP enzyme.

Identification of glucuronides of PAAH

Incubations of PAAH with HLM and recombinant UGT 1A1 and 2B7 in the presence of UDPGA were analysed by UPLC–MS. The *m/z* values corresponding to PAAH (predicted 347.18 Da; observed 347.19 Da) and PAAH-glucuronide (predicted 523.23 Da; observed 523.22 Da) were detected. Three peaks at the *m/z* value for PAAH-glucuronide were separated by UPLC; one major peak at 1.83 min and two minor peaks at 1.15 and 1.39 min (Figure 6). All three metabolite peaks were detected in incubations of both HLM (Figure 6) and recombinant enzymes (data not shown). Hydrolysis by β-glucuronidase resulted in complete loss of the major peak plus one of the minor peaks at 1.39 min, with little effect on the second minor peak. Hydrolysis under mild alkaline conditions resulted in complete loss of the major peak, with no effect on the minor peaks.

Table 2. Derived kinetic data (mean ± SD) for HLM mediated PAAH depletion in the presence of UDPGA, NADPH, and UDPGA plus NADPH.

Cofactor	$t_{1/2}$ (min)	CL_{int} (μL/min mg)
UDPGA	154 ± 12.2†	4.51 ± 0.37†
NADPH	636 ± 41.6*	1.09 ± 0.07*
UDPGA/NADPH	107 ± 2.12*,†	6.44 ± 0.13*,†

*$p < 0.05$ compared to UDPGA alone.
†$p < 0.05$ compared to NADPH alone.

Discussion

Incubations of PAA and PAAH with HLM were used to assess the metabolic stability of each compound by various enzyme systems. Ester hydrolysis may occur spontaneously under either alkaline or acidic conditions, but PAA hydrolysis was not observed in incubations conducted for 150 min at pH 7.4 and 37 °C in the absence of HLM. Enzyme catalysed hydrolysis of ester containing xenobiotics is mediated primarily by carboxylesterases, of which there are two primary isoforms (hCES1 and hCES2) in human liver (Sanghani et al., 2009). Since PAA hydrolysis was linked to the presence of HLM, it is likely that the extensive hydrolysis shown in Figure 2 is catalysed by a carboxylesterase. hCES1 appears to preferentially hydrolyse substrates with a small alcohol but large acyl moiety, while the converse applies to hCES2 (Hosokawa, 2008). However, overlapping substrate specificity may occur with hCES1. As PAA contains a large alcohol and a small acyl moiety, hydrolysis by hCES2 seems likely although a contribution of hCES1 cannot be discounted. As noted above, both hCES1 and hCES2 are expressed in liver, while expression of hCES2 additionally occurs in the gastrointestinal tract and kidneys (Hosokawa, 2008).

The hydrolysis of esters *in vivo* frequently occurs rapidly due to the involvement of hepatic, gastrointestinal and blood

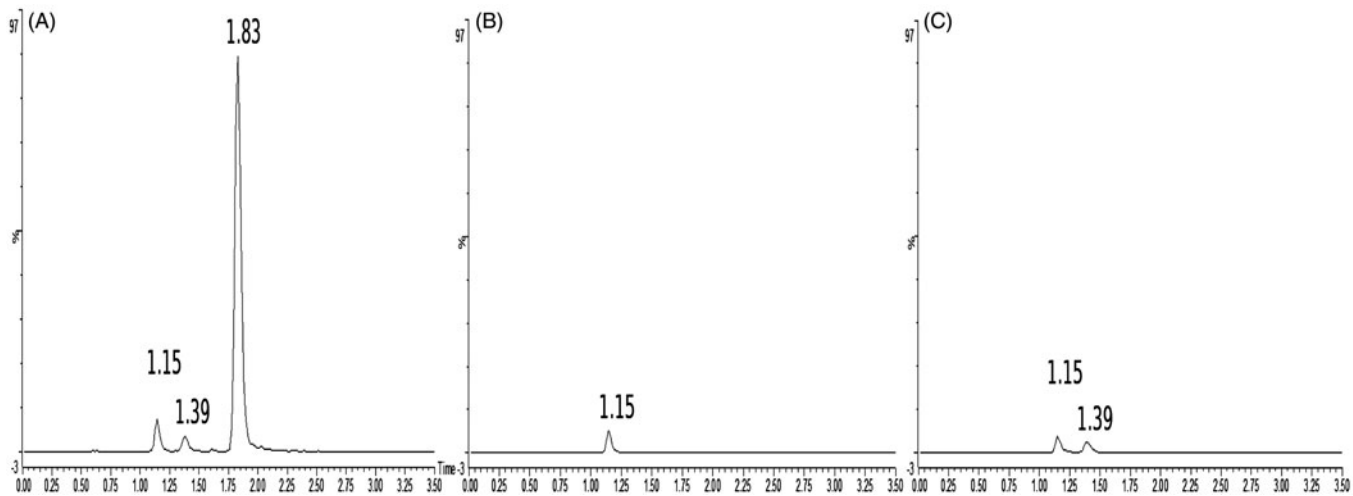

Figure 6. UPLC–MS traces showing the hydrolysis of PAAH-glucuronide peaks by weak base and β-glucuronidase. Peaks were selected for *m/z* 523.22 with a total ion count of 3.28e3. (A) Incubations of PAAH with HLM and UDPGA. (B) Incubations of PAAH with HLM and UDPGA, followed by β-glucuronidase hydrolysis. (C) Incubations of PAAH with HLM and UDPGA, followed by weak alkaline hydrolysis. Incubations were prepared with 2 mg/mL HLM.

Downloaded by [University Of South Australia Library] at 21:33 14 July 2016

esterases. It has been reported that salvinorin A, which is structurally similar to PAA (see later discussion), is hydrolysed rapidly in blood *ex vivo* (Schmidt et al., 2005). Thus, given the likely involvement of hepatic, gastrointestinal, renal and blood esterases in PAA hydrolysis, pre-systemic and systemic hydrolysis of PAA is expected to occur rapidly following oral administration and therefore PAAH is predicted to be the major circulating species in blood *in vivo.* Similarly, systemic hydrolysis will occur following dermal absorption. There is evidence that topically administered PAAH exhibits anti-inflammatory activity *in vivo.* The anti-inflammatory activity of PAAH is lower than that of PAA, which may be the result of either a weaker interaction between ligand and target or improved membrane perfusion of PAA due to the presence of the more hydrophobic ester group (Simpson et al., 2011).

The metabolism of PAAH by hepatic CYP and UGT enzymes, the two major xenobiotic metabolising enzyme families, was explored by incubations of PAAH with HLM in the presence of relevant enzyme cofactors. Substrate depletion was used initially to assess the contribution of UGT and CYP enzymes to PAAH metabolism. It was demonstrated that UGT-mediated glucuronidation is the major pathway of PAAH metabolism with HLM as the enzyme source, with a lesser contribution by CYP enzymes. The depletion observed with the combined CYP and UGT cofactors approximated the sum of the depletions determined in the presence of the individual cofactors. The *in vitro* CL_{int} for PAAH elimination by HLM in the presence of UDPGA was approximately four-fold higher than the CL_{int} for HLM supplemented with NADPH. Taken together, these data indicate that the elimination of PAAH by glucuronidation accounts for approximately 80% of the total elimination resulting from glucuronidation plus CYP-catalysed oxidation. A contribution of sulfotransferase to PAAH metabolism was excluded on the basis of a lack of depletion of PAAH by incubations of HLC supplemented with PAPS.

The contribution of individual UGT and CYP enzymes was characterised using reaction phenotyping methods with enzyme selective inhibitors and recombinant enzymes. UGT-mediated depletion of PAAH by HLM was inhibited by the addition of the inhibitors fluconazole, a relatively selective inhibitor of UGT2B7 (Uchaipichat et al., 2006b), and niflumic acid, an inhibitor of UGT1A9 that also exhibits inhibitory activity of UGT1A1 and UGT2B15 at higher concentrations (Miners et al., 2011). Significant inhibition of human liver microsomal PAAH glucuronidation occurred only at the higher niflumic acid concentration (100 μM, Figure 4), suggesting involvement of UGT 1A1 or 2B15 but not 1A9. Incubation of PAAH with recombinant enzymes provided further clarification of these data by demonstrating significant depletion of PAAH by recombinant UGT 1A1 and 2B7, but not UGT 1A9 and 2B15 (Figure 5). Taken together, these data indicate that UGT 1A1 and 2B7 are responsible for human hepatic PAAH glucuronidation. CYP mediated depletion of PAAH by HLM was inhibited by CYP3cide, a CYP3A4 selective inhibitor (Walsky et al., 2012), and sulfaphenazole, a CYP2C9 selective inhibitor (Miners et al., 1996). Incubation of PAAH with recombinant CYP enzymes provided further support for this observation, demonstrating significant depletion by CYP 3A4 and 2C9 but not by other CYP enzymes (Figure 5). Previous studies have demonstrated an important role of CYP3A4, with a lesser role of CYP2C9, in the oxidation of furan-containing substrates (Baer et al., 2005; Peterson, 2012).

Structural identification of the glucuronide metabolites of PAAH was performed by UPLC–MS and chemical hydrolysis. Inspection of the structure of PAAH reveals three positions amenable to glucuronidation: the hydroxyl groups located at C2 and C17 (Figure 1) and the carboxylic acid at C18. Three metabolites with *m/z* values corresponding to a PAAH-glucuronide were detected by UPLC/MS. The same three metabolites were detected by incubations of PAAH with HLM and recombinant UGT 1A1 and 2B7, consistent with a lack of regioselectivity. There was no evidence of a diglucuronide. Mild alkaline hydrolysis is a well-recognised method for the selective hydrolysis of acyl glucuronides (Shipkova et al., 2000). Mild alkaline hydrolysis resulted in almost complete loss of the major glucuronide formed by HLM, suggesting that this compound is the acyl glucuronide (Figure 1). The two remaining unassigned peaks are therefore likely to correspond to the (minor) hydroxy-glucuronides located at positions C2 and C17. Hydrolysis by β-glucuronidase resulted in complete loss of the peaks for the acyl glucuronide (retention time 1.83 min), and one of the minor glucuronides (retention time 1.39 min). The resistance of the second hydroxyl-glucuronide to β-glucuronidase hydrolysis is likely a result of structural differences between the C2 and C17 glucuronides. A similar phenomenon has been reported for the differential effects of β-glucuronidase on the morphine 3- and 6-glucuronides whereby the 3-glucuronide is hydrolysed faster than the 6-glucuronide, presumably due to steric hindrance of the latter (Romberg & Lee, 1995).

In vitro–in vivo extrapolation was employed to predict the hepatic clearance (CL_H) of PAAH. The mean microsomal CL_{int} for PAAH generated in the presence of UDPGA and NADPH (6.44 μL/min mg, Table 2) was scaled to a whole liver CL_{int} using a human liver microsomal yield of 32 mg/kg (Barter et al., 2007) and a liver weight of 21.4 g/kg (i.e. 1500 g for a 70 kg person) (Gill et al., 2012). The derived liver CL_{int} (309 mL/min, or 18.5 L/h) was substituted into the equation for the well-stirred model of hepatic clearance (Equation 3, Data Analysis) to provide an *in vivo* CL_H of 1.25 L/h. Given the contributions of UGT2B7 and CYP2C9 to hepatic PAAH metabolism, it is likely that this value underestimates the true hepatic clearance due to the inhibitory effects of long-chain unsaturated fatty acids released from the microsomal membrane during the course of an incubation (Rowland et al., 2007, 2008). Nevertheless, even a 10-fold underestimation of CL_H would still result in PAAH being classified as a ''low'' hepatic clearance compound (i.e. CL_H<18 L/h).

Salvinorin A (Figure 7) is a clerodane diterpenoid that bears close structural resemblance to PAAH. The central scaffold, incorporating the decalin moiety (C1–C10), alkyl chain (C11 and C12) extending to a furan ring (C13–C16), carbonyl group at C18 and methyl groups at C19 and C20, is conserved between the structures. Differences are found around oxygenated carbons, with several additional structural features present in salvinorin A. Similar to our findings with

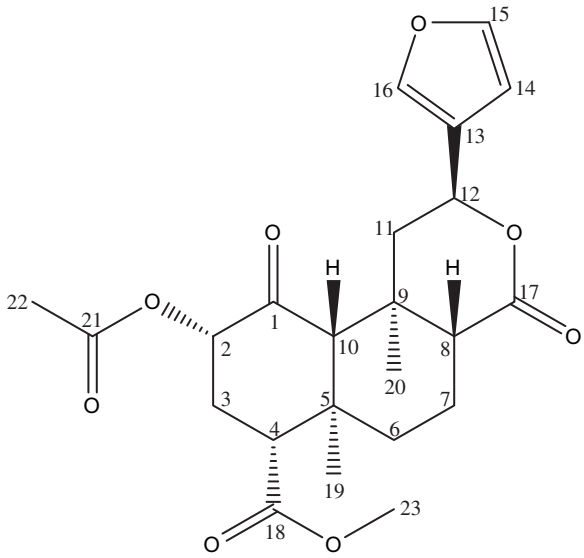

Figure 7. Chemical structure of salvinorin A.

PAAH, Teksin et al. (2009) reported initial carboxylesterase mediated hydrolysis of salvinorin A followed by UGT2B7-catalysed glucuronidation as the major metabolic pathways, with lesser contributions of CYP1A1, 2C18 and 2D6. Of particular note was the identification of UGT2B7 as the major enzyme involved in salvinorin A glucuronidation, which accords with data presented here for PAAH. Differences in the contributions of CYP enzymes are likely to result from structural differences between the two substrates, most notably the presence of the lactone ring of salvinorin A which significantly constrains the flexibility of the furan ring in comparison to PAAH.

Conclusions

The metabolism of a clerodane diterpenoid species isolated from an Australian Aboriginal medicinal plant is reported for the first time. PAA undergoes ester hydrolysis to form PAAH. PAAH is subsequently metabolised by UGT1A1, UGT2B7, CYP2C9 and CYP3A4, with UGT-catalysed formation of the acyl glucuronide being the major metabolic pathway. Microsomal intrinsic clearances were determined for UGT- and CYP-catalysed metabolism and then used to estimate *in vivo* CL_H. *In vitro–in vivo* extrapolation predicted that PAAH was a low hepatic clearance compound. The study contributes to knowledge of clerodane diterpenoid metabolism in humans and provides a basis for further pre-clinical studies with PAA.

Acknowledgements

The authors wish to acknowledge the Chuulangun Aboriginal Corporation, on behalf of the Kuuku I'yu Northern Kaanju people, for sharing their cultural knowledge and facilitating access to raw plant materials from their land, as well as Kushari Burns, Nuy Chau, Dr. Pramod Nair, Dr. Andrew Rowland and Dr. Chi Ndi for technical assistance with this work.

Declaration of interest

The authors have no declarations of interest to report. This work was partially supported by the National Health and Medical Research Council Development Grant 1017556.

References

ACD. (2010). PhysChem History, v12.0. Toronto, ON, Canada: Advanced Chemical Development, Inc.

Baer BR, Rettie AE, Henne KR. (2005). Bioactivation of 4-Ipomeanol by CYP4B1: adduct characterization and evidence for an enedial intermediate. Chem Res Toxicol 18:855–64.

Barter ZE, Bayliss MK, Beaune PH, et al. (2007). Scaling factors for the extrapolation of in vivo metabolic drug clearance from in vitro data: reaching a consensus on values of human microsomal protein and hepatocellularity per gram of liver. Curr Drug Metab 8:33–45.

Boase S, Miners JO. (2005). In vitroin vivo correlations for drugs eliminated by glucuronidation: investigations with the model substrate zidovudine. Br J Clin Pharmacol 54:493–503.

Bowalgaha K, Elliot DJ, Mackenzie PI, et al. (2005). S-Naproxen and desmethylnaproxen glucuronidation by human liver microsomes and recombinant human UDP-glucuronosyltransferases (UGT): role of UGT2B7 in the elimination of naproxen. Br J Clin Pharmacol 60: 423–33.

Boye SL, Kerdpin O, Elliot DJ, et al. (2004). Optimizing bacterial expression of catalytically active human cytochromes P450: comparison of CYP2C8 and CYP2C9. Xenobiotica 34:49–60.

Bramer SL, Suri A. (1999). Inhibition of CYP2D6 by quinidine and its effects on the metabolism of cilostazol. Clin Pharmacokinet 37:41–51.

Cuttle L, Munns AJ, Hogg NA, et al. (2000). Phenytoin metabolism by human cytochrome P450: involvement of P450 3A and 2C forms in secondary metabolism and drug-protein adduct formation. Drug Metab Dispos 28:945–50.

Druckova A, Marnett LJ. (2006). Characterization of the amino acid adducts of the enedial derivative of teucrin A. Chem Res Toxicol 19: 1330–40.

Druckova A, Mernaugh RL, Ham AJL, Marnett LJ. (2007). Identification of the protein targets of the reactive metabolite of teucrin A in vivo in the rat. Chem Res Toxicol 20:1393–408.

EMA. (2012). In: Committee for Human Medicinal Products, ed. Guideline on the investigation of drug interactions. London, UK: European Medicines Agency.

Fisher MB, Campanale K, Ackermann BL, et al. (2000). In vitro glucuronidation using human liver microsomes and the pore-forming peptide alamethicin. Drug Metab Dispos 28:560–6.

FDA. (2008). In: Center for Drug Evaluation and Research, ed. Guidance for industry: safety testing of drug metabolites. Rockville (MD): Food and Drug Administration.

Gill KL, Houston JB, Galetin A. (2012). Characterization of in vitro glucuronidation clearance of a range of drugs in human kidney microsomes: comparison with liver and intestinal glucuronidation and impact of albumin. Drug Metab Dispos 40:825–35.

Ha-Duong NT, Dijols S, Macherey AC, et al. (2001). Ticlopidine as a selective mechanism-based inhibitor of human cytochrome P450 2C19. Biochemistry 40:12112–22.

Hallifax D, Houston JB. (2006). Uptake and intracellular binding of lipophilic amine drugs by isolated rat hepatocytes and implications for prediction of in vivo metabolic clearance. Drug Metab Dispos 34: 1829–36.

Harper TW, Brassil PJ. (2008). Reaction phenotyping: current industry efforts to identify enzymes responsible for metabolizing drug candidates. AAPS J 10:200–7.

Hosokawa M. (2008). Structure and catalytic properties of carboxylesterase isozymes involved in metabolic activation of prodrugs. Molecules 13:412.

Jamei M, Marciniak S, Edwards D, et al. (2013). The SimCYP population based simulator: architecture, implementation, and quality assurance. In Silico Pharmacol 1:14.

Kumar GN, Surapaneni S. (2001). Role of drug metabolism in drug discovery and development. Med Res Rev 21:397–411.

Lowry OH, Rosebrough NJ, Farr AL, Randall RJ. (1951). Protein measurement with the folin phenol reagent. J Biol Chem 193:265–75.

Downloaded by [University Of South Australia Library] at 21:33 14 July 2016

Masimirembwa CM, Bredberg U, Andersson TB. (2003). Metabolic stability for drug discovery and development: pharmacokinetic and biochemical challenges. Clin Pharmacokinet 42:515–28.

Meng Q, Liu K. (2014). Pharmacokinetic interactions between herbal medicines and prescribed drugs: focus on drug metabolic enzymes and transporters. Curr Drug Metab 15:791–807.

Miners JO, Bowalgaha K, Elliot DJ, et al. (2011). Characterization of niflumic acid as a selective inhibitor of human liver microsomal UDP-glucuronosyltransferase 1A9: application to the reaction phenotyping of acetaminophen glucuronidation. Drug Metab Dispos 39: 644–52.

Miners JO, Mackenzie PI, Knights KM. (2010). The prediction of drug-glucuronidation parameters in humans: UDP-glucuronosyltransferase enzyme-selective substrate and inhibitor probes for reaction phenotyping and in vitro–in vivo extrapolation of drug clearance and drug–drug interaction potential. Drug Metab Rev 42:196–208.

Miners JO, Veronese ME, Birkett DJ. (1994). Chapter 31. In vitro approaches for the prediction of human drug metabolism. Annu Rep Med Chem 29:307–16.

Miners JO, Veronese ME, Birkett DJ. (1996). Use of tolbutamide as a substrate probe for human hepatic cytochrome P450 2C9. Methods Enzymol 272:139–45.

Parikh A, Gillam EM, Guengerich FP. (1997). Drug metabolism by *Escherichia coli* expressing human cytochromes P450. Nat Biotechnol 15:784–8.

Peterson LA. (2012). Reactive metabolites in the biotransformation of molecules containing a furan ring. Chem Res Toxicol 26:6–25.

Polasek TM, Elliot DJ, Somogyi AA, et al. (2006). An evaluation of potential mechanism-based inactivation of human drug metabolizing cytochromes P450 by monoamine oxidase inhibitors, including isoniazid. Br J Clin Pharmacol 61:570–84.

Romberg RW, Lee L. (1995). Comparison of the hydrolysis rates of morphine-3-glucuronide and morphine-6-glucuronide with acid and beta-glucuronidase. J Anal Toxicol 19:157–62.

Roth BL, Baner K, Westkaemper R, et al. (2002). Salvinorin A: a potent naturally occurring nonnitrogenous κ opioid selective agonist. Proc Natl Acad Sci U S A 99:11934–9.

Rowland A, Gaganis P, Elliot DJ, et al. (2007). Binding of inhibitory fatty acids is responsible for the enhancement of UDP-glucuronosyltransferase 2B7 activity by albumin: implications for in vitro–in vivo extrapolation. J Pharmacol Exp Ther 321:137–47.

Rowland A, Knights KM, Mackenzie PI, Miners JO. (2008). The ''albumin effect'' and drug glucuronidation: bovine serum albumin and fatty acid-free human serum albumin enhance the glucuronidation of UDP-glucuronosyltransferase (UGT) 1A9 substrates but not UGT1A1 and UGT1A6 activities. Drug Metab Dispos 36:1056–62.

Salinas-Sánchez DO, Zamilpa A, Pérez S, et al. (2015). Effect of hautriwaic acid isolated from *Dodonaea viscosa* in a model of Kaolin/Carrageenan-induced monoarthritis. Planta Med 81:1240–7.

Sanghani SP, Sanghani PC, Schiel MA, Bosron WF. (2009). Human carboxylesterases: an update on CES1, CES2 and CES3. Protein Pept Lett 16:1207–14.

Schmidt MS, Prisinzano TE, Tidgewell K, et al. (2005). Determination of Salvinorin A in body fluids by high performance liquid chromatography-atmospheric pressure chemical ionization. J Chromatogr B Analyt Technol Biomed Life Sci 818:221–5.

Sheffler DJ, Roth BL. (2003). Salvinorin A: the 'magic mint' hallucinogen finds a molecular target in the kappa opioid receptor. Trends Pharmacol Sci 24:107–9.

Shipkova M, Schütz E, Armstrong VW, et al. (2000). Determination of the acyl glucuronide metabolite of mycophenolic acid in human plasma by HPLC and Emit. Clin Chem 46:365–72.

Simpson BS, Claudie DJ, Gerber JP, et al. (2011). In vivo activity of benzoyl ester clerodane diterpenoid derivatives from *Dodonaea polyandra*. J Nat Prod 74:650–7.

Simpson BS, Claudie DJ, Smith NM, et al. (2010). Evaluation of the anti-inflammatory properties of *Dodonaea polyandra*, a Kaanju traditional medicine. J Ethnopharmacol 132:340–3.

Simpson BS, Luo X, Costabile M, et al. (2014). Polyandric acid A, a clerodane diterpenoid from the Australian medicinal plant *Dodonaea polyandra*, attenuates pro-inflammatory cytokine secretion in vitro and in vivo. J Nat Prod 77:85–91.

Simpson BS, Luo X, Wang J, et al. (2015). Development and evaluation of a topical anti-inflammatory preparation containing *Dodonaea polyandra* extract. J Pharm Pharm Sci 18:578–99.

Sykes MJ, Sorich MJ, Miners JO. (2006). Molecular modeling approaches for the prediction of the nonspecific binding of drugs to hepatic microsomes. J Chem Inf Model 46:2661–73.

Tassaneeyakul W, Birkett DJ, Veronese ME, et al. (1994). Direct characterization of the selectivity of furafylline as an inhibitor of human cytochromes P450 1A1 and 1A2. Pharmacogenetics 4: 281–4.

Teksin ZS, Lee IJ, Nemieboka NN, et al. (2009). Evaluation of the transport, in vitro metabolism and pharmacokinetics of Salvinorin A, a potent hallucinogen. Eur J Pharm Biopharm 72:471–7.

Uchaipichat V, Mackenzie PI, Elliot DJ, Miners JO. (2006a). Selectivity of substrate (trifluroperazine) and inhibitor (amytriptiline, androsterone, canreonic acid, hecogenin, phenylbutazone, quinidine, quinine, and sulfinpyrazone) ''probes'' for human UDP-glucuronosyltransferases. Drug Metab Dispos 34:449–56.

Uchaipichat V, Mackenzie PI, Guo XH, et al. (2004). Human UDP-glucuronosyltransferases: isoform selectivity and kinetics of 4-methylumbelliferone and 1-napthol glucuronidation, effects of organic solvents, and inhibition by diclofenac and probenecid. Drug Metab Dispos 32:413–23.

Uchaipichat V, Winner LK, Mackenzie PI, et al. (2006b). Quantitative prediction of in vivo inhibitory interactions involving glucuronidated drugs from in vitro data: the effect of fluconazole on zidovudine glucuronidation. Br J Clin Pharmacol 61:427–39.

VandenBrink BM, Foti RS, Rock DA, et al. (2011). Evaluation of CYP2C8 inhibition in vitro: utility of montelukast as a selective CYP2C8 probe substrate. Drug Metab Dispos 39:1546–54.

Walsky RL, Obach RS, Hyland R, et al. (2012). Selective mechanism-based inactivation of CYP3A4 by CYP3cide (PF-04981517) and its utility as an in vitro tool for delineating the relative roles of CYP3A4 versus CYP3A5 in the metabolism of drugs. Drug Metab Dispos 40: 1686–97.

Downloaded by [University Of South Australia Library] at 21:33 14 July 2016